DRAFT REPORT.

MASSACHUSETTS INSTITUTE OF TECHNOLOGY

DEPARTMENT OF NUCLEAR ENGINEERING

CAMBRIDGE, Massachusetts 02139, U.S.A.

NUCLEAR ENGINEERING
READING ROOM - M.I.T.

# ANALYSIS OF CONVENTIONAL AND PLUTONIUM RECYCLE UNIT-ASSEMBLIES FOR THE YANKEE (ROWE) PWR.

by

Paul G. MERTENS

November 1971

MITNE - 134

## ABSTRACT.

An analysis and comparison of Unit Conventional $UO_2$ Fuel-Assemblies and proposed Plutonium Recycle Fuel Assemblies for the Yankee (Rowe) Reactor has been made.
The influence of spectral effects, at the watergaps -and spectral-and transport effects at the $UO_2$ - Mixed Oxide interface, on the powerpeaking has been determined.
Two one thermal group methods have been developped for the calculation of powerpeaking in the two dimensional assemblies. The accuracy of the LEOPARD code and LASER code (thermal cut off 1.855 ev) for the calculation of the powerpeaking in conventional and plutonium recycle assemblies has been evaluated.
The power distribution and local power peaking factors during burnup, including spectral effects, were also calculated with a macroscopic depletion model.
Powergradients inside the peak $UO_2$ rod and peak mixed oxide rod were also determined, and the variations in the heat flux, at the pellet and cladding surface, around these peak pins were calculated. Finally preleminary comparisons of engineering factors for the peak $UO_2$ rod and the peak mixed oxide rod have been made.

ACKNOWLEDGMENT.

The author would like to express his sincere gratitude to his supervisor, Professor D.D. Lanning for his guidance, advice and encouragement throughout the course of this work.

He wishes to express his great appreciation for the interesting advice of W. Hinkle , D. Cacciapouti, B. Kirschner, A. Allan, H. Lurie from the Yankee Atomic Electric Company, and of Prof. A.F. Henry, H. Spierling and D. Farrar from the Nuclear Engineering Department M.I.T.

The financial aid for the computer calculations from the Nuclear Engineering Department M.I.T., and from the Yankee Atomic Electric Co. are gratefully acknowledged.

The calculations were done in part on the IBM-360 of the MIT Information Processing Center, Cambridge, Mass, and on the CDC-6600 terminal of the New-England Electric Company, Westboro, Massachusetts.

SUMMARY AND KEY CONCLUSIONS.

A) DESCRIPTIONS ASSEMBLIES : key Table I-4, key Figures : I-4, I-5, I-6, I-10.

B) KEY CONCLUSIONS CONCERNING THE EFFECTS THAT INFLUENCE THE CALCULATIONS OF THE POWERDISTRIBUTIONS & LOCAL POWER PEAKING FACTORS. (Chapter III-V)

1)-The much larger fluxgradient in the Pu-recycle assembly is responsible for differences in diffusion theory models. The effect on the power peaking factor is minor. The few group diffusiontheory calculations with standard unit cell codes such as LASER is adequate for the calculation of the powerdistributions.

2)-The accurate description of the Pu-240 resonance is a major factor of concern for the calculation of the power distribution and local power peaking in the Pu-recycle assembly, but is not too important in conventional applications even at high burnups.

3)-The spectral effects at the watergaps and at the mixed oxide - $UO_2$ interface are major factors of concern for the accurate calculation of local power peaking factors.

(Key Tables : Table III-4, IV-4, V-1, V-2, V-3. Key Figures : Fig.II-2, III-3, III-4, III-5, IV-15, IV-16, V-5, V-8)

C) KEY CONCLUSIONS ABOUT THE SIMPLE POWER PEAKING CALCULATION METHODS. (Chapter IV, V)

1)-The developed spectral- cross section Synthesis method (SXS) and the more simple generalised mixed number density method (GMND) which can be used with the LASER codes are adequate for the calculation of power peaking in the Pu-recycle assemblies.

2)-By comparison with experiment the standard LASER code to generate the X-sections was found to be more accurate tham the LEOPARD code for the calculation of the powerdistribution and local power peaking factors,

for Plutonium Recycle applications.

(Key Tables : IV-4, V-1, V-3. Key Figures : III-3, IV-12, IV-13, IV-14, IV-15, IV-16)

D) KEY CONCLUSIONS ABOUT THE POWERDISTRIBUTION AND LOCAL POWER PEAKING FACTORS (Chapter V) IN THE CONVENTIONAL AND PU-RECYCLE YANKEE ASSEMBLIES.

D -1 Beginning of Life

( Key Tables : Table V-1, V-3, V-4. Key Figures : Fig.V-5, V-9, V-10, V-11)

1)-The power peaking factor in a plutonium-recycle assembly increases with the w/o of $PuO_2$ used in the mixed oxide rods by about 10 % per w/o (Fig.V-11)

2)-At 4 w/o of $PuO_2$ the local nuclear power peak in the plutonium recycle assembly is about equal to the local power peaking factor in a conventional assembly (Fig.V-11)

3)-The local power peaking factor in a Pu-recycle assembly is rather insensitive to the number of mixed oxide rods and loading configuration.

4)-The spectral effects at the mixed oxide $UO_2$ interface increase by about 1.6 % per w/o of $PuO_2$ in the mixed oxide fuel.

D -2 Burnup.

(Key Figures : Fig. V-19, V-31, V-32, V-37, V-38, V-40, V-41)

1)- There is a considerable powerflattening in the Pu-recycle assembly with burnup (Fig.V-37) and no flattening in a conventional assembly (Fig.V-31).

2)-There is a decrease of the local power peaking factorwith burnup in a Pu-recycle assembly, especially for the peak mixed oxide rod; and an increase in the local power peaking factor in a conventional assembly (Fig.V-41).

3)-There is a shift in peak rod position from the peak mixed oxide rod to the peak $UO_2$ rod in a plutonium recycle assembly (Fig.V-41)

4)-The increase in local power peaking due to spectral effects remains strong, even at high burnups. In conventional applications the spectral effects at the fresh fuel - burned fuel interface are negligible.

5)-Both the isolated conventional and plutonium recycle assemblies reach zero reactivity at about 30,000 MWD/MTM. In a batch fueled Yankee Reactor, the plutonium recycle assemblies have a rather severe lifetime penalty. However equal lifetime conditions in the actual two zone out-in fueled Yankee reactor can probably be obtained.

E) KEY CONCLUSIONS ON THE POWER DISTRIBUTION INSIDE THE PEAK $UO_2$ AND PEAK MIXED OXIDE RODS. (Chapter VI)

(Key Figures : VI-12, VI-13, VI-14)

1)-The peak mixed oxide rods have a larger power gradient inside the pin than a peak $UO_2$ rod.

2)-The power distribution inside a mixed oxide rod is much more non uniform than in a $UO_2$ rod.

F) GENERAL KEY CONCLUSIONS ON HOT CHANNEL FACTORS.

(Chapters V, VII) (Key Tables : VII-3, VII-5. Key Figures : VII-2, VII-3)

1)-The peak mixed oxide rod has a larger circumferential heat flux hot channel factor than a $UO_2$ rod. The larger powergradient is responsible for this effect.

2)-Due to the beneficial "internal" location of the peak mixed oxide rod, next to the low power $UO_2$ rods and other mixed oxide rods, the engineering flow redistribution factor and nuclear enthalpy rise hot channel factor are lower.

3)-The non uniform power distribution inside the peak mixed oxide pin compared to the peak $UO_2$ pin has a potential to allow an increase of about 2.6 % in linear power in order to get the same maximum fuel temperature as in the $UO_2$ pin.

4)-It is estimated that due to the beneficial effects of internal location of the mixed oxide rods in the graded assembly design, an increase of at least 5 % in peak power can be allowed in the peak mixed oxide rod, relative to the peak $UO_2$ rod, to get the same minimum departure of nucleate boiling ratio(assuming equal nuclear power peaking factors.

<u>As an overall conclusion</u>, the analysis indicates that the conventional and plutonium recycle unit assembly designs, in which the 4 w/o mixed oxide rods of only one enrichment are loaded in the center of the assembly, are compatible in powerpeaking, heat flux and enthalpy rise hot channel factors, and have about the same lifetime in an infinite reactor.

A capsule comparison of the conventional and plutonium-recycle unit assembly design study is given on Table S-1.

TABLE S-1.

CAPSULE COMPARISON CONVENTIONAL AND PLUTONIUM RECYCLE YANKEE ASSEMBLY DESIGN

| Parameter | Pu-recycle | Reason for difference | Consequence. |
|---|---|---|---|
| - accuracy power distribution calculation. | reduced | larger flux gradients, Pu-240 description. | - Proper choice of the code (LASER or LOCALUX). |
| - local power peaking BOL | increased | spectral effects at mixed oxide and $UO_2$ interface, higher absorption in mixed oxide. | - limitation on the w/o of $PuO_2$ or 2 Pu enrichments necessary to flatten the power. |
| - local power peaking with burnup. | decreased | decrease of thermal absorption cross section with burnup. | - Improved power flattening with burnup. |
| - lifetime in an<br>- infinite reactor<br>- batch Yankee reactor | <br>about same<br>reduced | $k_\infty$ versus burnup mixed oxide rod. | - none or possible increase w/o $PUO_2$, reduce number of Pu rods, or other fuel management action. |
| - accuracy burnup calculations. | reduced | errors Pu cross-sections, buildup higher isotopes. | - lower lifetime, revision burnup codes, or reactivity bias necessary. |
| - powergradients inside peak rods. | increased | high absorption cross-section. | - higher circumferential heat flux hot channel factor, decrease MDNBR. |
| - powerdistribution inside the rods. | more non uniform | high absorption cross-section. | - lower fuel centerline temperature. |
| - enthalpy rise. | reduced | internal location, lower flowredistribution and nuclear enthalpy rise HCF. | - improved DNB margin. |

TABLE OF CONTENTS. Page #.

ABSTRACT 2

ACKNOWLEDGEMENTS - SUMMARY. 3 - 4

TABLE OF CONTENTS - LIST OF FIGURES - LIST OF TABLES. 9 -11 -17

CHAPTER I - INTRODUCTION 19

I-1 Background - Plutonium Recycle in Thermal Reactors. 19

I-2 Description of the Yankee (-Rowe) PWR (175 MWe) and comparison with current 1000 MWe PWR's. 24

CHAPTER II - STATUS OF COMPUTER METHODS - CODES AND DESCRIPTION OF THE COMPUTER CODES USED IN THIS STUDY. 46

II-1 Status of Computermethods and Codes. 46

II-2 Flow of the Nuclear Analysis Calculations 54

II-3 Description of the computercodes used in this study. 58

CHAPTER III - SPECTRAL EFFECTS & TRANSPORT EFFECTS IN ONE DIMENSIONAL CONVENTIONAL AND PU-RECYCLE ASSEMBLY MODELS. 69

III-1 Introduction 69

III-2 The thermos-35 Group Fuel Element Homogenization Procedure. 69

III-3 The thermal spectrum distribution in one dimensional conventional & Pu-recycle assemblies 72

III-4 Effects of one-group models, on the calculation of the powerdistribution. 77

CHAPTER IV-DEVELOPMENT OF GENERAL AND SIMPLE ONE THERMAL GROUP METHODS FOR THE CALCULATION OF POWERPEAKING IN ONE, TWO & THREE DIMENSIONS. 95

IV-1 Introduction 95

IV-2 Development of the Thermos-Spatial-Cross-Section Synthesis in X-Y dimensions. 99

Page #.

IV-3 Development of the Generalised MND Method. 114

IV-4 Evaluation of the SXS and GMND methods for the calculation of powerpeaking at watergaps and $UO_2$-Mixed Oxide Interfaces. 137

CHAPTER V : THE CALCULATION OF THE LOCAL POWERPEAKING FACTORS & POWERDISTRIBUTION IN CONVENTIONAL & PLUTONIUMRECYCLE ASSEMBLIES FOR THE YANKEE REACTOR AT BOL AND DURING LIFETIME. 161

V -1 Introduction 161

V -2 The influence of the Design Details of the Assemblies on the Calculation of the local Powerpeaking & Powerdistribution. 161

V -3 The Powerdistribution and Powerpeaking in the Conventional and Plutonium Recycle Assembly at beginning of life. 168

V -4 The variation of Local Powerpeaking Factors, Powerdistribution and $k_\infty$ in a conventional & Plutoniumrecycle Assembly during lifetime. 185

CHAPTER VI : THE CALCULATION OF POWERGRADIENTS AND POWERDISTRIBUTION INSIDE THE PEAK RODS OF CONVENTIONAL AND PU-RECYCLE ASSEMBLIES. 234

VI-1 Introduction 234

VI-2 Description of the calculation-method. 234

VI-3 Evaluation of the method by comparison with THERMOS. 238

VI-4 Results for the Conventional & PU-recycle assemblies. 240

CHAPTER VII : THERMAL-HYDRAULIC EVALUATION OF CONVENTIONAL AND PU-RECYCLE ASSEMBLIES. 260

VII-1 Thermal Hydraulic characteristics 260

VII-2 The Thermal Hydraulic Model 269

VII-3 Summary of calculated Engineering Factors & Comparison Peak $UO_2$ and peak Mixed Oxide Pin 293

VII-4 Conclusion. 296

APPENDIX A W-3 DNB Heat Flux Correlations. 297

REFERENCES 299

## LIST OF FIGURES.


CHAPTER I :

| | | Page #. |
|---|---|---|
| Fig. I - 1 | Representative Steady State Fuel Cycle Flow Rates, 430 MWe Reactor, one lot of fuel. | 20 |
| I - 2 | Vertical Section Reactor Yankee. | 26 |
| I - 3 | Horizontal Section Reactor Yankee, and SS.clad Fuel Assemblies. | 27 |
| I - 4 | Type A zircalloy Clad Assembly. | 31 |
| I - 5 | Type B zircalloy Clad Assembly. | 32 |
| I - 6 | Type B zircalloy Clad Assembly. | 33 |
| I - 7 | Fuel Assemblies with control cluster rods in large PWR's. | 35 |
| I - 8 | Enrichment Pattern for an All-Plutonium Fuel Assembly (Average enrichment = 3.8 w/o PU $O_2$). | 39 |
| I - 9 | Discreet Assembly Core Configuration Showing the relative Positions of Control Rods and Plutonium Fuel Assemblies. | 40 |
| I -10 | Loading of Conventional and Plutonium Recycle Assemblies. | 43 |

CHAPTER II :

| | | |
|---|---|---|
| Fig. II - 1 | Flow for the Analysis of Conventional & Plutonium Recycle Assemblies for the Yankee Reactor. | 55 |
| II - 2 | Comparison Cross-Sections U 236 and Plutonium isotopes. | 59 |
| II - 3 | Laser Lattice Cell Geometry. | 63 |

CHAPTER III :

| | | |
|---|---|---|
| Fig. III- 1 | Cylindrical Models of the Conventional and Plutonium Recycle Assemblies. | 70 |
| III- 2 | Spectra at different positions in the cylindrical $UO_2$ and Plutonium Recycle Assemblies. | 75 |
| III- 3 | Powerdistribution Cylindrical Conventional $UO_2$ assembly, Comparison Thermos 35 group, PDQ - 1 group. | 88 |
| III- 4 | Comparison powerdistribution using different diffusiontheory models - Pu-recycle assembly. | 90 |
| III- 5 | Comparison Transport Theory & Diffusiontheory Plutonium Recycle Assembly. | 91 |

CHAPTER IV.: Page #.


| | | |
|---|---|---|
| Fig. IV - 1 | Two Dimensional Spatial X-sections Synthesis. | 101 |
| IV - 2 | Geometry for the calculation of the spectrumdisturbance at the watergap. | 106 |
| IV - 3 | Geometry for the calculation of the spectral disturbances at the watergap and fuels interface. | 106 |
| IV - 4 | % Deviations in X-sections and thermal velocity vs. position away from the watergap. | 107 |
| IV - 5 | % Deviations in X-sections vs. watergap thickness at different positions. | 107 |
| IV - 6 | % Deviations in X-sections and Thermal velocity in the slab Pu-recycle section. | 108 |
| IV - 7 | Avg. Thermal Neutron velocity distribution in a portion of conventional $UO_2$ assembly. | 110 |
| IV - 8 | Avg. Thermal Neutron Velocity Distribution in a Pu-recycle Assembly. | 111 |
| IV - 9 | % Deviations in Cross-Sections in a conventional $UO_2$assembly. | 112 |
| IV -10 | % Deviations in macroscopic Cross-Sections in a Pu-recycle assembly. | 113 |
| IV -11 | Normalized activation of a 1/v absorber in a conventional & Pu-recycle assembly model. | 116 |
| IV -12 | Comparison 1/v an $1/v_{GRAD}$, Thermos, Breen's MND and our GMND method in a conventional assembly. | 135 |
| IV -13 | Comparison 1/v, 1/v grad, Thermos, Breen, our GMND-in a Pu-recycle assembly. | 135 |
| IV -14 | Comparison one group methods for the calculation of power-peaking in a Pu-recycle assembly. | 141 |
| IV -15 | Comparison standard powercalculation and GMND-method, relative to the SXS-method in a conventional $UO_2$ Yankee Assembly Portion. | 144 |
| IV -16 | Comparison Standard Powercalculation and GMND method, relative to the SXS method in a Piutonium-recycle Assembly Portion. | 146 |
| IV -17 | Experiment Loading Configuration | 150 |
| IV -18 | $UO_2$ Fuel Specification Experimental Loading | 151 |
| IV -19 | Mixed Oxide Fuel Specification | 152 |

CHAPTER V : Page #.


Fig. V - 1,2 Physical Boundary and Composition Overlay. 163

V - 3 % Increase in Normalised Power due to 50 % increase of holes in the SS-can. 166

V - 4 % Increase in Power due to Replacement of the SS-can by a zircalloy can. 166

V - 5 Total Normalised Powerdistribution in a Conventional $UO_2$ assembly using regular LASER & LEOPARD X-sections. 170

V - 6 Fraction of Total Power due to thermal neutrons in a portion of the Conventional assembly. 171

V - 7 Powerdistribution Conventional $UO_2$ assembly Portion using LEOPARD MND. 172

V - 8 Powerdistribution in the Plutonium Recycle Assembly using Regular LEOPARD X-sections, -and % error relative to the calculation with LASER Regular Cross-sections. 175

V - 9 Powerdistribution in the Plutonium Recycle Assembly using Regular LASER X-sections and GMND X-sections from LASER. 176

V -10 Lay-out and location of the local Powerpeaks in the two different Pu-recycle designs. 183

V -11 Local Powerpeakingfactors in a Conventional & Plutonium Recycle Assembly with different w/o of $PuO_2$. 184

V -12 Monte Carlo Result of the Spatial distribution of U-238 resonance captures. 190

V -13 Fraction of total power due to thermal neutrons in a portion of the plutonium-recycle assembly. 194

V -14 Thermal neutron spectra in a fresh $UO_2$ fuel cell. 196

V -15 Thermal neutron spectra in a depleted $UO_2$ fuel cell. 197

V -16 Neutron Balance in a $UO_2$ cell as a function of Burnup. 198

V -17 Fuel Region Averaged Isotopic concentrations in $UO_2$ vs. burnup. 200

V -18 Change of Plutonium Isotopic concentrations in $UO_2$ fuel. 201

V -19 Variation of $k_\infty$ and $k_{eff}$ with burnup of an all $UO_2$ or mixed oxide fueled Yankee reactor(without extra materials). 202

| | | Page #. |
|---|---|---|
| Fig. V -20 | Variations in the macroscopic X-sections vs. burnup in the $UO_2$ fuel. | 203 |
| V -21 | Thermal Neutron Spectra in a fresh plutoniumrecycle fuel cell. | 205 |
| V -22 | Thermal Neutron Spectra in a depleted plutonium recycle fuel cell. | 206 |
| V -23 | Neutron Balance in Mixed Oxide Fuel Cell as a function of burnup. | 208 |
| V -24 | Fuel Region Averaged Isotopic Concentation, in the mixed oxide fuel. | 209 |
| V -25 | Change of the Plutonium Isotopic Composition in the Mixed Oxide fuel. | 210 |
| V -26 | Variation of the macroscopic X-sections in the Mixed-Oxide fuel vs. burnup. | 203 |
| V -27 | Variation of the reciprocal avg. thermal velocity of the flux and flux gradient at the water and fuels interfaces, vs. burnup. | 212 |
| V -28 | Burnup Map Rod by Rod $UO_2$ assembly average burnup : 4800 MWD/MTM. | 214 |
| V -29 | Powerdistribution in $UO_2$ assembly at avg. Assembly burnup of 4800 MWD/MTM. | 215 |
| V -30 | Powerdistribution in the $UO_2$ assembly at an avg.burnup of 19200 MWD/MTM. | 216 |
| V -31 | Rod by Rod Burnupdistribution avg. assembly burnup 28800 MWD/MTM. | 217 |
| V -32 | Powerdistribution in the $UO_2$ assembly at an average burnup of 28800 MWD/MTM. | 218 |
| V -33 | k-infinity map $UO_2$ assembly at avg. 28800 MWD/MTM. | 219 |
| V -34 | Powerdistribution in the Plutonium Recycle Assembly at 4800 MWD/MTM avg. burnup. | 224 |
| V -35 | Powerdistribution in the Pu-recycle assembly at 9600 MWD/MTM avg. | 225 |
| V -36 | Powerdistribution in the Pu-recycle assembly at 19200 MWD/MTM avg. | 226 |
| V -37 | Powerdistribution in the Pu-recycle assembly at 28800 MWD/MTM. | 227 |

Page #.

Fig. V -38 Burnup distribution in the Pu-recycle assembly -avg. burnup 28800 MWD/MTM. 228

V -39 k-infinity map for the Pu-recycle assembly at 28800 MWD/MTM. 229

V -40 Comparison k-inf. and $k_{eff}$ vs. burnup for the conventional & Pu-recycle assemblies. (k-inf. without extra materials, $k_{eff}$ with extra materials & buckling). 230

V -41 Local Powerpeakingfactors in the Conventional and Pu-recycle assemblies vs. burnup. 231

V -42 Unit Assembly Power Distribution at the Beginning of Life for a Discreet Assembly Concept. 232

V -43 Unit Assembly Power Distributions at the End-of-Life for a Discrete Assembly Concept. 233

CHAPTER VI :

Fig. VI - 1 Comparison Thermos & Corrected Diffusion Theory. 239

VI - 2 Perturbed Spectral correctionfactors. 241

VI - 3 Spectral Correction Factors in the Unperturbed Cylindrical Pins. 241

VI - 4 Geometrical and Composition Layout of the 9 rod cluster at the cruciform watergap. 244

VI - 5 Geometrical & composition Layout of the 36 $UO_2$ Mixed Oxide Cluster. 245

VI - 6 Gradient Factor Distribution & Bowing Directions in the 9 rod cluster in the corner of the assemblies and in the 36 rod cluster in a plutoniumrecycle assembly (PDQ-5, uncorrected results). 247

VI - 7 Uncorrectd X-Y powerdistribution in the peak $UO_2$ pin number 1, in the 9 rod cluster at the cruciform watergap (conventional & Pu-recycle assembly). 248

VI - 8 Uncorrected X, Y powerdistribution in $UO_2$ pin number 3, in the 9 rod cluster at the watergap. 249

VI - 9 Uncorrected X-Y powerdistribution in the peak Mixed Oxide pin number 1, in the 36 rod cluster in the center of a plutonium-recycle assembly. 251

VI -10 Uncorrected X,-Y powerdistribution in the mixed oxide pin number 2. 252

Page #.

Fig. VI -11 Uncorrected X-Y powerdistribution in the mixed oxide pin number 3. 253

VI -12 Corrected Total powerdistribution in the peak $UO_2$ rod, compared to the normal powerdistribution. 256

VI -13 Corrected Total Powerdistribution in the peak Mixed Oxide Rod (compared to the normal powerdistribution). 257

VI -14 Comparison of the powerdistributions in the 0-180° plane, in the peak $UO_2$ and peak mixed oxide rod. 258

CHAPTER VII :

Fig. VII- 1 Different coolant channels in the Zirc Clad Assemblies. 270

VII- 2 R, $\theta$ Variation of the Circumferential Inner Clad Heat Flux, in the peak $UO_2$ and peak Mixed Oxide Pins. 280

VII- 3 Ratios of the Nuclear Enthalpy Rise Hot Channel Factor, to the Nuclear Peak Factor in the peak rod (peak $UO_2$ and peak Mixed Oxide). 284

LIST OF TABLES. Page #

SUMMARY.

Table S-1 Capsule comparison of the conventional and plutonium recycle Yankee Unit Assembly Design. 8

CHAPTER I :

Table I - 1 Makeup of Steady State Fuel Cycle cost in a Pressurized Water Reactor. 21

I - 2 Comparison of Yankee (Rowe) & recent PWR design characteristics. 28

I - 3 Capsule Comparison of Uranium & Plutonium Nuclear Design Characteristics. 37

I - 4 Description of UNC conventional Fuel Assembly Designs and Fuel Rods. 45

I - 5 Nuclear Characteristics of the Unloaded Fuel Assemblies of the Yankee Reactor. 44

CHAPTER II :

Table II - 1 Laser Energy Mesh. 64

CHAPTER III :

Table III- 1 Thermos Self Shielding Factors for the $UO_2$ fuel and Mixed Oxide fuel. 73

III- 2 Comparison of one group macroscopic X-section of an unperturbed $UO_2$ and mixed oxide unit cell, using the C.H. or M.H. method. 86

III- 3 Comparison of the one Group diffusion constants of unperturbed cells using different homogenization schemes. 87

III- 4 Flux by angle and by point in a Plutonium recycle Assembly (ANISN). 94

CHAPTER IV :

Table IV - 1 Comparison of Division Factors for Breen's MND X-sections (LEOPARD) and our GMND X-sections (LASER) for the calculation of powerpeaking at fuel/$H_2O$ interface. 131

IV - 2 Comparison between Breen's MND parameters and our GMND Parameters for the calculation of powerpeaking at fuel/fuel interfaces. 133

IV - 3 Comparison of Code Calculations for $UO_2$ -2.35 w/o U235 fuel, and 2.0 w/o $PuO_2$ - nat $UO_2$ fuel (8 a/o Pu 240). 156

IV - 4 Comparison of Experimental & Calculated Powerdistribution of an 11X11 2 w/o $PUO_2$ -nat $UO_2$(8 a/o Pu 240) clement in $UO_2$ - 2.35 w/o u235. 157

CHAPTER V : Page #.


Table V - 1 Comparison BOL-Local Powerpeaking Factors in a Conventional $UO_2$ Unit Assembly, using different Methods. 173

V - 2 Comparison LASER and LEOPARD unit cell calculations. 178

V - 3 Comparison BOL-Local Powerpeaking Factors in the Proposed Plutonium Recycle Assembly, using different Methods. 181

V - 4 Comparison of the Local Powerpeakingfactors for Different Designs. 182

V - 5 Spatial Distribution of U238 Resonance Capture Rate. 189

V - 6 2200 m/sec Parameters for Fissile Nuclides. 191


CHAPTER VI : ---

CHAPTER VII :


Table VII- 1 Core 10 Thermal-Hydraulic Parameters at Full Power, & Hot Channel and Hot Spot Parameters and Comparison with a Pu-recycle assembly. 264

VII- 2 Hydraulic Diameters and Flow-areas for the different channel Types. 279

VII- 3 Maximum HCF $F_{q''}^{n.u.}$ ( $\theta$ =0 ) for the Heat Flux at outer-and inner Cladding surface, in the peak $UO_2$ and peak mixed oxide pins. 279

VII- 4 Linear heat rate HCF for the fuel centerline temperature. 282

VII- 5 Summary Hot Channel Factors of the Unit Assemblies. 294

VII- 6 Estimated Plutonium Recycle Core Hot Channel Factor Ratios $F^{UO_2}/F_{MIX}$. 295

# CHAPTER I : INTRODUCTION.

## I - 1 BACKGROUND - PLUTONIUM RECYCLE IN THERMAL REACTORS.

### I - 1 - 1) Economic Aspects of Recycling Plutonium in Thermal Reactors.

The development of large FAST BREEDERS has proceeded slowly in the U.S. and elsewhere, whereas the demand for electric power doubles almost every ten years.

With this increasing demand for electricity and a spiraling increase of nuclear powerreactors, huge amounts of plutonium are expected to pile up within the next 10years or more, before this plutonium will be consumed by the first series of large fast breeder reactors.

In the U.S. alone 300 metric tons of Pu-fissile will be produced by 1985, representing a value of roughly 3 billion dollars.(Ref. 1).

In the U.S. and elswhere (except the U.K. where inventory charges for government holdings of Pu can be set quite low - and breeders are expected earlier) stockpiling the Pu and carrying the accumulated interest charges, has been considerednot economic and harmful for the development of future LMFBR's. (Liquid Metal Fast Breeders). Therefore effective the 1st January of 1971, the U.S. Atomic Energy Commission terminated the buy-back of plutonium produced in commercial powerreactors, and forced the electric utilities to take immediate action for recycling their Pu.

Before the Pu-fissile was sold at about 8 $ per gram. One typical Light Water Reactor of 430 MWe produces about 70 kg. of Pu 239, and 18 kg. Pu 241 fissile isotopes per year, representing a value of about 812,000 $ per year or roughly 16 % of the total fuel cycle cost. (Fig, I - 1, Table I - 1).

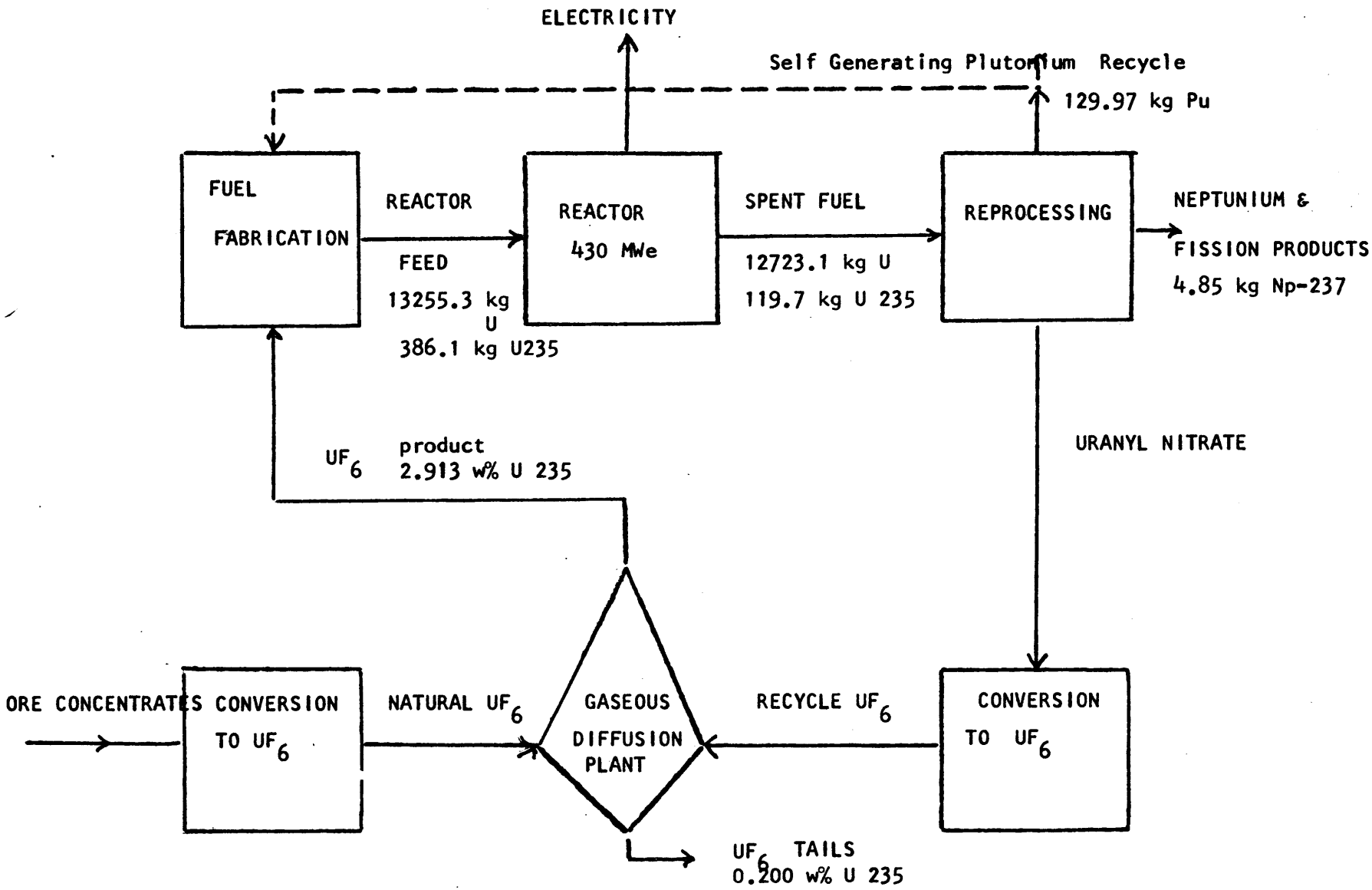


FIG I-1 Representative Steady State Fuel Cycle Flow Rates, 430 MWe PWR Reactor, one lot of fuel

Table I - 1 Makeup of Steady State Fuel Cycle Cost in a Pressurized Water Reactor.

2.913 w/o U-235 in Feed

0.8 Capacity Factor

(1969 prices - from Prof. M. Benedicts course : "Economics for Nuclear Reactors - MIT).

| Component | Dollars per Fuel Lot $Z_q$ | Mills per kwh $e_q$ |
|---|---|---|
| Uranium feed | $ 3,069,755 | 1.0441 |
| Uranium credit (subtract) | 531,286 | 0.1807 |
| Uranium burnup | 2,538,469 | 0.8634 |
| Plutonium credit (subtract) | 812,000 | 0.2762 |
| Net material cost | 1,726,469 | 0.5872 |
| Fabrication | 1,199,129 | 0.4078 |
| Reprocessing | 477,368 | 0.1624 |
| Conversion | 39,366 | 0.0134 |
| Total direct costs | 3,442,332 | 1.1708 |
| Fuel carrying charge | 1,669,371 | 0.5678 |
| Operations carrying charge | 224,313 | 0.0763 |
| Total fuel cycle cost | $ 5,336,016 | 1.8149 |

If Pu recoverable from U.S. Light Water Reactors were assigned zero value, the fuel cycle cost would be increased by 812,000 $ per year, for a 430 MWe reactor, but may reach 1.5 to 3 million $ for a 1000 MW(e) reactor.

In the evaluation of plutonium recycle economics the term "value" of plutonium is widely used. The value is defined as the maximum price that can be assigned to plutonium in a given reactor to produce the same unit power cost whether the reactor is fueled with plutonium or enriched uranium.

If no market for plutonium exists at the assumed price and it must be carried on inventory, the capital outlay for Pu would double every 7 years. Thus the capital-cost factor will become significant, if reactor use of plutonium is long delayed.

If a utility decides to store Pu in anticipation of a future price rise a storage cost of 0.20 $ per gram must be paid at AEC facilities and $\approx$ 0.35 $ per gram at commercial facilities.

The increase in Pu price due to potential increases in the cost of enriched uranium or reduction of the plutonium fabrication-cost penalty will not justify Pu storage for more than 2 or 3 years.

The high Pu-fabrication cost is one major drawback for economic recycling. It has been estimated that the minimum Pu-value required for recycling is 1 to 3 $ per gram. In a preliminary study after receiving the bids of fuel fabricators the Pu-value in the Yankee Reactor was found to be low, which was due to the very high present fabrication cost of Pu-fuels.

The low throughput of the facilities for Pu-fuels & its toxity are major factors for the high fabrication cost factor, presently about twice that of $UO_2$ rods.

## I - 1 - 2) Technical Aspects on Pu-Recycle Cores.

Based on preleminary design work for large PWR's Westinghouse concludes that (Ref.2)

1) during the 1970's plutoniumrecycle will constitute less than 15 % of the fuel for most LWR's, and the most likely mode is a self generated cycle where plutonium processed from discharged fuel is reloaded in a given reactor.

2) The reload region will have the same mechanical design for both the plutonium recycle and enriched uranium fuel assemblies. This will result in the same coolant flow conditions outside the mixed oxide rods since the same fuel rod pitch, outside diameter and grid designs will be used. In PWR's the same type of cladding (zircalloy 4) will be used.

3) The plutoniumrecycle assemblies for PWR reload regions will consist entirely of mixed-oxide fuel rods.

4) There will be minimum three different plutonium enrichments in each plutoniumrecycle assembly.

5) Additional design work will be required for each application of plutoniumrecycle to determine control worth and powerdistributioncontrol requirements for each reactor. Powerdistribution and adequate control rod worth are the principle concerns for plutonium recycle applications.

## I- 2 DESCRIPTION OF THE YANKEE (-ROWE) PWR (175 MWe) AND COMPARISON WITH CURRENT 1000 MWe PWR's.

### I- 2 -1) GROSS CORE DESCRIPTION & COMPARISION

The Yankee Nuclear Power Station is one of the first privately owned nuclear power stations and is located at Rowe in Massachusetts. It is owned and operated by the Yankee Atomic Electric Company, a combine of 10 electric utilities in New England.
The reactor is of a PWR type, water moderated and cooled, and using slightly enriched uranium.
The main contractors were Westinghouse Electric Corp. for the nuclear plant and Stone & Webster Engineering Corp. for the steam plant. The reactor reached full power in june 1961 and produced a gross heat output of 392 MW thermal, and a gross electric power of 110 MWe. Table I- 2 shows the differences in the design characteristics of the Yankee reactor compared to the initial design, and the differences that exist between this reactor and the more recent PWR's.

A vertical section of the Yankee reactorvessel isshown in Fig. I- 2, and a horizontal cut in Fig. I- 3.

Of specific importance for the interpretation of our results compared to other design studies of large PWR's is - the smaller reactor core, this

results in higher leakage, and a smaller effective multiplication factor which in turn has a marked effect on the burnup & the choice of the enrichment in order to get about 1 year of reactor operation.

Coastdown is a current practice in the Yankee reactor to extend the burnup according to the load demands, and the fuel management is of the out-in type, compared to the modified scatter refueling in large PWR's.

The presence of cruciform control rods with zirc followers in the Yankee, has for obvious space saving reasons (& other advantages) been replaced by controlrodclusters without followers in large PWR'S.

The followers in the Yankee serve 2 purposes, they reduce the powerpeaking due to the increased watergap when control rods are withdrawn, and they preserve the same flow distribution in the assemblies, for each control rod position.

It is further important to notice (Fig. I - 3) the particular asymmetric location of the cruciform controlrods & followers in the Yankee reactor respective to the location of the fuel assemblies.

This layout, although it gives the highest density of the core, makes it impossible to shuffle the assemblies freely, and makes it necessary to have 2 mechanically different assembly designs.

Furthermore the number of possible fuel assembly patterns for optimum fuelmanagement is obviously reduced.

- Not all the assemblies in current large PWR's contain control rod clusters.

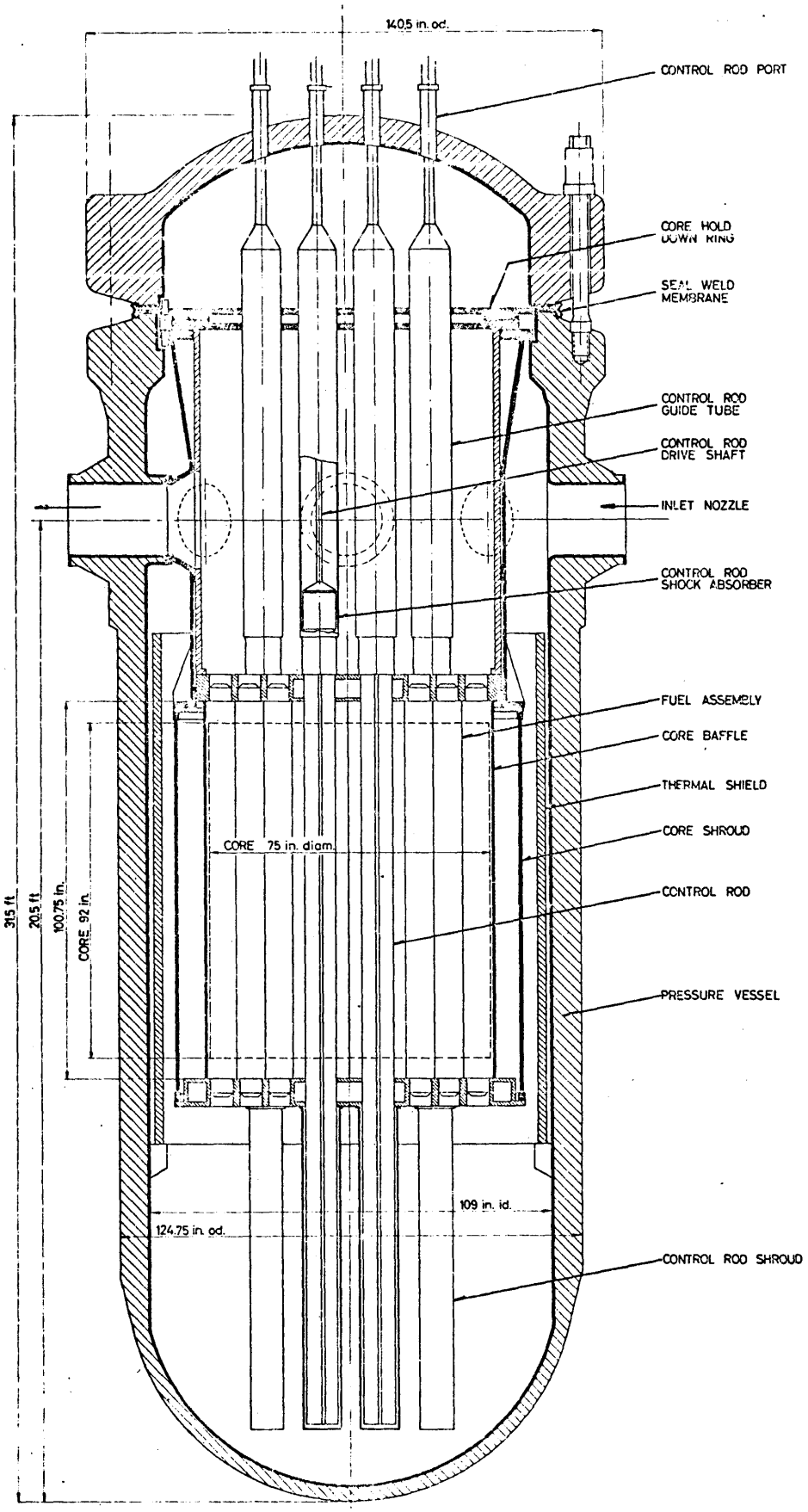


FIG 1-2, VERTICAL SECTION REACTOR YANKEE

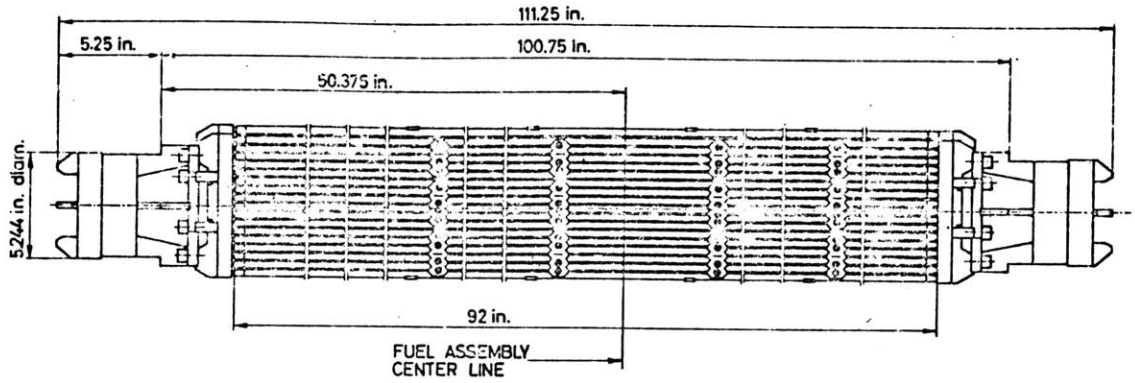


FIG 1-3, FUEL ELEMENT

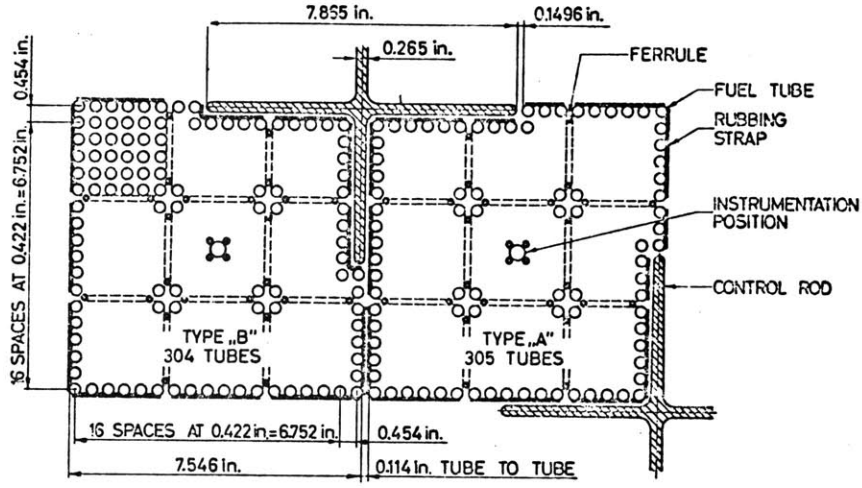


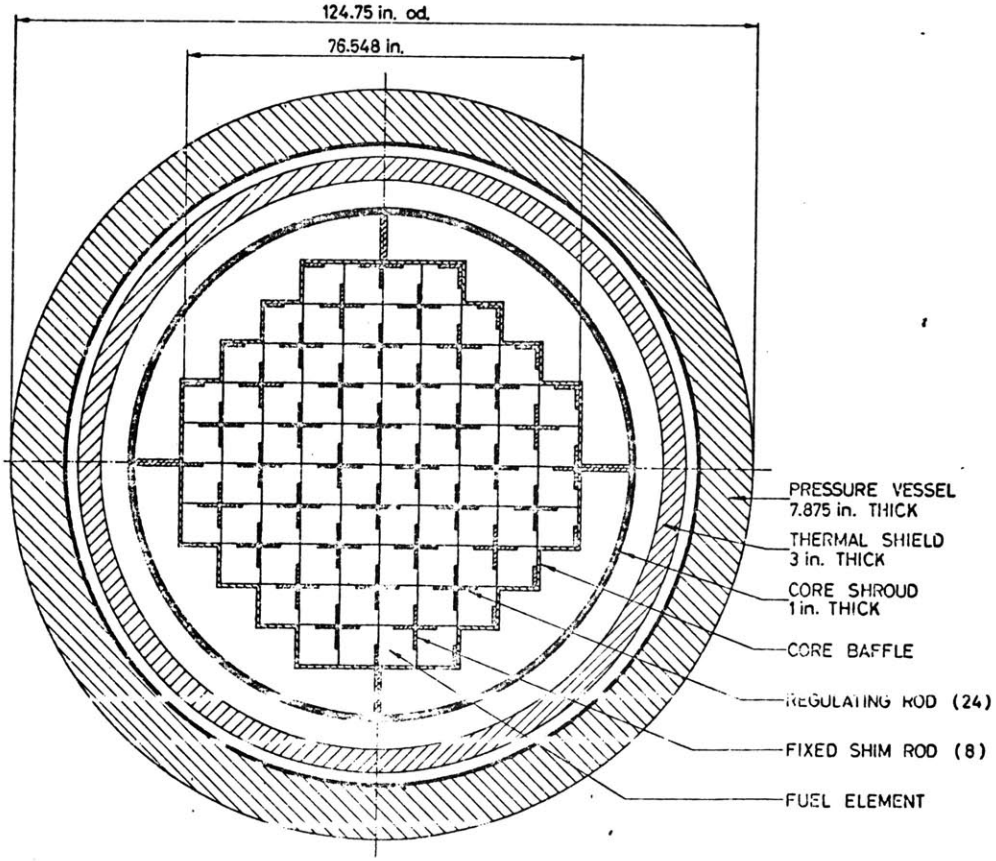


FIG1-3, HORIZONTAL SECTION REACTOR YANKEE

TABLE I - 2 : COMPARISON OF YANKEE (ROWE) & RECENT PWR DESIGN CHARACTERISTICS.

| | YANKEE (ROWE) INITIAL DESIGN | YANKEE (ROWE) CURRENT OPERATION | RECENT PWR DESIGN. |
|---|---|---|---|
| Power Level, MWt | 392 | 600 | 3,090 |
| Power Level, MWe (net) | 110 | 175 | 1,035 |
| Specific Power, KWt/Kg U | 18.8 | 28.12 | 35 |
| Power Density, KW/liter | 58.4 | 86.8 | 93.5 |
| Power per $ft^3$ coolant inventory KWt | 151 | 165 | 249 |
| Fuel Exposure (Discharge) MWD/MTU | 8,470 | 26,000 | 30,000 |
| Reactor Outlet temp ($^oF$) | 532 | 548 | 605 |
| Reactor $\Delta t$, $^oF$ | 33 | 42 | 59.6 |
| Pounds Coolant circulator/KWt/hr | 96.5 | 68 | 43.4 |
| Heat transfer surface (steamgenerators), $ft^2$/MWt. | 168 | 110 | 60 |
| Primary Pressure (psia) | | 2,000 | 2,250 |
| Secondary Steam Pressure psia, max | 465 | 533 | 780 |
| Loading Kg U | | 20,664 | 100,000 |
| Fuel Program | | OUT-IN | MODIFIED SCATTER |
| Core equivalent diameter inches (cold) | | 73.35 | 132.7 |
| Active Fuel height (cold) inches | | 91.0 | 144 |
| Number of Fuel Assemblies | | 76 | 193 |
| Avg KW/ft (nuclear) at 600 MWt | | 3.48 | |
| Heat Transfer area $ft^2$ (hot) | | 15,767 | 52,200 |
| Core heat deposited outside fuel rods % | | 2.7 | 2.7 |
| avg. heat flux at 600 MWt BTU/hr.$ft^2$ | | 126,372 | 207,000 |
| Movable control rods : | | 24 | 53 |
| Shape | | Cruciform | Rodclusters |
| Absorber material | | 5% Cd, 15% In. 80% Ag | 5% Cd, 15% In. 80% Ag. |

## I - 2 - 2) DESCRIPTION OF YANKEE FUEL ASSEMBLIES & COMPARISON WITH CURRENT DESIGNS.

### 2)A : The SS clad Yankee Assemblies.

In the Yankee Reactor and other PWR'S the fuel rods are assembled in "open" bundles, suitably shaped to provide control rod passage, and held in place between the upper and lower grid plates.

The two types A and B are not identical due to the mechanical lay out of the cruciform control rods.

The fuel rod matrix in the SS. type assemblies is 18 X 18, to provide slots for the passage of control rods, the actual number of rods in the SS.assemblies is either 304 or 305. As seen on Fig, I-3, either type of assembly contains 9 subassemblies, each of which is formed by nominally 6 by 6 square arrangement of fuel rods. The rods are joined to form the subassembly by 1/2 in.long tubular spacer or ferrules, brazed between the fuel rods at 8 inch axial intervals.

### 2)B : The Yankee Zircalloy-Clad Type Assemblies.

The reason for going to the zircalloy clad type assemblies are economic. The thermal macroscopic cross-section of SS is about $0.11050^{cm-1}$ and for zircalloy $0.0400^{cm-1}$. Because of this, neutrons are used more economically, and the result is substantial savings even with a higher cost of Zr-4. These assemblies again consist of 2 types A & B. The mechanical design of the two types of assemblies are pictured in Figs. I-4 and I-5.

From comparison between Fig. I-3 & Figs. 4,5, the mechanical design of the brazed SS.-clad type assemblies & the zircalloy clad types assemblies is obvious. The latter assemblies have a matrix of 16 X 16 rods as a base but actually contain 236 or 237 rods. No devision in subassemblies exist, no ferrules are used, no rods are brazed to the structure, which consists of a perforated 35 mils (.035 inches) stainless steel can (SS 304 L), with upper and lower end nozzles. The fuel rods are held in their matrix by 6 spacers of iconel.

The spacers are attached to the center instrumentation tube and form in this way an integral part of the assembly. The spacers are suitably designed to improve the turbulence & directional mixing of the coolant between the fuel rods. Westinghouse claims that a 10 % savings on the MNBR (minimum departure of nuclear boiling ratio) is obtained through their design of mixing vanes in the spacers. Usually spacers consist of an open box structure. Suitably designed Straps are attached to this box and form a matrix with the unit dimensions of the pitch. Depending on the design, the straps are shaped or contain special attachments to form a springtype structure in which the fuel rods are held in place in the center of the unit cell, still allowing some axial & radial expansion (without causing too much fretting or mechanical wear) due to coolant vibrations, thermal bowing & the like.

A little bit off-centered is the instrumentation tube on which the spacers are attached and which contain the SS. wire and instrumentation for the neutron flux measurement.

In the S-corners of the assembly, the fuel rods are replaced by solid zircalloy rods. Noticible on the Figs. I-4,5 are that the assembly can is perforated with holes, leaving the assembly an open structure, so that coolant mixing between assemblies can take placee. The dimensions of the holes in the assembly are such that roughly 16 % of the can is open (except near spacers).

In Fig.I-6 the type B assembly has been fitted in the control rod positions, thus showing more clearly the clearances that exist, in comparison with the SS.assemblies on Fig. I-3.

Yankee core N$^{o}$10will consist of 36 zircalloy assemblies and 40 SS assemblies. It is anticipated that Core 11 will consist entirely of zircalloy assemblies.

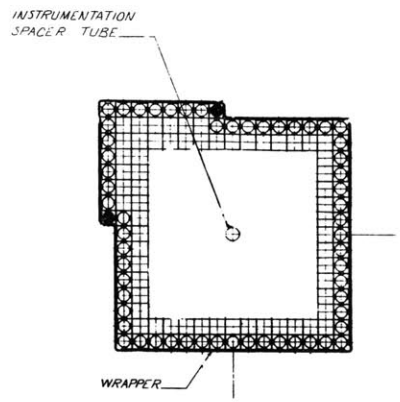


SECTION A-A
(TYP. 5 PLACES WITH 18.3" SPACING)

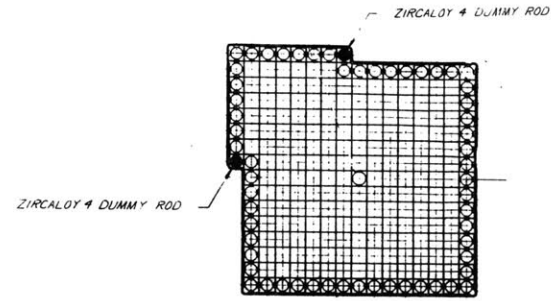


FUEL ROD LOADING

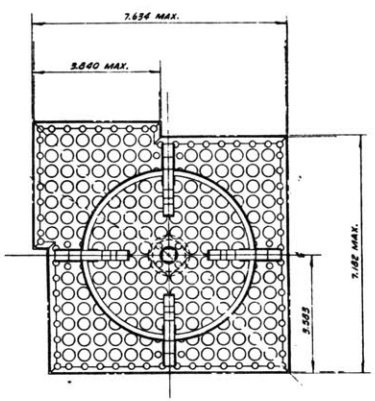


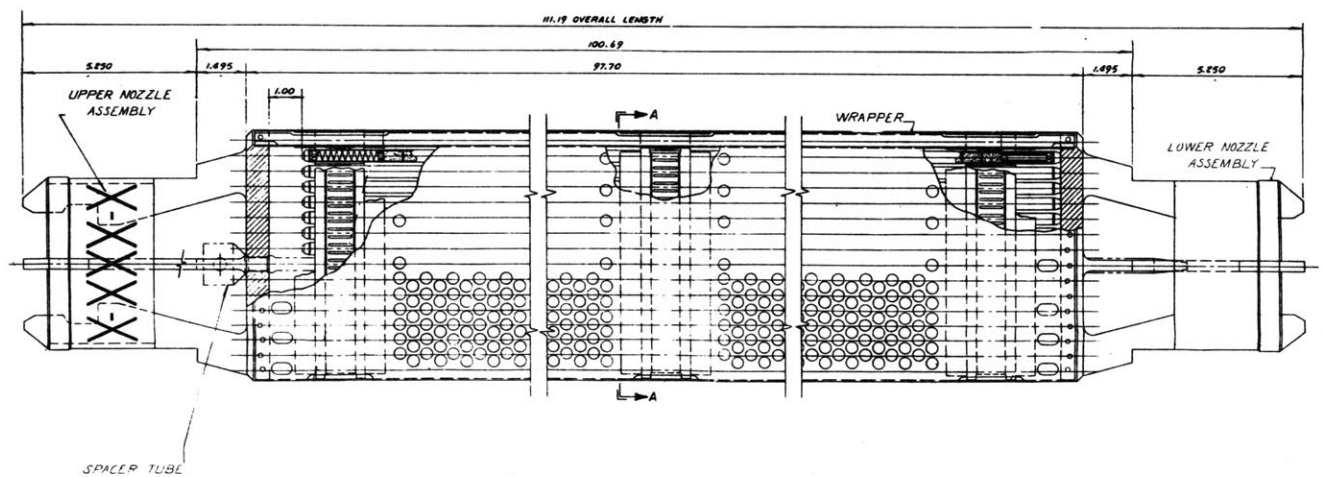


① FUEL ASSEMBLY-TYPE A

CORE I ZIRCALOY
ASSEMBLY-TYPE A

FIGURE I-4

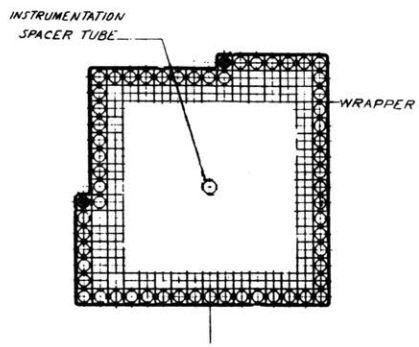


SECTION A-A

(TYP. 5 PLACES WITH 18.3 SPACING)

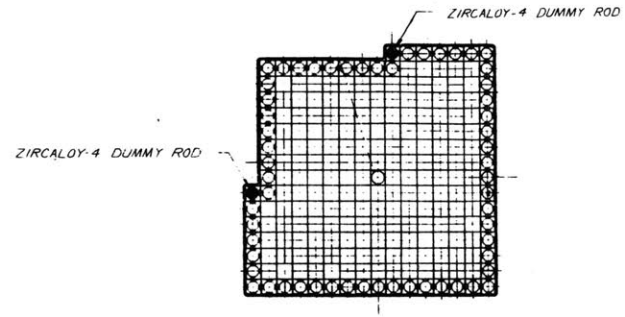


FUEL ROD LOADING

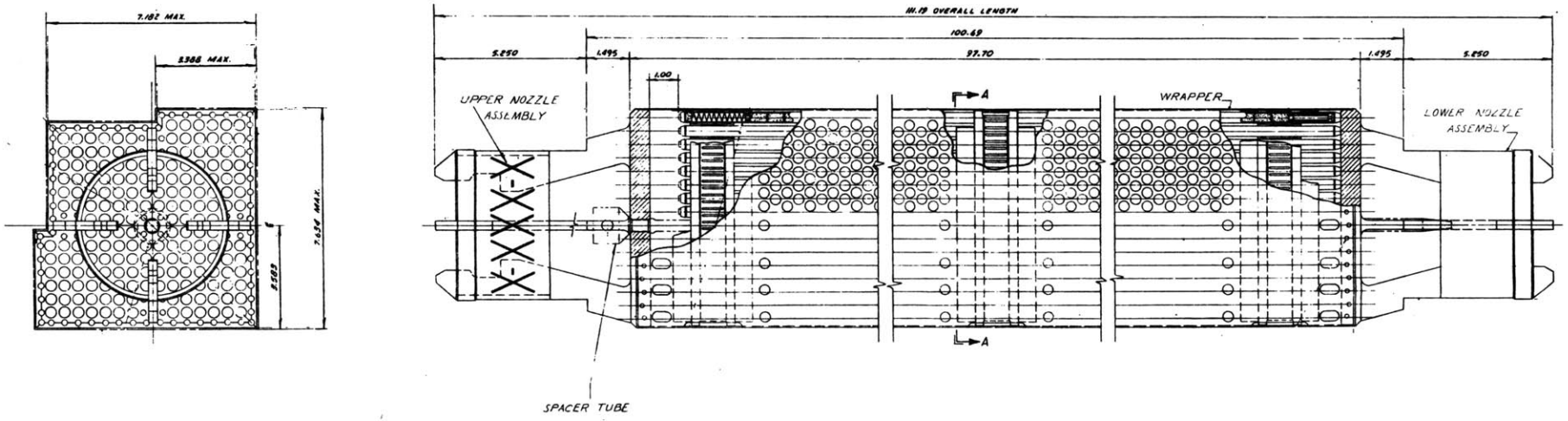


(1) FUEL ASSEMBLY - TYPE B

CORE X ZIRCALOY
ASSEMBLY TYPE B

FIGURE I-5

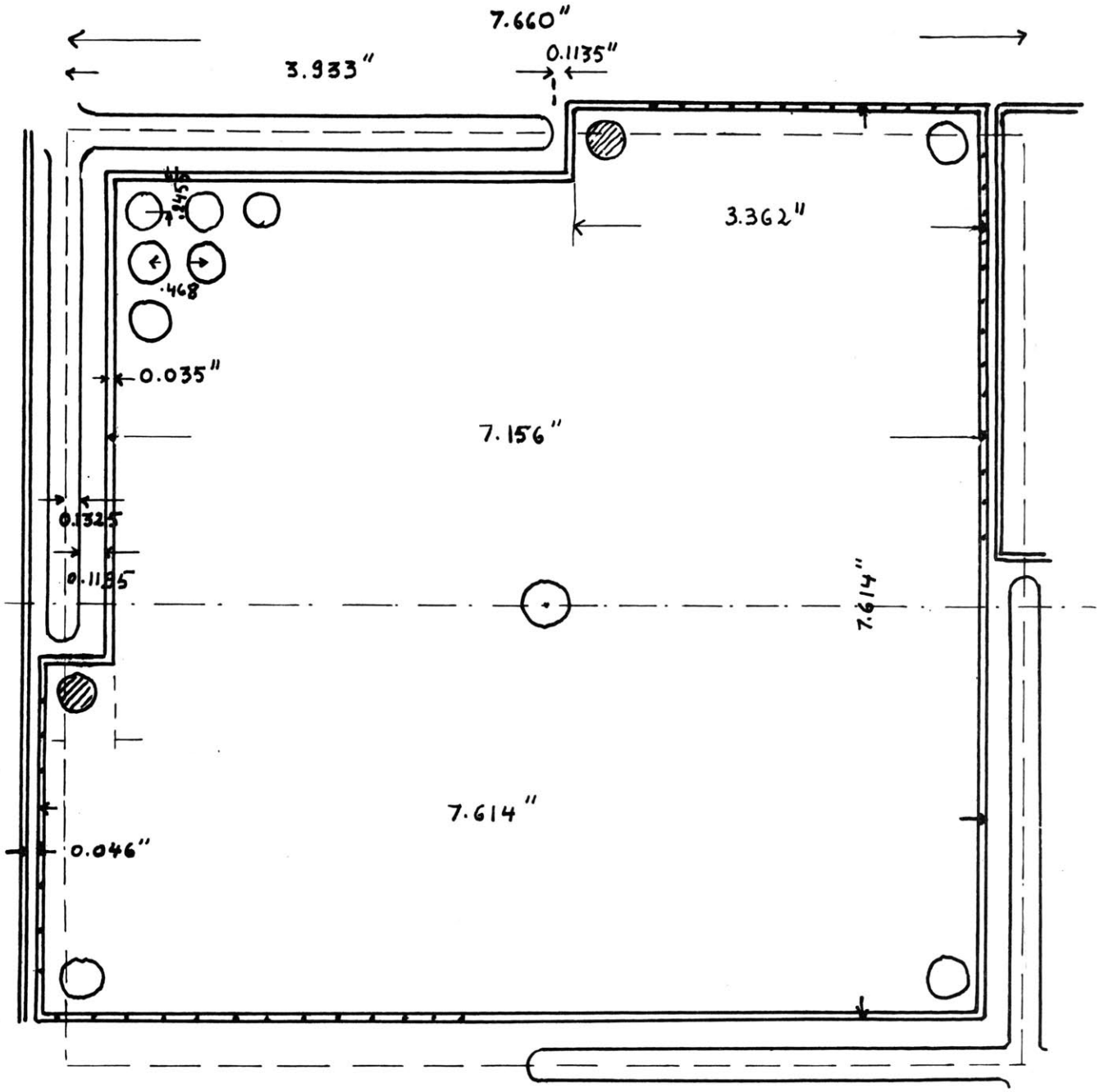


FIG 1-6 TYPE B ZIRCALLOY CLAD ASSEMBLIES SCALE =0.775/1

## 2)C : CURRENT 1000 MWe ASSEMBLY DESIGNS.

The current large PWR assemblies as shown on Fig. I-7 differ from the Yankee assemblies in the following aspects :

- the assemblies are square, with basic 16 X 16 matrix.
- the bundle is more open.
- cruciform control rods & attached followers are now replaced by control rod clusters, which are placed in selected assemblies in the core.
- when withdrawn the CRC (the control rod cluster ) leaves small watergaps with dimensions of a pitch - no followers are used.

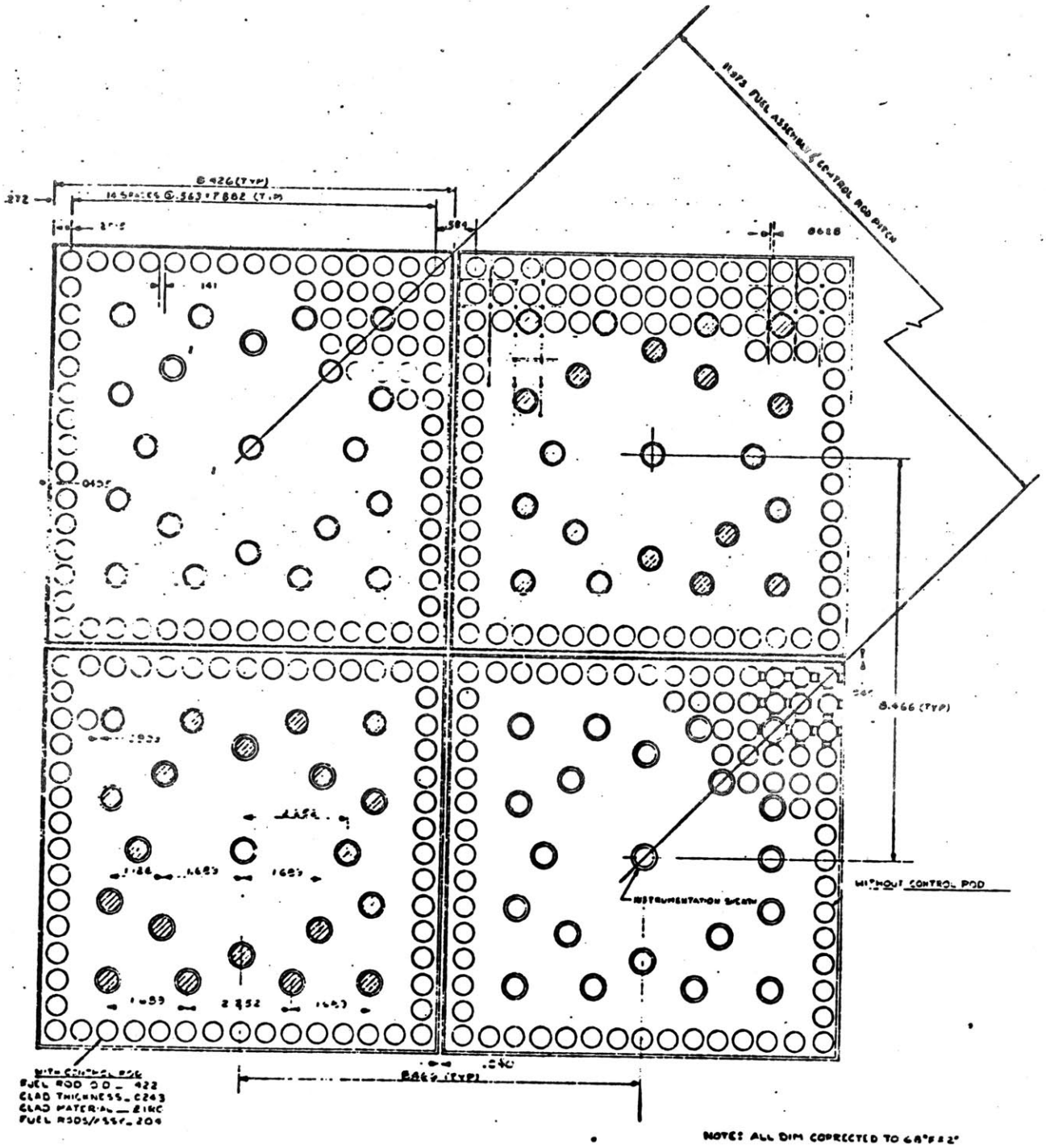


FIG I-7 ,FUEL ASSEMBLIES WITH CONTROL CLUSTER RODS IN LARGE PWR'S

## I- 2 - 3) DESCRIPTION OF THE PROPOSED PLUTONIUM RECYCLE ASSEMBLY AND COMPARISON WITH LARGE PWR PLUTONIUM RECYCLE ASSEMBLY DESIGNS.

### 3)A ; Key differences in Conventional & Pluton. Recycle cores.

Because of the short period involved for the recycle of Pu. in thermal reactors it is unlikely that a reactor will be build with an optimized design for Pu recycle. Although it has been shown that increasing the pitch or moderator-fuel ratio can increase the Keff & burnup substantially, and saving of .1 to .2 mills/$_{KWhr}$ (1) can be realized, the mechanical design of the core & fuel assemblies will be unaltered. The technical aspects will thus be mainly nuclear & of a fuel management character.

Extensive engineering studies were carried out e.g. in the Edison Electric-Westinghouse Plutonium Utilization Program in order to investigate the factors that influence the feasibility of recycling Pu-fuel in large PWR's.

During the course of this work the basic differences between the nuclear design characteristics of plutoniom & uranium fuels were identified, and the possible adverse effects were pointed out. A qualitative summary of these characteristics and their effect on the nuclear design are included in Table I-3 extracted from Ref. 2.

The basic key conclusions from the studies may be summarized as follows :

- An all plutonium fueled core has a more negative moderatortemperature coefficient an a more negative doppler coefficient than thus an all uranium fueled core. These more negative coefficients result in an increase in the control requirements. Furthermore the control rod worth is reduced in the core containing plutonium fuel. This reduction in control rod worth combined with an increased rod requirement has thus been identified as the principal problem area in converting an existing reactor to one fueled solely with plutonium.

TABLE 1-3

CAPSULE COMPARISON OF URANIUM AND PLUTONIUM NUCLEAR DESIGN CHARACTERISTICS

| Parameter | Plutonium Core | Reason for Difference | Consequence |
|---|---|---|---|
| Moderator Temperature Coefficient | More Negative | Increased resonance absorption and spectrum shift | Improved stability and transient characteristics except for steam break |
| Doppler Coefficient | More Negative | Pu-240 resonances | Improved transient characteristics |
| Cold-to-Hot Reactivity Swing | Increased | Larger moderator temperature coefficient | None-boron used for compensation |
| Installed Reactivity | Reduced | Reduced depletion rate-Reactivity saturates | None |
| Control Rod Requirement | Increased | Larger moderator and doppler coefficients | Possible increase in number of rods |
| Control Rod Worth | Reduced | Thermal flux reduced | Possible increase in number of rods |
| Boron Worth | Reduced | Thermal flux reduced | None |
| Xenon Worth | Reduced | Thermal flux reduced | Improved stability |
| Fission Product Poisons | Increased | Increased yields-Increased resonance absorptions | Reactivity penalty |
| Local Power Peaking | Increased | Increased water worth | Fuel management action required |
| Delayed Neutron Fraction | Reduced | $\beta_{pu} < \beta_u$ | Rod ejection accident |

- In mixed fuel cores, which contain both plutonium and the regular uranium fuel, we may expect that some of the conclusions of above also apply. However more flexibility in the loading exists. The main difficulty found in the study of mixed fuel cores was the power peaking near water slots and interfaces between the two fuels. Powerdistribution control is thus a principal problem.

From those key conclusions it is clear that careful design considerations must be given in order to convert an existing reactor to the plutonium recycle operation.

### 3)B : PROPOSED WESTINGHOUSE DESIGN OF A PU-RECYCLE ASSEMBLY FOR LARGE REACTORS.

After extensive engineering & fuel management studies, the proposed published design ( 2 ) of a Pu-recycle assembly is pictured on Fig. I-8 .

It may thus be noticed that in the W-proposed design :

- the Pu-recycle assembly contains only mixed oxide fuel.
- 5 different mixed oxide fuels are used to flatten the power.
- The Pu-recycle assemblies are located in selective positions in the core, mostly were no control rods are inserted. (Fig. I-9)

  The reason is mainly to avoid substantial reduction in control rod worth due to both the harder spectrum in an all Pu-assembly & the reduction of the neutron flux in the Pu-region.

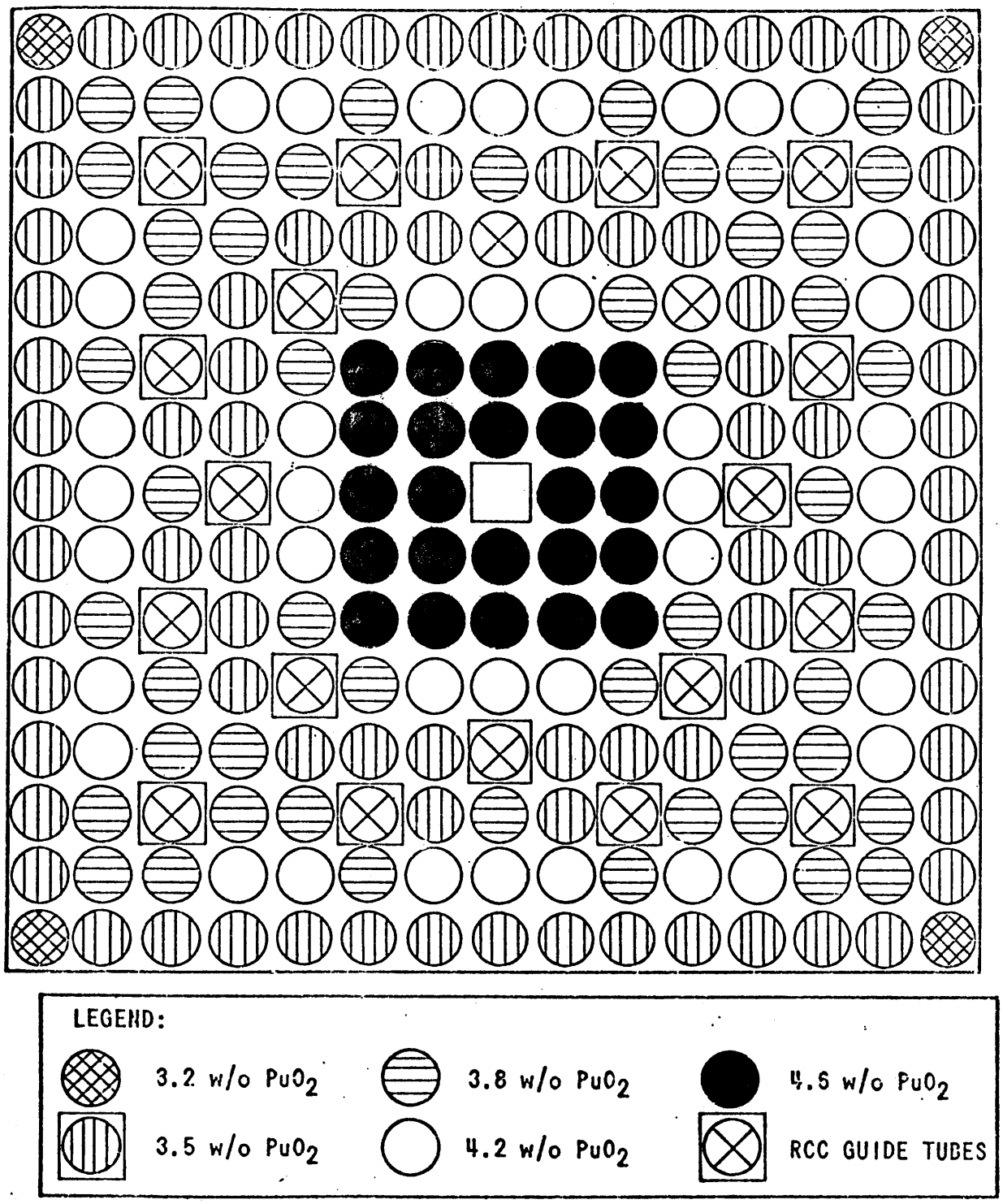


Figure 1-8 Enrichment Pattern for an All-Plutonium Fuel Assembly, Average Enrichment = 3.8 w/o $PuO_2$

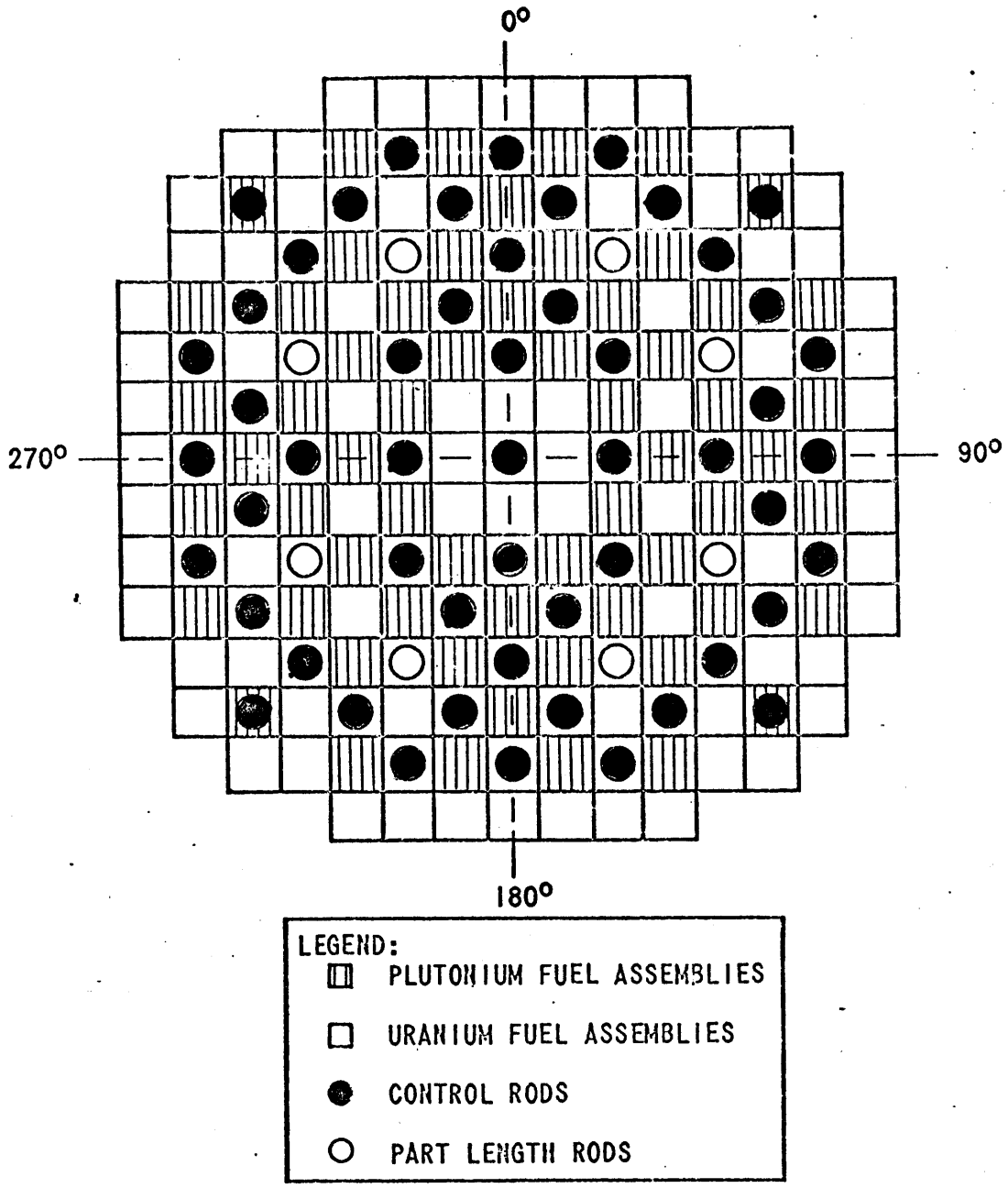


Figure 1-9 Discrete Assembly Core Configuration Showing the Relative Positions of Control Rods and Plutonium Fuel Assemblies

## 3) C : PROPOSED DESIGN OF A PU-RECYCLE ASSEMBLY FOR THE YANKEE REACTOR.

In the much smaller Yankee core, the presence of cruciform control rods & the specific layout makes it impossible to locate all mixed oxide assemblies from control and watergaps.

Therefore the proposed design which is pictured on Fig. I-10 together with the conventional cell $UO_2$ assembly :

1) contains both $UO_2$ & mixed oxide fuel.
   The latter fuel is loaded in an island in the center of the assembly, away from the watergaps & cruciform control rods.

2) All the assemblies contain the mixed oxide fuel & are, apart from the mechanical differences between type A & B assemblies, identical.

3) In the basic proposed design there is only 1 type mixed oxide fuel consisting of 4 w/o PU $O_2$ .

The reason is that in a small reactor as the Yankee, the smaller number of purchased rods would make the cost of different type fuel rods more disadvantageous.

However serious powerpeaking problems exist at the interface as will be shown further in the study.

This type of assembly design, is identical to the proposed design of the Belgian SENA reactor, (3) which is nearly identical to the YANKEE reactor. Although some calculations were made for a design with different mixed oxide fuels & another loading ine one assembly , the basic proposed design has been used for our study. No calculations have been performed with a mixed oxide slightly enriched $UO_2$ fuel, although in the SENA reactor study a slight economic advantage has been anticipated for that reactor.

The number of Mixed oxide rods in the assembly is dependent on the amount of Pu available from the reactordischarge and the W/O of $PUO_2$ choosen.

A 4 W/O $PUO_2$ - nat $UO_2$ mixed oxide fuel together with a regular conventional 4 W/O U235 $UO_2$ fuel has been tentatively choosen as the base fuel for the Pu-recycle assembly study and a 4 W/O U235 $UO_2$ fuel for the conventional assembly, (Fig. I-10 ).

The mixed oxide rod was assumed to be identical to the $UO_2$ rod, with the same % of theoretical density.

The discharge (Kg Pu-total) and the isotopic compositions of the previous & future Yankee-cores are shown on Table I-5.

$$* \text{ w/o PU } O_2 = \frac{\text{weight PU } O_2}{\text{weight PU } O_2 + \text{weight net } UO_2}$$

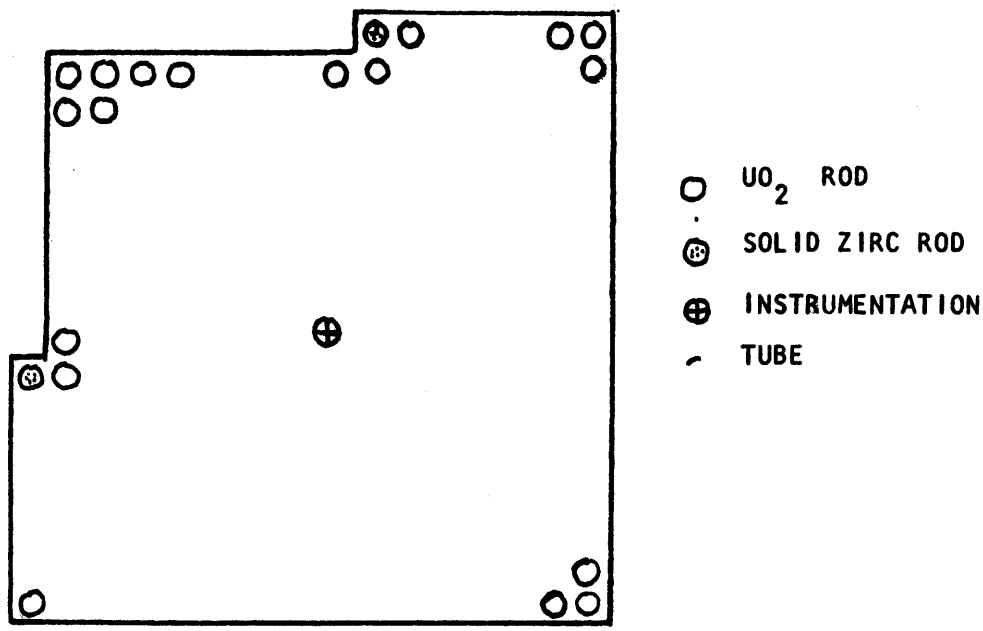


CONVENTIONAL TYPE B ASSEMBLY

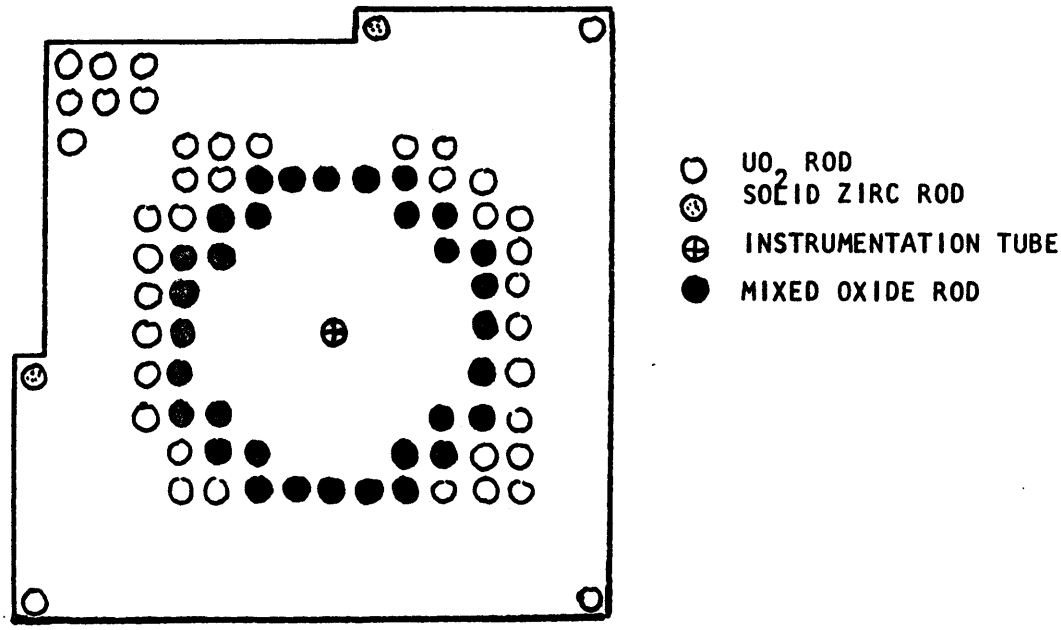


PROPOSED PLUTONIUM RECYCLE ASSEMBLY

FIG I-10 LOADING OF CONVENTIONAL AND PLUTONIUM RECYCLE ASSEMBLIES

TABLE I - 5 NUCLEAR CHARACTERISTICS OF THE UNLOADED FUEL ASSEMBLIES OF THE YANKEE REACTOR.

| YEAR. | CYCLE NUMBER | AVG. BURNUP (MWD/MT) | | TOTAL Kg | ISOTOPIC COMPOSITION. (W/O PU 239, PU 240, PU 241, PU 242) |
|---|---|---|---|---|---|
| | | SS. assemblies (number) | ZIRC assy. | PU | |
| 1970-71 | 8 | 23581 (36) | 0 (0) | 99.8 | 74.84 / 13.98 / 9.83 / 1.35 |
| 1971-72 | 9 | 24813 (36) | (0) | 103.2 | 73.97 / 14.28 / 10.27 / 1.48 |
| 1972-73 | 10 | 24667 (36) | (0) | 102.8 | 74.07 / 14.24 / 10.22 / 1.47 |
| 1973-74 | 11 | 30110 (4) | 26270 (32) | 86.7 | 66.87 / 18.45 / 11.93 / 2.75 |

Since there is no definite plan about the year when the Yankee Reactor will start recycling its plutonium, it has been assumed that the isotopic compositions of the design mixed oxide fuel is 66.87 W/O PU 239, 18.45 PU 240, 11.93 PU 241, 2.75 PU 242.

Further it has been assumed that a total of 99 kg PU was available.

From the choosen 4 W/O $PUO_2$, the 2 zones, the dimensions & characteristics of the rod shown in Table I- 4. The design of the base-case-assembly was calculated to contain 68 mixed oxide rods out of a total of 236 rods, and could be geometrically arranged as on Fig. I-10 .

In short the base case design was thought of being economical & representative.

TABLE I-4 : DESCRIPTION OF UNC CONVENTIONAL FUEL ASSEMBLY DESIGNS AND FUEL RODS.

| | |
|---|---|
| Enrichment w/o | 4.0 |
| $O.D._{rod}$, in, | .365 |
| $I.D._{rod}$, in. | .317 |
| Clad material | Zr-4 |
| $t_{clad}$, in. | .024 |
| $t_{gap}$, in. | .0065 |
| $O.D._{pellet}$, in. | .3105 |
| $L_{active\ fuel}$, in. | 91.0 |
| $N^o$ of rods / assembly | 236.5 |
| Heat transfer area, $ft^2$ | 171.4 |
| Max. permissible linear heat rate, kw/ft | 13.8 |
| Hydraulic diameter, in. | .368 |
| Flow area, $ft^2$ | .1951 |
| Fuel Rod Pitch, in. | .468 |
| Density $UO_2$ gm/cm | 10.153 |
| Weight $UO_2$ / Rod, Kg | 1.146 |
| Number of Spacers | 6 |
| Spacer Material | Inconel |
| Number of Poison Rods / Assembly | - |
| Linear Density of Poison in Poison Rods | - |

The Mixed oxide rods & Plutonium Recycle Assemblies are assumed to have identical characteristics, except for the nuclear specifications :

Basic Case, Mixed Oxide : 4 w/o $PUO_2$ - natural $UO_2$

PU-isotopic composition (a/o) : 66.87 PU 239, 18.45 PU 240, 11.93 PU 241, 2.75 PU 242

# CHAPTER II : STATUS OF THE COMPUTERMETHODS USED FOR NUCLEAR ANALYSIS IN THE U.S. INDUSTRY AND AT THE NUCLEAR ENGINEERING DEPT. M.I.T. - AND - DESCRIPTION OF THE COMPUTERCODES USED IN THIS STUDY.

## II - 1 STATUS OF COMPUTERMETHODS & CODES (REFS. 4,5,6)

The day of reactor-design calculations by handbook and slide rule has long since passed in the industry. Every major manufacturer has a package of codes that is flexible enough to treat everything from complete plant lifetime studies and safety, control, burnup, and fuel-management studies to fuel-inventory and plant-cost analyses. The adequacy as well as the costs of their code packages is of great financial importance to the manufacturer. For the smaller companies who cannot afford this expense, there exist computer-service organizations that provide expertise with comparable code packages.

Most of the codes used by the various manufacturers are in the public domain, but some refinements in code development, cross-section modification, thermal-hydraulic recipes, control, fuel management, or operating experience may be regarded as proprietary, and this has been found to be particularly true for Plutonium Recycle Applications.

Descriptions of the codes and methods used by manufacturers as well as considerable additional design information can be found in their PSARs(preliminary safety-analysis reports) for specific power plants.

Industrial practice in PWR reactor-physics calculations varies to some extent since a larger number of vendors are involved.

The basic tool in reactivity, power distribution, and depletion analysis is the LEOPARD-PDQ-7 (or the earlier AIM-5) sequence, with proprietary refinements related to user convenience, higher isotopes representation, and temperature feedback. For a very detailed analysis, a full 3D, few-group, nuclear-thermal-hydraulic program, THUNDER is available, it is clear that this code is not used for routine calculations. Experience on the IBM-7094 incicates that a 10,000-mesh-point problem can be solved in 2 hr. at a cost of about $ 1,000, and it is estimated that the same cost would permit the use of 30,000 mesh points on the CDC-6600. THUNDER indicates the trend in industry toward greater detail in the spatial representation of large, complex cores, such as those being proposed for water reactors in the 1000-MW(e) range. Greater detail in neutron energy and angular distributions would only increase the cost, as would greater detail in transient studies. It remains to be seen what impact the next generation of such large U.S. computers as the CDC-7600 and the IBM 360-195 will have on these costs.

At Combustion Engineering the basic lattice code is CEPAK, which is made up of MUFT, THERMOS and a group of subsidiary operator codes that connect these two basic blocks and introduce approximations for resonance shielding, fuel-temperature effects, and improvements in the cell approximation. In addition, the CEPAK code performs fuel-depletion calculations using few-group cross sections with occasional respectralization in the multigroup calculations at given points in fuel life. Resonance capture is based on formulas incorporating 0.7-b reduction in Hellstrand's correlation for the resonance integral of U238 and Levine's form of the equivalence principle

for lattices . Account is taken of the effect of fuel cladding and overlap of U235 and U238 resonances. Plutonium-240 self-shielding and Doppler-broadening are based on analytical fits to ZUT calculations. Since none of the fuel assemblies is entirely uniform, considerable work is continuing on the proper treatment of fuel-assembly boundaries, water-hole peaking effects, and non-uniform Dancoff corrections.

For spatial calculations, Combustion Engineering uses PDQ-7 on its CDC 6600 computer as the basic tool because if its reliability, speed an flexibility. The cross sections required for these diffusion calculations come from CEPAK, as do changes in cross sections with fuel depletion which are represented in the HARMONY adjunct to PDQ-7. For reactivity lifetime calculations a rather coarse mesh is generally adequate and is used in analyzing operating reactors. The use of coarse mesh requires awkward fuel-assembly heterogeneities to be incorporated somehow into CEPAK calculations and these studies are continuing. The normal design calculations employ a fine mesh 2D calculation with PDQ-7 to evaluate thermal conditions in various fuel assemblies. Thus far 3D synthesis methods have not been used, since it is hoped that Combustion Engineering reactors can be operated with soluble boron control throughout core life so that the resulting power distribution will be nearly separable.

Little difference has been found between coarse-mesh, 3D PDQ-7 calculations and those obtained by combining 1D and 2D depletion calculations.

The current methods employed by Babcock & Wilcox are described in the FSAR for the Oconee Nuclear Station. Their standard depletion calculations are made with a 1D depletion package code called LIFE, which is a composite of conventional codes, MUFT-5, KATE-1, RIP, WANDA-5, and a depletion routine. The 1D WANDA, calculation uses four-energy-group cross sections, which are

obtained by collapsing a 34-energy-group MUFT calculation and the use of the Wigner-Wilkins heavy-gas model for the thermal constants. Disadvantage factors for the thermal group are calculated with THERMOS.

Similarly 2D calculations are done with conventional PDQ-5, PDQ-6 or TURBO. codes. These calculations are carried out to determine the effects of strong localized absorbers such as their movable control-rod assemblies. Additional controls in Oconee include soluble boron, part-length axial-power-shaping (and xenon-control) rods, and, in Oconee 2, burnable poison rods. Burnable poison rods are used in Oconee 2 to compensate for fuel burnup an fission-product buildup to reduce total control requirements. The required properties of the 1D system are then matched to the 2D analysis. In this manner it is possible to analyze the simpler 1D system in a depletion survey problem with, it is stated, only a small loss in accuracy.

Current work at Babcock & Wilcox Co. involves the upgrading of their basic code library that apparently now includes PDQ-7 and its HARMONY adjunct.

All water-reactor manufacturers relate their basic lattice codes and cross-section data to critical experiments and other integral data. Agreement with critically data on enriched-uranium-fueled assemblies is generally quoted to within ± 0.5% in reactivity. This agreement offers some reassurance in reactor design, although it may be based in part on a cancellation of errors of opposite sign. There would be greater reassurance if these results could be compared with unadjusted cross sections and rigorous calculations.

However the standard U.S. cross-section library ENDF/B still has a number of important uncertainties and omissions, and thermal-reactor data have a low AEC priority. Rigorous calculations are also expensive, infrequently attempted, an then may come to grief because of an overeagerness to draw conclusions on the basis of an incomplete or insufficiently broad study.

Concerning plutonium-fueled water reactors, there seems to be general agreement that the available data are rather sparse. Many of the data available have been obtained on small, high-buckling assemblies, which should require more elaborate analysis. There is disagreement between industrial evaluators on the general adequacy of ENDF/B plutonium-isotype cross sections and concern about the adequacy of reactivity calculations for high burnup of U-enriched or plutonium-enriched fuels.

As a part of their Plutonium Recycle Program, Westinghouse has developped a modified LEOPARD version, which eliminated the reactivity bias needed in previous calculations (Ref. 2 ). The analytical improvement include :

1) The availability of ENDF/B cross-sections for PU-239, PU-240 and PU 241 containing appropriate modifications to improve the correlation with the ESADA Plutonium Critical Experiments.
2) The availability of a modified version of the LEOPARD code, which included a detailed treatment of the buildup and depletion of individual fission product and transuranic isotopes Np-237, Am-241, Am-243. These elements accounted for 99 % of the total reactivity penalty associated with the transuranic elements.
3) The availability of improved fission product and transuranic cross-sections. The use of these cross-sections significantly improved the correlation with depletion date in uranium fueled systems.
4) The availability of an improved L-factor treatment for different fuel rod diameters based on improved fits to Monte Carlo & LASER calculations.

The adequacy of a lattice code such as LEOPARD is very important and is the basic information on fuel input and discharge inventories. (details of 2D and 3D spatial calculations appear to be of secondary importance for the inventories).
The modified LEOPARD version however still remains proprietary to Westinghouse.

At M.I.T., a lot of work has been done the last years to acquire, (through the ANL Computor Code Center), the standard computorcode packages that have been developed at National Laboratories and Companies as Westinghouse.
The department has access to the IBM 360 computor of the MIT Information Processing Center.
Presently the Nuclear Engineering Department Code Library includes the released IBM 360 versions of LEOPARD, LASER ( 7 ) and the Argonne THERMOS package (with GAKER to generate scattering kernels) for the generation of cross-sections.
Errors in THERMOS have been repaired, and part of the LASER library with a cut-off at 1.855 eV has been included in the THERMOS code ( 8 ), also a self-shielding factor homogenization scheme has been included ( 8 ) as an option in the code.
For zero dimensional burnup calculations LASER and LEOPARD and the less accurate but cheap code CELL, developed at MIT ( 9 ), can be used to obtain cross-sections versus burnup, isotopic compositions verus burnup etc.
The determination of fluxes, powerdistribution reactivity using diffusion

calculations has been done frequently with EXTERMINATOR II ( 10 ), but are slowly being replaced by the elaborate PDQ-5, and PDQ-7 codes.

S-N, P-L Transport theory codes, such as the one dimensional ANISN code ( 11 ), have been used in the department mainly for fast reactor applications, but have occasionally been used for thermal reactors as a checkpoint for diffusiontheory.

Recently the Library acquired a 2-dimensional X-Y SN, PL Transporttheory Code TWOTRAN ( 12 ), but some calculations made with the code indicate that more meshpoints are needed than with diffusiontheory and that, due to steaming effects at reflectory boundaries, low order S.N. (e.g. S-4) calculations are inaccurate.

For diffusion depletion calculations, the PDQ-HARMONY ( 13 ) package has recently become available. The time for the set-up of a problem & the expense (one depletion step costs about 4 X more than a regular calculation, and the set up is estimated to take 3 months). are limitations to the easy use of this package. Simplified diffusion-depletioncalculations have been made for over years with the cheap CELL & MOVE codes, developed at MIT ( 9 ). Their use for Plutonium recycle work has been questioned ( 14 ), although ENDF/B X-sections haven been included in the CELL code ( 15 ).

Simplified 3 dimensional calculations for BWR studies and general core reactivity & lifetime-fuel management studies, have been made with the FLARE code ( 16 ), and the MIT modified FLARE-G ( 17 ).

An attempt for using both CELL-MOVE, and FLARE for our study failed.

For thermal hydraulic applications efforts have been underway to set up codes as COBRA and COBRA II-A ( 18, 19) for the study of mixing & general thermal hydraulics of fuel assemblies, and HEATING ( 20 ) for the calculation of 1, 2 and 3 dimensional temperature distributions in complex geometry

Presently HEATING is operational, whereas COBRA has only recently been put on the IBM 360 System, but still seems to have convergence problems.
With regard to the nuclear analysis of conventional $UO_2$ cores, the computorcode packages and methods used at MIT are very satisfactory , and are generally the codes and methods used in industry.
As far as analysis of Pu-recycle cores is concerned, the present study has indicated that the LASER code used with 2 groups (1 thermal up to 1.855 eV) gave very good results for the calculation of the powerdistribution,

The present LEOPARD codes have been found to be inaccurate for the calculation of the detailed powerdistribution. It has been identified that the treatment of the giant PU 240 resonance is probably responsible for the large part of the discrepancies in LEOPARD.
Modifications to the LEOPARD code have been made by H.Spierling, who introduced the ENDF/B X-sections and included the buildup of higher isotopes and a 1.4 fission product X-section modifier. Although substantial improvements seem to be achieved ( 14 ), the study performed by the author indicates that the modifications should also include a more detailed PU-240 resonance treatment.
In short, the present computercodepackage LASER, available at MIT seems to be adequate for the calculation of the powerdistribution in PU-recycle assemblies & cores. With respect to burnup, the present standard methods may be thought of as being of the same level of the methods used for the design of the Saxton Reactor, and in the later Phase I - Preliminary Study of PU-recycle in large PWR's by Westinghouse, where a bias of 2.5 % on $k_{\infty}$ was used in the LEOPARD code. The standard method is also probably as good as the any of methods used

at BNWL in their PU-recycle Program Report of Ref. 21 for the calculation of the powerdistribution of several critical experiments in the PRCF (Plutonium Recycle Critical Facility).

## II - 2 : FLOW OF THE NUCLEAR ANALYSIS CALCULATIONS.

The starting point for the nuclear analysis of conventional and plutonium-recycle assemblies (or in general for the whole core analysis) is a set of reactor, fuel assembly & fuel rod design characteristics including material compositions, dimensions, temperatures and thermal hydraulic parameters.

The overall problem of establishing the distribution of neutrons & the power in 3 space dimensions, in time and in neutron energy, must be broken down into smaller segments, each of which is small enough to be economical solvable with available techniques and computorcodes.

Fig. II - 1 shows the Flow Diagram for the nuclear analysis of the isolated assemblies and their behaviour in the Yankee Reactor Core.

The first calculations that are performed are those of generating the spectrum and the cross-sections of a unit cell consisting of the fuelrod, its cladding and the amount of moderator.

A small unit cell is thus isolated and the assumption is made that the core is composed of an infinite array of unit cells, only sensitive to their own spectrum. One dimensional codes such as LASER, LOCALUX and zero dimensional codes as LEOPARD may be used for generating the thermal, the fast & epithermal spectrum and the cross-sections of this unit cell. The cross-sections for extra regions, water, cans etc. can be obtained from these codes, or separate calculations can be performed with THERMOS, to get the thermal

FIG. II -1 FLOW FOR THE ANALYSIS OF CONVENTIONAL & PLUTONIUMRECYCLE ASSEMBLIES FOR THE YANKEE REACTOR.

Reactor, Fuel Assembly and Fuel Rod Characteristics

UNIT CELL CALCULATIONS (LASER, LOCALUX, THERMOS)

BURNUP

BOL

BURNUP OF UNIT ASSEMBLIES (PDQ-5)

- local powerpeaking factors vs burnup
- spectraleffects vs burnup

BOL-UNIT ASSEMBLYCALCULATIONS (PDQ-5)

- Spectrum coupling effects (PDQ-5, THERMOS)
- Space detail
- design influences
- local powerpeakingfactors
- fine in rod powerdistribution

ESTIMATE IN-CORE PERFORMANCE (simulation model)

- gross assembly radial powerpeaking(BOL-Burnup)
- estimate rod by rod powerdistribution in peak assembly.

EVALUATION OF THERMAL-HYDRAULIC ASPECTS.

- comparison peak mixed oxide & $UO_2$
- calculation circumferential engineering heat flux hot channel factors.

X-Sections, or LOCALUX , to get the fast & epithermal X-sections.
Detailed spectrumcoupling effects of more complicated structures can be obtained from THERMOS using a one dimensional model and eventually the SSF-homogenization option in the code.
The use and validity of unperturbed-1 thermal group diffusion theory calculations can be checked with a 35 thermal group THERMOS model to evaluate the spectral coupling effect, and with a 1 thermal group THERMOS (integral transporttheory) and a thansporttheory code ANISN to evaluate the use of 1 group "diffusion" theory calculations and homogenization procedures.
The generated X-sections from LASER, LOCALUX or LEOPARD, eventually with spectral coupling corrections from THERMOS, are then used in a 2 dimensional diffusiontheory calculation (PDQ-5) of the fuel assemblies, which are just as. the unit cells, isolated from the reactorcore.
The 2 dimensional rod by rod powerdistribution & powerpeaking in the assemblies can also be calculated with GMND (generalized mixed Number Density) X-sections, a method that has been developed (see Chapter V) to calculate the powerpeaking, taking spectral & transporteffects into account, in a very simple and direct way.
Using the method, comparisons and parametric studies may be performed for the design of the assemblies.
In order to calculate the burnup in an assembly, the unit cells are again isolated and zero demensional depletion is performed on the fuel rod with LASER, LOCALUX or (LEOPARD).
At each burnup step, the spectrum is recalculated and the micro & macroscopic X-sections are obtained, which can be fed in the PDQ-5 program to calculate the powerdistribution, rod by rod in an assembly versus burnup.
In order to make a core analysis of complicated assemblies, such as the ones

proposed for PU-recycle, macroscopic cross-sections are constructed from the unit-assembly calculations, in the same way as has been done with unit cells. These X-sections of a homogenized assembly are then inputted in a PDQ-5, diffusion theory run of the whole core at BOL. The Powerdistribution & reactivity, for a whole core are then obtained.

From the unit assembly calculations vs. burnup, the $k_\infty$ vs. burnup of a whole assembly can be put into FLARE which after tuning with a PDQ-5 core run, will give the 3 dimensional core behaviour (powerdistribution & burnup distribution per assembly at each axial mesh).

## II - 3 DESCRIPTION OF THE COMPUTORCODES USED IN THIS STUDY.

3- 1) The Argonne-MIT revised and extended THERMOS-code ( 22, 8 ), computes the scalar thermal neutronspectrum as a function of position in a lattice unit cell or other 1 dimensional arrangement, by solving the integrel transportequation with isotropic scattering (Eq. 2-1) with 35 thermal energy groups.

The code also computes flux & spectrum averaged values of $\Sigma a$. $\Sigma_f$ , $\nu\Sigma_f$ , $\Sigma_s$ , and D for the cell compositions and supplies values of $\Sigma_a$ , $\Sigma_f$ $\nu\Sigma_f$ , $\Sigma_s$ and $\Sigma_{TR}$ for the isotopic constituents.

The usefulness of THERMOS has also been increased by modifications ( 8 ) which permit an automated sequence in which one problem generates a correct, energy dependent, spatially averaged set of cross-sections for the use in the next problem. This "pseudo-material" generating feature, (which at MIT, refers to the moderator) facilitates the solution of geometrically complex systems in 1 dimension.

A library tape containing scattering kernels and absorption cross-sections as a primary input to THERMOS is prepared by the LIBP and GAKER codes.

Melkins scatteringkernel with transportcorrection by Honeck ( 23 ) is employed for $H_2O$, and for other elements the scattering is described by the Brown and St.John free gas kernel. The usefulness of THERMOS for PU-recycle applications has greatly been increased through the use of a library with a cutt-off at 1.855 eV, which was taken from LASER.

In this way a very detailed spectral description of the PU-isotopes was obtained as can be seen from Fig. II-2, picturing the cross-sections of U235 & PU-isotopes, and the LASER energymesh shown on Table II -1 .

2

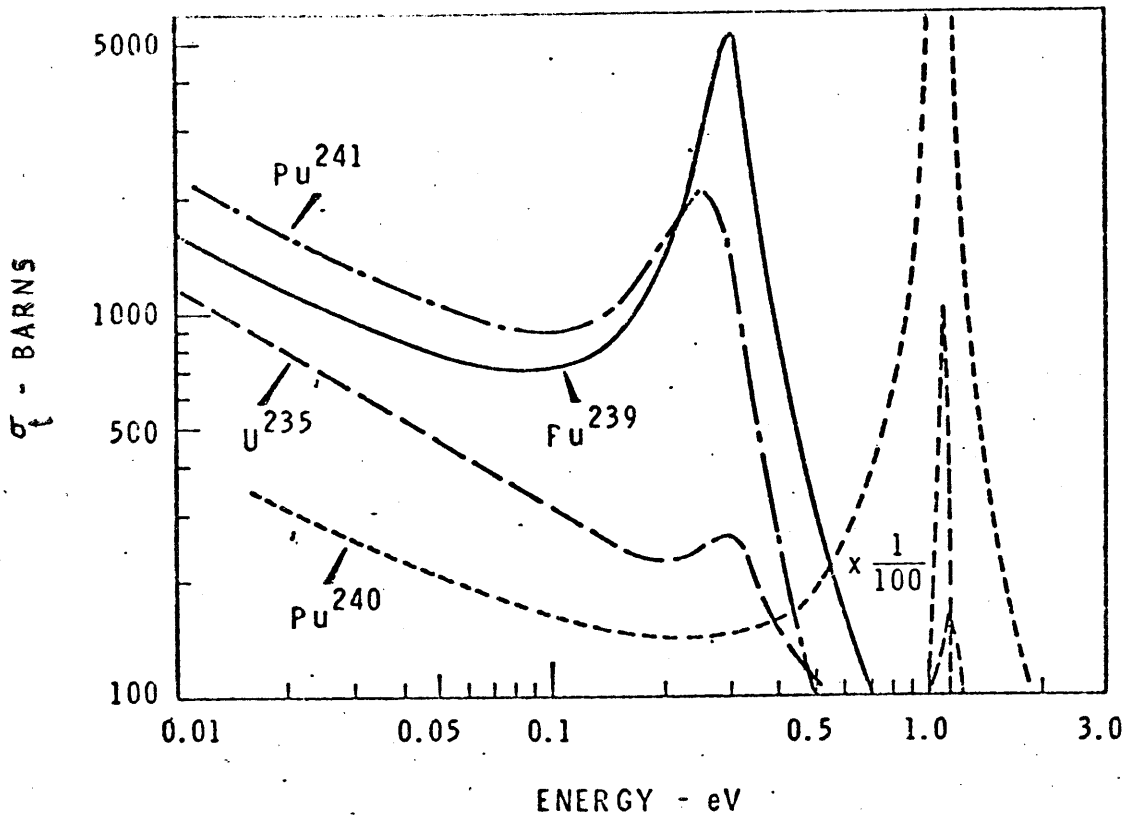


FIG II-2 Microscopic Cross Section Comparison $U^{235}$ and Plutonium Isotopes

in this way the important PU 240 giant resonance at 1.0 eV is completely described. Prior to this work the PU-isotopes and some other elements, were not included in the library. Therefore the PU, isotopes from LASER were extracted. For PU-240, 35 group doppler broadened cross-sections at 1100 °K, calculated seperately in the LASER code, was used.

The Integral Transport Eq. solved by THERMOS numerically by dividing the energy & geometric space into subintervals, using an iterative procedure, is :

$$\phi(r,E) = vN(\bar{r},v) = \int_{\text{all } r'} d\bar{r}\,' T(\bar{r},\bar{r}',v)\left[ S(\bar{r}',v) + \int_0^{v^*} dv'\, I(\bar{r}',v,v')\, vN(\bar{r}',v)\right.$$

were $N(\bar{r},v)$ is the neutrondensity at point $\bar{r}$, of neutrons with speed v.

$T(\bar{r}, \bar{r}', v)$ = the flux at $\bar{r}$ due to an isotropic point source at r'

(point kernel)

$$T(\bar{r},\bar{r}',v) = \frac{1}{4\pi(\bar{r}-\bar{r}')^2} \exp\left\{ -\left| \int_{\bar{r}'}^{\bar{r}} ds\, \Sigma_t(s,v) \right| \right\}$$

$S(\bar{r}', v)$ = the slowing down source

$$= \int_{v^*}^{\infty} dv'\, I(\bar{r}',v,v')\, N(\bar{r}',v)$$

V* = thermal cut-off = 1.855 eV (before a value of 0.625 or 0.78 eV was used)

Since V* is large enough so that thermal effects are ignored (even for PU 240 the cut-off is higher th n the peak res. at 1 eV) and small enough so that resonance in U 238 & U 235 can be ignored , the energy-dependence of $N(r,v')$ can be written as :

$$N(v') = N(v^*)\left(\frac{v^*}{v}\right)^2 \qquad \left(\frac{1}{E} \text{ law}\right)$$

let $S_d$ (P) be the spatial distribution of epithermal neutrons then

$$S(\bar{r},v) = S_d(\bar{r}) \int_{v^*}^{\infty} dv' \, P(\bar{r}, v, v') \, N(v^*) \left(\frac{v^*}{v}\right)^2$$

The high energy from the scattering kernel is given by :

$$\begin{aligned} P(v,v') &= 0 && v < \alpha v' \\ &= \frac{2v\Sigma_s}{v'(1-\alpha^2)} && \alpha v' \leq v \leq v' \\ &= 0 && v' < v \qquad \alpha = \frac{M-1}{M+1} \end{aligned}$$

$$\text{so} \quad S(\bar{r},v) = \epsilon \, \frac{v\Sigma_s(\bar{r}) \, S_d(\bar{r})}{1-\alpha^2} \left( \frac{1}{v^{*2}} - \frac{\alpha^2}{v^2} \right) \quad (\alpha v^* \leq v \leq v^*)$$

$$= 0 \quad (v < \alpha v^*)$$

The constant $\epsilon$ is determined from the condition that the total slowing down into the cell be one neutron/sec.

The scatteringkernel in the thermal energy region P (r',V, V') satisfies the condition.

$$\int_0^{\infty} dv' \, P(\bar{r}, v', v) = v\Sigma_s(\bar{r}, v)$$

This scatteringkernel is either the Nelkin kernel for $H_2O$ with a transport-correction by Honeck, ( 23 ) or the Brown-St.John free gas kernel for other elements.

Convergence problems have been noticed in THERMOS with PU-fuels, changing the iterationparameters helped but with varying success.

## 3-2) THE LASER CODE.

The LASER code ( 7 ) is a multi-energy, one dimensional (cylindrical) unit cell cross-section generating code and burnup-program. LASER is based on a modified version of the slowing down program MUFT ( 2 ), and the thermalisation transport-theory program THERMOS, and performs the calculation of the neutron spectrum in space, of a uniform lattice made up of cylindrical rods, cladding and surrounding moderator. The LASER program is only restricted to that geometry, which is pictured in Fig. II-3. An isotopic scattering ring surrounding the cell is automatically provided. Honeck has shown that the inclusion of a white scattering ring eliminates to a large extent the errors introduced by cylyndricalizing the unit-lattice cell.

The fuel compositions are allowed to vary spatially, this permits the code to allow for the non-uniform buildup and depletion of isotopes in the fuel rod when a burnupcalculation is performed.

The thermal cut-off in LASER is 1.855 eV & the energy mesh is shown in Table II-1.

The program will at option perform a burnup calculation for the lattice, and the spatial distribution of burnup within the fuel rods is explicitely calculated. A usual linear burnup option in which the flux is taken constant during a Time-step, as well as solving the non-linear system of equations can be choosen as options, the latter being more expensive but allowing a larger time step.

In LASER, the F.P. cross-section must be supplied in the form of a polynomial vs. burnup. In order to get the constants a separate CINDER code calculation must be performed.

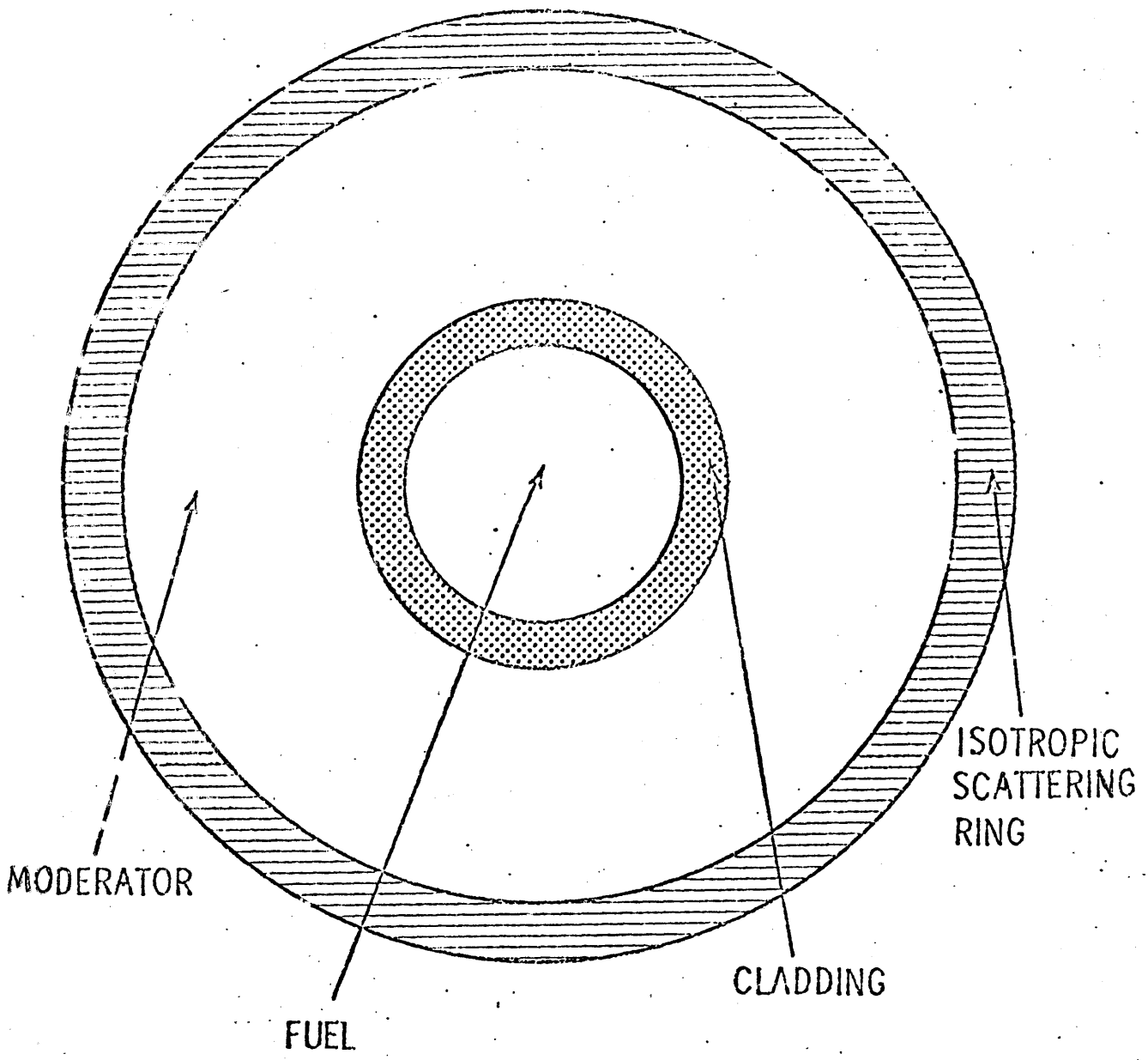


LASER LATTICE CELL GEOMETRY

Figure II-3

TABLE II-1

LASER Thermal Energy Mesh

| i | Speed[a] $v_i$ | Mesh Width[a] $\Delta v_i$ | Energy $E_i$(ev) | $E_{int}$(ev) |
|---|---|---|---|---|
| 1 | .2 | .2 | .001012 | .002277 |
| 2 | .4 | .2 | .004048 | .006325 |
| 3 | .6 | .2 | .009108 | .012397 |
| 4 | .8 | .2 | .016192 | .020493 |
| 5 | 1.0 | .2 | .0253 | .030613 |
| 6 | 1.2 | .2 | .036432 | .042757 |
| 7 | 1.4 | .2 | .049588 | .056925 |
| 8 | 1.65 | .3 | .068879 | .081972 |
| 9 | 1.95 | .3 | .096203 | .11157 |
| 10 | 2.25 | .3 | .12808 | .14573 |
| 11 | 2.55 | .3 | .16451 | .18444 |
| 12 | 2.85 | .3 | .20550 | .22770 |
| 13 | 3.075 | .15 | .23923 | .25104 |
| 14 | 3.21 | .12 | .26069 | .27053 |
| 15 | 3.33 | .12 | .28055 | .29075 |
| 16 | 3.42 | .06 | .29592 | .30113 |
| 17 | 3.505 | .11 | .31081 | .32064 |
| 18 | 3.66 | .2 | .33891 | .35768 |
| 19 | 3.91 | .3 | .38679 | .41704 |
| 20 | 4.26 | .4 | .45913 | .50326 |
| 21 | 4.715 | .51 | .56245 | .62493 |
| 22 | 5.265 | .59 | .70132 | .78211 |
| 23 | 5.845 | .57 | .86435 | .95070 |
| 24 | 6.23 | .2 | .98197 | 1.01374 |
| 25 | 6.375 | .09 | 1.02821 | 1.04277 |
| 26 | 6.435 | .03 | 1.04765 | 1.05254 |
| 27 | 6.465 | .03 | 1.05744 | 1.06236 |
| 28 | 6.495 | .03 | 1.06728 | 1.07222 |
| 29 | 6.55 | .08 | 1.08543 | 1.09873 |
| 30 | 6.69 | .2 | 1.13233 | 1.16645 |
| 31 | 6.99 | .4 | 1.23616 | 1.30791 |
| 32 | 7.39 | .4 | 1.38169 | 1.45748 |
| 33 | 7.765 | .35 | 1.52547 | 1.59500 |
| 34 | 8.10 | .32 | 1.65993 | 1.72616 |
| 35 | 8.41135 | .3027 | 1.79000 | 1.85500 |

[a] 1 unit = 2200 m/sec

## 3-3) THE LOCALUX CODE.

The LOCALUX code is a proprietary code from United Nuclear Corporation, and is essentially identical to LASER, with only a few modifications which include :

1) The inclusion of an extra region. This extra region is particularly useful for the calculation of a supercell. The output of LOCALUX essentially dual one with the extra region & one without.
2) The inclusion of a version of the CINDER program ( 25 ); which calculates the fission product X-section with burnup.
3) The inclusion of a modified version of the Dancoff-Jr. Code (26) which enables the user to calculate small 6 X 6 or 7 X 7 assemblies.
   Results have shown that the Dancoff-factor variations as a function of assembly configuration, damps out very rapidly & approaches that of an infinite lattice for a 10 X 10 lattice.
   The usual Dancoff-factor can also be calculated using the regular Sauers method.
4) Edit changes.
   The edit in LOCALUX has been reduced compared to LASER. However the code calculates , just as in the LEOPARD code, microscopic differential removal X-sections for each isotope of interest, and a pseudo-transport microscopic X-section $\sigma_{tr}$ for each isotope in fast, epithermal & thermal energies.
   The pseudo $\sigma_{tr}$ is defined as :

$$[\sigma_{tr}]^{-1} = \frac{\int_V d\bar{r} \int_0^{1.855\,eV} \phi(\bar{r},E)[\sigma_{tr}(E)]^{-1}\, dE}{\int_V d\bar{r} \int_0^{1.855\,eV} \phi(\bar{r},E)\, dE}$$

These cross-sections are of particular interest for the calculation of macroscopic cross-sections of extra regions, water, cans etc. without any need for making an other separate calculation. This procedure is simple & gives much better results

## 3-4) THE LEOPARD CODE, ( 27 ).

The LEOPARD computorprogram determines fast & thermal spectra using only basic geometry & temperature data. The code optionally computes fuel depletion effects for a dimensionless reactor and recomputes the spectra before each discrete burnup step.

LEOPARD as LASER, assumes that every reactor contains a large array of unit calls in either square or hexagonal lattice; consisting of the fuel rod, a metallic clad & moderator.

in a real reactor, this geometry is adequate in a large fuel bundle, but commonly 7 to 10 % of the core is taken up by control rod followers, waterslots, assembly cans, structure etc. LEOPARD accounts for this by allowing a fictituous extra region to be included in the unit cell (see e.g. also LOCALUX).

Spectrumcalculations are done on such an equivalent unit cell.

The method is based on MUFT-SOFOCATE( 28 ) for the homogeneous calculations.

A 54 group MUFT calculation in the B-1 approximation is used to cover the energy range from 10 eV to 0.625 eV.

The B-1 approimation is rigorous only to second moments in the slowing-down distribution and may therefore be inaccurate for high leakage systems.

The SOFOCATE code calculates the thermal group constants, avaraged over a Wigner-Wilkins (heavy gas) spectrum below 0.625 eV ( 29 ).

Thermal group X-sections are not too sensitive to thermalization models, provided integral quantities are preserved. Since the calculation is zero-

dimensional (in contrast to THERMOS, LASER, LOCALUX), the thermal disadvantage factors are obtained by a modification of a formula due to Amouyal and Benoist.

It is important to notice at this point that the thermal cut-off is at 0.625 et, although completely adequate for uranium fueled systems, it is inaccurate for the description of plutomiumrecycle fuel and for high burnup calculations (note the PU-240 resonance). The more that in the resonance range self shielding is neglected except for U 238.

The lattice self-shielding of U 238 is calculated by a recipe that is fitted to Hellstrand's correlation.

As has been discussed earlier, Westinghouse has modified the standard LEOPARD, although even at this company, the THERMOS-LASER procedure is gradually replacing LEOPARD. The low running cost of LEOPARD (5 X less then LASER) makes this code however very attractive for parametric studies & the results of beginning of life powerdistribution calculations for uranium systems is very good ( 30) . Its use, in an unmodified form is unfortunately not recommended for PU-recycle applications as this study has shown.

## 3-5) THE ANISN CODE.

The ANISN computor program ( 11 ) solves the one-dimensional multi-group neutron transport equation in slab, cylindrical & sferical geometry using Carlson's S-N method.

It has a large number of options, including higher oder anisotropic scattering and the ability to use any order of SN calculation desired.

Boundary conditions include vacuum, reflection, periodic & white/ albedo options. A complete shell source option described by group and angle is available, and void streaming corrections can be made.

Fixed source, $k_{eff}$ calculation, concentration search & other options are available. Cross-sections can be input on cards or can be called from a tape, the code will as on option also collapse cross-sections to any desired few-group scheme.

3 -6) THE PDQ-5 CODE.

The PDQ-5 program ( 31 ) solves the one or 2 dimensional neutron diffusion equations in x, r, r-z, or x-y geometry. Zero flux, zero derivative (zero current), and 180° degrees rotational Symmetry boundary conditions are available. Up to 5 energygroups (1 thermal), can be used. Between 300 to 500 meshpoints are permitted in each coordinate direction, with variable mesh-sparing allowed. Up to 100 compositions and up to 500 edit regions may be asked.

Diffusioncalculations are relatively easy to imput, but depletion problems including the HARMONY package in PDQ-5 which does the point depletioncalculations is difficult and very timeconsuming. Although the PDQ-5 HARMONY package is extremely flexible in terms of types of reactors analysed, the input becomes quite complex.

For depletioncalculations one must set up his own depletion chains, and microscopic input X-sections in function of burnup.

Even experienced people require about 3 months to set up one depletionproblem, which costs for one time step about 4 X as much as a regular calculation. Therefore onother procedure has been used in this study without need of the HARMONY package to make a rod by rod unit assembly burnup study.

# CHAPTER III : SPECTRAL EFFECTS & TRANSPORT EFFECTS IN ONE DIMENSIONAL CONVENTIONAL & PU RECYCLE ASSEMBLY MODELS.

## III - 1 : INTRODUCTION.

In this chapter a one dimensional analysis of conventional and Pu-recycle assemblies is made with the 35 group THERMOS code (cut.off 1.855 eV). Detailed spectraleffects were obtained. Comparisons have also been made with a 1 group THERMOS integral transporttheory, 1 group ANISN S-N transport-theory code with the P-1, S-4 approximation and 1 group diffusiontheory PDQ runs using different homogenisation models.

The geometrical model of the assemblies that have been used in these calculations is shown on Fig. III - 1.

## III -2 : THE THERMOS - 35 GROUP FUEL ELEMENT HOMOGENIZATION PROCEEDURE.

Since the THERMOS code is a one dimensional code with a maximum of 20 spacepoints, it is impossible to treat the 2 dimensional assembly. Even with a circular 1 dimensional assembly model, the fine details of a unit cell consisting of the fuel, clad and moderator (Fig. II - 3 ) can not be treated.

The usual procedure for homogenizing the unit cell, and to preserve the reaction-rates in the unit cell consists of using self-shielding factors in the macroscopic parameters.

In such a 1 group homogenizing scheme the macroscopic and effective microscopic cross-sections are calculated from

$$\Sigma_{cell} = \frac{\int_{cell} d\bar{r} \int_0^{V^*} \Sigma(\bar{r},E)\, N(\bar{r},v)\, v\, dv}{\int_{cell} d\bar{r} \int_0^{V^*} dv\, N(\bar{r},v)\, v} \qquad (3-1)$$

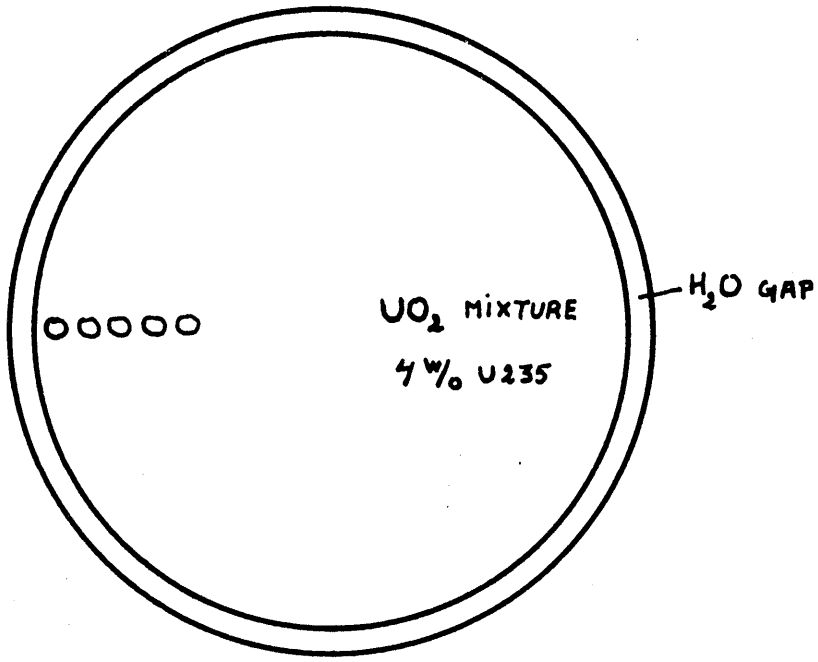


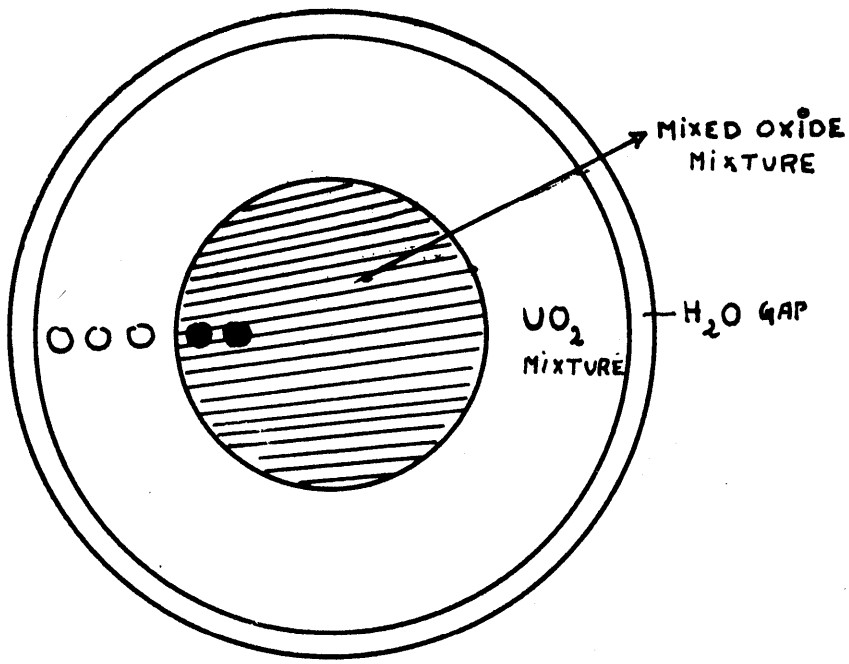


FIG III-1 CYLINDRICAL MODELS OF THE CONVENTIONAL AND PLUTONIUM RECYCLE ASSEMBLIES

where N $(\bar{r},V)$ is the neutrondensity at point $\bar{r}$, of neutrons with a velocity $v$, in a more explicit form (1) is also :

$$\Sigma_{cell} = \Sigma_{fuel} V_F \frac{\bar{\Phi}_{fuel}}{\bar{\Phi}_{cell}} + \Sigma_{clad} V_{cl} \frac{\bar{\Phi}_c}{\bar{\Phi}_{cell}} + \Sigma_{mod} V_{mod} \frac{\bar{\Phi}_{mod}}{\bar{\Phi}_{cell}} \quad (3\text{-}2)$$

where $\bar{\phi}_{CELL}$ is the spectrum & spaceavgd. flux in the cell & $\bar{\phi}_i$ the spectrum and spaceavgd. flux in region i. $V_i$ is the volumefraction of region i, and $\Sigma_i$ is the energy avgd. macroscopic X-section.

The ratio $SSF(i) = \bar{\Phi}_i / \bar{\Phi}_{cell}$ is called the self-shielding factor of region i, and is thus in a one group model only dependent on that region.

The effective 1 group microscopic X-sections are thus defined as :

$$\sigma^i_{eff} = \sigma^i \times SSF(i) \quad (3\text{-}3)$$

A similar homogenizing procedure but for 35 groups has been included in the THERMOS code at MIT ( 8 ), and is available in the code as an option. With this option, a unit cell (Fig. II-3 ) is calculated with THERMOS, and self-shielding factors are calculated for each element M, each region L, and each of the 35 thermal energy groups K according to :

$$SSF(K,L,M) = \frac{\int_{region L} \phi(\bar{r}, K, L)\, d\bar{r}}{\int_{moderator} \phi(\bar{r}, K, mod)\, d\bar{r}} \quad (3\text{-}4)$$

It is important to notice that in this scheme the self-shielding factors are calculated <u>relative to the moderator</u> ! and all the materials in the moderator have unity self-shieldingfactors in all the groups.

These self-shieldingfactors (Eq.4) are then punched out on cards which are included in the next THERMOS calculation using a homogenized cell input. In the next calculation, the code uses now a fictitious cross-section set

$$\sigma^*(K,L,M) = SSF(K,L,M).\sigma(KLM) \qquad (3\text{-}5)$$

(for each of the 35 thermal groups)

instead of $\sigma(K,M,L)$ to calculate the spectrum, fluxes and homogenized 1 group macroscopic parameters .

As an input the user has to supply the volume-homogenized atomdensities of the materials in a unit cell.

<u>Using this procedure it is thus possible to include the spatial effects of a unit cell into a 35 thermal group calculation of a more complex arrangement such as an assembly or a core</u>.

This procedure describes thus the spatial & spectral effects in a unit cell in a cell homogenized calculation.

Table III - 1 shows the calculated self shielding factors of some elements as U 235 in a $UO_2$ unit cell and of the elements U235, PU 239, PU 240 in a mixed oxide (4 W/O PU $O_2$ - nat $UO_2$) unit cell.

## III - 3 : THE THERMAL SPECTRAL-DISTRIBUTION IN ONE DIMENSIONAL CONVENTIONAL & PLUTONIUMRECYCLE ASSEMBLY.

### 3-1) INTRODUCTION.

The SSF homogenization procedure described above has been used with THERMOS to calculate the conventional $UO_2$ assembly and the PU-recycle assembly. First 2 unit cell calculations (Fig. II-3 ) were made for the $UO_2$ & mixed oxide fuel in order to get the punched output self-shielding factors.

ISOTOPE 23592-- 3

HOMOGENISED CONC 3.0614E-04

CALCULATED SELF-SHIELDING FACTORS BY GROUP

| | | | | | | | | | | | | | | | |
|---|---|---|---|---|---|---|---|---|---|---|---|---|---|---|---|
| 1 | 0.33285 | 2 | 0.52556 | 3 | 0.62983 | 4 | 0.68985 | 5 | 0.72804 | 6 | 0.75185 | 7 | 0.77278 |
| 8 | 0.79481 | 9 | 0.81389 | 10 | 0.83577 | 11 | 0.85612 | 12 | 0.86771 | 13 | 0.87533 | 14 | 0.87533 |
| 15 | 0.87298 | 16 | 0.87821 | 17 | 0.88052 | 18 | 0.89628 | 19 | 0.91370 | 20 | 0.92948 | 21 | 0.94382 |
| 22 | 0.95449 | 23 | 0.95744 | 24 | 0.96533 | 25 | 0.94970 | 26 | 0.94712 | 27 | 0.94529 | 28 | 0.94240 |
| 29 | 0.93800 | 30 | 0.92274 | 31 | 0.96185 | 32 | 0.97254 | 33 | 0.96091 | 34 | 0.93926 | 35 | 0.90552 |

EFFECTIVE MICROSPIC CROSS-SECTIONS OVER GROUPS 1 AND 35

| SIGMA | SIGMF | SIGMS | SIGMTR |
|---|---|---|---|
| 2.21200E 02 | 1.87512E 02 | 8.53001E 00 | 2.29706E 02 |

GROUP AVERAGE SELF-SHIELDING FACTOR = 8.52115

ISOTOPE 23994-- 3

HOMOGENISED CONC 1.9830E-04

CALCULATED SELF-SHIELDING FACTORS BY GROUP

| | | | | | | | | | | | | | |
|---|---|---|---|---|---|---|---|---|---|---|---|---|---|
| 1 | 0.26188 | 2 | 0.44336 | 3 | 0.55029 | 4 | 0.60897 | 5 | 0.64787 | 6 | 0.66516 | 7 | 0.67773 |
| 8 | 0.68904 | 9 | 0.68415 | 10 | 0.66174 | 11 | 0.62124 | 12 | 0.52072 | 13 | 0.41770 | 14 | 0.35082 |
| 15 | 0.30791 | 16 | 0.31125 | 17 | 0.33135 | 18 | 0.43493 | 19 | 0.62782 | 20 | 0.81059 | 21 | 0.88234 |
| 22 | 0.88846 | 23 | 0.80549 | 24 | 0.38890 | 25 | 0.10733 | 26 | 0.07787 | 27 | 0.07502 | 28 | 0.07925 |
| 29 | 0.10832 | 30 | 0.38327 | 31 | 0.39039 | 32 | 0.93665 | 33 | 0.94450 | 34 | 0.92953 | 35 | 0.89972 |

EFFECTIVE MICROSPIC CROSS-SECTIONS OVER GROUPS 1 AND 35

| SIGMA | SIGMF | SIGMS | SIGMTR |
|---|---|---|---|
| 4.82405E 02 | 3.16761E 02 | 6.47107E 00 | 4.88857E 02 |

GROUP AVERAGE SELF-SHIELDING FACTOR = 6.73437

**TABLE III-1 : THERMOS SELF SHIELDING FACTORS IN $UO_2$ FUEL (UPPER), AND MIXED OXIDE FUEL (LOWER)**

A second run with the circular assembly model (see Fig. III-1 ), was then made using volume homogenized material concentrations and the SSF deck. Using this procedure detailed results of the important thermal spectrum distribution in the assemblies have been obtained for both the conventional & PU-recycle assembly and its effects have been studied. The results have been compared with a THERMOS calculation using only 1 thermal group library. This 1 thermal group library included the macroscopic, unperturbed X-sections, obtained from homogenized unit cell calculations (with SSF's). (Note that no diffusion constant is needed in the THERMOS code, solving the integral transport-theory equations).

In this way, the details of the thermal spectrum distribution and its influence in the assemblies were obtained without disturbances of any other effects due to the use of different codes & different calculation procedures.

## 3-2) RESULTS FOR THE CONVENTIONAL ASSEMBLY.

Fig. III-2 shows the spectrum in a regular $UO_2$ assembly at 3 positions

1- in the watergap

2- in the $UO_2$ - at the watergap

3- in the $UO_2$ at the center (asymptotic - unperturbed spectrum).

It is thus easily noticed that compared to the asymptotic unperturbed spectrum of a unit cell, the spectrum distribution in an assembly varies with the position. The spectrum in the $UO_2$-fuel is thus noticed to be softer near the watergap. In Fig. IV-11, the pointwise thermal velocity distribution of the neutrons (in units of 2200 m/sec) in the conventional assembly, has been drawn, together with the 1 group velocity distribution model.

It is thus easily observed that the velocity of the neutrons is continuous

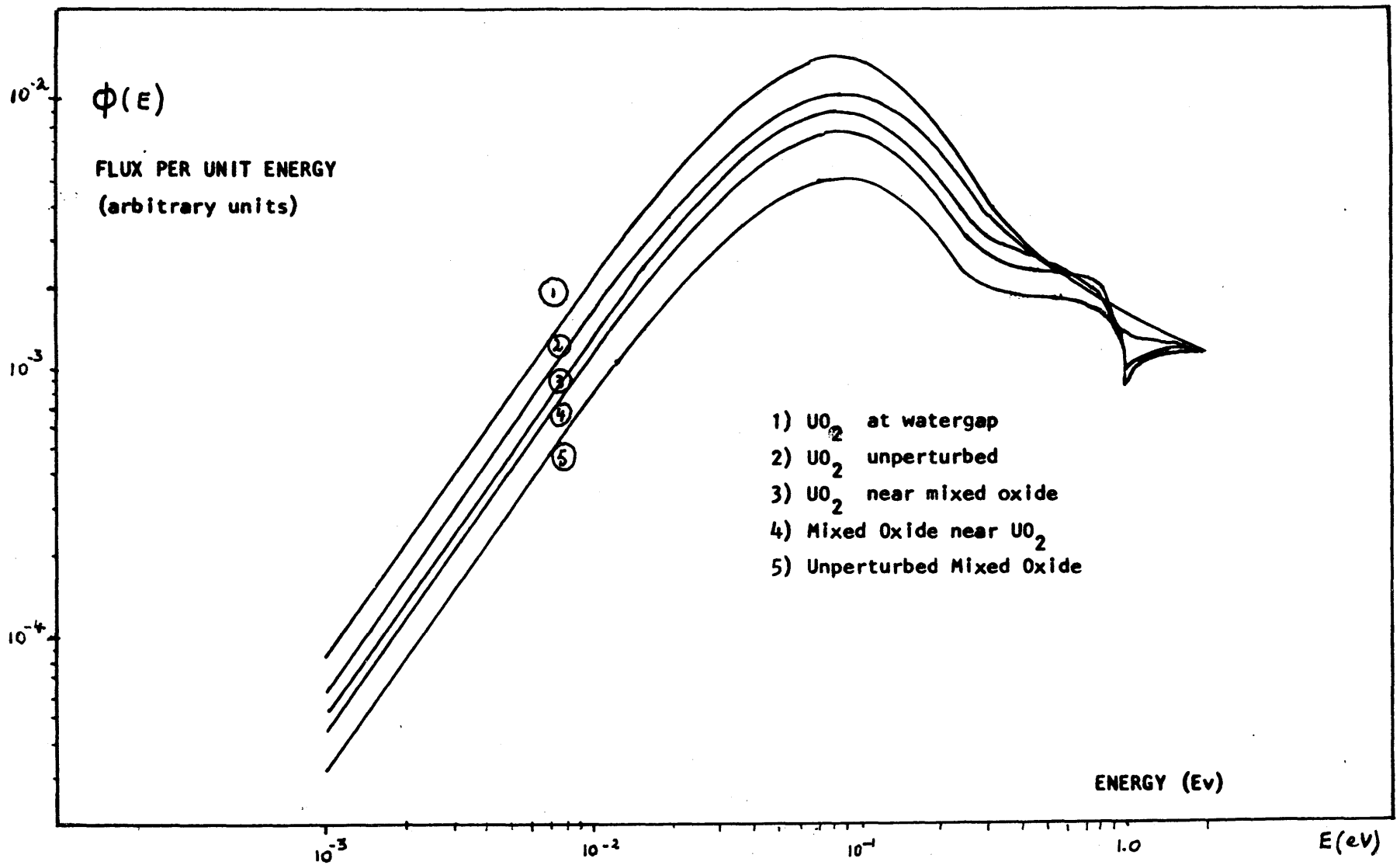


FIG III-2 Spectra at different Positions in the cylindrical $UO_2$ and Plutonium Recycle Assemblies

whereas the standard model, thus assuming the unit cells from an infinite unperturbed array is unable to predict the spectral effects near interfaces.

Fig. III-3 finally shows the powerdistribution of thermal neutrons in a conventional assembly as calculated with the 35 groups THERMOS library compared to the calculation of the powerdistribution using the standard unperturbed 1 group X-sections.

It is thus important to notice from a practicle point of view that the standard 1-group calculation underpredicts the powerpeaking by about 5%.

The spectralsoftening effect near the watergap is thus responsible for a supplementary powerpeaking.

## 3-3) RESULTS FOR THE PLUTONIUM RECYCLE ASSEMBLY.

Fig. III-2, shows the spectrum in a plutonium recycle assembly at 4 positions :

1- in the $UO_2$ near the watergap
2- in the $UO_2$ near the mixed-oxide region
3- in the mixed oxide near the $UO_2$ region
4- in the center of the mixed oxide region together with the unperturbed spectra in the $UO_2$ & mixed regions.

It is thus easily noticed that the unperturbed spectra in the $UO_2$ and mixed oxide are entirely different, in the mixed oxide the spectrum is harder, which is evidently due to the much higher (about twice) absorption X-sections of the PU 239 compared to the U235 (Fig. II-2 ).

Noteworthy is also the dip in the mixed oxide spectrum at the giant 1- 0 eV PU 240 resonance.

When looking at the spectra at different positions in the assembly it is noticed that now compared to the $UO_2$-assembly,spectraleffects at the boundary of as well the $UO_2$-mixed oxide interface as the watergap are introduced.

In the mixed oxide the spectrum is softened at the interface & in the $UO_2$ the spectrum is hardened at the interface & softened near the watergap.

Fig. IV-11, pictures the neutron-velocity versus the distance in the assembly, compared to the 1 group velocity distributionmodel.

Again the strong spectralvariations in a PU-recycle assembly can be noticed.

It is however important to notice that the spectraleffects are only felt approximately within the distance of one unit cell from a boundary.

The rest being virtually unperturbed.

## III- 4 : THE EFFECTS OF ONE-GROUP MODELS ON THE CALCULATION OF THE POWERDISTRIBUTION IN CONVENTIONAL AND PLUTONIUMRECYCLE ASSEMBLIES.

### 4 -1) THE DIFFERENT ONE GROUP CALCULATION MODELS.

The 3 basic techniques that can be used to calculate the flux & powerdistribution are :

1- S-N, P-L TRANSPORTTHEORY (ANISN, TWOTRAN)

2- INTEGRAL TRANSPORTTHEORY (THERMOS)

3- DIFFUSION THEORY (PDQ)

In order to get the one-group macroscopic X-sections of a homogenized unit cell needed for the calculations basically 2 methods can be used for the homogenization of the heterogeneous unit cell.

1- CELL HOMOGENIZATION (C.H.) which is the regular & standard procedure.

In this procedure the macroscopic X-sections are calculated from :

$$\Sigma = \Sigma^F V^F \frac{\Phi_F}{\Phi_{cell}} + \Sigma^c V^c \frac{\Phi_c}{\Phi_{cell}} + \Sigma^{Mod} V^{mod} \frac{\Phi_{mod}}{\Phi_{cell}}$$

2- MODERATOR EDGE FLUX-HOMOGENIZATION ( 21 ), abbreviated M.H.

In this procedure the macroscopic X-sections are calculated from

$$\Sigma = \Sigma^F V_F \frac{\Phi_F}{\Phi_{MOD}} + \Sigma^c V^c \frac{\Phi_c}{\Phi_{MOD}} + \Sigma^{Mod} V^{mod}$$

This homogenization scheme is sometimes used in $D_2O$ systems (SGHWR group at Winfrith)

There is no theoretical justification for either of the 2 definitions, but sometimes it is claimed that the M.H. model should be better because the flux in the water must be continuous between cells or between core & reflector.

It must be remarked that the effective microscopic cross-sections used in the, THERMOS 35 group, SSF-homogenized calculations were generated with the M.H. scheme (the only version built in the MIT-THERMOS option).

The 1 group output follows thus a M.H. scheme, whereas a heterogeneous unit cell calculation with THERMOS follows a C.H. scheme.

Both cell homogenizationschemes can thus be used te generate the 1 group macroscopic cross-sections for THERMOS, ANISN and PDQ. In THERMOS and ANISN no

use is made of the diffusionconstant (only $\Sigma_a$, $\Sigma_s$, $\Sigma_{tot}$ are needed). In diffusion theory however the definition of the diffusionconstant varies wildely ; and therefore different diffusion theory models can be constructed according to the energy and $\Sigma_{tr}$ weighting & the use of the C.H. or M.H. procedure.

## 4 -2) THE DIFFERENT DIFFUSION THEORY MODELS :

Since the definition of the diffusion constant through its derivation from transporttheory is highly mathematical (which is beyond our scope), no attempt has been made to go in too much detail. Interested readers may consult references ( 32 , 33 ) or any other book on transporttheory.

Instead we will start with Pomranings discussion of the energy weighting of the diffusionconstant (33), to clarify the subject.

If one expands the transportequation in a low order (P-1) spherical harmonic series, making use of the transport X-section to account for P-1 scattering, one obtains the energy dependent diffusionapproximation i.e. the conservation equation :

$$\nabla . J(\bar{r},E) + \Sigma_t(\bar{r},E)\phi(\bar{r},E) = \int_0^\infty dE\, \Sigma_s(\bar{r},E'\rightarrow E)\phi(\bar{r},E') + S(\bar{r}) \qquad (3\text{-}6)$$

and Fick's law of diffusion

$$J(\bar{r},E) = -\frac{1}{3\Sigma_{tr}(\bar{r},E)} \nabla\phi(\bar{r},E) \qquad (3\text{-}7)$$

where $\Sigma_t = \Sigma_a + \Sigma_s$ = total macroscopic X-section

$\phi(\bar{r},E)$ = scalar flux, $J(\bar{r},E)$ = current, $\Sigma_s(\bar{r},E' \rightarrow E)$ is the macroscopic differential scattering X-section, & $\Sigma_{tr}(\bar{r},E)$ =

$$\Sigma_{tr}(\bar{r},E) = \sum_{\ell} \left[ N_\ell \sigma_a^\ell(\bar{r},E) + (1-\mu_0^\ell)\sigma_s(\bar{r},E)N^\ell \right] \qquad (3-8)$$

Integration the eq.(7) over the i th group

$$J_s^i(\bar{r}) = -\left[\frac{1}{3\Sigma_{tr}(\bar{r})}\right]_i \frac{\partial \Phi^i(\bar{r})}{\partial s} \qquad (3-9)$$

where $$\Phi^i(\bar{r}) = \int_i dE\, \phi(\bar{r},E) \qquad (3-10)$$

$$J_s^i(\bar{r}) = \int_i dE\, J(\bar{r},E) \qquad (3-11)$$

and $$\left[\frac{1}{\Sigma_{TR}(\bar{r})}\right]_i = \frac{\int_i dE\, 1/\Sigma_{TR}(\bar{r},E) \frac{\partial \phi(\bar{r},E)}{\partial s}}{\int_i dE\, \frac{\partial \phi(\bar{r},E)}{\partial s}} \qquad (3-12)$$

from this definition it is thus seen that parallel averaging $\Sigma_{tr}(E) = \Sigma_a(E) + (1-\bar{\mu})\Sigma_s(E)$

with respect to the gradient seems appropriate

However Eq. 7 can be written equally well as

$$3\Sigma_{tr}(\bar{r},E)\, J(\bar{r},E) + \nabla \phi(\bar{r},E) = 0 \qquad (3-13)$$

integrating (13) over the i th group gives :

$$3\left[\Sigma_{tr}(\bar{r})\right]_i J_s^i(\bar{r}) + \frac{\partial \Phi^i(\bar{r})}{\partial s} = 0 \qquad (3-14)$$

where we have defined

$$\left[\Sigma_{tr}(\bar{r})\right]_i = \frac{\int dE\, \Sigma_{tr}(\bar{r},E)\, J(\bar{r},E)}{\int dE\, J(\bar{r},E)} \qquad (3\text{-}15)$$

Eq. (15) indicates that one should series average $\Sigma_{tr}$ with respect to the current.

Comparing Eqs. 12with 15 we deduce

$$\left[\frac{1}{\Sigma_{tr}(\bar{r})}\right]_i = \frac{1}{\left[\Sigma_{tr}(\bar{r})\right]_i} \qquad (3\text{-}16)$$

Thus if one has the exact solution of the current $J(\bar{r},E)$ of equations 6 & 7 the 2 procedures should be equal.

However neither $\emptyset(\bar{r},E)$ or $J(r,E)$ are known in advance, therefore the $\emptyset(\bar{r},E)$'s or $J(\bar{r},E)$'s of the unit cell calculations are used as approximations, in the thermal group, or a zero dimensional calculation is performed from which we get the spectrum (usually in the higher groups -MUFT).

The most commonly used approximation is to assume the seperability of flux & current in space & energy.

In this way $\emptyset(\bar{r},E) = \emptyset(\bar{r})\,\phi(E)$ , $\nabla\phi(\bar{r},E) = (\nabla\phi(\bar{r}))\cdot\phi(E)$ and we obtain the formulas 8 & 15 in which now the fluxspectrum $\emptyset(E)$ replaces the $J(\bar{r},E)$ call 8 * and 15 *).

<u>If this seperability holds</u>, then again the statement of eq. (16) can be assumed.

Another assumption is to assume a seperability of the directional flux $\psi(\bar{r},\bar{\Omega},E) = \psi(\bar{r},\bar{\Omega})\cdot\psi(E)$ , in this case coming from transporttheory one should use the series avaraging. However since this

seperability assumption is more restrictive,(all angular components have the seperability) this is generally not used in practice.

In short, 2 practicle methods can be used : parallel or series avaraging $\Sigma_{tr}$ (r,E) over the flux.

Thus far nothing has been said about the space & volumeweighting of the diffusionconstant in the unit cell. Taking those possibilities into account the following definitions exist usually :

D 1) first space and volumeweighting the transport X-section using cell homogenization & then parallel avg. $\Sigma_{tr}$ over the spectrum of the cell

Calling M = material , L = region

$$\Sigma_{tr}(E) = \frac{\int_{CELL} \Sigma_{tr}(E,M)\,\phi(\bar{r},E)\,d\bar{r}}{\int_{CELL} \phi(\bar{r},E)\,d\bar{r}} \qquad (3\text{-}17)$$

where
$$\Sigma_{tr}(E,M) = \sum_{L} N(L,M)\,\sigma_{tr}(L,E) \qquad (3\text{-}18)$$

thus
$$\Sigma_{tr}(E) = \sum_{M}\sum_{L} V(L)\,N(L,M)\,\sigma_{tr}(M,E)\,SSF_{cell}(L,E,M) \qquad (3\text{-}18)$$

and then :
$$D = \frac{1}{3}\,\frac{\int_0^{E^*} dE\,\left[\Sigma_{tr}(E)\right]^{-1} \int_{cell} \phi(\bar{r},E)\,d\bar{r}}{\int_0^{E^*} dE \int_{cell} d\bar{r}\,\phi(\bar{r},E)} \qquad (3\text{-}19)$$

or with Ø (E) the spectrum of the cell

$$\phi(E) = \frac{\int_{cell} d\bar{r}\,\phi(\bar{r},E)}{\int_0^{E^*} dE \int_{cell} d\bar{r}\,\phi(\bar{r},E)} \qquad (3\text{-}20)$$

(19) becomes :

$$D = \frac{1}{3} \int_0^{E^*} dE \left[ \sum_{L,M} V(L)\, N(L,M)\, \sigma_{tr}^{EFF}(L,E) \right]^{-1} \phi(E) \qquad (3\text{-}21)$$

D 2) first space & volume weighting $\Sigma_{tr}$ using M.H., and then parallel avg. $\Sigma_{tr}$ over the spectrum of the cell.

in this way we get :

$$D = \frac{1}{3} \int_0^{E^*} dE \left[ \sum_{L,M} V(L)\, N(L,M)\, \sigma_{tr}^{*}(M,E) \right]^{-1} \phi(E) \qquad (3\text{-}22)$$

where

$$\sigma_{tr}^{*}(M,E) = \sigma_{tr}(M,E) \cdot SSF_{mod}(L,M,E)$$

D 3) First space & volumeweighting in the $\Sigma_{tr}$ over the spectrum of the cell.

In this case :

$$D = \frac{1}{3} \Big/ \int_0^{E^*} dE \left[ \sum_{L,M} V(L)\, N(L,M)\, \sigma_{tr}^{EFF}(L,E) \right] \phi(E) \qquad (3\text{-}23)$$

D 4) same as (3) but M.H.

$$D = \frac{1}{3} \Big/ \int_0^{E^*} dE \left[ \sum_{L,M} V(L)\, N(L,M)\, \sigma_{tr}^{*}(L,E) \right] \phi(E) \qquad (3\text{-}24)$$

D 5) FIRST energyweighting the parallel $\Sigma_{tr}$ over a region and then volume and fluxweighting.

in this case :

$$[\Sigma_{tr}(L)]^{-1} = \frac{\int_L d\bar{r} \int_0^{E^*} dE\, [\Sigma_{TR}(M,E)]^{-1} \phi(\bar{r},E)}{\int_L d\bar{r}\, \phi(\bar{r},E)}$$

then :

$$D = \frac{1}{3} \sum_L V(L) \frac{\Phi(L)}{\Phi_{cell}} [\Sigma_{tr}(L)]^{-1} \qquad (3\text{-}25)$$

D 6) FIRST energy weighting the parallel $\Sigma_{tr}$ over a region, and then density, volume and fluxweighting.

$$[\sigma_{tr}(M)]^{-1} = \frac{\int_L d\bar{r} \int_0^{E^*} dE\, [\sigma_{tr}(M,E)]^{-1} \phi(\bar{r},E)}{\int d\bar{r}\, \phi(\bar{r},E)} \qquad (3\text{-}26)$$

$$D = \frac{1}{3} \sum_{M,L} V(L) \frac{\Phi(M)}{\Phi_{cell}} [\sigma_{tr}(M,L)]^{-1} \qquad (3\text{-}27)$$

After careful examination of the most important unit cell codes, THERMOS, LASER, LOCALUX, LEOPARD it was found that ;

- SCHEME D-1 <u>IS THE MOST COMMON USED</u>.

LASER-LOCALUX AND LEOPARD calculate the diffusionconstant of a unit cell according to this scheme and eqs. (17) to (19).

- SCHEME D-2 is used by THERMOS IN HOMOGENIZED UNIT CELL-SELF SHIELDING FACTOR OPTION AT MIT.
- SCHEME D-3 CAN BE OBTAINED FROM THERMOS IN A HETEROGENEOUS UNIT CELL CALCULATION; since THERMOS prints out $\Sigma_{tr}^{eff}(M)$ for each material.

- SCHEME D-5 has been found to be the STANDARD OUTPUT FROM A HETEROGENEOUS UNIT CELL CALCULATION WITH THERMOS.

-SCHEME D-6, CAN BE OBTAINED FROM LOCALUX OR LEOPARD SINCE IN THOSE CODES PSEUDO MICROSCOPIC X-SECTIONS as calculated from Eq. 26 are also printed on the output. Those pseudo-microscopic X-sections are especially useful for the calculation of the diffusion-ct. of extra-materials, such as watergap, cans, reflector etc.

Table III - 2 shows a comparison between the one-group macroscopic cross-sections as determined with the homogenization -(C.H.) or moderator edge flux homogenization (M.H.) schemes for both a $UO_2$ and mixed oxide unit cell and for the water.

Table III - 3 shows the different diffusionconst,ants for both the $UO_2$ & mixed oxide unit cells & the water as calculated with the 6 different schemes described above.

From Table III-2, it is thus noticed that the differences in the macroscopic X-sections are mainly due to the differences in weighting $\frac{\bar{\Phi}_i}{\bar{\Phi}_{MOD}}$ (M.H.) versus $\frac{\bar{\Phi}_i}{\bar{\Phi}_{CELL}}$ (C.H.).

For a mixed oxide cell for which the $\frac{\bar{\Phi}_{MOD}}{\bar{\Phi}_{CELL}}$ is higher the difference are thus higher.

From Table III -3, a large deviation in the diffusion constants is noticed between the different schemes. The normal scheme but using the moderator edge flux homogenization (THERMOS-homogenized SSF procedure) (scheme 2), seems to give a particularly high diffusion constant. The other schemes give rather similar results, although the deviations between the schemes are much larger than the deviations between the macroscopic cross-sections. In the water (which was taken with a $UO_2$ cell generator spectrum), large deviations exist in the diffusion-constants between the different methods.

The usual adopted practible Technique generating a water-diffusionconstant from a unit cell calculation is through the scheme D-6 using the LEOPARD or LOCALUX CODES.

TABLE III - 2 COMPARISON OF ONE GROUP MACROSCOPIC X-SECTIONS OF AN UNPERTURBED $UO_2$ AND MIXED OXIDE UNIT CELL USING THE C.H. OR M.H. METHOD. (cut-off 1.855 eV - THERMOS).

| $UO_2$ CELL | | | MIXED OXIDE CELL. | |
|---|---|---|---|---|
| CELL HOM. (C.H.) | | MOD.HOM. (M.H.) | C.H. | M.H. |
| $\Sigma_a$ | .09514 | .09177 | .18960 | .16610 |
| $\nu\Sigma_f$ | .1490 | .14780 | .26540 | .23423 |
| $\Sigma_f$ | .06102 | .05921 | .09247 | .08458 |
| $\Sigma_{tr}$ | .67108 | .63450 | .72759 | .63815 |
| $H_2O$ PARAMETERS (1400 ppm B). | | | | |
| $\Sigma_a$ | .02697 | .02886 | | |
| $\Sigma_{tr}$ | .77420 | .82070 | | |

TABLE III- 3 : COMPARISON OF THE ONE GROUP DIFFUSION CONSTANTS OF UNPERTURBED CELLS USING DIFEERENT HOMOGENIZATION SCHEMES (1.855 eV CUT-OFF).

| | | $UO_2$ | $H_2O$ + 1400 ppm B | MIX OXIDE. |
|---|---|---|---|---|
| (SCHEME 1) | D1 | .43818 | | .41499 |
| (SCHEME 2) | D2 | .74272 | .24550 | .73079 |
| | D3 | .50489 | .43055 | .45692 |
| | D4 | .52545 | .40616 | .49234 |
| | D5 | .37510 | .12913 | .3751 |
| | D6 | .43860 | .33605 | |

4 -3) RESULTS OF THE CALCULATION OF THE POWER DISTRIBUTION IN A CONVENTIONAL ASSEMBLY & PU-RECYCLE ASSEMBLY USING DIFFERENT ONE GROUP MODELS (WITH UNPERTURBED UNIT CELL CONSTANTS).

a) the $UO_2$ assembly Fig. III-3, shows the powerdistribution for a conventional $UO_2$ assembly calculated with two different methods.

1) the THERMOS - group M.H. model (integral transporttheory).

2) PDQ - 1 group diffusiontheory, M.H. model, with a M.H. diffusionsonconstant from scheme D2.

It is thus noticed that there is a rather good agreement between the 2 methods,

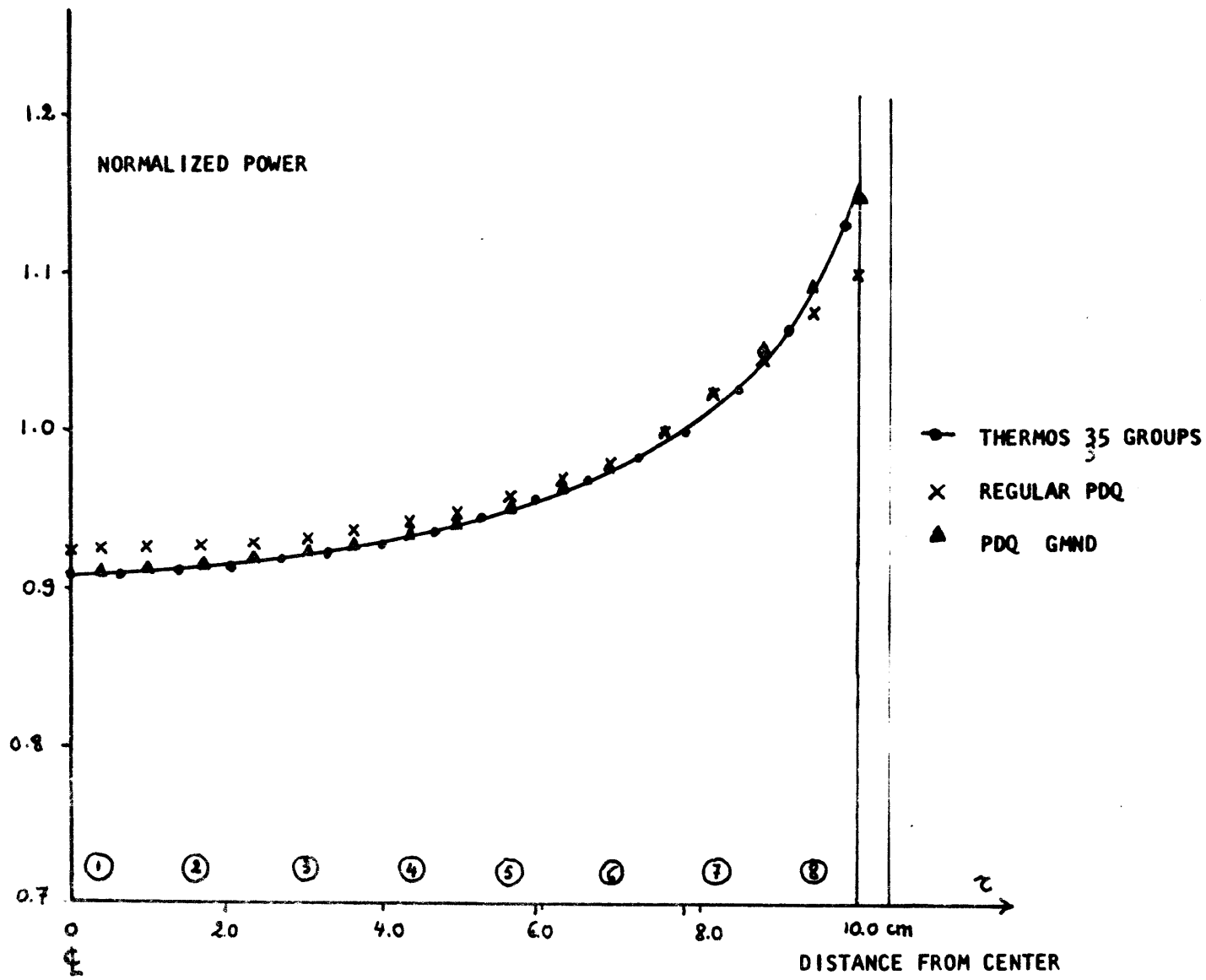


FIG III-3 Circulized Conventional $UO_2$ Assembly, Comparison Thermos 35 group, PDQ- 1 group

In general, because of the differences in the diffusionconstant, diffusiontheory calculations using the moderator edge flux homogenization scheme (M.H.) underpredicts the powerdistribution compared to the cell homogenezation (C.H.) scheme. It should therefore not be recommended for the study of $H_2O$ cooled & moderated reactors. However the results are rather insensitive to the 1 group model choosen (see also reference 21).

b) The PU-recycle assembly.

As can be seen from Figs III-4,5 the powerdistribution varies wildely according to the choosen calculationmodel.

5 models have been used :

1) THERMOS - 1 group M.H. method.

2) ANISN - 1 group M.H. method

3) PDQ - 1 group M.H. method, diffusionconstant D-2.

4) PDQ - 1 group M.H., diffusionct. D-4

5) PDQ - 1 group, C.H., diffusion constant D-5.

From the comparison between THERMOS & ANISN, using the same M.H. method, it is seen that transporttheory gives more powerpeaking compared to integral transporttheory. This suggest that angular effects are present in a PU-recycle assembly. Table III - 4, shows the angular flux in the $UO_2$ region and the angular flux in the mixed oxide region

The differences are small but noticible. Also from Fig. III-4, the PDQ-1 group M.H. method with the diffusionconstant D-2 (regular M.H. method), is thus seen to be very inaccurate.

Deviations in power of about 12 % may be noticed. Decreasing the diffusionconstant using the series $\Sigma_{TR}$ (M.H.) weighting already gives a substantial improvement. However the errors are still substantial.

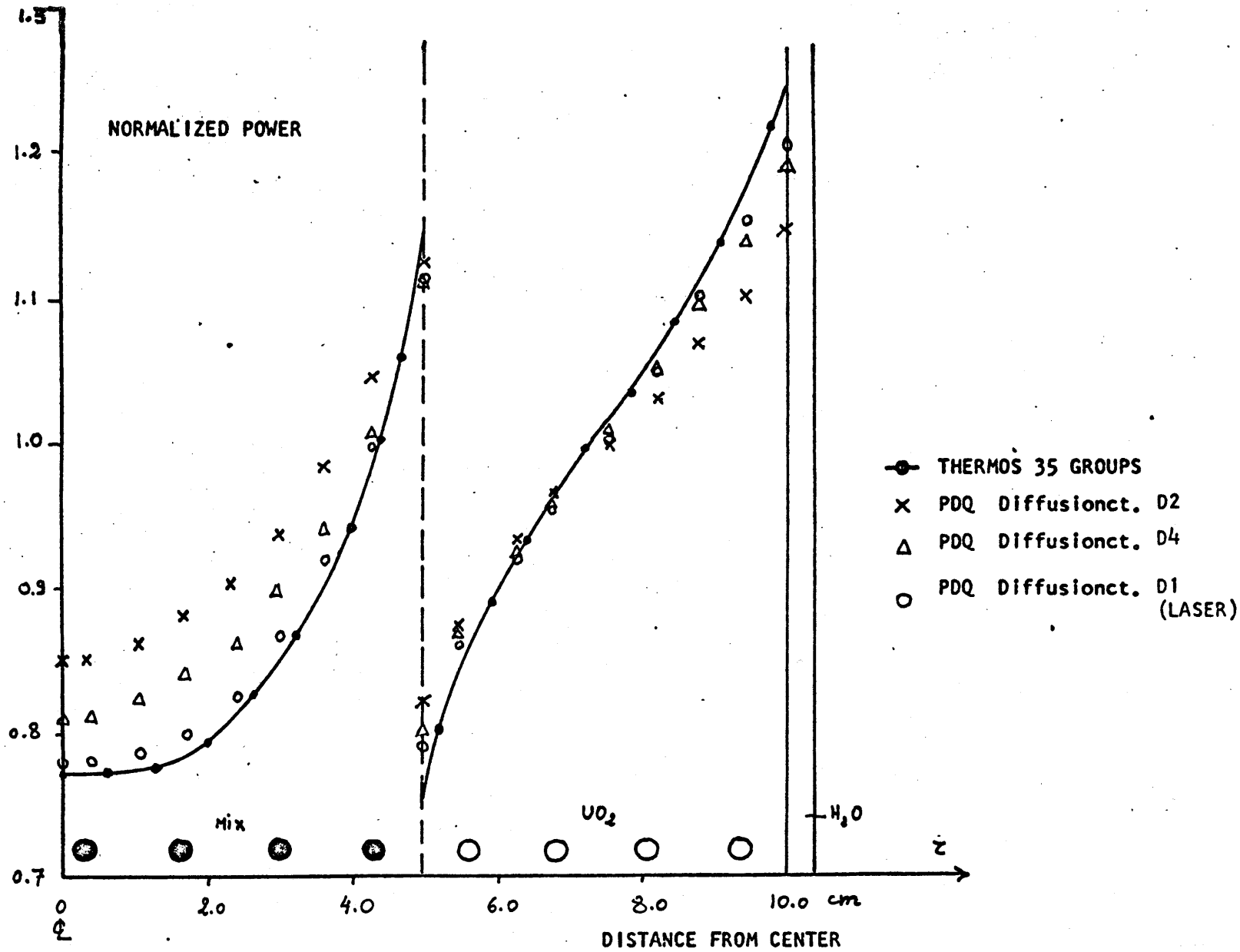


FIG III-4 Comparison Different Diffusiontheory Models- Plutonium Recycle Assembly

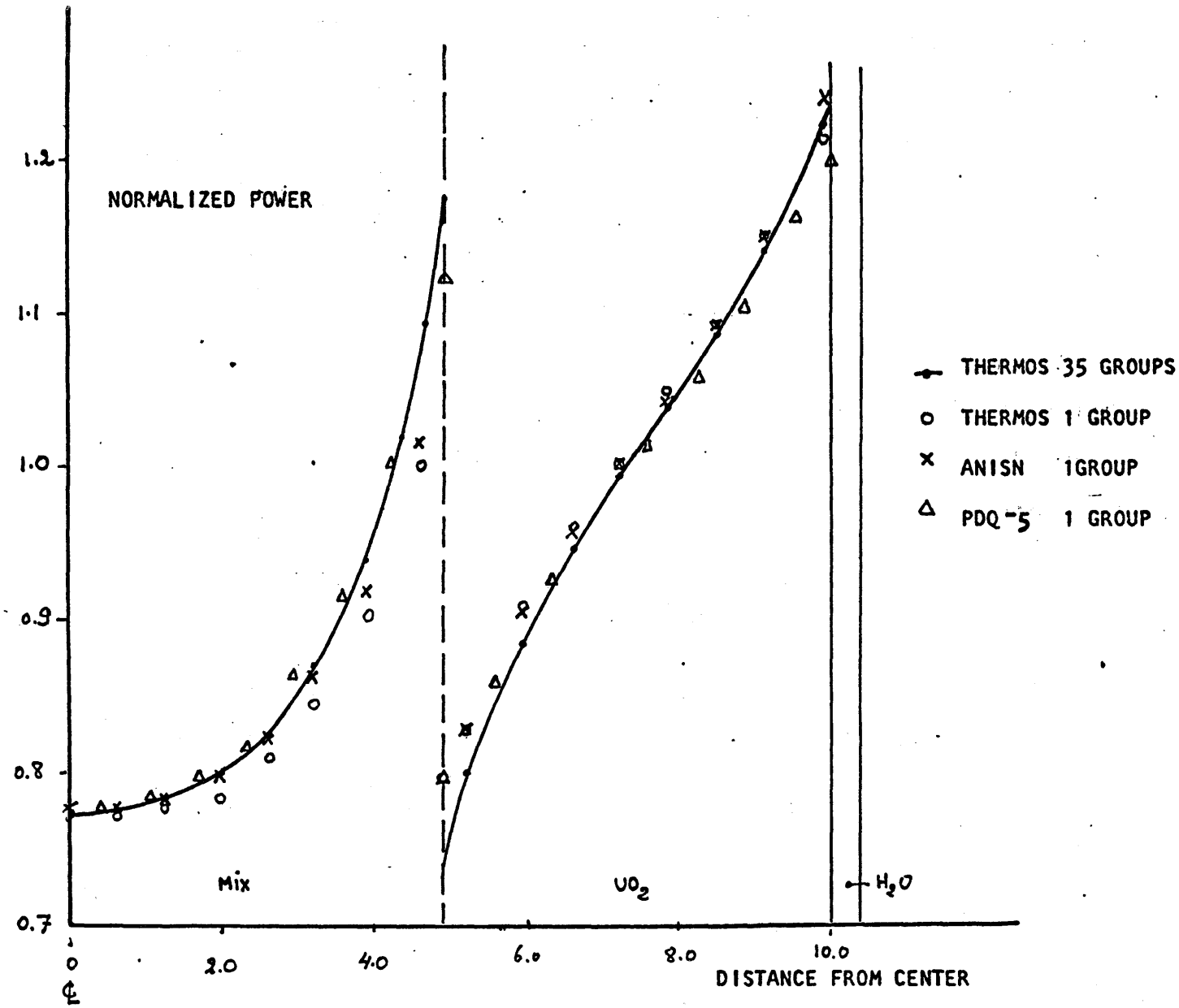


FIG III-5 Comparison Transport Theory and Diffusion Theory In a Plutonium Recycle Assembly

FLUX BY ANGLE AND POINT FOR GROUP 1

| | PNT. | ANGL 1 | ANGL 2 | ANGL 3 | ANGL 4 | ANGL 5 | ANGL 6 | ANGL 7 | ANGL 8 |
|---|---|---|---|---|---|---|---|---|---|
| | 1 | 1.69185E-02 | 1.69144E-02 | 1.69144E-02 | 1.70540E-02 | 1.70518E-02 | 1.70504E-02 | 1.70504E-02 | 1.70518E-02 |
| | 2 | 1.70099E-02 | 1.69862E-02 | 1.69212E-02 | 1.72363E-02 | 1.72184E-02 | 1.71489E-02 | 1.70488E-02 | 1.69797E-02 |
| | 3 | 1.71920E-02 | 1.71458E-02 | 1.70042E-02 | 1.75462E-02 | 1.75099E-02 | 1.73473E-02 | 1.71249E-02 | 1.69933E-02 |
| | 4 | 1.74942E-02 | 1.74170E-02 | 1.71726E-02 | 1.80348E-02 | 1.79729E-02 | 1.76730E-02 | 1.72901E-02 | 1.70918E-02 |
| Mix | 5 | 1.79694E-02 | 1.78449E-02 | 1.74546E-02 | 1.87831E-02 | 1.86860E-02 | 1.81813E-02 | 1.75717E-02 | 1.72919E-02 |
| | 6 | 1.87099E-02 | 1.85091E-02 | 1.78978E-02 | 1.99145E-02 | 1.97725E-02 | 1.89501E-02 | 1.80129E-02 | 1.76282E-02 |
| | 7 | 1.98956E-02 | 1.95281E-02 | 1.85803E-02 | 2.16068E-02 | 2.14187E-02 | 2.01545E-02 | 1.87069E-02 | 1.81585E-02 |
| | 8 | 2.20613E-02 | 2.13004E-02 | 1.96292E-02 | 2.41061E-02 | 2.39023E-02 | 2.18454E-02 | 1.97203E-02 | 1.89887E-02 |
| | 9 | 2.61106E-02 | 2.57055E-02 | 2.16071E-02 | 2.73808E-02 | 2.72423E-02 | 2.60338E-02 | 2.20934E-02 | 2.03437E-02 |
| | 10 | 2.79899E-02 | 2.76873E-02 | 2.55276E-02 | 2.90708E-02 | 2.89452E-02 | 2.79521E-02 | 2.60704E-02 | 2.30419E-02 |
| | 11 | 2.93816E-02 | 2.93093E-02 | 2.75676E-02 | 3.04540E-02 | 3.03249E-02 | 2.93584E-02 | 2.77903E-02 | 2.54653E-02 |
| | 12 | 3.06249E-02 | 3.03469E-02 | 2.90077E-02 | 3.17896E-02 | 3.16493E-02 | 3.06065E-02 | 2.91496E-02 | 2.73784E-02 |
| $UO_2$ | 13 | 3.18837E-02 | 3.15614E-02 | 3.02468E-02 | 3.32162E-02 | 3.30621E-02 | 3.18511E-02 | 3.03432E-02 | 2.89138E-02 |
| | 14 | 3.33297E-02 | 3.28965E-02 | 3.14502E-02 | 3.48497E-02 | 3.46896E-02 | 3.32240E-02 | 3.15197E-02 | 3.02663E-02 |
| | 15 | 3.52523E-02 | 3.45718E-02 | 3.27557E-02 | 3.67854E-02 | 3.66459E-02 | 3.48926E-02 | 3.28177E-02 | 3.15897E-02 |
| | 16 | 3.82695E-02 | 3.72443E-02 | 3.43641E-02 | 3.90244E-02 | 3.89676E-02 | 3.72191E-02 | 3.44770E-02 | 3.30458E-02 |
| | 17 | 4.30563E-02 | 4.30716E-02 | 3.69107E-02 | 4.10035E-02 | 4.10959E-02 | 4.28723E-02 | 3.75884E-02 | 3.49257E-02 |
| $H_2O$ | 18 | 4.32404E-02 | 4.34177E-02 | 4.05626E-02 | 4.03353E-02 | 4.04121E-02 | 4.33813E-02 | 4.12582E-02 | 3.71162E-02 |
| | 19 | 4.26229E-02 | 4.26229E-02 | 4.26244E-02 | 3.90300E-02 | 3.90300E-02 | 4.32470E-02 | 4.32486E-02 | 3.90312E-02 |

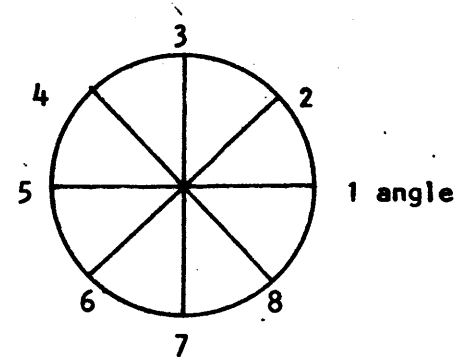


**TABLE III-4, FLUX BY ANGLE AND BY POINT IN A PLUTONIUM RECYCLE ASSEMBLY AS DETERMINED WITH ANISN**

The best agreement of diffusiontheory with transporttheory was obtained using the standard THERMOS cell homogenization scheme (D-5) and the standard LASER scheme (D-1).

As a general conclusion it has thus been found that large differences in the calculated powerdistribution exist, between the different calculation methods applied to a PU-recycle assembly. In particular M.H. diffusiontheory seems to underpredict the powerpeaking to a great extend.

The M.H. method used with diffusiontheory is completely inadequate.

The best results were obtained with the standard cell homogenized (C.H.) THERMOS 1 group parameters (scheme D-6) & the standard LASER & LOCALUX schemes (D-1).

SUMMARY.

In summary it has been found that very good agreement exits between different methods in a conventional $UO_2$ assembly, although the M.H. slightly underpredicts the powerpeaking.(21)

In a PU-recycle assembly, large deviations (up to 13 %) in powerdistribution exits between a regular diffusiontheory calculation using the M.H. method for the macroscopic X-sections & diffusion constant, and transportcalculations with THERMOS & ANISN.

The alarm that had been risen, was greatly tempered when diffusion-theory with the standard C.H. and diffusionconstants were used.

Although some differences of about 2 % remain between diffusion theory & transporttheory, the standard 1 group LASER & LOCALUX diffusiontheory procedures, in comparison with 1 group transporttheory, should be considered adequate in practice for the calculation of the powerdistribution and powerpeaking in both $UO_2$ en PU-recycle assemblies.

Due to the influence of the diffusionconstant for the calculation of PU-recycle assemblies this parameter requires special attention. Careful examination of the scheme adapted in the code to calculate the diffusionconstant as well as the particular use made of the codes is thus recommended.

Angular flux effects have also been noticed in a PU-recycle assembly and an additional 1 to 2 % increase in powerpeaking may result from these effects.

With regard to the spectraleffects it has been found that in a conventional assembly powerpeaking is increased by about 5 % due to spectralsoftening near the watergap.

In a PU-recycle assembly spectralsoftening in the mixed oxide region increases the powerpeak by a 5 %, and spectralhardening decreases the power in the $UO_2$ fuel near the interface by about 2 %; whereas the softening near the watergap takes a 4 % increase in the powerpeak.

Because of the special importance of the peak power in the design of nuclear reactors, it is thus necessary to take into account the additional powerpeaking produced by thermal spectrumcoupling of the different fuel rods between each other and between fuel rods & extra materials such as water. For the calculation of angular transporteffects there is only one solution :

one & 2 dimensional transporttheory codes. Because of the expense involved and special need for generating scatteringcross-section, it is unlikely that they will be used as standardcalculations.

The effect, even in a PU -recycle assembly however is small & the 1 % error is also in the range of experimental errors.

# CHAPTER IV DEVELOPMENT OF GENERAL AND SIMPLE ONE THERMAL GROUP METHODS FOR THE CALCULATION OF POWERPEAKING IN ONE-TWO & THREE DIMENSIONS.

## IV- 1 INTRODUCTION - DESCRIPTION OF EXISTING METHODS.

In the preceeding chapter we have noticed that the standard methods of using 1-thermal group X- sectionsets of unperturbed unit cells underpredicts the powerpeaking produced at watergaps & $UO_2$- Mixed Oxide interfaces.
For simple one-dimensional geometries, the THERMOS code using 35 energy-groups & the most accurate scattering-kernels for $H_2O$ can be used. In the case of 2D and 3D geometries, generally no such codes exist or have serious limitations.
Although in principle the 2D diffusiontheory codes, which allow several thermal groups & upscattering could be used, the problem is generally to find multi-hermalgroup collapsed X-sections, & especially up-scattering cross-sections.
Another big disadvantage is cost, since the cost of a computorrun is roughly proportional to I . J . K . G where I, J, K are the # of meshes in the X, Y,Z coordinates and G is the number of groups.
Therefore several more simple 1-thermal group methods have already been proposed for the calculation of watergap-peaking.
The most popular methods for the calculation of watergap-peaking are :

1)- spatially varying 1-group cross-sections as determined from a 1 dimensional THERMOS model.
2)- Calumes overlapping group model ( 34 ).
3)- Breen's MND (mixed Number Density Model) ( 35 )
4)- Correctionfactors of Leve dahl ( 36 )
5)- using X-sections of a supercell.
6)- the use of a Maxwellian spectrumavgd. diffusionconstant.

An excellent treatment of the most simple methods 2, 3, 4, 5 & 6 for the calculation of <u>watergap peaking</u> in BWR's using the LEOPARD code with some extensions

can be found in Ref. 30

Because of the importance, a discussion of the several methods also in the light of the new problem introduced at the $UO_2$-Mix interface will be given here.

1-1) The Spatial X-Sections Method.

This is probably the most accurate, but also the most time consuming & costly method, since it involves making a 35 thermal group calculation with THERMOS. The method is general, in the sence that it is accurately applicable to $UO_2$-Mixed Oxide interfaces & other structures as burnable poison rods as well.

One particular drawback is the need for a 1 dimensional model of a more complicated structure such as a X-Y assembly in our case.

Since the method however is general & considered to be the most exact, a particular effort has been made to improve the restriction on the geometry & a relatively simple 2 D spatial-X-Section Synthesis method based on 1 D THERMOS calculations has been developed.

1-2) CALUME'S OVERLAPPING GROUP MODEL.

In complexity, Calume's overlapping groupmodel may be thought of being between the THERMOS-Spatial X-section Model and more simple methods as Breen's MND model. It is easily applicable to 1, 2 & 3 D calculations.

Calume's basic assumption is that in diffusing, the neutrons maintain their original asymptotic spectrum, even in media were they are not born.

They will not in fact, retain that spectrum, but will through energy exchange collisions slowly become distributed in the spectrum of that medium.

So, for an arrangement with a watergap e.g., if we assume that the source of thermal neutrons (slowing down source $\Sigma_R$, $\emptyset$ ) in the $UO_2$ fuel region is zero, it is assumed that neutrons from the $H_2O$ diffuse in the $UO_2$ region, without their spectrum being altered, & vice versa if the source in the water is put to zero neutrons from the $UO_2$ region diffuse in the water without a change in their spectrum. In short Calume's method consits of : <u>first</u> finding the X-sections of the material L ( U235 e.g.) in region A (water e.g.), of materials M in their own region B, materials M in region A & L in B;
<u>second</u> making 2 diffusiontheory runs : in the first the source of thermal neutrons in region A is put to zero (zero $\Sigma_R$ fast removal X-section in 2 group calculations, or zero fixed source in fixed source problems) & the X-sections of region A are those of the materials M in region B, in the second the source in B is put to zero & the cross-sections of materials M & L are taken over region A.

From a study performed with THERMOS, in which alternatively the sources of 2 regions were removed, it had been found that Calume's basic assumptions break down, In order to overcome this problem for watergap peaking Calume has suggested some variational methods, which makes the problem more complicated. Especially for the treatment of the $UO_2$-Mixed Oxide interface, this method should not be recommended.
Futhermore Calume's method requires a lot of preparation, it needs <u>cell averaged</u> X-sections of materials in a region which are not present in this region, and requires at least 2 diffusiontheory calculations in which the sources are removed alternatively. (for a PU-recycle assembly, 3 calculations are necessary).
Therefore the method has not been used in this study.

## 1-3) BREEN'S MIXED NUMBER DENSITY (MND) MODEL. ( 35 )

Breen has developed a very interesting & simple one group model for the calculation of powerpeaking near watergaps.

Several comments & limitations of the model are noteworthy after reading the article & some familiarity with the LEOPARD ( 27,28 ) Code, which contains the SOFOCATE program for the calculation of the thermal spectrum.

1) Breen's model seems only applicable to watergap peaking & not to mixed oxide $UO_2$ interface peaking.
2) In the water, the same spectrum and $1/v$ * is used as in the unit cell.
3) The assumption that the gradient spectrum near a watergap approaches a Maxwellian spectrum, is not always correct.
4) The LEOPARD code is the only standard code which prints out the Mixed Number Density Cross-sections needed for the application of the model.
5) The Standard LEOPARD code has been found, apart from spectraleffects, to be inaccurate for the calculation of powerpeaking in PU-recycle assemblies.
6) The LEOPARD code has a cut-off at 0.625 eV, and is thus insufficient to describe the Thermal spectrum in a mixed oxide fuel completely.

Because of those limitations a more general one-group model, based on ideas of the MND model has been developed, which can : *

1) be used with unit cell codes LEOPARD, THERMOS, LASER, LOCALUX and probably other, without a need for any modifications in these codes , and
2) be used for Mixed-Oxide $UO_2$ interface peaking as well as for watergap peaking.

As the original MND model, the developed General MND model is easy & quick to apply.

* see further.

1-4) CORRECTION FACTORS OF LEVEDAHL.

The method of Levedahl seems to give similar results to Calumes method (34). The method however suffers from the drawbacks that it is only applicable to watergap peaking and that the diffision constants must be obtained over spectra which are not directly available from a standard unit cell code.

1-5) THE USE OF X-SECTIONS OF A SUPERCELL.

The use of X-sections of a supercell, or a unit cell with the extra region, which volume fraction in the super cell is the same as the volume fraction of the extra materials (other materials than the regular fuel unit cell) in an assembly core, may improve the calculation of the power peaking somewhat in BWR'S(30). The smeared spectral effects and smeared X-sections over the whole assembly are insufficient to describe the much larger spectral effects and X-section variations at the peak locations.

1-6) THE USE OF A DIFFUSION CONSTANT AVGD. OVER A MAXWELLIAN SPECTRUM.

This approach is evidently not applicable to Pu-recycle applications, since the assumption of a maxwellian gradient at the $UO_2$ - Mixed Oxide interface, has been found to be inexact

IV - 2 : DEVELOPMENT OF THE THERMOS SPATIAL CROSS-SECTION SYNTHESIS METHOD (*) IN X - Y DIMENSIONS.

As mentioned earlier the THERMOS code is a one dimensional code and it is therefore impossible to obtain directly the spectrum variation and spectrum averaged 1-group X-sections at a position I, J in a 2 dimensional X - Y structure such as the conventional and Pu-recycle assemblies pictured on the Fig. IV - 1 (only a portion of the assemblies are shown).
Therefore a 2-dimensional synthesis method was developed, based on the following reasoning.

* abbreviated SXS method.

## 2-1) 2D SPECTRUMSYNTHESIS.

Assume that we have a complicated assembly such as the PU-recycle assembly portion pictured on Fig. IV - 1.

The cell homogenized flux at each unit cell or node I, J, & each neutronenergy E can be written as :

$$\Phi(I,J,E) = \Phi(I,J)\,\psi(E,I,J) \qquad (4-1)$$

where $\psi$ (E, I, J) is the unperturbed spectrum at node I, J.

Assume that a one dimensional calculation has been made in the X-direction, and one in the Y direction such that the 2 directions cross each other at I, J; and that no spectrumcoupling exits.

These fluxes can be written at the positions I and J as :

$$\Phi_x(I,E) = \Phi_x(I)\,\psi_x(E,I) \qquad (4-2)$$

$$\Phi_y(J,E) = \Phi_y(J)\,\psi_y(E,J) \qquad (4-3)$$

Let us now write at each mode I, J

$$\Phi(I,J)\,\psi(E,I,J) = \Phi_x(I)\,\Phi_y(J)\,\psi_x(E,I)\,\psi_y(E,J) + \Delta\Phi_o(I,J)\,\psi_o(I,J,E) \qquad (4-4)$$

where the first term on the right hand side makes up for a complete separability in X, Y and energy, and the second term takes the correction of this assumption in account.

Since no spectralcoupling has been ssumed :

$$\psi(E,I,J) = \psi_x(E,I) = \psi_y(E,J) = \psi_x(E,I)\,\psi_y(E,J) = \psi_o(E,I,J) \qquad (4-5)$$

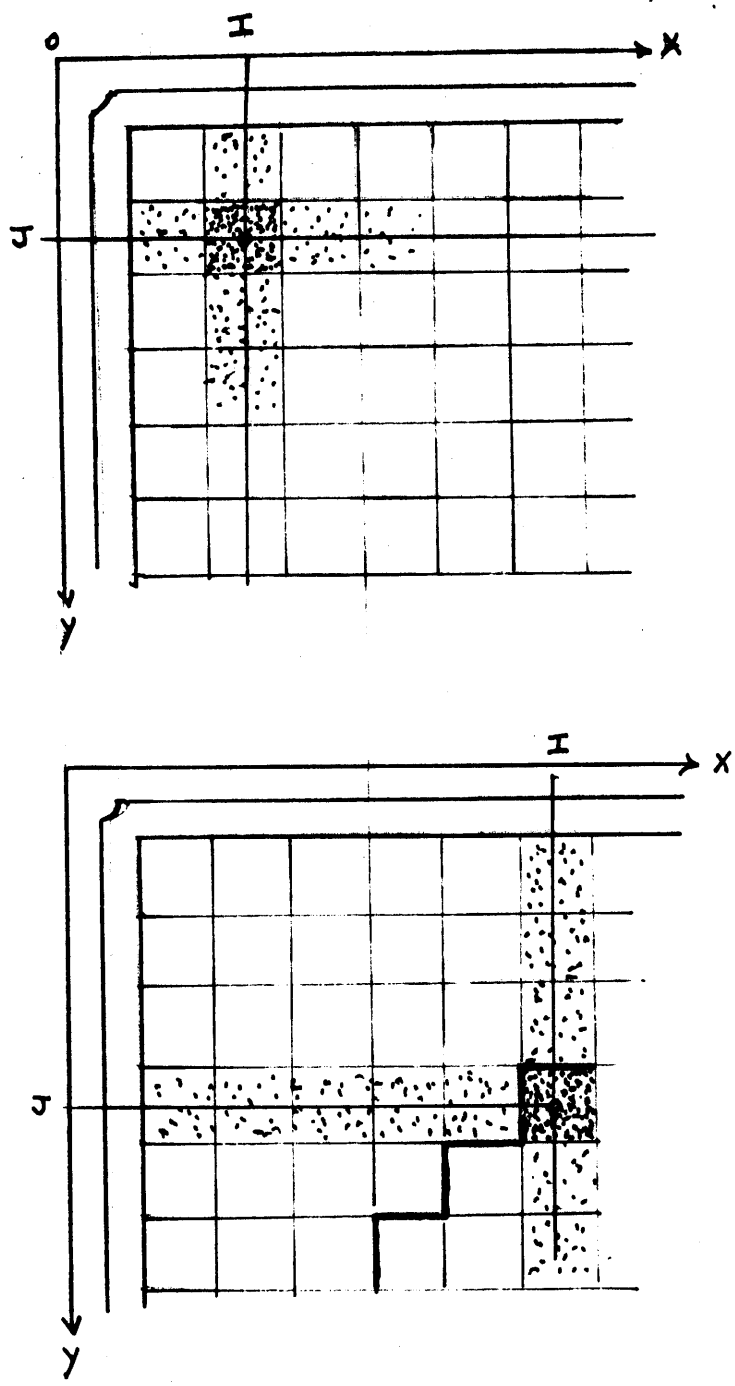


FIGS. IV-1 TWO DIMENSIONAL SPATIAL X-SECTION SYNTHESIS

In the case that we have spectrumcoupling, and assuming that the perturbation-effects are small we can write :

$$[\Phi(I,J) + \delta\Phi(I,J)][\psi(E,I,J) + \delta\psi(E,I,J)] =$$
$$[\Phi_x(I) + \delta\Phi_x(I)][\Phi_y(J) + \delta\Phi_y(J)] *$$
$$[\psi_x(I,E) + \delta\psi_x(I,E)][\psi_y(E,J) + \delta\psi_y(J,E)]$$
$$+ [\Delta\Phi_o(I,J) + \delta\Delta\Phi_o(I,J)][\psi_o(I,J,E) + \delta\psi_o(I,J,E)] \quad (4\text{-}6)$$

After taking only first order perturbations and after dividing the resulting eqs. by $\Phi_x(I)\,\Phi_y(J)\,\psi_x(I,E)\,\psi_y(J,E)$

we get taking (4-4) and (4-5) into account :

$$\frac{\delta\Phi(I,J)}{\Phi(I,J) - \Delta\Phi_o(I,J)} + \frac{\delta\psi(I,J,E)}{\psi(I,J,E)} =$$

$$\frac{\delta\Phi_x(I)}{\Phi_x(I)} + \frac{\delta\Phi_y(J)}{\Phi_y(J)} + \frac{\delta\psi_x(E,I)}{\psi_x(E,I)} + \frac{\delta\psi_y(E,J)}{\psi_y(E,J)} \quad (4\text{-}7)$$

Since spatial effects only affect spatial terms I, J we have :

$$\frac{\delta\Phi(I,J)}{\Phi(I,J) - \Delta\Phi_o(I,J)} = \frac{\delta\Phi_x(I)}{\Phi_x(I)} + \frac{\delta\Phi_y(J)}{\Phi_y(J)} \quad (4\text{-}8)$$

$$\frac{\delta\psi(I,J,E)}{\psi(I,J,E)} = \frac{\delta\psi_x(I,E)}{\psi_x(I,E)} + \frac{\delta\psi_y(J,E)}{\psi_y(J,E)} \quad (4\text{-}9)$$

Since the purpose is not to make a spatial synthesis (2-D diffusiontheory codes are available) only EQ (4-9) is of interest.

EQ (4-9) thus says that the spectrumdisturbance $\delta\psi$ (E, I, J) at a mode I, J is the <u>superposition</u> of the spectrum disturbance $\delta\psi_x(I, E)$ at I, from the X direction and the spectrumdisturbance $\delta\psi_y(J, E)$ at J, from the Y direction; which can be calculated with a 1 dimensional spectrumcode like THERMOS.

2-2) <u>2D VELOCITY DISTRIBUTION.</u>

From Eq. (4-9), the 2 dimensional velocitydistribution can be calculated with the following reasoning :

Assume a $1/v$ absorber with a unity cross-section at 2200 m/sec.

The activation of this absorber, in a disturbed spectrum at node I, J can be written as :

$$\frac{\int_0^{E^*} \frac{1}{v}\left[\psi(E,I,J) + \delta\psi(E,I,J)\right] dE}{\int_0^{E^*} \left[\psi(E,I,J) + \delta\psi(E,I,J)\right] dE} \cong$$

$$\frac{\int_0^{E^*} \frac{1}{v}\psi(E,I,J)\left[1 + \frac{\delta\psi(I,J,E)}{\psi(I,J,E)}\right] dE}{\int_0^{E^*} \psi(E,I,J)} \cong \frac{\int_0^{E^*} dE\, \frac{1}{v}\psi(E,I,J)\left[1 + \frac{\delta\psi_x(E,I)}{\psi_x(E,I)} + \frac{\delta\psi_y(E,J)}{\psi_y(E,J)}\right]}{\int_0^{E^*} dE\, \psi(E,I,J)}$$

(4-10)

Since $\psi_x = \psi_y = \psi$ we get after some manipulations :

$$\delta\left(\frac{1}{\bar{v}}\right) = \delta\left(\frac{1}{\bar{v}(I,J)}\right) = \delta\left(\frac{1}{v_x(I)}\right) + \delta\left(\frac{1}{v_y(J)}\right) \qquad (4\text{-}11)$$

or assuming $\bar{v}(I,J) \cong v_x(I) = v_y(J)$

$$\delta\bar{v}(I,J) = \delta v_x(I) + \delta v_y(J) \qquad (4\text{-}12).$$

## 2-3) 2D CROSS-SECTION SYNTHESIS.

Of much more practicle importance is the synthesis of the 1-group macroscopic X-sections $\Sigma$ ( $\Sigma_a$, $\nu\Sigma_f$, $\Sigma_f$ ) and the diffusionconstant D. Replacing now in general the $1/v$ X-section in EQ. (4-10) by $\Sigma$ (E, I, J) Eq. (4-11) can be written as :

$$\delta\Sigma(I,J) = \delta\Sigma_x(I) + \delta\Sigma_y(J) \qquad (4\text{-}13)$$

Thus all the spectraldisturbed macroscopic data at any position (I, J) in a 2 dimensional X-Y assembly can be calculated approximately from one dimensional THERMOS-calculations and the superposition principle of EQ (4-13).

## 2-4) APPLICATION OF THE S X S-METHOD TO THE CONVENTIONAL & PU-RECYCLE ASSEMBLIES.

a) Preliminary runs :

The THERMOS Spatial-X-section Synthesis Method has been applied to determine the velocity distributions and deviations of the macroscopic X-Sections in the portions of the conventional & PU-recycle assemblies pictured in Fig. IV-1

From the diagonal symmetry in the conventional assemblies, it is noticed that only 1 THERMOS calculation is necessary. The SSF-homogenizationscheme (*) in THERMOS was used on a geometry pictured in Fig. IV-2 for the conventional assembly.

Fig. IV-4 shows the % deviations in the macroscopic cross-sections (defined as $\frac{\Sigma - \Sigma^{\sigma}}{\Sigma^{\sigma}}$ were $\Sigma^{\sigma}$ = the unperturbed cross-section); and the (-%) deviations in the thermal neutronvelocity, avgd. over the unit cell positions I or J from 1 to 8.

It was noticed that the % deviations in $\Sigma_a, \Sigma_f, \nu\Sigma_f$ were very close, so that only one % deviation in $\Sigma$ is necessary.

The % deviation in D was max. 2 %, and its effect has been neglected.

Fig. IV-5 shows the % deviations in macroscopic X-sections for the positions 1, 2, 3 when the watergapthickness was varied from .135" original up to .30inches. As can be noticed the % deviations, especially for the most important position 1, increases nearly linearly with the watergapthickness. Therefore the % deviations due to spectralcoupling of a watergap with thickness t can be thought of being the superpositon of 2 deviations due to a watergap thickness $t_1$ and $t_2$, were $t_1 + t_2 = t$. This observation is consitent with the S X S model equations 4-13.

For the PU-recycle assembly portion of Fig. IV-1-B, the above results of the 1 dimensional configuration of Fig. IV-3 were used for the region were only the watergapeffects are present. (region bounded by the I = 0 to 3 & J = 0 to 3 positions). The 1 D model pictured in Fig. IV-3, was used to determine the spectraldisturbances of both watergap & $UO_2$ - MIXED OXIDE interface, bounded by the I = 4 to 8 and J = 4 to 8 positions).

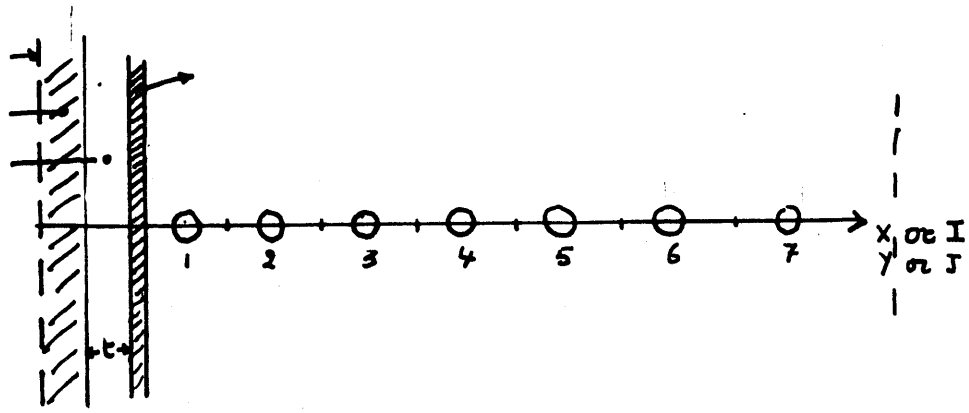


FIG IV-2 GEOMETRY FOR THE CALCULATION OF THE SPECTRUM DISTURBANCE AT THE WATERGAP

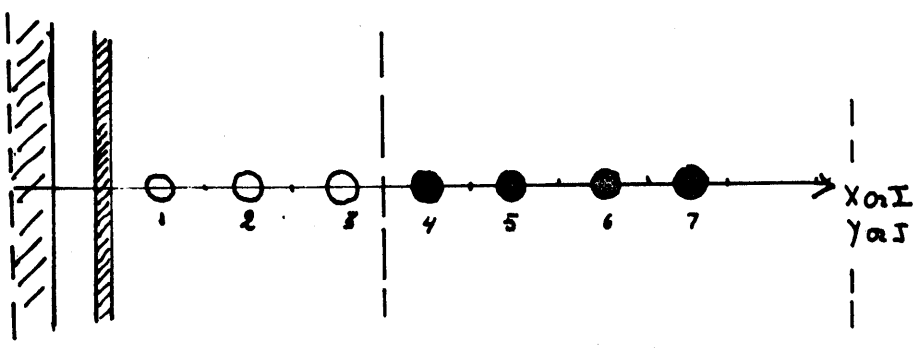


FIG IV-3 GEOMETRY FOR THE CALCULATION OF THE SPECTRAL DISTURBANCES AT THE WATERGAP AND FUELS INTERFACE

(the circles represent the fuel rods and their positions and have been included to make the notation that the unit cell has been taken in account through self-shielding factors in the homogenization).

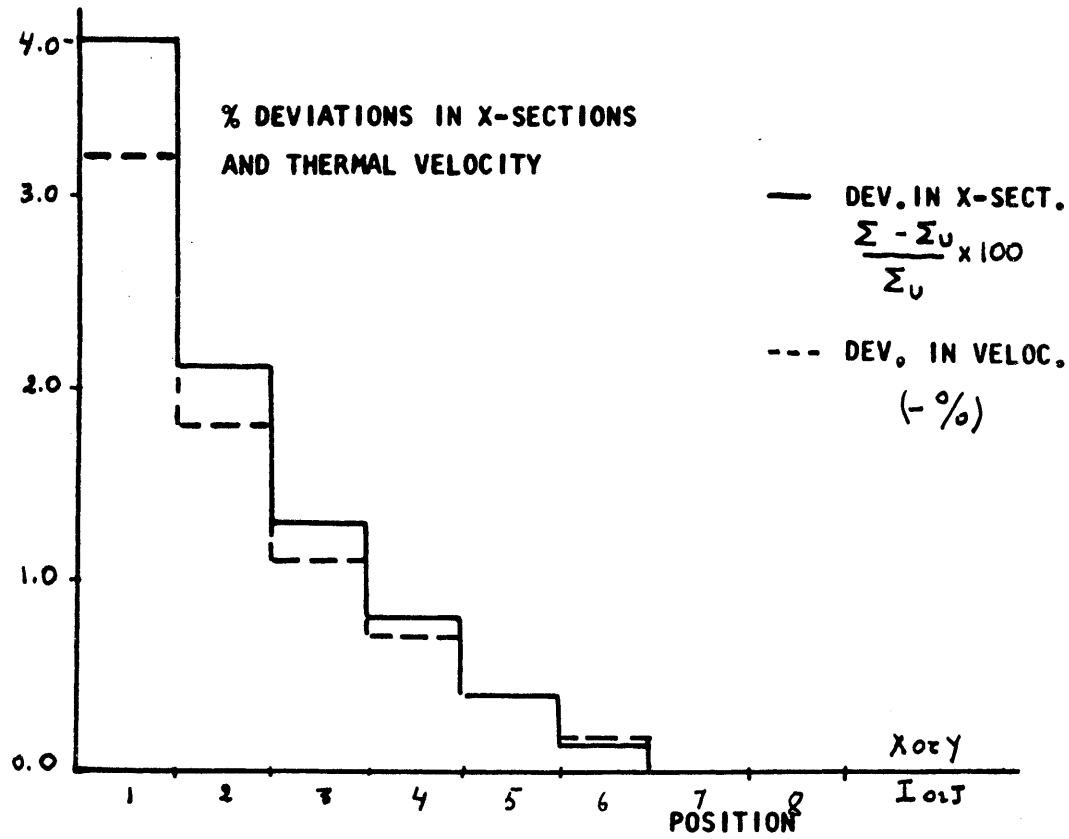


FIG IV-4 % DEVIATIONS IN X-SECTIONS AND THERMAL VELOCITY VS. POSITION AWAY FROM THE WATERGAP

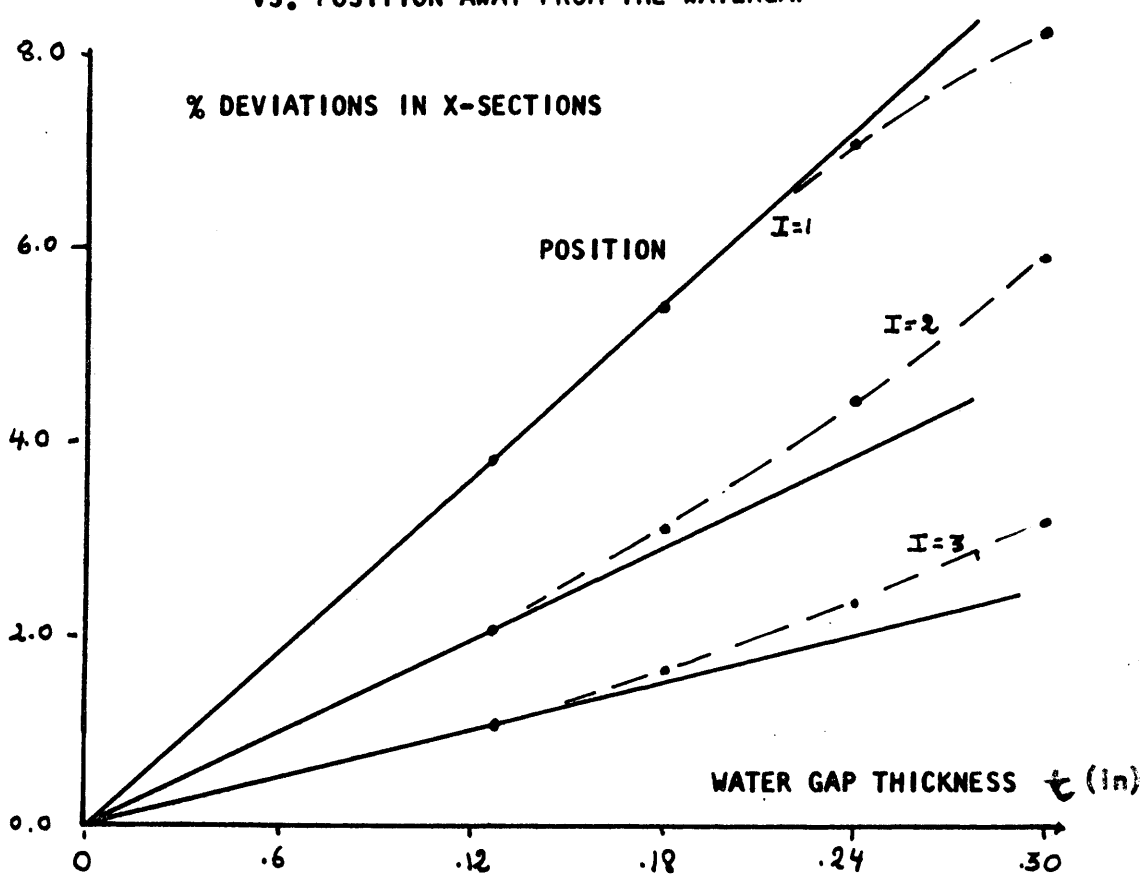


FIG IV-5 % DEVIATION IN X-SECTIONS VS WATERGAP THICKNESS AT DIFFERENT POSITIONS

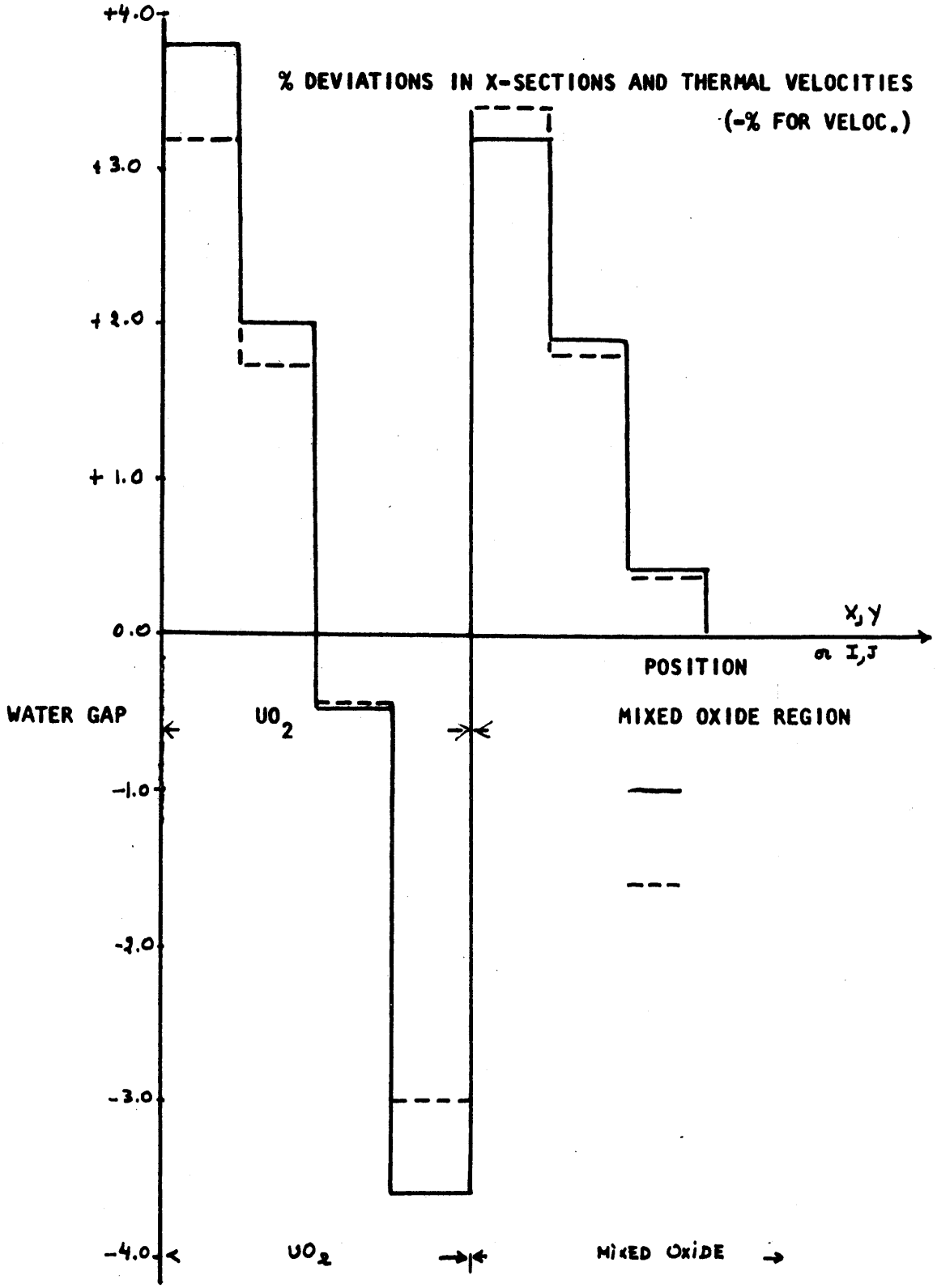


FIG IV-6 % DEVIATIONS IN X-SECTIONS AND (-) THERMAL VELOCITY IN THE SLAB PU- RECYCLE SECTION

Fig. IV-6 shows the % deviations in X-sections and ($\bar{v}$) thermal velocity, due to the watergap & $UO_2$-MIXED OXIDE boundary at various positions, as the determined with THERMOS on the geometry of Fig. IV -3.

b) <u>The 2-D Synthesis</u>.

From the preliminary 1D THERMOS calculations & the 2D synthesismethod, the 2 D velocity distribution & 2D spatial distribution of 1 thermal group cross-sectiondeviations has been obtained for the portions of the conventional & PU-recycle assemblies, (Figs IV-1, A & B).

Fig. IV-7, shows the thermal neutronvelocitydistribution (in units of 2200 m/sec) in the conventional assembly, whereas Fig. IV-8 shows the result for the PU-recycle assembly.

It is thus noticed that now the velocities change more continuously from one region to the other, in contrast to the unperturbed model in which the velocities changed abruptly from 2.129 (in units 2200 m/sec) in the water to 2.304 in the $UO_2$ cells. Due to the more continuous change in spectrum, the macroscopic X-sectionschange near the interfaces, compared to their unperturbed values.

Fig. IV-9 & Fig. IV-10, show the 2D distribution of the macroscopic X-section changes, relative to their unperturbed values, in respectively a conventional & PU-recycle portion of the assemblies.

As an example how these perturbations were obtained at each location (I, J) consider e.g. in the conventional assembly the node (3,1).

From Fig. IV-4, the perturbation from the watergap along X alone in the Y direction at location J = 1 is seen to be + 3.8 %, whereas the perturbation from the watergap along Y in the X direction alone, at location I = 3 is + 1.3%.

According to the superposition $\delta\Sigma(I, J) = \delta\Sigma_x(I) + \delta\Sigma_y(J)$ the perturbation due to the watergaps along X & Y is thus : (+1.3%) + (+3.8%) = + 5.1%.

Fig. IV -7 : AVG. THERMAL NEUTRON VELOCITY DISTRIBUTION IN A PORTION OF CONVENTIONAL $UO_2$ ASSEMBLY.

2.129

| | 1 | 2 | 3 | 4 | 5 | 6 | 7 | 8 |
|---|---|---|---|---|---|---|---|---|
| 1 | 2.157<br>-6.4% | 2.189<br>-5.0 | 2.205<br>-4.3 | 2.214<br>-3.9 | 2.221<br>-3.6 | 2.226<br>-3.4 | 2.230<br>-3.2 | 2.230<br>-3.2 |
| 2 | | 2.221<br>-3.6 | 2.237<br>-2.9 | 2.246<br>-2.5 | 2.253<br>-2.2 | 2.258<br>-2.0 | 2.263<br>-1.8 | 2.263<br>-1.8 |
| 3 | | | 2.253<br>-2.2 | 2.264<br>-1.8 | 2.269<br>-1.5 | 2.274<br>-1.3 | 2.279<br>-1.1 | 2.279<br>-1.1 |
| 4 | | | | 2.272<br>-1.4 | 2.279<br>-1.1 | 2.283<br>-0.9 | 2.288<br>-0.7 | 2.288<br>-0.7 |
| 5 | | | | | 2.286<br>-0.8 | 2.290<br>-0.6 | 2.295<br>-0.4 | 2.295<br>-0.4 |
| 6 | | | | | | 2.295<br>-0.4 | 2.300<br>-0.2 | 2.300<br>-0.2 |
| 7 | | | | | | | 2.304<br>-0.0 | 2.280<br>-1.0 |
| 8 | | | | | | | | |

Unperturbed Velocity 2.304 (in units 2200 m/sec)
Average Velocity in this portion : 2.262 - whole ass. 2.283 (avg. v circ.ass.2.2500

| | |
|---|---|
| 2.157<br>-6.4 | THERMAL N°VELOCITY IN 2200 m/sec UNITS<br>% DEV. FROM UNPERTURBED. |

Fig. IV-8 : AVG. THERMAL NEUTRON VELOCITY DISTRIBUTION IN A PU-RECYCLE ASSEMBLY. (IN UNITS 2200 m/sec).

2.129

| | 1 | 2 | 3 | 4 | 5 | 6 | 7 | 8 |
|---|---|---|---|---|---|---|---|---|
| 1 | 2.157<br>-6.4% | 2.189<br>-5.0 | 2.205<br>-4.3 | 2.214<br>-3.9 | 2.221<br>-3.6 | 2.226<br>-3.4 | 2.230<br>-3.2 | 2.230<br>-3.2 |
| 2 | | 2.221<br>-3.6 | 2.237<br>-2.9 | 2.246<br>-2.5 | 2.253<br>-2.2 | 2.260<br>-1.9 | 2.265<br>-1.7 | 2.265<br>-1.7 |
| 3 | | | 2.253<br>-2.2 | 2.263<br>-1.8 | 2.283<br>-0.9 | 2.369<br>+2.8 | 2.373<br>+3.0 | 2.373<br>+3.0 |
| 4 | | | | 2.299<br>-0.2 | 2.442<br>+6.0 | 2.468<br>-6.4 | 2.553<br>-3.2 | 2.553<br>-3.2 |
| 5 | | | | | 2.468<br>-6.4 | 2.537<br>-3.8 | 2.560<br>-2.9 | 2.576<br>-2.3 |
| 6 | | | | | | 2.616<br>-0.8 | 2.626<br>-0.4 | 2.626<br>-0.4 |
| 7 | | | | | | | 2.637<br>-0.0 | 2.597<br>-1.5 |
| 8 | | | | | | | | |

Unperturbed velocity $UO_2$ : 2.304

MIX : 2.637

Avg. velocity in this portion : $\bar{v}$ $UO_2$ = 2.267, v assy. = 2.293 (whole assembly)

$\bar{v}$ MIX = 2.567, v assy. = 2.567 (whole assembly)

| | |
|---|---|
| 2.157<br>-6.4 | THERMAL NEUTRONVELOCITY (IN UNITS 2200 m/sec)<br>% DEVIATIONS FROM UNPERTURBED. |

Fig. IV-9 : % DEVIATIONS IN CROSS-SECTIONS IN A CONVENTIONAL $UO_2$ ASSEMBLY.

| | 1 | 2 | 3 | 4 | 5 | 6 | 7 | 8 |
|---|---|---|---|---|---|---|---|---|
| 1 | +8.0 | +5.9 | +5.1 | +4.6 | +4.2 | +3.9 | +3.8 | +3.8 |
| 2 | | +4.2 | +3.4 | +2.9 | +2.5 | +2.2 | +2.1 | +2.1 |
| 3 | | | +2.6 | +2.1 | +1.7 | +1.4 | +1.3 | +1.3 |
| 4 | | | | +1.6 | +1.2 | +0.9 | +0.8 | +0.8 |
| 5 | | | | | +0.8 | +0.5 | +0.4 | +0.4 |
| 6 | | | | | | +0.2 | +0.1 | +0.1 |
| 7 | | | | | | | 0 | +0.8 |
| 8 | | | | | | | | |

Avg. % dev. in this portion 2.2 %, whole assembly : 1.1 %

| | |
|---|---|
| +8.0 | % INCREASE MACROSCOPIC CROSS-SECTIONS (relative to unperturbed) |

Fig. IV-10 : % DEVIATIONS IN MACROSCOPIC X-SECTIONS IN A PU-RECYCLE ASSEMBLY.

| | | | | | | | |
|---|---|---|---|---|---|---|---|
| +8.0 | +5.9 | +5.1 | +4.6 | +4.2 | +3.9 | +3.8 | +3.8 |
| | +4.2 | +3.4 | +2.9 | +2.5 | +2.1 | +2.0 | +2.0 |
| | | +2.6 | +2.0 | -0.1 | -3.5 | -3.6 | -3.6 |
| | | | -1.0 | -7.2 | +6.4 | +5.1 | +3.6 |
| | | | | +6.4 | +3.8 | +2.3 | +1.9 |
| | | | | | +0.8 | +0.4 | +0.4 |
| | | | | | | +0.0 | +1.6 |
| | | | | | | | |

Avg. % Dev. $UO_2$ : 1.7 %

% Dev. Mix :+2.8 %

| + 8.0 | % INCREASE IN MACROSCOPIC CROSS-SECTIONS. (relative to unperturbed). |
|---|---|

In a similar way, but making now use of both Figs. IV-4 and 6; the % deviations in macroscopic X-sections at each location I, J in the PU-recycle assembly were obtained.

## IV-3 DEVELOPMENT OF THE GENERALISED MND METHOD.

### 3-1) INTRODUCTION.

In the previous section a method was developed which enabled us to get the spectraleffects in 2D X - Y geometries. The method is however time consuming & involves making 1 D THERMOS calculations.

In this section we will develop a much simplier method. We will first show, based on one D, THERMOS results, that the suggested continuity of activation by M. Goldsmith and S. Stein is much more powerful than Breen emphasizes in his article on the development of his MND method, which is applied exclusively to the problem of watergappeaking.

Second we will show that it is possible to obtain macroscopic & microscopic MND cross-sections with unit cell codes such as LASER and LOCALUX, and that they are not exclusively intrinsic to the SOFOCATE-LEOPARD code which calculates the MND cross-sections.

Afterwards we will develop a method for the calculation of the avg.$\left(\frac{1}{v}\right)_{GRAD}$ of the gradientspectrum at a watergap and a method for the calculation of the avg.$\left(\frac{1}{v}\right)_{GRAD}$ of the gradientspectrum at the $UO_2$-MIXED OXIDE interface or any other 2 difficult fuels interface, with any other unit cell codes such as LASER & LOCALUX.

The results are compared to calculations made with the THERMOS code and the LEOPARD code,

Finally the results are blended to a new Generalised Mixed Number Density (GMND) Method for the calculation of powerpeaking at both watergaps & $UO_2$- mixed oxide

interface (or any other multifuel boundary).

## 3-2) THE CONTINUITY OF ACTIVATION OF A $1/v$ ABSORBER AND ITS IMPORTANCE FOR THE PREDICTION OF POWERPEAKING.

In the standard 1 thermal group calculations, the cross-sections were obtained from a unit-cell calculation. Since one unit cell has been isolated, the intrinsic assumption has been made that the reactor consists of an infinite array of such unit-cells. Therefore no coupling between other regions such as the watergap, other fuels ($UO_2$-MIXED OXIDE) are assumed.

The normalised activation of a 1/V absorber with a unity 2200 m/sec absorption-cross-section (normalised activation = $\int \phi(r,E)\, 1/v\, dE \Big/ \int \phi(r,E)\, dE$ )

will therefore be discontinuous in the standard model.

Because of spectrumcoupling it is not surprising to find a continuity in the activation in an actual case, such as a conventional assembly consisting of $UO_2$ cells & watergaps, and a PU-recycle with 2 fuels Mixed-Oxide & $UO_2$ & a watergapregion.

Fig. IV-11, shows the results that were obtained with the 1-D THERMOS calculation on a circulized conventional & PU-recycle assembly. (see Chapter III ).

It is thus clearly noticed that the activation of a $1/v$ absorberfoil is continuous in both assemblies. The effect in the PU-recycle is particularly striking.

In a real physical model this continuity should appear, therefore instead of writing the usual diffusion eq.

$$D^i \nabla^2 \phi^i(E) - \Sigma_a^i \phi^i(E) + S^i = 0 \qquad (4\text{-}14)$$

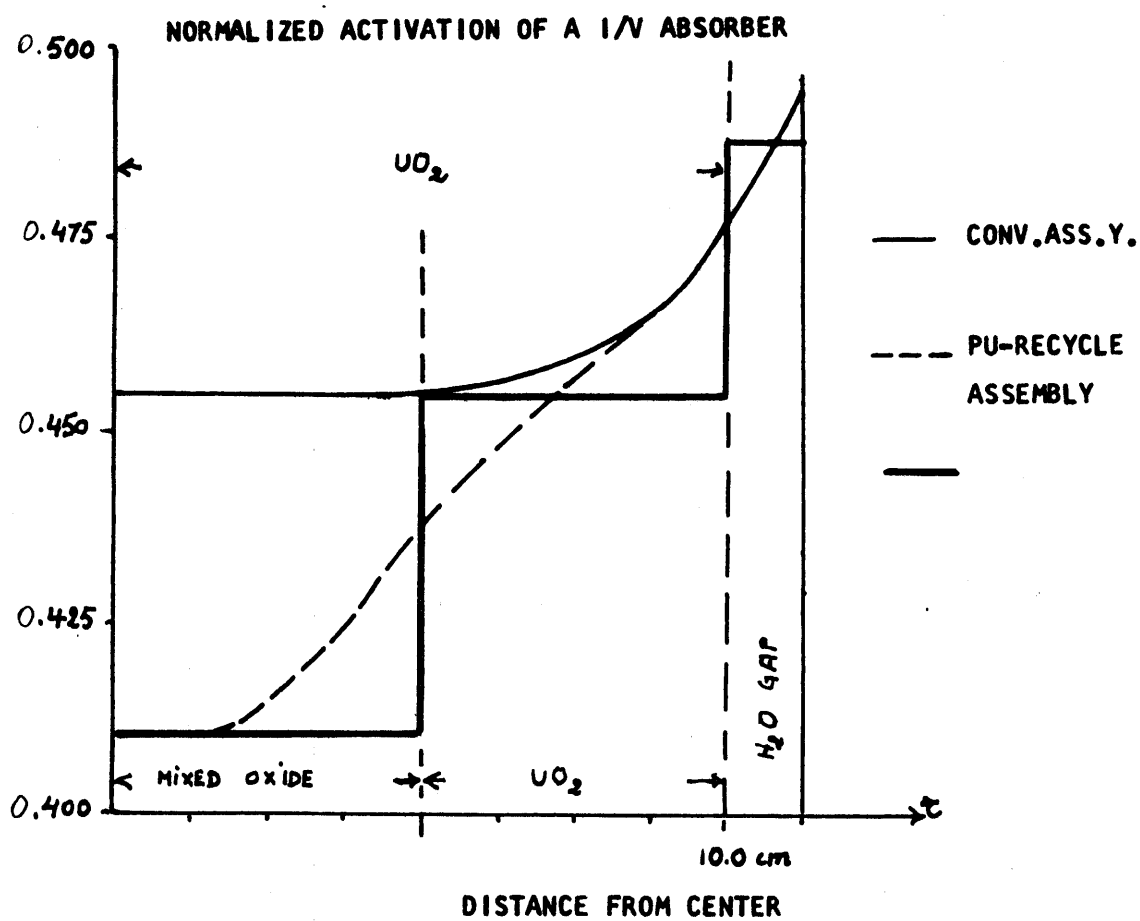


FIGIV- 11 NORMALIZED ACTIVATION OF A I/V ABSORBER IN A CONVENTIONAL AND PLUTONIUM RECYCLE ASSEMBLY MODEL

with the boundary condition at an interface :

$$\phi^1(R_1) = \phi^2(R_1)$$
$$D_1 \nabla\phi^1(R_1) = D_2 \nabla\phi^2(R_1) \qquad (4\text{-}15)$$

where the activation of a 1/V absorber would be

$$\overline{\left(\frac{1}{v}\right)}_1 \bar{\phi}^1(R_1) \neq \overline{\left(\frac{1}{v}\right)}_2 \bar{\phi}^2(R_1) \qquad (4\text{-}16)$$

or

$$n^1(R_1) \neq n^2(R_2) \qquad (4\text{-}17)$$

(where n is the neutrondensity.)

we could write : the boundary condition

as

$$\int_0^{E^*} \frac{1}{v}\, \phi^1(E,R_1)\,dE = \int_0^{E^*} \frac{1}{v}\, \phi^2(E,R_1)\,dE \qquad (4\text{-}18)$$

or $n_1 = n_2(R_1)$

$$\& \quad \int_0^{E^*} D_1\, 1/v\, \nabla\phi^1(E,R_1)\,dE = \int_0^{E^*} \frac{1}{v} D_2\, \nabla\phi^2(E,R_1)\,dE \qquad (4\text{-}19)$$

Since the usual diffusion eq. with 1 thermal group for region i is :

$$D^i \nabla^2 \phi_i(\bar{r}) - \Sigma_a^i\, \phi^i(\bar{r}) + S^i(\bar{r}) = 0 \qquad (4\text{-}20)$$

where $D^i, \Sigma_a^i$ have been averaged over the unperturbed spectrum of this region, we can write since $\phi^i(\bar{r}) = \dfrac{n^i(\bar{r})}{(1/v)_i}$, $\nabla\phi^i = \dfrac{\nabla n^i}{(1/v)_{i\,GRAD}}$ (4-21)

$$\frac{D^i_{GRAD}}{(1/v)_{i\,GRAD}} \nabla^2 n^i(\bar{r}) - \frac{\Sigma_a^i}{(1/v)_i}\, n^i(\bar{r}) + S^i = 0 \qquad (4\text{-}22)$$

So if we use, in a diffusiontheory code with 2 groups ( 1 thermal & 1 fast + epithermal) the thermal group X-sections;

$$\frac{D^i_{GRAD}}{(1/v)_{i\,GRAD}}, \quad \frac{\Sigma_a{}^i}{(1/v)_i}, \quad \frac{\nu\Sigma_f{}^i}{(1/v)_i}, \quad \frac{\Sigma_f{}^i}{(1/v)_i}$$

the code will automatically handle : $n_1 = n_2$ , $D_1 \nabla n_1 = D_2 \nabla n_2$

at an interface.

In order to clarify the use of the principle, at this point, for the calculation of the powerpeaking, it is instructive for the reader to calculate by hand to compare the normalised powerdistribution of a simple geometry such as 2 different infinite slab media in contact with each other (e.g. $H_2O$ - $UO_2$ interface or MIXED-OXIDE $UO_2$ interface), using the regular 1-group diffusioneq. (4-14) & boundarycondition (4-15) & the eq. (4-22) with the B.C. (4-19).

It is very easy to show that for such a simple case the normalised power at the peak location X = 0 is given by :

$$P^i_{REG}(x=0) = 1 + \frac{1}{1 + L_j/L_i}\left(\frac{S_j}{S_i}\frac{\Sigma_{ai}}{\Sigma_{aj}} - 1\right) \qquad (4\text{-}23)$$

and with the model of eqs. 4-19 & 22 by :

$$P^i_{MND}(x=0) = 1 + \frac{1}{1 + \bar{L}_j/\bar{L}_i}\left(\frac{S_j}{S_i}\frac{\Sigma_{ai}}{\Sigma_{aj}}\frac{(1/v)_j}{(1/v)_i} - 1\right) \qquad (4\text{-}24)$$

Thus if the spectrum in J is softer than in i,

$$P^i_{MND}(x=0) > P^i_{REG}(x=0)$$

For a mixed-oxide; $UO_2$ fuels the $(1/v)^{UO_2} / (1/v)_{Mix}$ was found to be 1.145, whereas the $(1/v)^{UO_2} / (1/v)_{H_2O}$ was about 1.083

The differences in powerpeak are thus significant.

Spectrumhardening & softening-effects can thus efficiently be treated with the 1 group model of equations (4-19) and (4-22).

In Breen's article it is stated that the application of "only the 1/V continuity is insufficient & gives essentially the same results as the regular method. The reason is that in the cases of particle interest before PU-recycling the differences in spectrum in unperturbed $UO_2$ fuels (e.g. interface of 2.5. & 3.5 w/o U235) is very small, so $(1/v)_1 \cong (1/v)_2$ in those cases.

In the case of a watergap, $(1/v)_{H_2O}$ is taken to be equal to $(1/v)_{UO_2}$, since the same spectrum from LEOPARD is used as well in the $UO_2$ fuel cell as in the water.

Therefore in Breen's model the application of the activationcontinuity alone for the prediction of watergap-peaking gives essentially the same results as the regular method; which is thus generally an oversimplified model.

Breen however goes one step further & argues that the diffusionconstant should not be weighted over a fluxspectrum Ø (E), but over a gradient-spectrum $\nabla\phi(E)$

As Breen noticed with his SLOP-1 calculations, this was found to be the case, and in Chapter III it was also observed that this is a more exact definition.

It was furthermore found that the gradientspectrum approaches a Maxwellian spectrum at the watergap.

Therefore in Breen's MND model for the calculation of <u>watergap peaking</u>;

$$\frac{D^{i\,MAX}}{(1/v)_{MAX}} \nabla^2 n^i(\bar{r}) - \frac{\Sigma_a^i}{(1/v)_i} n^i(\bar{r}) + S^i = 0 \qquad (4\text{-}25)$$

MITLibraries
Document Services

Room 14-0551
77 Massachusetts Avenue
Cambridge, MA 02139
Ph: 617.253.2800
Email: docs@mit.edu
http://libraries.mit.edu/docs

# DISCLAIMER

**MISSING PAGE(S)**

Page 120

However we have :

$$\overline{\left(\frac{1}{v}\right)}_{CELL} = \frac{\int_0^R d\bar{r} \int_0^{E^*=1.855} \frac{1}{v}\,\phi(\bar{r},E)\,dE}{\int_0^R dr \int_0^{E^*=1.855} \phi(r,E)\,dE} =$$

$$\frac{\int_0^R d\bar{r} \int_0^{1.855} N(\bar{r},E)\,dE}{\int_0^R d\bar{r} \int_0^{1.855} v\,N(\bar{r},E)\,dE} = \frac{1}{\bar{v}_{CELL}} \qquad (4\text{-}27)$$

Since $\bar{v}_{CELL}$ as well as a pointwise velocity V in the unit cell is calculated in the LASER & LOCALUX codes, it is thus possible to get the MND X-sections from

$$\Sigma_a\,\bar{v}_{CELL}\ ,\quad \nu\Sigma_f\,\bar{v}_{CELL}\ ,\quad \Sigma_f\,\bar{v}_{CELL} \qquad (4\text{-}28)$$

Thus by multiplying the spectrum cell averaged cross-sections with the average thermal velocity $\bar{v}_{CELL}$ of the cell, the MND X-sections can be obtained.
So the only thing missing in order to obtain all the MND X-sections is to find the $1/v$ of the gradient spectrum at the water & the $(1/v)_{GRAD}$ at the mixed-oxide, $UO_2$ interface.

## 3-4) THE METHOD TO GET $1/v$ OF THE GRADIENTSPECTRUM AT THE WATERGAP AND TO GET THE GMND X-SECTIONS.

The gradient at each point $\bar{r}$, and energy E is defined as :

$$\nabla\Phi(\bar{r},E) = \lim_{\Delta r \to 0} \left[\frac{\Phi(E,\bar{r}+\Delta\bar{r}) - \Phi(\bar{r},E)}{|\Delta\bar{r}|}\right] \qquad (4\text{-}29)$$

Considering the unit cell consisting of fuel, clad & moderator, EQ 4-29 may be approximated as :

$$\nabla \phi_{H_2O}(r,E) \cong \frac{\phi(R_{CELL},E) - \overline{\phi(E)}^{CELL}}{\Delta r} \qquad (4\text{-}30)$$

where $\phi(R_{cell}, E)$ is the flux at any energy E at the edge point in the moderator (point 12 in LASER & LOCALUX), or simply the Ø avg.flux in the moderator, and $\overline{\phi}(E)^{CELL}$ is the whole cell avgd fluxspectrum =

$$\overline{\phi}(E)^{CELL} = \int_{CELL} dr \int_0^{1.855} \phi(r,E)\, dE \qquad (4\text{-}31)$$

which is also printed out by LASER or LOCALUX.

$\Delta$ r is an arbitrary value, e.g. taken as the distance of the center of the first unitcell to the center in the watergap.

The $(1/v)_{GRADIENT}$ is now difined as :

$$\left(\frac{1}{v}\right)_{GRAD.\,H_2O} = \frac{\int_0^{1.855} 1/v\, \nabla\phi(E)\, dE}{\int_0^{1.855} \nabla\phi(E)\, dE} \qquad (4\text{-}32)$$

or with EQ (4-30) ; (4-27) & (4-33) :

$$\left(\frac{1}{v}\right)_{GRAD.\,H_2O} = \frac{1}{\overline{v}_{GRAD.\,H_2O}} \cong \frac{\frac{1}{\overline{v}(R)}\overline{\Phi}(R) - \frac{1}{\overline{v}_{CELL}}\overline{\Phi}_{CELL}}{\overline{\Phi}(R) - \overline{\Phi}_{CELL}} \qquad (4\text{-}33)$$

$$= \frac{\bar{N}(R) - \bar{N}_{CELL}}{\bar{\Phi}(R) - \bar{\Phi}_{CELL}} \qquad (4\text{-}34)$$

$$= \frac{1/v_{MOD} - 1/v_{CELL} \cdot \bar{\Phi}_{CELL}/\bar{\Phi}_{MOD}}{1 - \bar{\Phi}_{CELL}/\bar{\Phi}_{MOD}} \qquad (4\text{-}35)$$

where N is the neutrondensity.

In absence of the edge point in the moderator, the moderator avgd. values can be used

Therefore EQS (4-33) can be us ed to obtain an approximate value of $(1/v)_{GRAD}$ of the gradientspectrum at the FUEL CELL-WATER interface.

We will call the macroscopic X-sections multiplied with $\bar{v}$, $\bar{v}_{GRAD}$ the GENERALISED MIXED NUMBER DENSITY CROSS-SECTIONS (GMND).

Thus a method has been developed, for the calculation of the GMND X-SECTIONS with LASER or LOCALUX, or any other unit cell code which prints out the fluxes of the cell, the flux at the edge of the moderator (or eventually over the whole moderator), or the moderator disadvantage factors, the avg. velocity of the edge moderatorpoint (or eventually the whole moderator).

It may be observed that in our model :

1) the diffusionconstant D is not averaged over the gradient-spectrum; only the gradient $(1/v)_{GRAD}$ is used. The reason is that codes generally do not calculate the gradient-spectrum, & would therefore require a change,

but the most important reason is that the difference between a model in which the gradient spectrum is assumed to be the flux-spectrum & the MND model in which the gradientspectrum is used, is not only in the energy averaging of the diffusionconstant but mainly in the difference : $\overline{\left(\frac{1}{v}\right)}_{CELL}$ & $\overline{\left(\frac{1}{v}\right)}_{GRAD}$ .

As a whole the knowledge of the diffusion constant is rather vague, since no general expression exists for the diffusion constant, coming from general transporttheory; & no general gradientspectrum exists.

2) It has not been assumed that the gradientspectrum is Maxwellian.
This is certainly more general, since now in our model, the $(1/v)_{GRAD.\,H_2O}$ can vary from case to case, in contrast with Breen's MND method, in which once the temperature of the moderator is fixed, every gradientspectrum is assumed to be the same.

3) It has not been assumed that the $\overline{\left(\frac{1}{v}\right)}$ in the $H_2O$ = $\overline{\left(\frac{1}{v}\right)}_{CELL}$.
Therefore the MND X-Sections in the water are obtained by multiplying the regular X-sections with $\bar{v}_{H_2O}$ & not with $\bar{v}_{CELL}$.

As far our GMND is ready for the calculation of powerpeaking near a watergap. In the next section our GMND method is further extended to the MIXED OXIDE / $UO_2$ INTERFACE;

## 3-5) THE METHOD TO GET THE $(1/v)_{GRAD}$ OF THE GRADIENTSPECTRUM AND GMND X-SECTIONS AT THE MIXED-OXIDE / $UO_2$ INTERFACE.

With respect to the GMND macroscopic X-Sections, the method has already been indicated in section 3-3.

Neglecting again averaging of the diffusionconstant D over a gradient-spectrum, the problem is to find $1/v_{\text{GRADIENT MIXED OXIDE}/UO_2}$ interface from two <u>unit-cell</u> runs.

However it may be observed that in all practicle applications, powerpeaking is avoided, therefore the average power in a mixed oxide fuel will be very close to the avg. power in the $UO_2$ fuel.

<u>Thus, assuming an equal power in the MOx and $UO_2$</u> , the gradient can be approximated by :

$$\nabla\phi(E)_{MOx-UO_2} \cong \frac{\bar{\Phi}^{CELL}_{UO_2}(E) - \bar{\Phi}^{CELL}_{MOX}(E)}{\Delta r} \qquad (4\text{-}36)$$

Thus after the same manipulations as above :

$$\left(\frac{1}{\bar{v}}\right)_{GRAD\ MOx-UO_2} = \frac{1}{\bar{v}_{GRAD\ MOX-UO_2}} = \frac{\frac{1}{\bar{v}_{UO_2}}\bar{\Phi}^{CELL}_{UO_2} - \frac{1}{\bar{v}_{MOX}}\bar{\Phi}^{CELL}_{MOX}}{\bar{\Phi}^{CELL}_{UO_2} - \bar{\Phi}^{CELL}_{MOX}} \qquad (4\text{-}37)$$

Thus it is possible to get an approximate value of the 1/v of a gradientspectrum at any-different fuel interface by making, two sperate unit cell runs & EQ (4-37). Since all the codes print out $\bar{v}_{CELL}$ & the flux $\bar{\Phi}_{CELL}$ , the method can be applied with any unit cell code.

## <u>3-6) COMPARISON BREEN'S MND X-SECTIONS & OUR GMND X-SECTIONS. AN EVALUATION OF THE ASSUMED GRADIENT SPECTRA.</u>

### <u>3-6)-a) INTRODUCTION.</u>

In the preceeding section, we have developed a method to calculate the generalised MND X-sections with codes as LASER, LOCALUX or others, for both applications of watergap powerpeaking and mixed oxide / $UO_2$ interface powerpeaking

(or any other different fuel interface).

The method to obtain these GMND X-sections is entirely different from Breen's method built in the LEOPARD code. It should therefore be useful to compare the GMND X-sections obtained with LEOPARD.

One particular difficulty for the comparison is that LASER has a cut-off at 1.855 eV, & LEOPARD at 0.625 eV.

Since the LASER code only prints out the macroscopic cross-sections at 1.855 eV a direct comparison of the MND X-Sections is impossible.

However the MND X-Sections are obtained from

$$\frac{\Sigma_{SOF}}{(1/v)_{SOF}} \quad , \quad \frac{D^{MAX}}{(1/v)_{MAX}}$$

& with our GMND method

$$\frac{\Sigma}{1/\bar{v}_{LASER}} \quad , \quad \frac{D}{1/\bar{v}_{GRAD}} .$$

Therefore the only pertinent information for the comparison is :

$$(1/v)_{WW} \text{ or } (1/v)_{SOF} \ \& \ (1/\bar{v})_{LASER} \quad \text{both at 0.625 eV}$$

$$D_{MAX} , D_{W.W.} , (\overline{1/v})_{MAX} , (1/\bar{v})_{GRAD,LASER}$$

at 0.625 eV.

Fortunately LASER prints out values for $\bar{v}_{CELL}$ , $\bar{v}_{MOD}$ , $\bar{\phi}_{CELL}$ , $\bar{\phi}_{MOD}$, $D_{LASER}$ for both cut-offs at .625 eV an 1.855 eV.

Therefore a direct comparison of our GMND 1/V values (obtained with LASER) & Breen's 1/V values (obtained from LEOPARD) is possible.

Particular attention has been paid to make the LEOPARD & LASER imputs identical, such that no other effects could disturb the comparison.

## 3-6)b) COMPARISON OF THE MND & GMND X-SECTIONS FOR WATERGAP POWERPEAKING CALCULATIONS.

3 cases were examined :

- the regular $UO_2$ (4 W/O U235) fuel at a $H_2O$ gap.
- the regular MIXED OXIDE fuel (4 W/O $PUO_2$ - nat $UO_2$) at a $H_2O$ gap.
- the regular MIXED-OXIDE fuel but with the PU-240 removed.

The first case consits of standard fuel & a watergap, therefore we should expect, that our GMND values as determined with LASER at a cut off of 0.625 be very close to the MND values as obtained with LEOPARD; since Breen's MND method was developed for such standard cases.

The second case is already much more stringent, since the spectrum in a mixed oxide fuel is much harder and we should expect Breen's method, with respect to his assumption of a Maxwellian gradient spectrum to break down.

In the third case we would expect the same as the second, however now since we removed PU 240 with a giant resonance at 1.0 eV; some information with respect to the importance of the 1.855 eV cut-off should become apparent.

Table IV-1, shows the results of the comparison of the 2 methods.

In order to obtain the 1/V of the gradient spectrum at the FUEL/$H_2O$ interface, 2 methods were used with LASER, 1.855 eV cut off :

The first is using the velocity & fluxvalues averaged over the moderator in the cell & the second using the velocity & fluxvalues in the outermost edgepoint of the moderator (pt 12 in LASER).

The first observation that we can make, after comparison of the divisionfactors $1/v$ WIGNER WILKINS & $1/v$ LASER at 0.625 eV, is that <u>in all cases</u>, those factors are very close. The only difference comes from the intrinsic differences in the code such as LEOPARD is a zero dimensional code using the Wigner-Wilkins

equations for the calculation of the spectrum.

Therefore our method, if used with a cut-off at 0.625 eV would give the same MND macroscopic X-sections $\Sigma_{MND}$ . If we use the cut-off at 1.855 eV, the values will evidently differ, but this is only due to the intrinsic cut-off & has nothing to do with the MND or GMND method.

Another remark that we can make is that in Breen's MND method the (1/V) in the $H_2O$ is the same as for the fuel cell; whereas in our GMND method they are different, as they should be. However the difference is so small (the order of 2 %) that with fair confidence the same 1/V values could be used.

With respect to the gradient-spectrum, near the watergap, it is this noticed that the $V_{GRAD}$ is much smaller than the $V_{CELL}$ in all cases & with both methods. However in Breen's MND Nodel, $\left(\frac{1}{v}\right)_{GRADIENT}$ is the same in <u>all</u> cases and is 0.63443.

This is due to his assumption that the gradientspectrum is a Maxwellian in all cases, which differs only when the temperature of the moderator is varied. On the contrary with our method, different values for $\frac{1}{v}$ GRAD are found according to the fuel in contact with the water. E.g. in the case of the Mixed oxide fuel it is observed that the avg. velocity $V_{GRAD}$ is greater than the avg. velocit $V_{GRAD}$ in the $UO_2$-/ $H_2o$ interface case, which is to be expected physically & the influence of the cut-off is also remarkebly.

It is very interesting to note that in case of the standard fuel $UO_2/H_2O$ interface, our GMND method gives values which are very close to Breen's MND method. Which proves not only the validity of our method, but also Breen's assumption that in case of conventional fuel/$H_2O$ interfaces the gradientspectrum approaches a Maxwellian spectrum.

Another argument is that now the $(1/V)_{GRAD}$ for a cut-off at .625 eV is very close to the value with a cut-off at 1.855 eV, which is to be expected with a spectrum close to a Maxwellian, since the Maxwellian spectrum drops off very quickly beyond .20 eV. Comparison of the gradient avg.velocities (or its reciprocal) in case of the MOX fuel with our method proves that the gradientspectrum is much harder than a Maxwellian.

From comparison of the colums of $(1/V)_{GRAD}$) taken with the moderatoraveraged flux & velocity values at 1.855 eV, & the $(1/V)_{GRAD}$ taken at the edge of the moderator, it is seen that both methods agree very well. Therefore both methods can be used, maybe with same slight preference to the moderatoredge, since it will be somewhat more conservative.

From comparison of $D_{WW}$ & $D_{LASER}$ at 0.625 eV, it is noticed that the values disagree by about 5 %, which is mostly due to the use of the more accurate Nelkin scatteringkernel for $H_2O$ in the LASER code.

The values of the diffusionconstants averaged over a Maxwellianspectrum are seen to be a 15 % to 20 % lower than the Wigner-Wilkins averaged values. Therefore, strictly speaking, the diffusionconstant should be averaged over the gradientspectrum. Since this would require a basic modification in codes like LASER, the diffusionconstant is our method averaged over the cell spectrum. (in the GMND method however D is multiplied by $V_{GRAD}$).

Although this is recognized as a drawback there are many reasons to accept this shortcoming. The first argument is that in Breen's model the assumption of a Maxwellian spectrum breaks down anyway, the second is that the diffusionconstant is the least sensitive parameter, the third is that our method for obtaining a gradient-spectrum is by itself an assumption, the forth that the influence of $(1/V)_{GRAD}$ instead of $(1/V)_{CELL}$ is as big or even bigger than the averaging over the spectrum and the fifth is that the knowledge of the diffusionconstant is

the most inaccurate through its basic assumptions from transporttheory & the inaccuracies of the scattering kernels; and the last argument is that although it is possible to get the gradient-spectrum at the $H_2O$-gap approximately with our method from only one unit cell calculation, the same cannot be said for the gradient spectrum at e.g. the MIXED-OXIDE/$UO_2$ interface.
Therefore, since most of the gradient-effects are already taken care of by the calculation of $(1/V)_{GRAD}$ or V Gradient, the proposed GMND method in its simpliest format (without special averaging of the diffusion-constant over the different spectra) should be as accurate as Breen's MND method & does not require any changes in the codes.

TABLE IV-1, COMPARISON OF DIVISIONFACTORS FOR BREEN'S MND X-SECTIONS (LEOPARD) & OUR GMND X-SECTIONS (LASER), FOR THE CALCULATION OF POWERPEAKING AT A FUEL / $H_2O$ INTERFACE.

| CASE : | BREEN'S MND (LEOPARD) | | | | OUR GMND (LASER) | | | | | |
|---|---|---|---|---|---|---|---|---|---|---|
| FUEL/$H_2O$ INTERFACE | $(\overline{\frac{1}{\xi}})$ WIGNER WILKINS .625 eV cut off | $(\overline{\frac{1}{\xi}})$ MAXW. (.625eV) or approx. also 1.855 eV | D WIGNER WILKINS (.625 eV) | D MAXW. (.625 eV) | $(1/\xi)$ LASER .625 eV cut off | $(1/\xi)$ LASER 1.855 eV | $(1/\xi)$ GRAD. AT $H_2O$ INTERFACE MOD. AVG. 'D .625 eV | MOD. AVG. 'D 1.855 eV | MOD. EDGE 1.855 eV | D LASER (.625 eV) |
| 4 w/o $UO_2$ | .514403 | .634443 | .402488 | .338317 | .502083 | .433990 | .677031 | .65485 | .660786 | .38547 |
| $H_2O$ at $UO_2$ | .514403 | .634443 | .323520 | .265228 | .509606 | .442008 | .677031 | .65485 | .660786 | |
| 4 w/o MIXOX. | .48587 | .634443 | .353405 | .291208 | .482649 | .379291 | .50941 | .441622 | .450996 | .33623 |
| $H_2O$ at MIXOX. | .48587 | .634443 | .301922 | .249076 | .485296 | .384600 | .50941 | .441622 | .450996 | |
| 4 w/o MIXOX. without PU 240 | .488128 | .634443 | .356733 | .293489 | .483270 | .374830 | .51080 | .50001 | .50880 | .33992 |
| $H_2O$ at MIXOX. | .488128 | .634443 | .301976 | .249000 | .485910 | .383318 | .51080 | .50001 | .50880 | |

## 3-6-c : COMPARISON OF THE MND & GMND X-SECTIONS FOR MIXED OXIDE/ $UO_2$ OR FUEL / FUEL INTERFACE POWERPEAKING CALCULATIONS.

Using the same unit cell calculations as above 3 cases were examined :

- $UO_2$ / MIXED OXIDE - interface
- $UO_2$ / MIXED OXIDE w.o PU 240 - interface
- MOX / MOX (w/o PU 240), interface.

Using the standard MND-LEOPARD outputs , & the LASER outputs together with the EQS. (4-27), (4-38), Table IV-2 was prepared.

From this table it is again noticed that in the unit cells both MND methods agree for a cut-off at 0.625 eV. With respect to the gradient-spectrum at the interface, Breen's MND method breaks down, since it is noticed that the gradientspectra, more realistically obtained with our method, is not as soft as a Maxwellian.

In case of the w/o Mix-Oxide Fuel without PU 240/ 4 w/o Mix-Oxide fuel interface, the particular influence of the 1.855 eV cut-off is noticible.

In short Breen's MND method with the assumption for a maxwellian gradient spectrum at the interface is unrealistic in PU-recycle applications, but will be remarkably close in conventional applications.

## 3-7) EVALUATION OF BREEN'S MND & OUR GMND METHOD THROUGH COMPARISON OF 1/V, 1/VGRAD WITH THERMOS.

The THERMOS 35 group code has been used to calculate the pointwise average gradientvelocity $V_{GRAD}$ or ( $1/\bar{v}_{GRAD}$) & the pointwise average fluxvelocity $V_{CELL}$ or ( $1/\bar{v}$)$_{CELL}$.

Since THERMOS doesn't calculate the gradient $\nabla\phi$ explicitly, the finite difference formula (4-29) & more directly :

$$\frac{1}{\bar{v}_{GRAD}} = \frac{N(\tau_{k+1}) - N(\tau_k)}{\Phi(\tau_{k+1}) - \Phi(\tau_k)}$$

was used.

TABLE IV -2, COMPARISON BETWEEN BREEN'S MND PARAMETERS & OUR GMND PARAMETERS FOR THE CALCULATION OF POWERPEAKING AT FUEL/FUEL INTERFACES.

| CASE : | BREEN'S MND (LEOPARD) | | | | OUR GMND (LASER) | | | | |
|---|---|---|---|---|---|---|---|---|---|
| FUEL 1 / FUEL 2 | $(\overline{1/v})_{WW}$ .625 eV | $(\overline{1/v})_{MAX}$ .625 eV or also 1.855 eV | $D_{WW}$ .625 eV | $D_{MAX}$ | $(1/v)_{LASER}$ .625 eV | $(1/v)_{LASER}$ 1.855 eV | $(1/v)_{GRADIENT}$ AT FUEL/ FUEL .625 eV | .1.855 eV | D LASER .625 eV |
| 4 w/o MOX | .48587 | .634443 | .353405 | .291208 | .482649 | .50941 | .51875 | .49849 | .33623 |
| 4 w/o $UO_2$ | .514403 | .634443 | .402488 | .338317 | .502083 | .433990 | .51875 | .49849 | .38547 |
| 4 w/o MOX wo PU 240 | .488128 | .634443 | .356733 | .293489 | .483270 | .374830 | .51995 | .51768 | .33992 |
| 4 w/o $UO_2$ | .514403 | .634443 | .356733 | .338317 | .502083 | .433990 | .51995 | .51768 | .32547 |
| 4 w/o MOX wo PU 240 | .488128 | .634443 | .356733 | .293489 | .483270 | .374830 | .49465 | .32080 | .33992 |
| 4 w/o MOX | .485870 | .634443 | .353405 | .291208 | .482649 | .50941 | .49465 | .32080 | .33623 |

Fig IV-12, shows the results of the comparison between the 1/V , $1/v_{GRAD}$ pointwise values obtained from THERMOS & the values obtained with BREEN'S MND model (extrapolated to 1.855 eV) & our GMND model, in a conventional circulized assembly.

As a first observation, it is thus indeed seen from THERMOS, that the average velocity of the flux-gradient is smaller than the average velocity of the flux & as a second remark it is noticed that the 1/V & $1/v_{GRAD}$ values of both Breen's MND model & our GMND model are very close. However our model follows the 1/V curve, a little bit closer since now the 1/V in the water was not taken to be the same as in the cell.

This Breen's MND model & our GMND model give nearly identical 1/V parameters, for conventional applications.

Fig. IV-13, shows the results for a PU-recycle assembly.

Again Breen's MND & our GMND have the same 1/V values for the fluxspectra (except in the $H_2O$-gap).

For the 1/V GRAD of the fluxgradient-spectra however it is observed that our GMND method gives much better agreement with the THERMOS calculations, which is particularly important for PU-recycle applications since large fluxgradients exist, therefore the $\frac{D}{(1/v)_{GRAD}} \nabla^2 n$ term in the GMND diffusionequation (EQ-39) or the MND diff, EQ (4-25) has a greater influence on the powerdistribution.

$$\frac{D^i}{\frac{1}{\bar{v}_{GRAD}}} \nabla^2 n^i(\bar{r}) - \frac{\Sigma_a^i}{\frac{1}{\bar{v}_i}} n^i(\bar{r}) + S = 0 \qquad (4\text{-}39)$$

$$\frac{D^{MAX}}{(\frac{1}{v})_{MAX}} \nabla^2 n^i(\bar{r}) - \frac{\Sigma_a^i}{(\frac{1}{v})_i} n^i(\bar{r}) + S = 0 \qquad (4\text{-}25) .$$

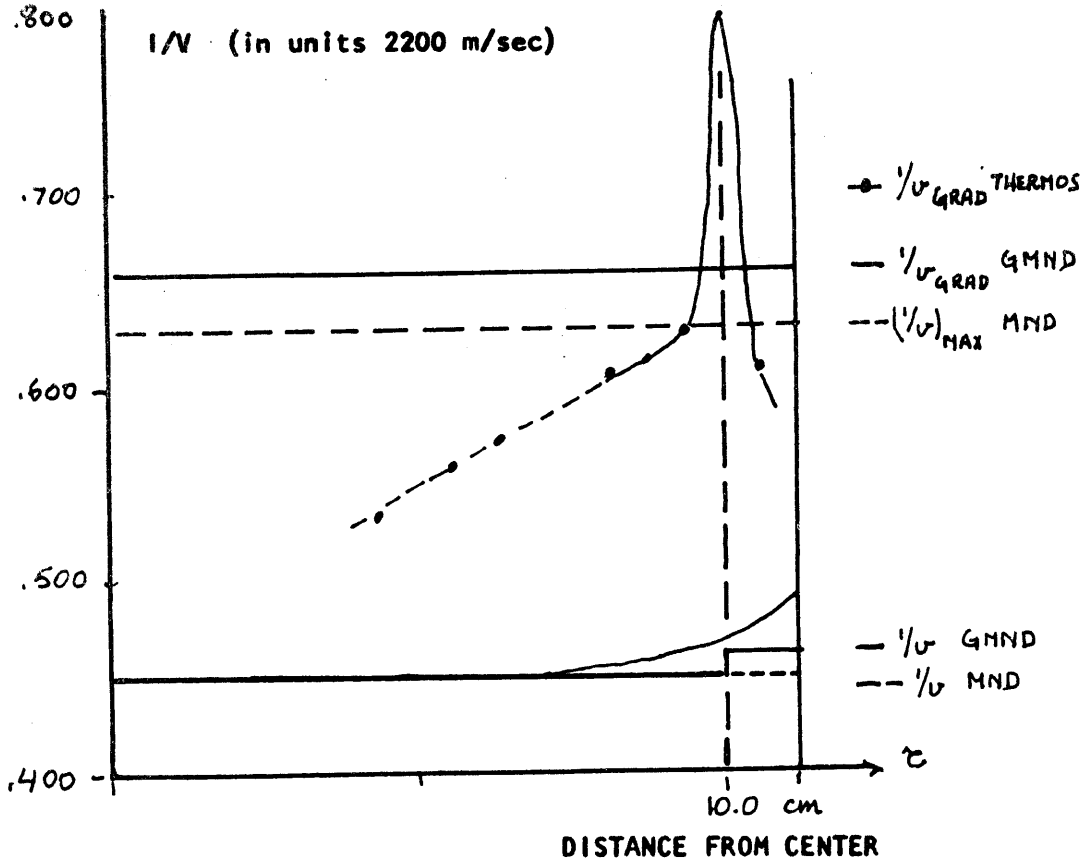


FIG IV- 12 COMPARISON I/V AND I/V GRAD THERMOS, BREEN'S MND AND OUR GMND METHOD, IN A CONVENTIONAL ASSEMBLY

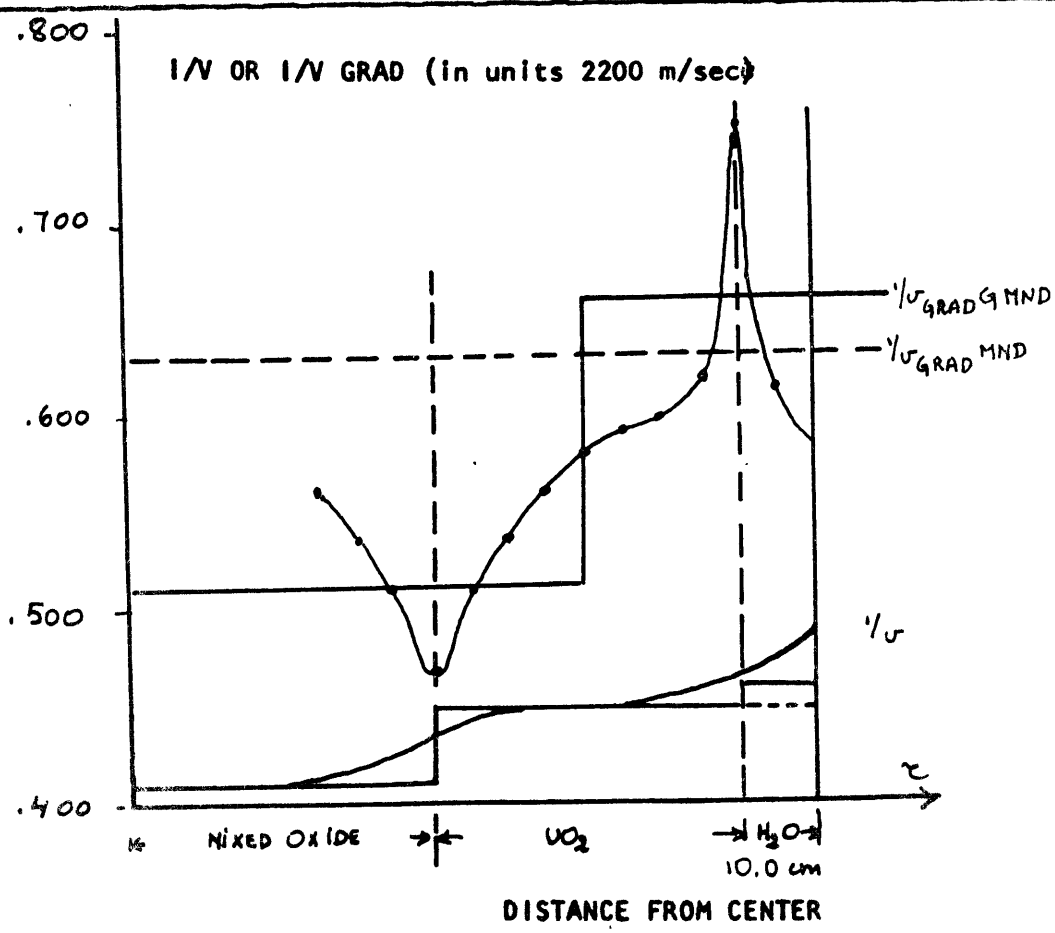


FIG IV-13 COMPARISON I/V, I/V GRAD, THERMOS, BREEN, OUR GMND IN A PU-RECYCLE ASSEMBLY

Although it is thus seen that our GMND method, is more realistic for PU-recycle applications, it is thus also noticed from Fig. IV-13, that whereas the MND method of Breen only requires 3 zones (mixed oxide, $UO_2$, $H_2O$) in which the MND macroscopic X-sections are fed, our GMND-method requires 1 more zone, namely a $UO_2$ zone with MIX-OX/$UO_2$ boundary GMND X-sections an a $UO_2$ zone with GMND X-sections of the $UO_2/H_2O$ interface (however only the $\frac{D^c}{1/v_{GRAD}}$ values differ).
It is also observed that , a continuity of activation in a gradient-spectrum ( $\frac{1}{v}\nabla\phi$ ) or continuity of $\nabla n$ is implicitly taken into account.

## 3-8) CONCLUSION.

A simple Generalised Mixed Number Density method has been developed, which can be used with more accurate unit cell codes such as LASER & LOCALUX. From comparison with Breen's MND method, it has been noticed that our GMND method & Breen's MND method are essentially identical for conventional $UO_2/H_2O$ interface applications. For Pu-recycle applications, Breen's Maxwellian gradient spectrum breaks down, whereas our GMND method describes the gradient spectrum more realistically, as has been shown with THERMOS calculations. Further refinement could be introduced in the model if the diffusion-constant is averaged over the gradientspectrum.
Especially for the $UO_2$/MIX.OX. interface this is not easy & a modification in the unit cell codes and the writing of a separate program would be necessary, which would greatly complicate the standard procedures from a practicle standpoint.

## IV -4) EVALUATION OF THE SXS AND GMND METHODS FOR THE CALCULATION OF POWERPEAKING AT WATERGAPS AND $UO_2$-MIXEDOXIDE INTERFACES.

### 4)-1 Introduction.

Three methods have been used to evaluate the use of the Spatial Cross-section Synthesis method (SXS) and the Generalised Mixed Number Density (GMND) method.

The first is through comparison of the 2 methods with the THERMOS code on a one dimensional $UO_2$ conventional assembly & a PU-recycle assembly.

Since no codes as THERMOS exist for 2 dimensions, the second evaluation consits of the inter comparison of the SXS & GMND methods & the standard method.

Finally the standard method & most practicle GMND method have been compared to an experiment & other calculations of a small inter-reflected core (19 X 19 rods) containing mixed oxide fuel in the middle, surrounded by $UO_2$, on its turn surrounded by the reflectorwater. The powerdistribution which was calculated with 2-group X-sections generated with the LASER code are also compared to the powerdistribution obtained with 2 group X-sections from a modified LEOPARD code & other Battelle calculations.

### 4)-2 COMPARISON of SXS & GMND METHODS FOR THE CALCULATION OF POWERPEAKING, WITH ONE DIMENSIONAL THERMOSCALCULATIONS.

The normalised powerdistribution (avg. value = 1.0) in a one dimensional conventional & PU-recycle assembly model (Fig. III- 1 ) was calculated with the THERMOS - 35 thermalgroup code & a cut-off at 1.855 eV, using the self-shieldingfactor homogenizationscheme.

These powerdistributions were compared with one thermalgroup diffusiontheory-calculations using PDQ-5.

Fig. III -3 shows the powerdistribution from thermal neutrons in a conventional assembly using ;

1) THERMOS-integral transport-theory (35 groups)
2) PDQ-5, 1-group fixed source diffusiontheory in which the unperturbed X-sections of a THERMOS (ssf-homogenized)unit cell were used.
3) PDQ-5, 1 group-fixed source diffusiontheory, in which the GMND X-sections were used. (which were thus obtained from the unperturbed X-sections from THERMOS unit cell after division by (1/V) values in Table IV.-1

From the comparison it is thus noticed that the GMND X-sections are a substantial improvement for the calculation of the powerdistribution & powerpeaking.
Whereas a standard calculatiom underpredicts the powerpeak by about -5%, due to spectralsoftening at the watergap. The use of the GMND X-sections reduce the error to about -0.2 %.
In the case of a PU-recycle assembly, the comparison between THERMOS & integral transport-theory & PDQ-5 diffusion theory is complicated by the different weighting schemes that can be used for the diffusionconstant, as has been investigated in Chapter III.

Several PDQ-5 calculations were made :

1) Using the regular unperturped X-Sections from the unit cell.
2) Using spatially varying X-Sections at each point, as determined from THERMOS (SXS-method, but without a need for synthesis).

3) Using GMND X-sections over 4 zones ($H_2O$, $UO_2$ / $H_2O$, $UO_2$/MIX, MIX /$UO_2$) with the $1/V_{GRAD}$ at the $UO_2$ / MIX interface as determined with our method (Table IV- 2 )

4) Using GMND X-sections over 4 zones, but now with a $1/V_{GRAD}$ at the $UO_2$/MIX interface = $1/V_{CELL}$

Fig IV - 14 shows the results.

Several observations may be made :

1) it is noticed that :

regardless the diffusionconstantscheme used, the SXS & GMND methods are a substantial improvement in the calculation of the powerpeaks at the $H_2O$-gap & MIX/$UO_2$ interface, compared to the standard calculation using unperturbed unit cell X-sections.

2) The influence of the diffusion-constant is substantial for the calculation of the powerdistribution in the mixed oxide especially. But whereas the powerpeak at the watergap is appreciably affected with the use of different diffusionconstants, the powerpeak at the MIX/$UO_2$ interface is not so much influenced. It is thus observed that in a PU-recycle assembly, a 100 % reduction in diffusionconstant, increases the powerpeak at the $H_2O$ / $UO_2$ interface by 8 %, and less than 1 % at the MIX/$UO_2$ interface, but reduces the error at the center of the assembly from 12 % to 2.5 %.

3) The Spatial varying X-section method; (which is thus essentially the SXS method without a need for synthesis) gives in both cases a very good agreement with our GMND method.

4) The influence of the $1/V_{GRAD}$ in the GMND mathod at the MIX/$UO_2$ interface can be substantial. In both cases an improvement can be noticed with the use of the more realistic $1/V_{GRAD}$ from Table IV- 2 instead of the $1/V_{CELL}$.

Since $1/V_{MAX}$ is > $1/V_{GRAD}$ > $1/V_{CELL}$ it is noticed that our method is more conservative than Breen's assumption of a maxwellian gradient.

5) At the $H_2O$-gap & using the <u>standard</u> diffusion constants (C.H.), both pseudo-SXS & GMND methods seem to overpredict the powerpeaking, compared to THERMOS. If we compare these peaks with the ANISN, transporttheory calculation ( Fig 3-5 ), (including the angular effects), it is seen that the conservatism is not unjustified.

<u>CONCLUSION.</u>

From the preceeding results it may be concluded that the developed GMND method for the calculation of powerpeaking, gives substantial improvement compared to the regular diffusiontheory practice, which underpredicts quite heavily the powerpeaks in the Yankee assemblies.

Furthermore the much simplier GMND method gives results which are essentially identical to the use of Spatialy varying X-sections as determined from THERMOS (pseudo SXS-method). Since both are different methods the very good agreement between the pseudo SXS and GMND, emphasizes the use & worth of the much simplier GMND method.

## 4)-3 INTERCOMPARISON OF THE SXS- AND GMND METHOD, ON THE 2 DIMENSIONAL YANKEE ASSEMBLIES.

In the preceeding section a direct comparison of diffusiontheory 1 thermalgroup methods was possible with the 35-thermalgroup integral transport-theory code THERMOS. Since this is impossible in 2 dimensions, we will evaluate the SXS and GMND methods through comparison with a standard calculation in which spectralcoupling effects are negleted. Since both methods are very different, the intercomparison would also add to the evaluation of both methods,

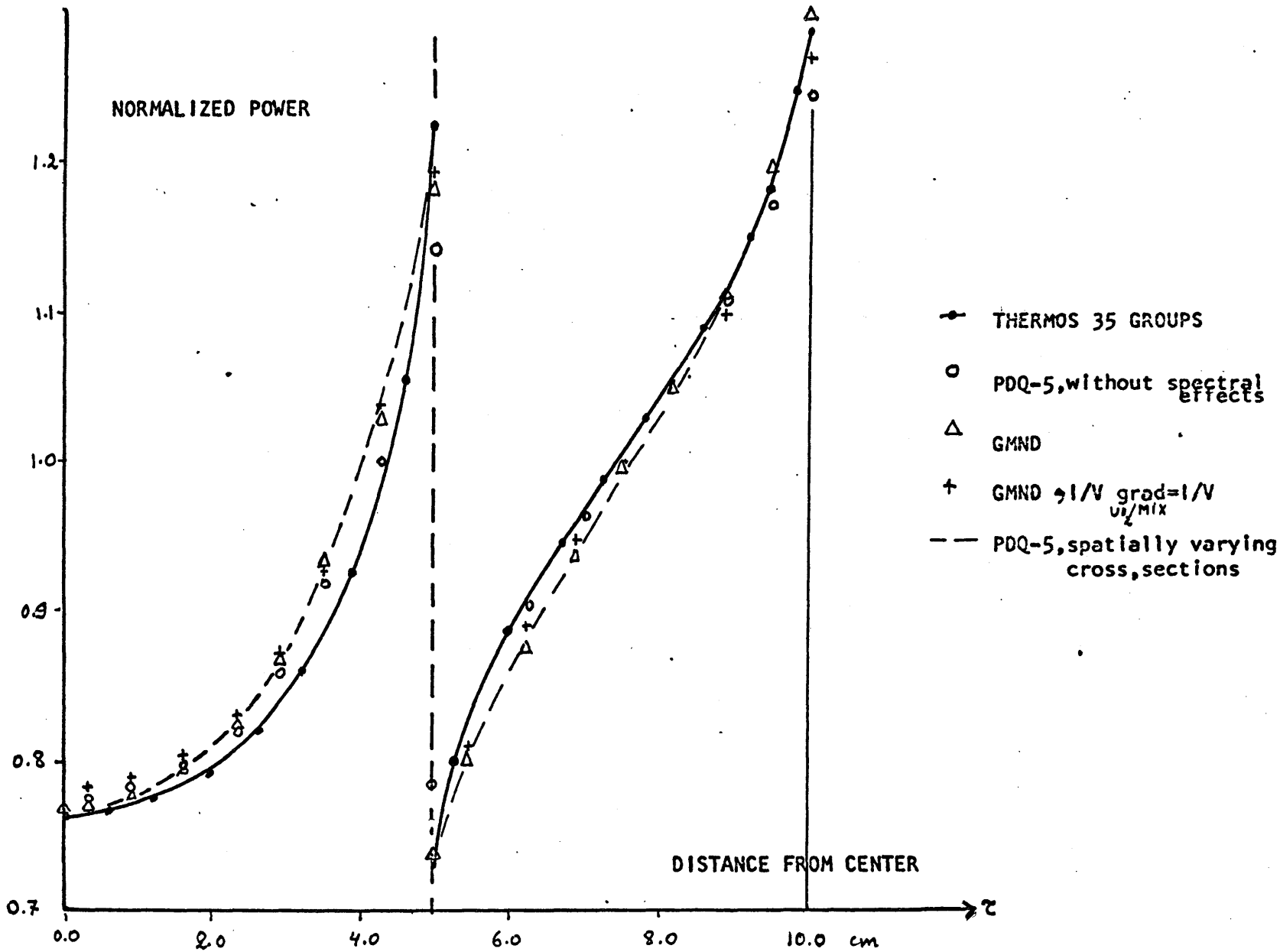


FIG IV- 14 Comparison one group methods for the calculation of powerpeaking in a Pu-recycle Assembly

& in particular to the much simplier GMND.

All the calculations were done with PDQ-5 diffusiontheory code, with 2 groups. The basic 2 group macroscopic X-sections of the 4 w/O U 235 $UO_2$ unit cell & the 4 w/o PU $O_2$-nat $UO_2$ unit cell were generated with the LASER-code using 1400 ppm B in the $H_2O$ (1 thermal group from 0-1,855 eV, 1 fast + epithermal group from 1.855 eV to 10 MeV). The diffusion-constants of the homogenized-follower, can, watergap region as well as the internal instrumentation cell were calculated from pseudotransport-cross-sections obtained with LOCALUX. 2 X 2 meshes per unit cell were used in the PDQ-5 calculations & 4 meshes in the smeared watergap. The deviations of the X-sections in the 2D assembly due to spectralcoupling effects were calculated & Synthesized with THERMOS in section 2-4 & are shown for the conventional assembly on Fig. IV-9 & for the PU recycle assembly on Fig. IV-10 . These corrections were applied to the unperturbed unit cell calculated thermal macroscopic X-sections from LASER, except the diffusionconstants which were unaltered since the deviations were too small ($< 3$ %). In this way thermal spectrumcoupled, macroscopic X-sections, for each unit cell in the 2D assembly were obtained for both the conventional & PU-recycle assemblies. Thus for the SXS-method there were 36 different compositions (diagonal symetry), which were put in the PDQ-5 code.

In case of the GMND-method, the unperturbed unit cell <u>thermal</u> macroscopic X-sections from LASER were divided by the 1/V factors displayed on Tables IV-1,2 , & the diffusionconstants by the $1/V_{GRAD}$ according to our method.

The fast & epithermal X-sections are unchanged.

For the conventional $UO_2$ assembly only 3 compositions had to be taken namely : the homogenized can, follower & watergap, the central instrumentation cell & the $UO_2$ unit cells. In the PU-recycle Assembly 5 compositions were necessary :

the region at the watergap, instrumentation cell, the $UO_2$-region with GMND X-sections of the $UO_2/H_2O$ interface (see Table IV - 1 ), the $UO_2$-region with GMND X-sections of the $UO_2$/MIX interface (Table IV-2 ) & the mixed oxide region with GMND X-sections of the MIX/$UO_2$ interface (Table IV-2 ).
In the 2 $UO_2$ regions only the thermal GMND diffusionconstant changes, & the separation of the region corresponding to $H_2O$-spectralcoupling was arbitrarily taken to be 2 fuel cells from the $H_2O$ interface.

Fig. IV - 15 shows the results of comparison of the total powerdistribution (thermal + epi & fast) for the conventional $UO_2$ assembly; in the form of percent underprediction of the power, calculated using the standard procedure (unperturbed X-sections) - relative to the calculation of the power using the Spatial X-section Synthesis SXS), & compared to the percent underprediction of the power (relative to SXS) using the GMND method.
It is thus noticed that relative to the SXS method, the GMND method greatly improves the calculation of the powerpeaking near the watergap.
The max. underprediction using the standard method is 4.3 %, in the peak rod & 2.1 % using the GMND; whereas the average absolute % deviation of the whole assemblyportion drops from 0.8 % using the standard, to 0.2 % using the GMND method.
Fig. IV- 16 shows the results of the comparison of the total powerdistribution (thermal + Epi & fast) calculations for the Plutonium Recycle Assembly-portion, using the same format as above.

FIG. IV-15 : COMPARISON STANDARD POWERCALCULATION & GMND METHOD, RELATIVE TO THE SXS METHOD IN A CONVENTIONAL $UO_2$ YANKEE ASSEMBLY PORTION.

| | | | | | | | |
|---|---|---|---|---|---|---|---|
| +4.3%<br>+2.1 | +1.6<br>+0.2 | +1.0<br>+0.1 | +1.1<br>+0.2 | +1.1<br>+0.2 | +1.2<br>+0.2 | +1.3<br>+0.2 | +1.3<br>+0.2 |
| | -0.4<br>-0.6 | -0.7<br>-0.5 | -0.6<br>-0.3 | -0.4<br>-0.1 | -0.4<br>-0.2 | -0.4<br>-0.2 | -0.4<br>-0.2 |
| | | -1.0<br>-0.6 | -0.9<br>-0.3 | -0.7<br>-0.1 | -0.7<br>-0.1 | -0.7<br>-0.2 | -0.6<br>-0.1 |
| | | | -0.7<br>-0.0 | -0.5<br>+0.1 | -0.5<br>+0.1 | -0.4<br>+0.1 | -0.3<br>+0.1 |
| | | | | -0.5<br>+0.1 | -0.4<br>+0.1 | -0.4<br>+0.1 | -0.3<br>+0.1 |
| | | | | | -0.3<br>+0.1 | -0.3<br>+0.1 | -0.3<br>+0.1 |
| | | | | | | -0.3<br>-0.0 | -0.3<br>-0.2 |
| | | | | | | | |

Standard Avg. $|\delta|$ = 0.8 %; Max. $\delta$ + 4.3 % Location 1-1, Min $\delta$ = 0.3 %
GMND Avg. $|\delta|$ = 0.2 %; Max. $\delta$ + 2.1 % Location 1-1, Min $\delta$ = 0.0

| | |
|---|---|
| + 4.3 | % UNDERPRED. IN TOTAL POWER, USING STANDARD METHOD RELATIVE TO THE SXS METHOD |
| + 2.1 | % UNDERPRED. IN TOTAL POWER, USING GMND METHOD, REL. TO SXS METHOD. |

Here in particular, it is thus observed that the GMND method greatly improves the calculation of powerpeaking near a watergap and also near the $UO_2$/ Mixed Oxide interface. The maximum overprediction of 6 % with the standard method at the location D-5, at the $UO_2$-MIX interface in the $UO_2$ rod, reduces to 2.2 % with the GMND method, in another position D-6, this overprediction drops from 3.0 % to 0.9 %. The maximum underpredictions are also greatly improved from 4.3 % at location A-1, with the standard method to 1.8 % with the GMND, & also in the mixed oxide the underprediction of 3 % at the interface using the standard method reduces to+0.9 % & 0.2 % at locations D-6 & E-5 . Only 2 particular locations seem to be worse, however they are not the peak powerlocations (see Fig. V-16 shown in the next chapter). On the average the errors using the GMND method, are reduced considerably from 1.50 % to 0.9%.

CONCLUSION.

The GMND method applied to the 2D powerdistribution calculation with 2 groups of neutrons, greatly improves & eliminates the underprediction of the power-peaking that exists in both $UO_2$ & PU-recycle assemblies when the standard unperturbed unit-cell macroscopic data are used.

Although the comparisions were done to the ( to us considered most accurate) SXS method, (since more accurate calculations are not available) the evaluation is useful in the sence that no other e.g. transport effects are present which could mask some of the effects. Since there is a very good agreement, between the SXS & GMND method, both being entirely different, both methods are thusconsidered to be a substantial improvement.

The GMND method is however much more practicle since nothing else than the results from the unit cell calculations have been used, whereas the SXS method requires other rather elaborous THERMOS calculations.

FIG. IV-16 : COMPARISON STANDARD POWERCALCULATION & GMND METHOD, RELATIVE TO THE SXS-METHOD IN A PLUTONIUM-RECYCLE ASSEMBLY PORTION.

| | | | | | | | |
|---|---|---|---|---|---|---|---|
| +4.3%<br>+1.8% | +1.8<br>+0.3* | +1.1<br>+0.1 | +1.1<br>+0.3 | +1.3<br>+0.6 | +1.3<br>+0.8 | +1.3<br>+0.8 | +1.4<br>+0.8 |
| | -0.2<br>+0.4 | -0.6<br>+0.3 | -0.3<br>+0.2 | -0.3<br>+0.5 | -0.3<br>+0.8 | -0.2<br>+0.9 | -0.1<br>+1.1 |
| | | -0.9<br>+0.2 | -0.7<br>+0.3 | -0.7<br>+1.1 | -3.4*<br>+0.7* | -3.2<br>+0.1 | -3.4<br>0.0 |
| | | | -0.6<br>+1.3 | -6.0*<br>-2.2* | +3.0*<br>+0.9* | +1.1<br>-1.7 | +1.2<br>-1.3 |
| | | | | +3.0*<br>-0.2* | -0.9<br>+2.9* | -0.7<br>+0.5 | -0.7<br>+1.1 |
| | | | | | -0.6<br>+2.8* | -0.3<br>+1.1 | -0.3<br>+1.2 |
| | | | | | | -0.3<br>+0.3 | -0.3<br>+0.1 |
| | | | | | | | |

Standard Avg. $|\delta|$ Assembly : 1.50 % Max. $\delta$ -6.0% Location D-5
$\delta UO_2$ = 1.55%, $\delta$ MIX =1.40 Min. $\delta$ +4.3% Location A-1

GMND Avg. $|\delta|$ 0.9 % Max. $\delta$ -2.9% Location E-6
$\delta UO_2$ = 0.70%, $\delta$ MIX =1.20 Min. $\delta$ +1.8% Location A-1

| | |
|---|---|
| +4.3 | % UNDERPREDICTION OF TOTAL POWER USING STANDARD METHOD, RELATIVE TO SXS |
| +1.8 | % UNDERPREDICTION OF TOTAL POWER, USING GMND, RELATIVE TO SXS |

The GMND method requires furthermore much less preparation. A PDQ-5 powerdistribution calculation as the one above would require about 1 1/2 day of preparation with the standard method; maybe 2 hours more with the GMND method, and about a working week with the SXS method.

## 4-4 COMPARISON OF OUR STANDARD & GMND METHOD WITH EXPERIMENT & OTHER CALCULATIONS.

### 4-a) Introduction.

As a further check on the accuracy of the chosen standard method, for the analysis of conventional & proposed PU-recycle assemblies for the Yankee reactor - namely the LASER code with 2 groups (1 thermal & 1 epi + fast) as well as further evaluation of our GMND method; a PDQ-5 powerdistribution calculation was made on, what was thought to be a representative experiment. In the experiment the powerdistribution was measured in a 19 X 19 rod water-reflected configuration, consisting of a mixed oxide island of 11 X 11 rods embedded in $UO_2$ rod region, surrounded by water.

Although the w/o of $PUO_2$ (2 w/o) as well as the 8 atom % PU 240, in the mixed oxide fuel, is rather low, (our fuel has 4 w/o $PUO_2$ & 19 % PU 240) and the configuration is essentially a small high buckled core (in contrast to our assembly calculations, which are done assuming an infinite reactor consisting of such unit assemblies) it was the best experiment with the most detailed published results available to us.

4-b) DESCRIPTION OF THE BATELLE PRCF EXPERIMENT.

Under auspices of the Plutonium Utilization Program experiments were conducted at the (Batelle)-Pacific Northwest Laboratoreies, to obtain experimental information on the neutronic characteristics of plutonium and uraniumenriched fuels in prototype loading schemes.

The main neutronic parameters investigated were the determination of local power peaking factors and the worth of reactor control systems.

The results of these experiments and the comparison of calculational methods used in their analysis are reported in Reference 21 . The experiments included single region $UO_2$ and PU $O_2$ - $UO_2$ lattice criticals & powerdistribution measurements in varying degrees of non uniformities such as waterholes, waterslabs, watercrosses etc.

Since those more conventional applications have been extensively analysed ( 30 , 37 ) no calculations were performed by us on these experiments.

Also included in the experiments were multiregion measurements of typical fuel elements (mixed oxide or $UO_2$) surrounded by $UO_2$ or PU $O_2$ - $UO_2$ loadings.

One particular experiment, (see further) has been chosen, because it represented the most closely our assemblies.

The powerdistribution measurements were deduced from fissionproduct gamma activity at the fuel midplane, and the different fuel types ($UO_2$ & mixed oxide) were intercalibrated by caloric measurements. The fuel rods were rotated circumferentially during thecounting periods in order to average the fuel rod activity. The excess reactivity of the investigated loading was determined by measurement of the critical moderatorlevel.

A description of the Plutonium Recycle Critical Facility (PRCF) used in the experiment can be found in Ref. 21

The critical loading configuration, that was used in our study is pictured on Fig. IV - 17 .

The fuel rods were 36 inches long and placed on a square pitch of 0.75 inches. A detailed description of the $UO_2$ rods & PU $O_2$ - $UO_2$ rods are pictured on Figs. IV -18 , and IV-19 .

## 4-c) DESCRIPTION OF THE CALCULATION PROCEEDURE.

The calculation of the macroscopic X-sections of the unperturbed $UO_2$ & Mix Oxide unit cells was done with LASER (cut off 1.855 eV).

Since the MUFT calculation is rather sensitive to the buckling calculation (the core is small !) a total core buckling value of 0.00934 $cm^{-2}$ was used in both unit cells. A temperature of $25^{o}$ C was used in the calculations.

For the PDQ-5 calculation of the loading of Fig. IV- 17 , a 2 X 2 mesh per unit cell was used in the core region ( the same mesh chosen by Batelle after several trials), and 2 neutron-groups were used (1 thermal).

An axial buckling of 0.00089 $cm^{-2}$ was used in this 2D calculation, which

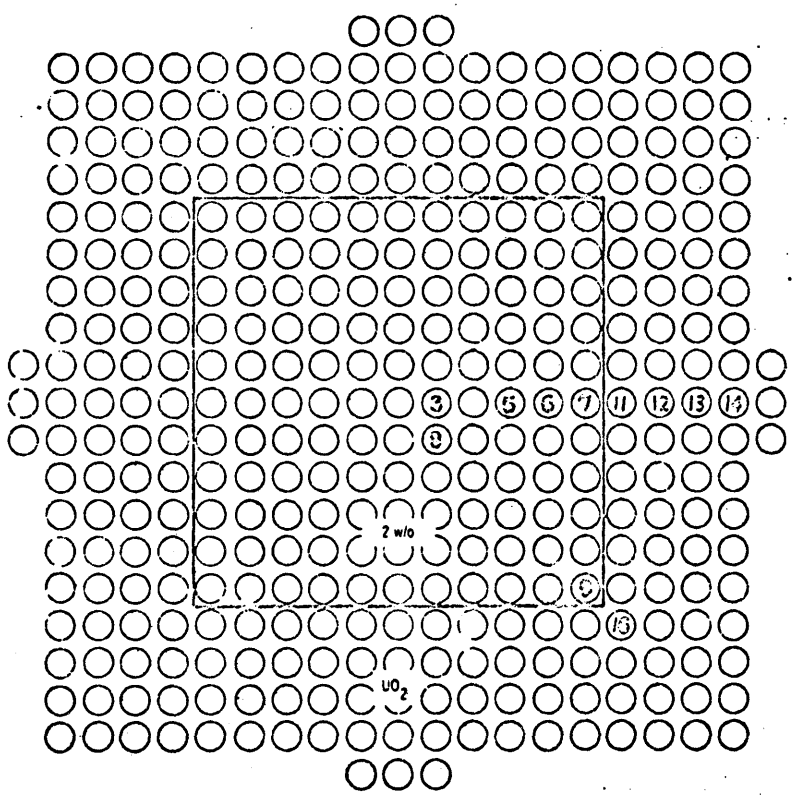


FIG. IV-17 : 11 X 11, $UO_2$ - 2 WT % $PuO_2$ (8% $^{240}Pu$) ELEMENT IN $UO_2$-2.35 % $^{235}U$.

EXPERIMENTAL LOADING CONFIGURATION.

FUEL SPECIFICATIONS: $UO_2$ - 2.35% $^{235}U$

FUEL RODS

1. ROD DIMENSIONS

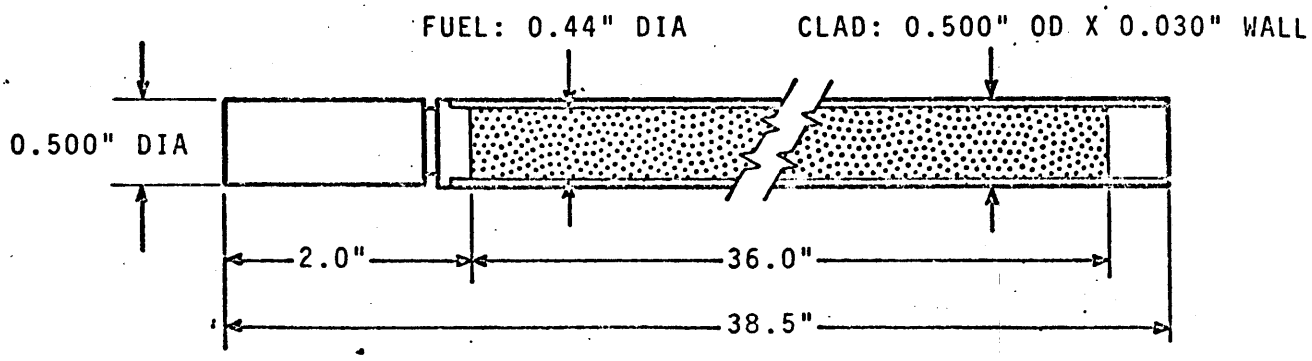


2. CLADDING: 6061 ALUMINUM TUBING SEAL WELDED WITH A LOWER END PLUG OF 5052-H32 ALUMINUM AND A TOP PLUG OF 1100 ALUMINUM.
3. TOTAL WEIGHT OF LOADED FUEL RODS: 917 GM (AVERAGE).

FUEL LOADING

1. FUEL MIXTURE VIBRATIONALLY COMPACTED.
2. 825 GM OF $UO_2$ POWDER/ROD. 726 GM OF U/ROD, 17.1 GM OF $^{235}U$/ROD.
3. ENRICHMENT - 2.35 ± 0.03% $^{235}U$.
4. FUEL DENSITY - 9.20 GM/CM$^3$ (84% THEORETICAL DENSITY)

FIG IV-18

FUEL SPECIFICATIONS: $UO_2$ - 2 WT% $PuO_2$

FUEL RODS

1. ROD DIMENSIONS

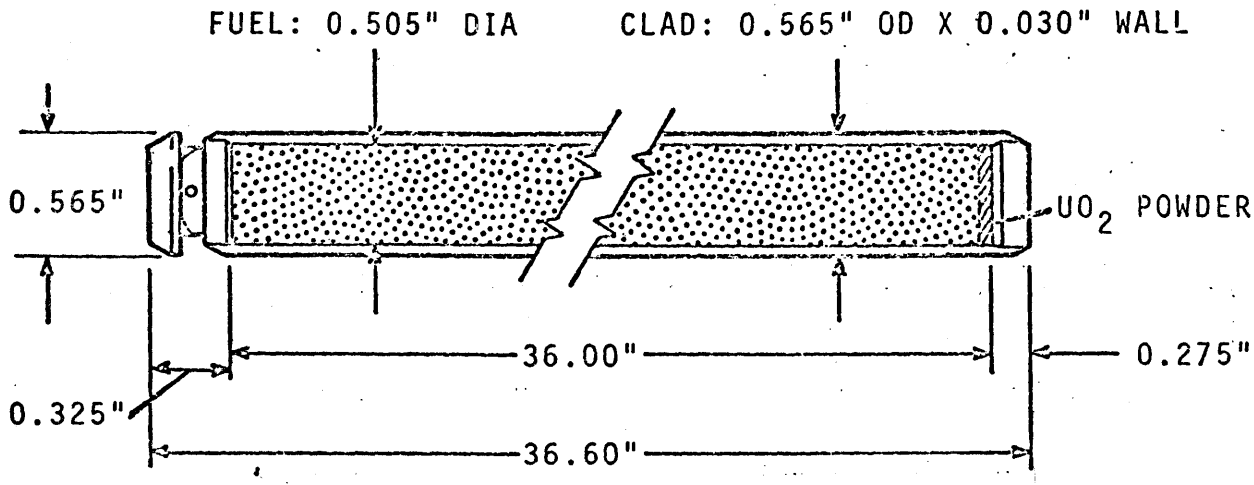


FIGURE IV-19

2. CLADDING: ZIRCALOY-2 TUBING WITH PLUGS SEAL WELDED AT BOTH ENDS.
3. TOTAL WEIGHT OF LOADED FUEL RODS: 1340 GMS (AVERAGE)

FUEL LOADINGS

1. $PuO_2$ MIXED IN NATURAL $UO_2$ AND VIBRATIONALLY COMPACTED.
2. 1128 GMS OF $UO_2$-$PuO_2$ MIX/ROD.
3. $PuO_2$ IS 2 WT% OF TOTAL MIXTURE.
4. $PuO_2$ - 22.56 GMS/ROD.
5. Pu - 19.85 GMS/ROD (AVERAGE).
6. NATURAL U.
7. FUEL DENSITY - 9.54 GM/CC (~87% THEORETICAL DENSITY).
8. $UO_2$ POWDER AT THE END OF FUEL COLUMN.
9. THE ISOTOPIC DISTRIBUTION OF PLUTONIUM IN THE TWO TYPES OF RODS REFERRED TO AS 8% AND 24% IS GIVEN BELOW:

1. 8% (NOMINAL) $^{240}Pu$

| ATOM PERCENT | |
|---|---|
| 91.615 | $^{239}Pu$ |
| 7.654 | $^{240}Pu$ |
| 0.701 | $^{241}Pu$ |
| 0.031 | $^{242}Pu$ |

2. 24% (NOMINAL) $^{240}Pu$

| ATOM PERCENT | |
|---|---|
| 71.762 | $^{239}Pu$ |
| 23.503 | $^{240}Pu$ |
| 4.08 | $^{241}Pu$ |
| 0.656 | $^{242}Pu$ |

corresponds to the full axially reflected core as given in Reference 21 .
The mesh sparing of 1/2 pitch = 0,9525 cm was extended for 3 lattice units in the reflector, after which the meshspacing was increased, such that the remainder of the 20 cm reflector contained 6 meshes.
There was no boron in the moderator.
The diffusionconstant in the water was obtained from a THERMOS calculation.

4-d) RESULTS OF THE CALCULATIONS.

Table IV- 3 compares the LASER (1.855 eV) code calculations for the $UO_2$ - 2.35 w/o U235 fuel, and the 2 w/o PU $O_2$ -nat $UO_2$ (8 at % PU 240) fuel, to other code calculations using .625 or .683 eV cut-offs. The cut off at .625 eV is used in the LEOPARD code, whereas the .683 eV cut-off is used in the Battelle analysis, using codes as RIBOT, HTH, THERMOS-BATELLE-HRG, which are described in Reference 21 .
In the case of the $UO_2$ fuel the LASER & LEOPARD codes give values of keff which are about.3 % lower than the values calculated by Batelle analysts.
For the mixed oxide fuel the laser code agrees very well with the RIBOT code, whereas the standard LEOPARD as well as the modified LEOPARD by H.Spierling at MIT (*) gave keff values which are about 3.5 to 4.5 % lower than the codes used by Batelle analysts.
Fig IV-17 shows the plan view of the calculated loading configuration.
The numbering scheme has no specific significance, but was used by Batelle analysts & are retained here.

* The Spierling-LEOPARD code includes, modifications such as :
the ENDF/B X-Sections, & inclusion of higher isotopes but does not include a better PU 240 resonance treatment.

Table IV. -4 shows the comparison between experiment and calculated powerdistribution using the standard (1.855 eV) LASER proceedure, the GMND method applied with LASER, and the Spierling-LEOPARD code (in all methods only 2 groups of neutrons were used). The calculated powerdistributions were normalised to the rod location number 13, in the same way as in reference 21 .

The calculated powerdistributions were also compared to the best result obtained at Batelle, using the RIBOT code with 4 groups of neutrons.

The experimental Rod Power is in arbitrary units, and is in this Table the average measured power at 3 symetrypoints in the lattice. The max. variation of the measurements between the symetrypoints defined as $\frac{P_e^s - P_e}{P_e} \times 100$ % is indicated in the colum of the experimental rod power as $\varepsilon_s$.

They are thus an indication of the range of variations that may be expected in a practicle loading, were e.g. not every fuel rod is identical. The deviation $\delta$ in % in the colums of the calculated poerdistributions, are defined as $\frac{P_c - P_e}{P_e} \times 100$ were $P_c$ is the calculated poerdistribution and $P_c$ is the experimental powerdistribution, avgd. over symmetrical points.

The group average $|\delta|$ is defined as the sum of all the absolute values of in % devided by the number of values.

At this point it is worthwhile to notice that at Batelle & other organizations the group average % deviation $\delta$ is defined as the root of the avg. sum of the mean square deviations. If this definition is used the errors are smaller & seemingly better results are obtained.

In Table IV-4, it is thus observed that the standard LASER code method gives the best results of all, especially in the mixed oxide region, compared to the experimental results. The agreement is really surprisingly good, especially if we compare the max. deviations that exist between a symmetry point & the average experimental power to the deviations of the calculated

power & the experimental power. The errors even at the peak locations 7 & 9 are completely within the experimental nonuniformity errors.
The GMND method is seen to give the most conservative results (4.8 % more power at the MIX/$UO_2$ interface positions vs. the standard calculation), but the conservatism is confined near the $UO_2$/MIX interface & further away the agreement is again good. The best available LEOPARD code (LEOPARD-Spierling) gives large deviations in the mixed oxide region, it overpredicts quite heavily the power at the interface & underpredicts it heavily at the center of the mixed oxide region. This behaviour has been found to be intrinsic to the available LEOPARD codes and the errors increase with the amount of PU 240 in the mixed oxide fuel. (see later).
Finally the standard RIBOT method with 4 groups of neutrons, which gave the best results at Batelle for this loading, is seen to overpredict the power-distribution in the mixed oxide region uniformly. It is also observed that the average % error is the largest of all cases. (*)
The keff values are observed to be quite close in all cases. However caution must be applied to the value of these agreements, since it has been frequently observed (see later) that powerdistributions can vary quite a bit and unit cell $k_\infty$ & keff values can vary largely and still give a keff of a core configuration to be in seemingly good agreeement.

## 4-e) CONCLUSION ABOUT OUR METHODS IN COMPARISON WITH EXPERIMENT.

From the calculations it has been observed that the chosen standard method using the LASER code with a cut-off at 1.855 eV and 2 groups of neutrons, gives surprisingly good results for the calculation of the powerdistribution in PU-recycle lattices.

(*) After completion of the work in Ref 21, the methods have been revised, and better results were obtained.

TABLE IV-3 COMPARISON OF CODE CALCULATIONS FOR $UO_2$ - 2.35 w/o U235 FUEL AND 2.0 w/o $PUO_2$ - nat $UO_2$ FUEL (8 a/o PU 240) FUEL.

$UO_2$ - 2.35 w/o U235 FUEL.

| CODE | $k_\infty$ | $k_{eff}$ ($B^2$=0.00934cm$^2$) | $\tau$(cm$^2$) |
|---|---|---|---|
| (1.855 eV) LASER | 1.319 | 0.966 | 35.1 |
| (0.625 eV) LEOPARD | 1.330 | 0.971 | 36.1 |
| (0.683 eV) RIBOT | 1.303 | 0.997 | 36.4 |
| HTH | 1.300 | 0.992 | 32.1 |
| TH/B-HRG | 1.301 | 1.005 | 31.8 |

2.0 w/o $PUO_2$ -nat $UO_2$ FUEL (8a/o PU 240).

| CODE | $k_\infty$ | $k_{eff}$ ($B^2$=0.00934 cm$^2$) | $\tau$(cm$^2$) |
|---|---|---|---|
| (1.855 eV) LASER (1) | 1.364 | 0.9976 | 37.2 |
| LEOPARD(ARGONNE) (2) | 1.399 | 0.965 | 46.5 |
| LEOPARD(SPIERLING) | 1.381 | 0.951 | 46.6 |
| RIBOT | 1.364 | 0.999 | 37.4 |
| HTG-L.W.(2) | 1.355 | 0.990 | 35.0 |
| HTG-S.W.(3) | 1.352 | 1.002 | 35.0 |
| TH/B-HRG | 1.333 | 1.010 | 32.5 |

(1) LASER & LEOPARD(ARGONNE) use the Sher 1965 PU239 thermal representation ($\eta$ 2200 = 2.116)
(2) LEONARD-Westcott PU239 representation ($\eta$ 2200 = 2.11)
(3) Schmidt-Westcott PU239 thermal representation ($\eta$ 2200 = 2.079)

TABLE IV-4 COMPARISON OF EXPERIMENTAL & CALCULATED POWERDISTRIBUTION OF AN 11X11 2 w/o $PUO_2$-nat $UO_2$ (8 a/o PU 240) ELEMENT IN $UO_2$ - 2.35 w/o U 235.

| ROD LOCATION | EXPERIMENTAL ROD POWER | | STANDARD LASER (1.855 eV 2 GROUPS) | | GMND METHOD LASER (1.855 eV) | | LEOPARD ( ) (SPIERLING) 0.625 eV, 2 GROUPS | | STANDARD RIBOT 4 GROUPS (0.683 eV) (BATELLE) | |
|---|---|---|---|---|---|---|---|---|---|---|
| | | $\varepsilon_s$ % | MIT | $\delta$ % | MIT | $\delta$ % | MIT | $\delta$ % | | $\delta$ % |
| 3 | 1.209 | + 1.5 | 1.191 | - 1.5 | 1.202 | - 0.6 | 1.170 | - 3.2 | 1.248 | + 3.2 |
| 8 | 1.194 | + 2.4 | 1.195 | + 0.1 | 1.195 | + 0.1 | 1.163 | - 2.6 | 1.239 | + 3.8 |
| 5 | 1.146 | - 1.1 | 1.138 | - 0.7 | 1.152 | + 0.5 | 1.123 | - 2.0 | 1.183 | + 3.2 |
| 6 | 1.114 | + 1.1 | 1.125 | + 1.0 | 1.140 | + 2.3 | 1.116 | + 0.2 | 1.159 | + 4.0 |
| 7 | 1.201 | + 2.2 | 1.209 | + 0.6 | 1.265 | + 5.3 | 1.241 | + 3.3 | 1.267 | + 5.5 |
| 9 | 1.128 | + 3.6 | 1.170 | + 3.7 | 1.235 | + 9.5 | 1.209 | + 7.2 | 1.201 | + 6.5 |
| GROUP AVERAGE | $\lvert\delta\rvert$ | 2.0 | | 1.3% | | + 3.0 | | + 3.1 | | + 4.4 |
| 11 | 0.832 | - 1.0 | 0.828 | - 0.5 | 0.808 | - 2.9 | 0.831 | - 0.1 | 0.837 | + 0.6 |
| 12 | 0.890 | - 0.6 | 0.874 | - 1.8 | 0.873 | - 1.9 | 0.891 | + 0.1 | 0.887 | - 0.3 |
| 13 | 0.840 | - 0.6 | 0.840 * | 0 | 0.840 * | 0 | 0.840 * | 0 | 0.840 * | 0 |
| 14 | 0.804 | + 0.4 | 0.813 | - 1.1 | 0.807 | + 0.4 | 0.797 | - 0.9 | 0.806 | + 0.2 |
| 16 | 0.726 | + 0.8 | 0.739 | + 1.8 | 0.730 | + 0.5 | 0.740 | + 0.5 | 0.729 | + 0.4 |
| GROUP AVERAGE | $\lvert\delta\rvert$ | .7 | | 1.3 % | | 1.4 | | 0.4 | | 0.4 |
| AVERAGE $\lvert\delta\rvert$ FOR ALL RODS | | 1.5 | | 1.3 % | | 2.4 % | | 2.0 % | | 2.8 % |
| $k_{eff}$ | 1.0033 | | 1.0035 | | 1.0026 | | 1.0044 | | 1.0028 | |

*rod used for normalisation.

The results are considerably better than with any other code as the Table IV-4 clearly demonstrates. Although it has been found that for conventional applications, the standard LEOPARD code is as accurate as LASER, (see also chapter 5) & because of its low cost (1/4 to 1/5 of LASER or LOCALUX) should be used for conventional applications, it has been noticed that the best available LEOPARD code (Spierling) (which for this purpose essentially differs from the standard LEOPARD through the inclusion of the ENDF/B X-sections) is inadequate for the calculation of the powerdistribution in PU-recycle applications. It has been identified that the inadequate treatment of the 1.0 eV PU 240 giant resonance in the LEOPARD code is responsible for the large deviations, which evidently increase with the w/o of the $PUO_2$ and the a/o of PU 240. Therefore although the LEOPARD code gives results which are seemingly better than the standard RIBOT in this case, it should break down completely for the practicle applications were the w/o of PU $O_2$ is about 4 w/o & the a/o of 240 PU is about 19 %. Assuming that the errors are due to the PU 240 treatment we may anticipate that relative to LASER the standard LEOPARD will deviate on the average by 9 % in the mixed oxide.

The developed GMND method, here applied with the LASER code, gives as expected the conservatism due to spectraleffects at the $MIX/UO_2$ boundary. An increase in rod power of about 4.7 % in the mixed oxide rod and a decrease of 2.4 % in the $UO_2$ rod at the boundary are the results of including the spectraleffects. Although compared to experiment, those values seem toohigh & are too conservative, specific caution must be exercised. First, the experiment consists of a small core, in which the thermal & epi + fast fluxes change largely. Therefore the assumptions in the methods & the errors in the experiment vs.

calculation will be larger than in an actual powerreactor, & other effects may mask the spectraleffects completely.

Second, it has been found in conventional loadings, that ( 30 ) all methods, introduced to calculate powerpeaking more realistically thus including spectral-effects, & applied to small loadings overpredict the power at the peak locations. In short the GMND method, invented to predict powerpeaking, including spectral-effects, shouldbe used in practice since it is known that the spectraleffects exist, & it is probably only fortunately that a standard method neglecting the effects, gives better results for high buckling loadings, which are known to be the most troublesome. In practice it seems thus advisable to use the GMND-X sections for the calculation of the local powerpeakingfactor in a unit-assembly, but to use the standard X-sections for whole core calculations & overall core radial powerpeaking*. In this way too much conservatism is avoided, and at the same time the spectraleffects are included in a realistic way for the safe evaluation of the hot channelfactors in the reactorcore.

* Overall core nuclear hot channelfactor $F_N = F_z^N F_r^N F_{local}^N$

where $F_n^Z$ axial hot channelfactor, $F_N^R$ : radial hot channelfactor excluding local powerpeaking effects such as watergaps, MIX/$UO_2$ spectral interface effects and F LOCAL : local hot channelfactor as determined with a detailed unit assembly calculation.

## IV - 5 OVERALL CONCLUSIONS ABOUT THE DEVELOPED METHODS.

Two methods have been developed for the calculation of local power-peakingfactors in conventional and plutoniumrecycle assemblies.
The Spectral Cross-section Synthesis methods (SXS) and the Generalised Mixed Number Density (GMND) method, which are both applicable with codes as e.g. LASER & LOCALUX, are both very different in concept. The much simplier & practicle GMND method was found to be in very good agreement with the SXS method. Both methods give considerable improvement in the calculation of local power-peaking in both conventional & PU-recycle assemblies. The methods have been evaluated on THERMOS calculations in a one dimensional model, and have been intercompared with the standard method on 2 D assembly models. Comparison with experiment on a high buckling loading, showed that the GMND method introduces the safer desired conservatism. The method should be applied in preference however, to the calculation of local powerpeaking in the assemblies, whereas the standard method should be preferred for whole core calculations.
The comparison with experiment showed furthermore a very good agreement with the adopted standard LASER-code 2-group scheme with a thermal cut-off at 1.855 eV. The results of the powercalculations were much better than any other reported calculations made with a 2 group-LEOPARD (cut off 0.625 eV) and the Standard 4 group RIBOT (cut-off 0.683 eV) schemes.

# CHAPTER V. THE CALCULATION OF THE LOCAL POWERPEAKING FACTORS & POWERDISTRIBUTION IN CONVENTIONAL AND PLUTONIUMRECYCLE ASSEMBLIES FOR THE YANKEE REACTOR AT BOL AND DURING LIFETIME.

## V-1 INTRODUCTION.

In the previous chapters the GMND method has been developed for the calculation of the powerpeaking factors in conventional and PU-recycle assemblies, using the LASER or LOCALUX unit cell codes to generate the X-sections.

In this chapter the local powerpeaking factors and powerdistributions have been calculated for the conventional $UO_2$ and PU-recycle assemblies, using the GMND & standard methods with X-sections from LASER & the MND & standard methods with X-sections from LEOPARD.

A burnupstudy on a simplified 2 dimensional assemblymodel has been made, using the GMND method and the LASER code for the X-sections during burnup.

All diffusiontheory calculations were done with PDQ-5; at BOL the differences in energy released from fission in the $UO_2$ & mixed oxide fuels were taken into account. It amounts to a roughly 3 % increase in power in the mixed oxide region.

## V-2. THE INFLUENCE OF THE DESIGN DETAILS OF THE ASSEMBLIES ON THE CALCULATION OF THE LOCAL POWERPEAKING AND POWERDISTRIBUTION.

### 2-1) THE INFLUENCE OF THE GEOMETRICAL MODELS.

The mechanical design of the assemblies have been described in Chapter I, section 2-2 and are displayed on the figures I, 4, 5, 6.

It is thus noticed that two different assemblies type A & B exist; with a different geometry. Figure V-1 shows an exagerated drawing of a type B assembly.

. The boundary of e.g. a type B assembly should be choosen where the fluxgradient $\nabla\phi$ is zero, assuming that the reactor consits of an infinite array of such unit assemblies. According to this model the boundary would follow a rather peculiar contour arround the assembly as shown on Fig. V-1.

A rather close boundary that follows the pysical $\nabla\phi = 0$ in the most important zirc followers-watergap regions is also pictured on Fig. I-6.

Using this geometrical boundary the composition-overlay of the assembly is pictured on Fig. V-2.

The composition 1 consists of unitcells of $UO_2$ in a conventional assembly.

The compositions 2, 3, 4 are homogenized regions of the SS.can, the watergap & the followers. Since different volumefractions of water & other material exist at those different locations, the compositions are taken different & the X-sections are thus different.

Compositions 5 & 7 are homogenized regions of the solid zirc-rod cell with associated can, and respectively the homogenized instrumentation channel.

The composition 6 consist of homogenized regions of $UO_2$-unitcells, the can & watergap between the cans.

In total here are thus 7 compositions in the assembly according to this model 1.

Since the composition 6, contains also fuel this model is somewhat difficult to work with, therefore a second model was used in all the calculations (except for the evaluation of the change - SS can, zirc can )where composition 6 was taken to be the same as 1. In this 2nd. model the can & watergap between the cans away from the followers are thus neglected.

Another model which is commonly used, in order to avoid the complication of variable mesh-sparing & rescaling of the poweredit in the fuel region with the thickness t; is to expand the outer assembly region to one with a thickness t equal to the pitch. Although this 3rd. model is the simpliest to prepare,

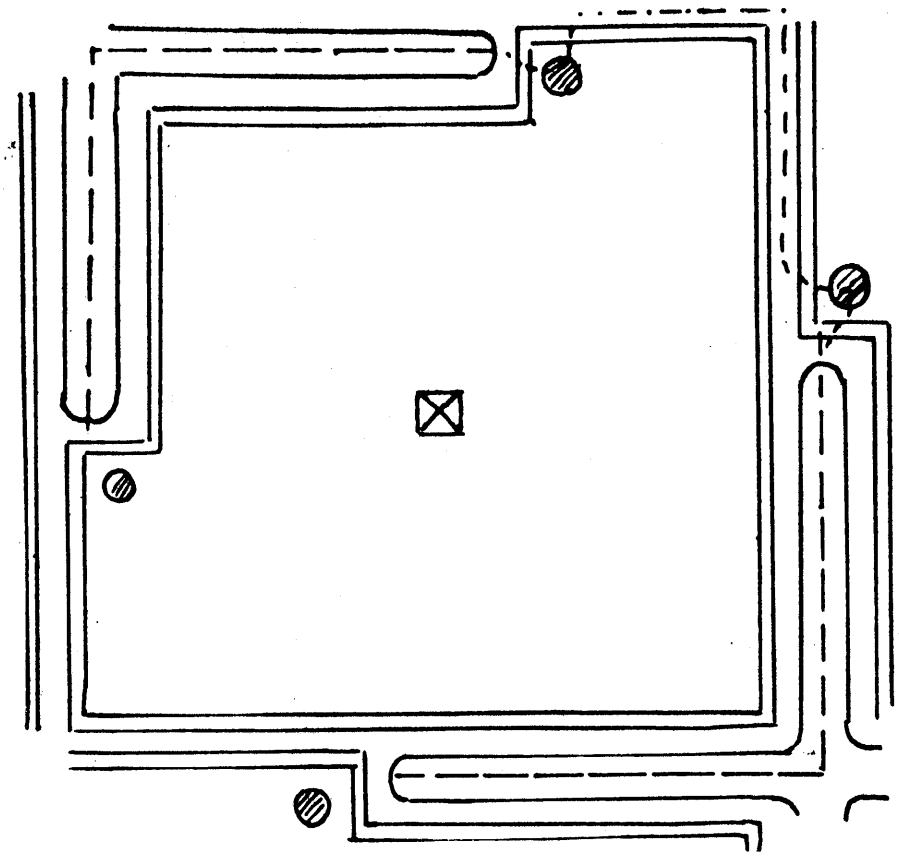

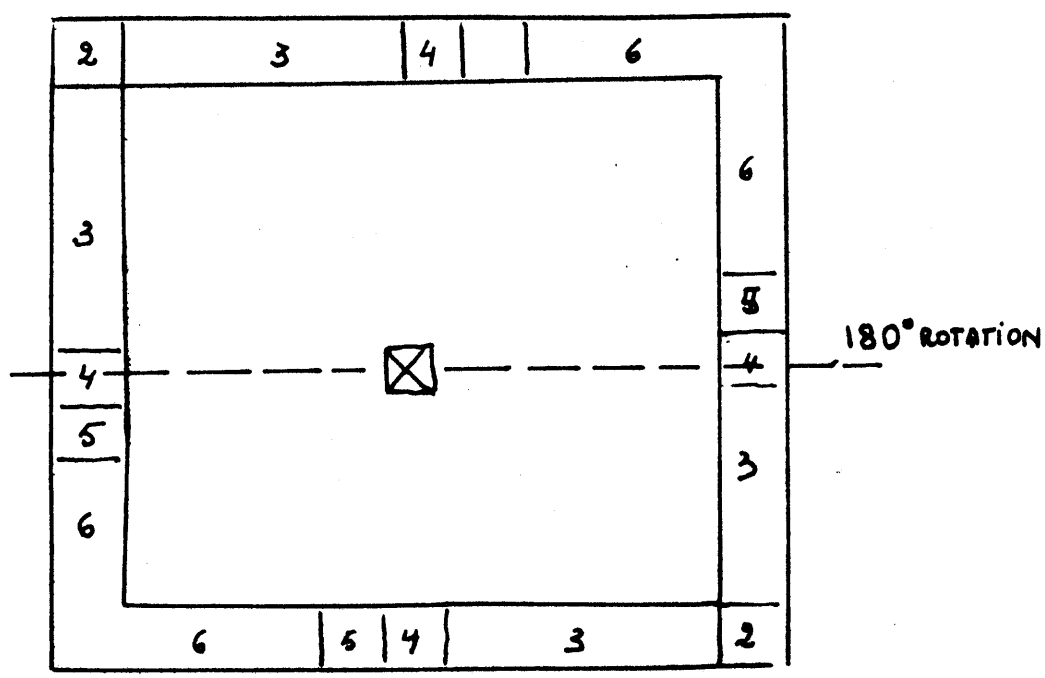


FIG V-1,e PHYSICAL BOUNDARY AND COMPOSITION OVERLAY

and the simpliest for using the output, it deviates too much from the physical model since now the extrawatergap & follower regions are also expanded, with an obvious result that the powerpeakingfactor is increased to an unusual high value.

It must be remarked that the accuracy of the geometrical model that is desired depends a lot on the type of calculation one wants to perform. In an application where two assemblies are compared, it does not matter too much what model is used, as long as the comparison is consistent. In applications where only a more accurate calculation is desired, e.g. with a 2 X 2 mesh/unit cell, which has to be compared to a e.g. 1 X 1 mesh/unit cell also used in a complete core calculation, it doesn't matter too much what kind of model is used to obtain the local powerpeakingfactor "corrections". In a rather small core as the Yankee, where a detailed (e.g. rod by rod) calculation can be performed, e.g. on a rod by rod basis in the peak assembly, the local powerpeaking correctionfactors are not sensitive to the model used; and the most simple model 3 can be applied.

If the core is large, or if only preliminary results are desired, the local powerpeakingfactor as determined with a unit-assemblycalculation is very useful, since the whole core calculation can be performed with less accuracy, neglecting the details of the watergaps, followers, & or peculiar lay-out of the mixed oxide rods. For such applications the 2nd, model seems more appropriate, since it is close to the physical model, and will thus give more realistic nuclear "local powerpeaking factors ".

Therefore in our study the second model has been used mostly.

In order to obtain the error introduced in the 2nd, model (relative to the first) in which the watergap between the cans & the can was neglected away from the followers, two calculations were made for a conventional assembly with the PDQ-5 code, taking 2 X 2 meshes per unit cell, and regular X-sections obtained

from LASER for the unit cells & from LOCALUX for the extra materials.
The results of the comparison showed that the powerdistribution in the $UO_2$, near the cans away from the follower (using the simplified model) was underpredicted by 1.8 % at the first row and about 0.8 % at the second. The simple model overpredicted the powerpeaking-factor at position A-1 by a 0.9 % & in much of the assembly by about 0.7 %.
Since the errors at the most important positions are conservative & were less than 1 %, the simplier 2nd model in which the cans were neglected away from the followers, was used in most of the calculations in this study except for the calculations on the influence of the design of the assembly can on the powerpeaking.

## 2-2) THE INFLUENCE OF THE DESIGN OF THE ASSEMBLY CAN ON THE POWERPEAKING & POWERDISTRIBUTION IN A CONVENTIONAL YANKEE ASSEMBLY.

In the present design of the Yankee-assemblies, a stainless steel 35 mils (0.035 inches) can is employed, and is perforated with holes away from the followers. To examine the influence of the stainless-steel can versus a zircalloy can and the influence of perforating holes everywhere in the can, two calculations were made, one with a zircalloy can of the same dimensions, one with a half closed SS can and one with a completely perforated SS.can with 50 % holes. Regular LASER X-sections & 2 groups were used in the calculations, 2 X 2 meshes per unit cell were taken except near the cruciform followers & watergap were 3 X 3 meshes were taken. A 180 $^{o}$ rotational symmetry at the midplane was used with model 1.
The results of the calculations are shown on the Figs. V-3 and V-4.
Fig. V-3 shows the <u>% increase</u> in the powerdistribution when the SS. can is completely perforated with 50 % holes, in order to improve fluid mixing.

FIG V-3 % INCREASE IN POWER DUE TO 50% INCREASE OF HOLES IN THE SS - CAN

| | | | | | | | |
|---|---|---|---|---|---|---|---|
| +3.0 | | | | | | | |
| +2.4 | +1.5 | | | | | | |
| +2.0 | +1.1 | +0.6 | | | | | |
| +1.8 | +0.8 | +0.2 | -0.1 | | | | |
| +1.7 | +0.7 | +0.0 | -0.3 | -0.4 | | | |
| +1.4 | +0.5 | +0.0 | -0.4 | -0.5 | -0.6 | | |
| +1.2 | +0.3 | -0.2 | -0.5 | -0.6 | -0.6 | -0.6 | |
| +0.9 | +0.1 | +0.1 | -0.2 | -0.4 | -0.5 | -0.6 | X |

% increase
k = 12 millik.

FIG V- 4 % INCREASE IN POWER DUE TO REPLACEMENT OF THE SS-CAN BY A ZIRCALLOY CAN

| | | | | | | | |
|---|---|---|---|---|---|---|---|
| +6.5 | | | | | | | |
| +5.2 | +3.6 | | | | | | |
| +4.3 | +2.7 | +1.7 | | | | | |
| +3.8 | +2.1 | +1.0 | +0.4 | | | | |
| +3.2 | +1.7 | +0.5 | -0.1 | +0.0 | | | |
| +2.8 | +1.0 | +0.2 | +0.2 | -0.4 | -0.2 | | |
| +2.2 | +0.8 | +0.1 | -0.4 | -0.2 | -0.3 | -0.4 | |
| +1.8 | +0.4 | -0.4 | -0.8 | -0.7 | -0.4 | -0.2 | X |

% increase
k * 16 millik.

Fig. V-4 shows the % increase in powerdistribution when a 35 mils, (unperforated at the followerpositions) zircalloy can is used instead of stainless-steel. Although the calculations were performed with the 1st. model, with a 180° rotational symmetry arround the midplane, only the most important assembly positions are shown.

The results thus show that perforating the can at the follower positions would increase the local peakingfactor by about + 3 %, which is due to the extra-account of water, but would decrease $\Delta$ k by about 12 milli-k . Replacement of the SS. can by a zircalloy can, would increase the local powerpeaking by as much as + 6.5 %. The $\Delta$ k would however be reduced by : 16 milli-k.

It is thus observed that the stainless steel can with a higher mechanical strength than zircalloy 4, but low neutroneconomy, reduces the powerpeaking by as much as 6.5 %. Therefore although the SS-fuel-cladding has been replaced by the zircalloy 4 cladding on the fuel rods, replacement of the SS-can by a zircalloy can is undesirable.

## V-3 : THE POWERDISTRIBUTION AND POWERPEAKING IN THE CONVENTIONAL AND PLUTONIUM-RECYCLE ASSEMBLY AT BEGINNING OF LIFE (BOL).

### 3 -1 CALCULATIONS FOR THE CONVENTIONAL $UO_2$ - ASSEMBLY.

The powerdistribution in the conventional $UO_2$ assembly (4.0 w/0 U235 fuel) has been calculated with PDQ-5, using the 2nd. model and a 180 $^{o}$ rotational symmetry. 2 X 2 meshes per unit cell were used except in the extraregions and adjacent $UO_2$ cells were 3 X 3 meshes were used. A buckling of 0.00071 $cm^{-2}$, corresponding to the full core buckling & a boronconcentration of 1400 ppm was assumed in the calculations.

First two calculations were made, in order to evaluate the need for the more expensive LASER code with a cut-off at 1.855 eV versus the less expensive LEOPARD code with a cut-off at 0.625 eV.

The regular 2 group LASER & LEOPARD X-sections were used in these calculations. Fig. V-5 shows the result of the calculated powerdistribution in the assembly using the regular LEOPARD & LASER code 2 group X-sections.

It is thus noticed that the agreement in the powerdistribution and $k_\infty$ in a conventional $UO_2$-assembly is very good. For conventional applications the four to five times less expensive LEOPARD code with a cut-off at 0.625 eV & using 2 groups can thus be used with good confidence.

Fig. V-6, shows the powerfraction due to thermal neutrons in the most important portion of the $UO_2$ assembly. About 25 % of the total power is thus due to fast & epithermal neutrons and 75 % to thermal neutrons. Note that the fractional power due to thermal neutrons is larger in LASER than in LEOPARD, which is

evidently due to the thermal cut-off of 1.855 eV versus 0.625 eV.
The fast & epithermal flux was noticed to be very flat over the whole assembly.
Fig. V-7, shows the powerdistribution in the most important $UO_2$ assemblyportion as calculated with the MND X-sections from LEOPARD for the whole assembly.
The local powerpeakingfactor is 1.189 in the corner of the $UO_2$ assembly at the cruciform watergap.
The use of the MND X-sections to take the spectralsofteningeffects in account, increase the powerpeak by about 3.2 %.
From the results of the previous chapter, on a 1/4 assembly, the use of the GMND X-sections with LASER would have increased the local powerpeakingfactor at lo-cation A-1, by about 2.3 %, whereas the SXS method would have increased this factor by about 4.3 %.
In Table V-1 a comparison is made of the local powerpeakingfactors (at location A-1) for the conventional assembly, as calculated with different methods.
The LASER, spatial X-section synthesis method gives the highest value, but is very close to the LEOPARD MND value (since the regular LASER peaking was somewhat lower).
For conventional applications the use of the LEOPARD-MND method, would be recommended for the practicle and inexpensive calculation of the powerpeaking & powerdistributions.

## 3-2) CALCULATIONS FOR THE PLUTONIUM-RECYCLE ASSEMBLY.

Similar powerdistributioncalculations have been made for the proposed plutoniumrecycle assembly, consisting of 68 mixed oxide rods (4 w/o $PUO_2$-nat $UO_2$, 19 % nominal PU 240 a/o) loaded in the middle of the assembly, & surrounded by 168 $UO_2$ rods (4 w/o U235). The loading & fuel rod descriptions were described in Chapter I, section 2-3 .

| | | | | | | | | | | | | | | |
|---|---|---|---|---|---|---|---|---|---|---|---|---|---|---|
| 1.073<br>1.076 | 1.033<br>1.038 | 1.013<br>1.017 | 1.003<br>1.005 | 0.996<br>0.996 | 0.996<br>0.995 | 1.002<br>1.003 | X | 1.002<br>1.003 | 0.997<br>0.996 | 0.998<br>0.995 | 1.002<br>0.998 | 1.012<br>1.012 | 1.031<br>1.029 | 1.070<br>1.070 |
| 1.076<br>1.079 | 1.035<br>1.039 | 1.014<br>1.018 | 1.003<br>1.005 | 0.998<br>0.997 | 0.997<br>0.996 | 0.998<br>0.997 | | 0.998<br>0.999 | 0.997<br>0.996 | 0.998<br>0.994 | 1.002<br>0.997 | 1.010<br>1.008 | 1.026<br>1.025 | 1.060<br>1.058 |
| 1.078<br>1.081 | 1.038<br>1.042 | 1.016<br>1.021 | 0.998<br>1.000 | 0.997<br>0.997 | 0.998<br>0.997 | | | | 0.998<br>0.996 | 0.998<br>0.994 | 1.001<br>0.997 | 1.008<br>1.006 | 1.017<br>1.015 | 1.040<br>1.035 |
| 1.082<br>1.085 | 1.040<br>1.045 | 1.018<br>1.023 | 1.007<br>1.010 | 0.997<br>0.996 | | | | | | 0.998<br>0.994 | 1.000<br>0.996 | 1.003<br>0.999 | 1.009<br>1.002 | 1.016<br>1.013 |
| 1.087<br>1.091 | 1.045<br>1.052 | 1.024<br>1.029 | 1.012<br>1.015 | | | | | | | | 1.001<br>0.995 | 1.001<br>0.996 | 1.003<br>0.998 | 1.006<br>0.999 |
| 1.097<br>1.101 | 1.055<br>1.062 | 1.034<br>1.040 | | | | | | | | | | 1.000<br>0.995 | 1.001<br>0.996 | 1.002<br>0.997 |
| 1.113<br>1.121 | 1.075<br>1.083 | | | | | | | | | | | | 1.001<br>0.996 | 1.001<br>0.996 |
| 1.142<br>1.151 | | | | | | | | | | | | | | 1.000<br>0.995 |
| | | | | | | | | | 1.045<br>1.047 | 1.022<br>1.019 | 1.013<br>1.007 | 1.015<br>0.999 | 1.001<br>0.995 | 1.000<br>0.994 |

$k_\infty$ (LASER) = 1.20472 $k_{eff}$=1.129935 COMPARISON LASER-LEOPARD REGULAR X SECTIONS.

$k_\infty$ (LEOPARD)=1.20594

FIG. V-5 : TOTAL NORMALISED POWERDISTRIBUTION IN A CONVENTIONAL $UO_2$ ASSEMBLY - USING REGULAR LASER & LEOPARD X-SECTIONS.

FIG. V-6 : FRACTION OF TOTAL POWER DUE TO THERMAL NEUTRONS IN A PORTION OF THE CONVENTIONAL $UO_2$ ASSEMBLY.

| | | | | | | | |
|---|---|---|---|---|---|---|---|
| 0.797<br>0.792 | 0.791<br>0.783 | 0.786<br>0.777 | 0.784<br>0.774 | 0.782<br>0.772 | 0.774<br>0.763 | 0.779<br>0.769 | 0.778<br>0.768 |
| | 0.782<br>0.771 | 0.776<br>0.765 | 0.773<br>0.761 | 0.772<br>0.759 | 0.770<br>0.758 | 0.769<br>0.756 | 0.768<br>0.755 |
| | | 0.771<br>0.757 | 0.767<br>0.753 | 0.765<br>0.751 | 0.764<br>0.757 | 0.763<br>0.749 | 0.762<br>0.748 |
| | | | 0.764<br>0.749 | 0.762<br>0.747 | 0.761<br>0.750 | 0.760<br>0.745 | 0.756<br>0.744 |
| | | | | 0.760<br>0.745 | 0.759<br>0.744 | 0.758<br>0.743 | 0.758<br>0.743 |
| | | | | | 0.758 | 0.758<br>0.743 | 0.758<br>0.743 |
| | | | | | | 0.758<br>0.743 | 0.758<br>0.743 |
| | | | | | | | |

| | |
|---|---|
| 0.797 | AVG. FRACTION LASER |
| 0.792 | AVG. FRACTION LEOPARD |

FIG. V-7 : POWERDISTRIBUTION CONVENTIONAL $UO_2$ ASSEMBLY PORTION USING LEOPARD MND.

| | | | | | | | |
|---|---|---|---|---|---|---|---|
| 1.189<br>+3.2 | 1.145<br>+2.1 | 1.124<br>+1.9 | 1.111<br>+1.8 | 1.106<br>+1.9 | 1.103<br>+2.0 | 1.102<br>+2.1 | 1.099<br>+2.1 |
| | 1.093<br>+0.9 | 1.068<br>+0.6 | 1.058<br>+0.6 | 1.052<br>+0.7 | 1.049<br>+0.7 | 1.048<br>+0.9 | 1.047<br>+0.9 |
| | | 1.042<br>+0.2 | 1.031<br>+0.2 | 1.026<br>+0.3 | 1.024<br>+0.3 | 1.021<br>+0.5 | 1.022<br>+0.5 |
| | | | 1.017<br>+0.2 | 1.013<br>+0.3 | 1.004<br>+0.4 | 1.009<br>+0.5 | 1.009<br>+0.5 |
| | | | | 0.998<br>+0.2 | 1.001<br>+0.4 | 1.001<br>+0.5 | 1.002<br>+0.6 |
| | | | | | 1.002<br>+0.5 | 1.003<br>+0.6 | 1.003<br>+0.7 |
| | | | | | | 1.003<br>+0.7 | 1.010<br>+1.0 |
| | | | | | | | |

Max. Powerpeak : 1.189 Location A-1.

| | |
|---|---|
| 1.189<br>+3.2 | NORMALISED ROD POWER<br>% INCREASE RELATIVE TO STANDARD CALCULATION. |

TABLE V-1 COMPARISON BOL-LOCAL POWERPEAKING FACTORS IN A CONVENTIONAL $UO_2$ UNIT ASSEMBLY, USING DIFFERENT METHODS.

| METHOD | LOCAL POWER-PEAKING FACTOR | % INCREASE VS. REGULAR X-SECTIONS. |
|---|---|---|
| LASER (REG.) | 1.142 | |
| LEOPARD (REG.) | 1.151 | |
| LASER (GMND) | 1.168 | + 2.3 % |
| LEOPARD (MND) | 1.189 | + 3.2 % |
| LASER (SXS) | 1.191 | + 4.3 % |
| AVG. OF SPECTRAL CORRECTED METHODS : | 1.183 | 3.3 % |
| MAX. (LASER SXS) | 1.191 | |

The PDQ-5 code wasused to calculate the powerdistribution in a similar way as for the conventional assembly. A mesh of 2 X 2 per unit cell was used, except at the boundaries near the watergaps & at the $UO_2$-MIX interface, where 3 X 3 meshes were taken. Two groups of neutrons were used.

Fig. V-8 shows the total powerdistribution as calculated with regular LEOPARD X-sections, whereas the first numbers on Fig. V-9 show the powerdistribution as calculated with the regular LASER X-sections.

It is thus observed that the differences between the calculated powerdistribution with LASER & LEOPARD are very substantial. Errors at the peak locations of 13.9 to 9.4 % are found. On the avg. there is a 5.10 % error in the $UO_2$ region & 6.9 % in the MIX.oxide region.

In contrast to the verification with experiment in chapter IV, the errors are not confined to the mix-oxide region alone. This comes because the total power in the assembly is normalised to 1.0, whereas in the experimental mock up Batelle analysts normalized their results to a high power $UO_2$ rod, such that the errors in the $UO_2$ were minimized in that scheme. The errors are thus seen to be particular at the most important locations : around the watergaps & mixed oxide region, but also in the center mixed oxide region the powerdistribution using LEOPARD varies wildely.

It is particularly interesting to note that whereas the $k_\infty$ in the Mixed Oxide region using LEOPARD was found to be about 1.106 & with LASER 1.35, the overall $k_\infty$ of the assemblies is very close. It seems thus very dangerous to evaluate the accuracy of a X-Sectiongenerating code on the overall $k_{eff}$ of a core.

Since it was more or less felt that the influence of the cut-off for the PU-240 resonance was responsible for the breakdown of the standard LEOPARD code, the PU 240 was removed in the LASER & LEOPARD unit cell codes & $k_\infty$ 's were compared.

| | | | | | | | | | | | | | | |
|---|---|---|---|---|---|---|---|---|---|---|---|---|---|---|
| 1.094<br>+5.2 | .963<br>-0.3 | .810<br>-7.2 | 1.154<br>+4.6 | .939<br>-5.2 | .864<br>-8.5 | .867<br>-7.8 | X | .867<br>-7.8 | .863<br>-8.6 | .938<br>-5.3 | 1.152<br>+4.7 | .808<br>-7.3 | .958<br>-0.6 | 1.086<br>+4.7 |
| 1.103<br>+5.5 | .973<br>+0.2 | .822<br>-6.6 | 1.177<br>+5.6 | .956<br>-4.4 | .873<br>-8.1 | .856<br>-8.6 | | .856<br>-8.6 | .872<br>-8. | .953<br>-4.7 | 1.169<br>+5.0 | .812<br>-7.3 | .952<br>-1.1 | 1.064<br>+3.3 |
| 1.118<br>+6.2 | .993<br>+0.9 | .856<br>-4.9 | 1.273<br>+9.4 | 1.028<br>-1.0 | .915<br>-6.3 | | | | .911<br>-7.0 | 1.021<br>-1.5 | 1.255<br>+8.4 | .835<br>-6.4 | .949<br>-1.6 | 1.023<br>+1.1 |
| 1.136<br>+6.7 | 1.023<br>+2.1 | .917<br>-2.2 | .787<br>-8.4 | 1.208<br>+6.9 | | | | | | 1.192<br>+6.0 | .770<br>-9.7 | .884<br>-4.3 | .956<br>-1.6 | 1.000<br>-0.1 |
| 1.160<br>+7.5 | 1.057<br>+3.3 | .977<br>+0.1 | .892<br>-3.4 | | | | | | | | .864<br>-5.3 | .929<br>-2.7 | .970<br>-1.3 | .995<br>-0.6 |
| 1.192<br>+8.8 | 1.096<br>+4.7 | 1.032<br>+2.2 | | | | | | | | | | .962<br>-1.6 | .984<br>-1.1 | .998<br>-0.7 |
| 1.237<br>+10.6 | 1.149<br>+6.9 | | | | | | | | | | | | .995<br>-0.8 | .995<br>-1.3 |
| 1.310<br>+13.9 | | | | | | | | | | | | | | 1.006<br>-0.7 |
| | | | | | | | | | 1.067<br>+2.8 | 1.018<br>+0.5 | 1.004<br>-0.4 | 1.003<br>-0.6 | 1.002<br>-1.0 | 1.007<br>-0.7 |

$k_\infty$ : 1.178631

FIG. V-8 POWERDISTRIBUTION IN THE PLUTONIUM RECYCLE ASSEMBLY USING REGULAR LEOPARD X-SECTIONS & % ERROR RELATIVE TO THE CALCULATION WITH LASER REGULAR X-SECTIONS.

| | | | | | | | | | | | | | | |
|---|---|---|---|---|---|---|---|---|---|---|---|---|---|---|
| 1.040<br>1.045 | .966<br>.958 | .873<br>.848 | 1.103<br>1.131 | .990<br>.998 | .944<br>.935 | .940<br>.935 | X | .940<br>.935 | .944<br>.935 | .990<br>.988 | 1.102<br>1.131 | .872<br>.847 | .964<br>.956 | 1.037<br>1.042 |
| 1.045<br>1.049 | .971<br>.964 | .880<br>.855 | 1.115<br>1.146 | 1.000<br>1.000 | .950<br>.942 | .937<br>.929 | | .937<br>.929 | .950<br>.943 | 1.000<br>1.000 | 1.113<br>1.144 | .876<br>.851 | .963<br>.955 | 1.030<br>1.031 |
| 1.053<br>1.057 | .984<br>.978 | .900<br>.880 | 1.164<br>1.210 | 1.039<br>1.048 | .976<br>.971 | | | | .975<br>.971 | 1.037<br>1.047 | 1.158<br>1.205 | .892<br>.872 | .964<br>.957 | 1.012<br>1.010 |
| 1.065<br>1.069 | 1.002<br>.999 | .938<br>.925 | .859<br>.825 | 1.130<br>1.166 | | | | | | 1.125<br>1.162 | .853<br>.825 | .924<br>.911 | .972<br>.967 | 1.001<br>1.000 |
| 1.079<br>1.085 | 1.023<br>1.023 | .976<br>.969 | .923<br>.908 | | | | | | | | .912<br>.897 | .955<br>.948 | .983<br>.981 | 1.001<br>1.000 |
| 1.096<br>1.106 | 1.047<br>1.050 | 1.010<br>1.008 | | | | | | | | | | .978<br>.948 | .995<br>.975 | 1.005<br>.994 |
| 1.118<br>1.135 | 1.075<br>1.083 | | | | | | | | | | | | 1.003<br>1.004 | 1.009<br>1.010 |
| 1.150<br>1.182<br>+2.8% | | | | | | | | | | | | | | 1.013<br>1.014 |
| | | | | | | | | | 1.038<br>1.071 | 1.013<br>1.044 | 1.008<br>1.038 | 1.009<br>1.040 | 1.012<br>1.043 | 1.014<br>1.046 |

k-INF. = 1.17985 (REG.), 1.17937(GMND)

FIG. V-9. POWERDISTRIBUTION IN THE PLUTONIUM RECYCLE ASSEMBLY USING REGULAR LASER X-SECTIONS (UPPER) AND GMND X-SECTIONS FROM LASER (BOTTOM)

Table V-2 shows the results of the comparison of the LEOPARD & LASER unit cell results for the three fuels. Noticeble is that the LEOPARD code gives good agreement except for the mixed oxide fuel with 19 a/o nominal PU 240 concentration. Therefore we may conclude that the very detailed resonance description of PU240 at 1.0 eV, in the thermal region of the LASER code, and the crude description and complete neglecting of PU240 self-shielding in the fast & epithermal group MUFT calculation in the Standard LEOPARD code, are responsible for the large discrepancies in $k_\infty$ & powerdistribution. The influence of the PU240 on $k_\infty$ is thus extremely important for mixed oxide fuels, and should be described accurately.

Fig. V-13, shows the fraction of the power, due to thermal neutrons in a portion of the PU-recycle assembly as determined with the PDQ-5 code, using regular LASER X-sections. The fast & epithermal flux over the whole assembly was 79.9, whereas the thermal flux was10.27. The fast & epithermal fluxes in the $UO_2$ region was on the average 79.2 , and in the MIX OXIDE region 80.7. The thermal fluxes were respectively 11.5 in the $UO_2$ an 7.14 in the mixed oxide region *. It is thus observed that the powerfractions also change discontinuously from the $UO_2$ to the Mixed Oxide region, and that the power due to thermal neutrons is more important in the $UO_2$ fuel than in the mixed oxide fuel. However at peaking locations, the importance of the thermal neutrons for the power increases.

The powerdistribution in the PU-recycle assembly has also been calculated with the thermal GMND X-sections obtained from our recipe & the LASER code. For simplicity only one $UO_2$ region was considered and the GMND X-Sections for the $UO_2$-MIX interface were used. The results are also shown on Fig.V-9 and are thus easely compared to the results with the regular LASER X-sections.

* The fluxes are normalised such that the total power in the assembly = 1.0

TABLE V-2 COMPARISON LASER AND LEOPARD UNIT CELL CALCULATIONS.

($B^2$ = 0.00071 $cm^{-2}$) (1400 ppm B, 19.8 % B-10)

$k_\infty$

| CASE | $k_\infty$ LASER (cut-off 1.855 eV) | $k_\infty$ LEOPARD | % DIFFERENCE $k_\infty$ (LEOP-LASER) |
|---|---|---|---|
| 1)- $UO_2$ FUEL (4.0 w/o U235) | 1.20594 | 1.20472 | -0.1 % |
| 2)- MIX.OXIDE (4 w/o $PUO_2$- nat $UO_2$) | 1.13510 | 1.10539 | -2.6 % |
| 3)- MIX.OXIDE (PU 240 removed) | 1.31425 | 1.30748 | -0.5 % |

In comparison with the results obtained in chapter IV, it is thus noticed that the increase in the powerpeakingfactor is nearly the same in both $UO_2$ MIX OXIDE regions. A slight fainting of the effect at the watergap away from the intersection may be noticed.

Table V-3 shows the comparison at the beginning of life of the local powerpeakingfactors in the proposed plutonium recycle assembly, using different methods and the results obtained in this chapter & chapter IV. The results obtained with the LEOPARD code have also been included, although the local powerpeakingfactors are not recommended in view of the results obtained in this chapter and the verification with experiment. It is thus observed that there are two powerpeakingfactors, one in the mixed oxide & one in the $UO_2$ and that they are nearly equal. The local powerpeakingfactor in the Mix-Oxide seems a little bit higher than in the $UO_2$.

From Table V-3 it is thus also noticed that the spectraleffects at the watergap and mixed oxide have an influence of about 4 % on the local powerpeakingfactor. The influence of the detailed PU240 resonance is on the order of 14 % to 10 %, this is thus a major factor of concern for calculations with codes such as LEOPARD with a cut-off smaller than the 1.0 eV resonance of PU 240.

In order to evaluate the influence of the weight percent of $PUO_2$ in the mixed oxide rods, two more calculations were made. Using the basic proposed PU-recycle assembly design of 68 Mixed Oxide rods in the assembly of 236 rods, the % increase in the Local powerpeakingfactors was calculated for 3.5 & 4.5 w/o $PUO_2$ relative to the standard 4.0 w/o case. Since the number of Mixed Oxide rods is inversily proportional to the w/o of $PUO_2$, another run was made using 4.5 w/o in which only 56 mixed oxide rods were used in a layout pictured on Fig. V-10.

The effects of changing the w/o of $PUO_2$ in the mixed oxide rods, as well as the

effect of the change of the number of mixed oxide rods for a 4.5 w/o PU $O_2$ loading from 68 to 56 rods, shown in Table V-4 and on Fig, V-11

The values of the peaking-factors include a spectrumcorrectionfactor relative to the base case of 4.0 w/o, which was from the calculations noticed to change by 1.6 % per 1 w/o of $PUO_2$.

From Table V-4 & Fig. V-11 it is thus seen that :

1) the local powerpeakingfactors are only slightly higher in a PU-recycle assembly than in a conventional assembly. But the $k_\infty$ is substantially lower.

2) the local powerpeakingfactor in the PU-recycle assembly increases with increasing weight percent of $PUO_2$ used in the mixed oxide rods. The changes are only of the order of -3 to + 4.4 % when going from 4.0 % $PUO_2$ to 3.5 w/o & 4.5 w/o respectively.

3) the local powerpeakingfactor seems not very sensitive to the geometrical lay-out & number of mixed oxide rods; a reduction of the rods from 68 to 56 only reduces the peakfactor by 0.4 %. On the other hand the $k_\infty$ of the assembly is increased by 44 millik with decreased number of Mixed Oxide rods.

4) From Fig. V-10, showing the location of the powerpeaks, it is thus seem that there are only 2 powerpeaks in the conventional assembly, whereas there are 10 power-peaks in a PU-recycle assembly. According to a statistical model of Judge & Bowl ( 38 ), it should be expected that there are more chances to get an overpowersituation in a PU-recycle assembly than with a conventional assembly.

TABLE V-3 COMPARISON BOL-LOCAL POWERPEAKING FACTORS IN THE PROPOSED PLUTONIUMRECYCLE ASSEMBLY, USING DIFFERENT METHODS.

LOCATIONS A-1 AND F-4

| METHOD. | LOCAL POWERPEAKING FACTOR IN $UO_2$ | % INCREASE VS. REGULAR LASER | LOCAL POWERPEAKING IN MIXED-OXIDE | % INCREASE VS. REGULAR LASER |
|---|---|---|---|---|
| 1)- LASER (REG) | 1.150 | | 1.164 | |
| 2)- LASER (GMND) (1 $UO_2$ region) | 1.182 | + 2.8 % | 1.210 | + 4.0 % |
| 3)- LASER (GMND) (2 $UO_2$ regions) | 1.179 | + 2.5 % | 1.209 | + 3.9 % |
| 4)- LASER (SXS) | 1.200 | + 4.3 % | 1.199 | + 3.0 % |
| 5)- LEOPARD (REG)* | 1.310 | +13.9 % | 1.273 | + 9.4 % |

The recommended values are underlined, reflecting some conservatism.

* The powerpeaking with the standard LEOPARD is not recommended (see text and Table V-2, & experimental results , Chapter IV)

**Table V-4 COMPARISON OF THE LOCAL POWERPEAKINGFACTORS FOR DIFFERENT DESIGNS.**

CASE : POWERPEAKINGFACTORS IN UNIT ASSEMBLY.

| | in $UO_2$ | in MIX-OXIDE | $k_\infty$ (LASER X-SECT. |
|---|---|---|---|
| - CONVENTIONAL<br>- PU-RECYCLE (68 RODS) | 1.191 (1) | - | 1.2062 |
| 3.5 w/o $PUO_2$ | 1.198 (1) | 1.168 (2) | 1.1781 |
| 4.0 | 1.200 (1) | 1.210 (3) | 1.1799 |
| 4.5 | 1.205 (1) | 1.278 (4) | 1.1831 |
| - PU-RECYCLE (56 RODS)<br>4.5 w/o $PUO_2$ | 1.195 (1) | 1.273 (4) | 1.1875 |

(1) Includes the conservative spectralcorrectionfactor of 4.3 % (Table V-2)

(2) Includes the conservative spectral C.F. of 3.2 %. *

(3) Includes the conservative spectral C.F. of 4.0 % see Table V-3

(4) Includes the conservative spectral C.F. of 4.8 % *

* The Spectrumcorrectionfactors at the peak Mix-oxide locations (at the $UO_2$/MIX interface) were found from the calculations to change by an additional 1.6 % per 1 w/o of $PUO_2$ relative to the base case of 4 w/o of $PUO_2$,

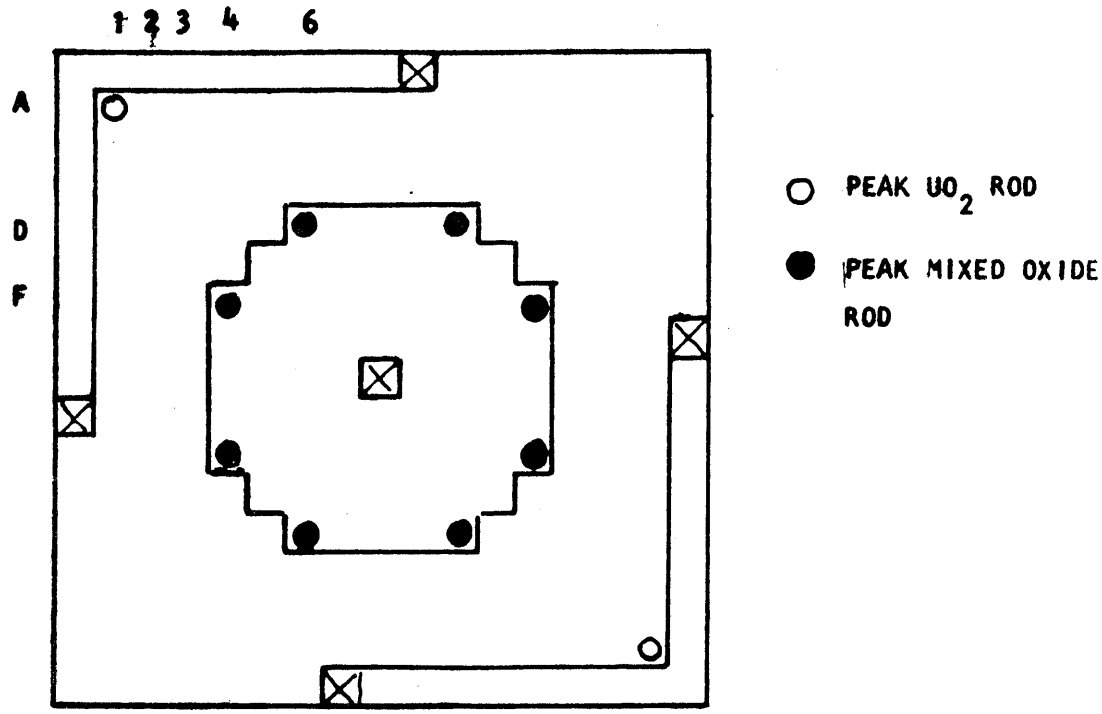


PROPOSED DESIGN -67 MIXED OXIDE RODS

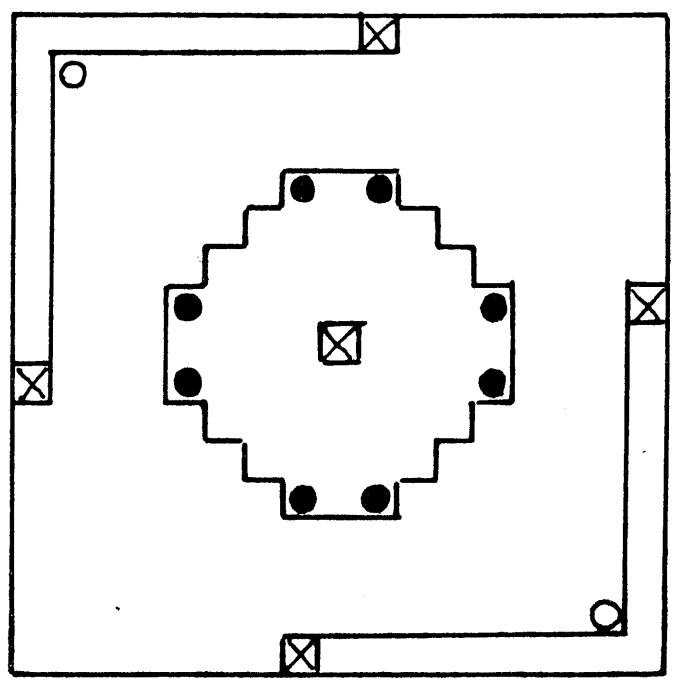

LAY OUT WITH 55 MIXED OXIDE RODS

FIG V-10 lay out and location of the local powerpeaks in the two different Pu-recycle designs

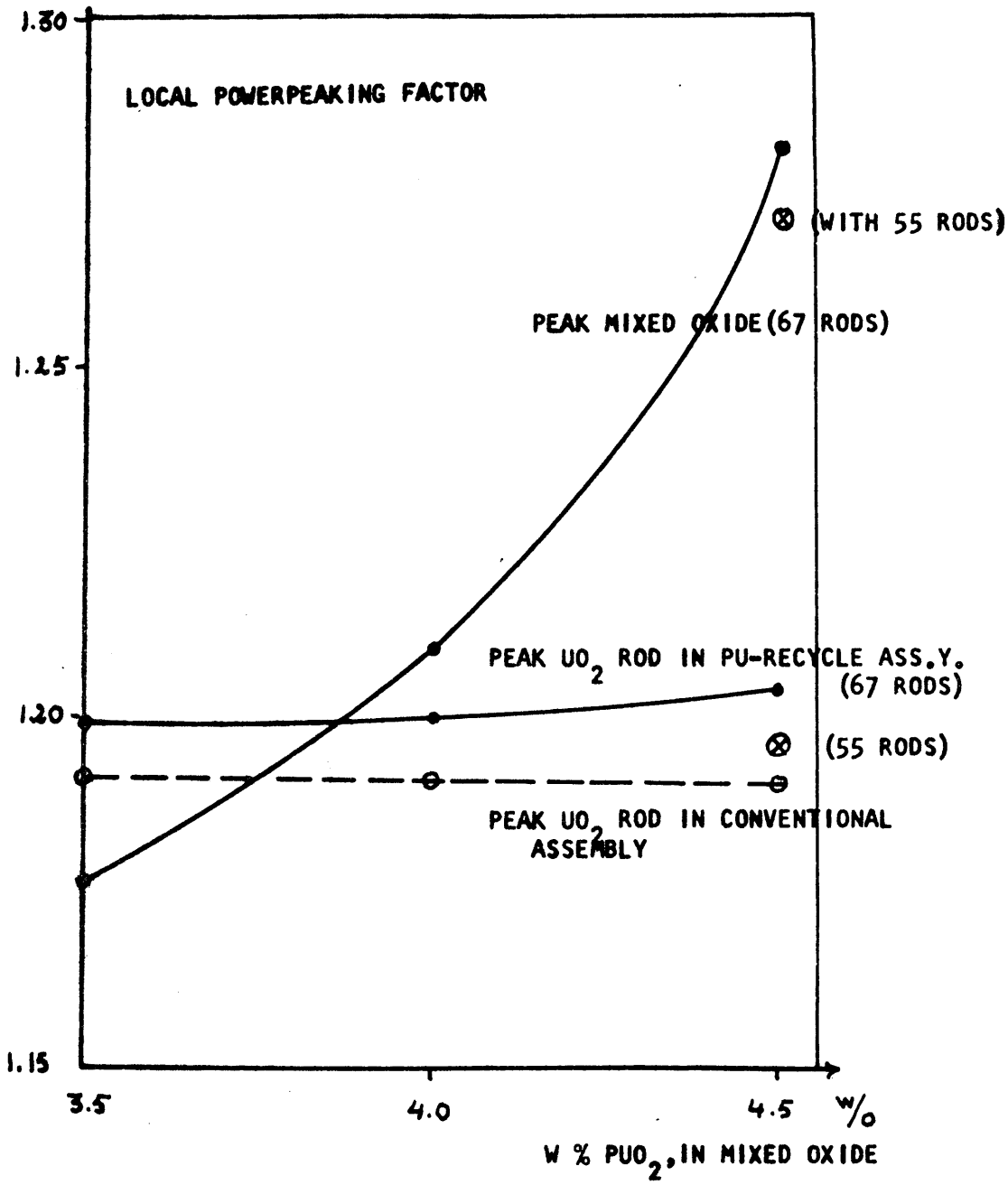


FIG V-11 LOCAL POWERPEAKING FACTORS IN A CONVENTIONAL & PLUTONIUM RECYCLE ASSEMBLY WITH DIFFERENT W% OF $PUO_2$

## V-4. THE VARIATION OF LOCAL POWERPEAKING FACTORS, POWERDISTRIBUTION AND $k_\infty$ IN A CONVENTIONAL & PLUTONIUMRECYCLE ASSEMBLY DURING LIFETIME.

### 4-1) INTRODUCTION :

In the previous section the powerdistributions & local powerpeaking-factors of the assemblies were calculated at beginning of life. Although in general the powerdistribution flattens out with burnup, such that the overall powerpeakingfactor for a reactor core decreases with burnup, the detailed situation of the local powerpeaking is much more complex and more or less unpredictable. Furthermore the new designs for plutoniuumrecycle applications are entirely different, and peculiar effects could be attributed to the different behaviour of $k_\infty$ versus burnup of conventional & mixed oxide fuel. It had e.g. been speculated that because the mixed oxide fuel starts with a large difference in $k_\infty$ between the $UO_2$ & mixed oxide fuel (which gradually diminishes and possibly even changes of sign), it could be possible that the local powerpeaking factor in the mixed oxide fuel increases with burnup. Because of these questions, as well as the question on how the spectral-coupling correction factors change with burnup, a simplified burnupstudy has been made on both the conventional & plutoniumrecycle assembly in order to evaluate the change in powerdistribution, local powerpeakingfactors & spectral-effects in both conventional & PU-recycle assemblies.

### 4-2) DESCRIPTION OF THE USED METHOD TO CALCULATE THE POWERDISTRIBUTION VS. BURNUP.

The accurate method that is used for the calculation of the fluxes, powerdistribution an $k_{eff}$ of a reactorcore or other fuel layout, consits of making unitcell-burnup calculations with codes as LEOPARD & LASER.

The input of such codes consit of e.g. the dimensions of fuel rod, clad and moderator, the temperatures, the overall core buckling (for the MUFT calculations), the materials & their initial atom-numberdensities (in units $10^{24}$).
For burnupapplications an average thermalreactorpower, the time step, fuel loading & other data e.g. on the fissionproducts are needed.
The codes calculate all the spectralaveraged microscopic cross-sections & other data at beginning of life, and the fast & thermal fluxes corresponding to the input average reactorpowers.
In the burnup-options, the codes calculate then, usually assuming that the fluxes remain constant during the time-step, the new concentrations of all burned & built-up materials from the burnupequations such as e.g. for the burnup of U238 & buildup of PU239

$$\frac{dN^{28}}{dt} = -\sigma_a^{28} \phi N_{28}$$

$$\frac{dN^{49}}{dt} = -\sigma_a^{49} \phi N_{49} + \sigma_c^{28} \phi N_{28}$$

,and a new spectrumcalculation is made which gives the new cross-sections & macroscopic data (such as $k_\infty$ & $k_{eff}$) after this timestep $\Delta$ t or burnupstep $\Delta$ B.
This is repeated until the final specified burnup has been reached.
In this way spectralcorrected microscopic cross-sections, macroscopic & isotopic inventories are obtained of an <u>average</u> fuel cell versus burnup or time t.
The standard proceedure to calculate the reactor characteristics versus burnup, is, after having obtained all the <u>microscopic</u> X-sections versus time, to make diffusiontheory calculations in 3 dimensional reactormodel using e.g. the PDQ-5 or 7-HARMONY code package. The PDQ-5 or 7 code solves the diffusion equation at each avg. specified burnupstep, gives the group-fluxes to HARMONY which solves <u>again</u>

the burnup-equations using an elaborate input deck of microscopic X-sections versus time as obtained with e.g. LEOPARD or LASER, and obtains at each flux-point the macroscopic reactordata which are fed in PDQ-5 for the subsequent flux & powerdistributioncalculation.

Although with the PDQ-HARMONY package all calculations are automatically done with the computor without human interventions, the set up is quite elaborate, and requires about 3 to 4 months of preparation.

Furthermore the calculations are about 4 times more costly than regular diffusiontheory calculations.

To avoid these drawbacks at the stage where no final design characteristics are known, the following relatively inexpensive method has been used.

The geometrical Model.

Instead of isolating one assembly, we will isolate one quarter of an assembly containing the cruciform follower & watergap. The use of this geometry permits a description with 16 X 16 meshes (2 X 2 meshes/ unit cell), instead of 42 X 21 meshes needed to describe the whole assembly with a $180^{o}$ rotational symmetry.

A savings of half the computorcost and half the input preparationtime is therewith possible. This model was found to underpredict the powerdistribution, in a conventional assembly by maximum 3.6 % compared to a whole assembly description, and by maximum 1 % in a PU-recycle assembly.

The effect on the $k_{\infty}$ (excluding the extra regions - other than fuel) was less then 1 milli-k for the conventional assembly and PU-recycle assembly.

The burnupcalculations.

Since the Standard LEOPARD code had been found to be in error, the more expensive LASER code had to be used for the burnup unit cell calculations of both the $UO_2$ (4 w/o U 235) and MOX fuel (4.0 w/o $PUO_2$ (19 w/o PU 240)-nat $UO_2$).

Burnupsteps of 2400 MWD/MT (U+PU)were used up to 24,000 MWD/MT.

The input was identical to the input for a normal unit cell calculation except for the following additions necessary for burnup applications in the LASER code. In the LASER code, fission products are separated into Xe-135, Sm-149 and all fissionproducts lumped into one pseudo fission product. The cross-sections for the lumped fission products are defined such that one fissionproduct is produced per fission event. These pseudo fissionproduct cross-sections, in the form of polynominal equations are required as an input to the LASER code. Results of CINDER calculations by Celnik et al ( 39 ) have been correlated by Rim ( 40 ) to derive the following equations :

For $UO_2$ FUEL :

$$\sigma_{ao}^{th} = 116.1 - 2.443\times10^{-3}B + 3.50\times10^{-8}B^2 - 1.70\times10^{-13}B^3 \quad \text{for } 0 \leq E \leq 1.855\,eV$$

$$\sigma_{a\,epi} = 23.72 + 1.563\times10^{-4}B - 2.146\times10^{-8}B^2 + 3.63\times10^{-13}B^3 \quad \text{for } 1.855\,eV \leq E \leq 5530\,eV$$

$$\sigma_{a\,FAST} = 0 \quad \text{for } 5530\,eV \leq E \leq 10\,MeV$$

FOR THE 4 w/o $PUO_2$ - $UO_2$(nat) FUEL,

$$\sigma_{ao}^{th} = 190.6 - 7.362\times10^{-3}B + 2.032\times10^{-7}B^2 - 2.26\times10^{-12}B^3 \quad \text{for } 0 \leq E \leq 1.855\,eV$$

$$\sigma_{a}^{epi} = 32.93 - 9.47\times10^{-5}B - 1.545\times10^{-8}B^2 + 2.58\times10^{-13}B^3 \quad \text{for } 1.855 \leq E \leq 5530$$

$$\sigma_{a\,FAST} = 0 \quad \text{for } 5530 \leq E \leq 10\,MeV$$

where B is the burnup in MWD/$_{MTM}$, $\sigma_{ao}^{th}$ is the 2200 m/sec value of a 1/v cross-section in (b/fission) and $\sigma_a^{epi}$ is the epithermal cross-section (taken constant with energy) in (b/fission).

To account for the non-uniform buildup of PU-239, LASER requires as input a spatial distribution of the U-238 resonance capture rate. Fig. V-10 shows this distribution in a fresh $UO_2$ fuel obtained from a Monte Carlo calculation ( 41 ). The volume averaged values in each region (5 regions in the usual LASER mesh) obtained from Fig. V-10 are given on Table V-5.

Table V-5.

Spatial Distribution of U-238 Resonance Capture Rate.

| Region (fractional radius). | U-238 absorption per neutron. |
|---|---|
| 0 - 1/9 | 0.0135 |
| 1/9 - 3/9 | 0.0140 |
| 3/9 - 5/9 | 0.0150 |
| 5/9 - 7/9 | 0.0180 |
| 7/9 - 1 | 0.0299 |

The cross-section data used in the LASER calculations are mostly those used in the standard PWR designs at WAPD ( 42 ).

Thermal U.235 and PU-239 cross-sections are normalized to the 2200 m/sec parameters of Sher et al ( 43 ), and thermal PU-241 data were normalised to the 2200 m/sec parameters of Westcott et al ( 44 ). These parameters are listed in Table V-6.

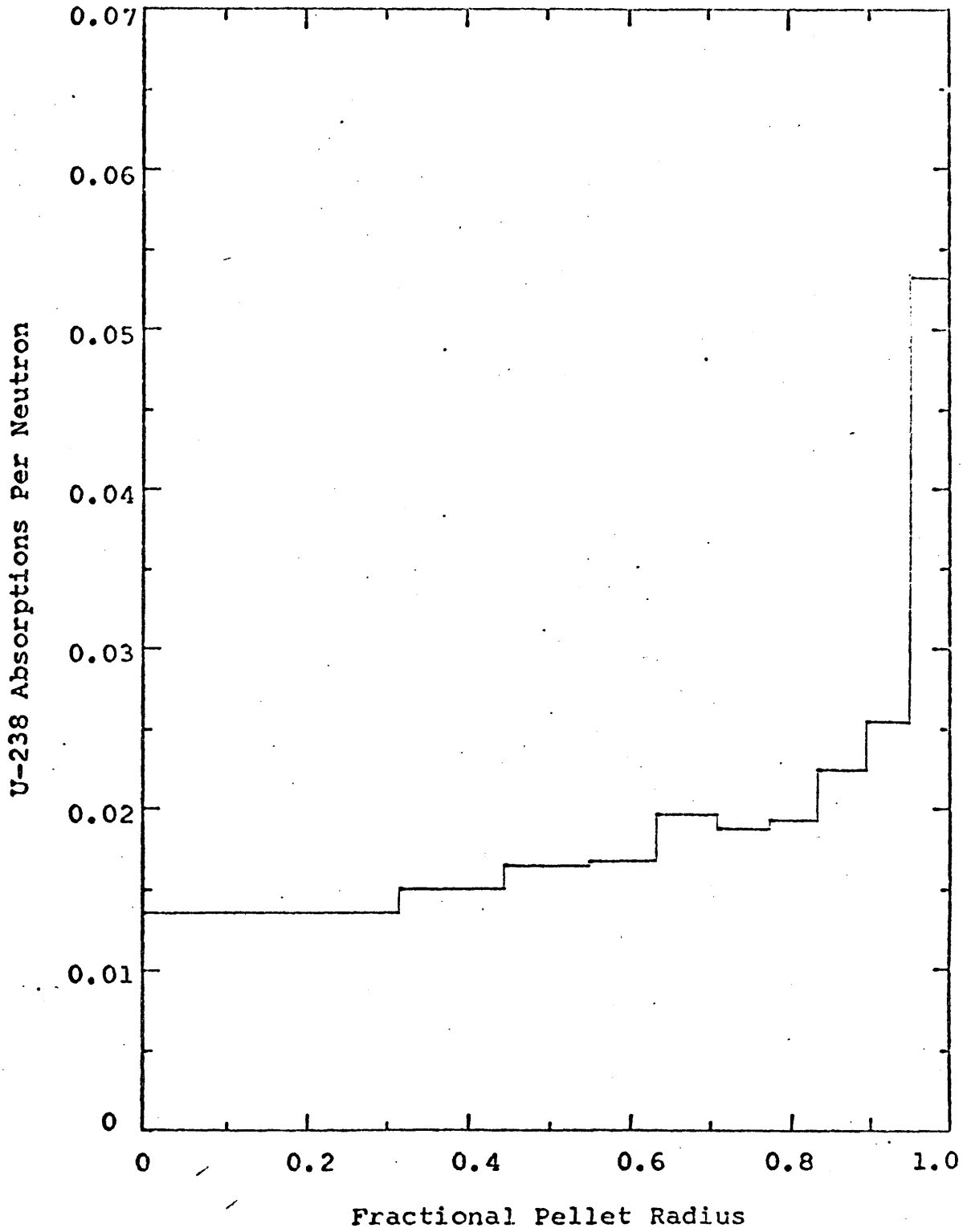


Fig. V-12, Monte Carlo result of the spatial distribution of U-238 resonance captures.

TABLE V-6.

2200 m/sec Parameters for Fissile Nuclides.

| cross-section | U-235 | PU-239 | PU-241 |
|---|---|---|---|
| $\sigma_f$ (barns) | 578 | 742 | 1,013 |
| $\sigma_a$ (barns) | 679 | 1,015 | 1,376 |
| $\nu$ | 2,442 | 2,898 | 2,978 |

The 2-Dimensional Burnup Calculation method.

Instead of feeding microscopic X-sections versus time, obtained from the LASER program into the HARMONY code. the macroscopic X-sectiondata of 2 groups have been fed into the PDQ-5 code in each of the 59 fuel cells. The PDQ-5 code was thus set up to contain 35 different compositions, making use of the diagonal symmetry.

The method used consited of essentially the following steps :

1) From a beginning of life calculation the powerdistribution was obtained in the 1/4 of the conventional and PU-recycle assembly.
2) Assuming that during a certain assembly-average burnupstep $\Delta B$, the power-distribution remains constant, a two dimensional burnupmap is obtained since the burnup distribution is proportional to the normalized powerdistribution, according to :

$$\Delta B = \frac{P' . \Delta t}{\rho . A(M)/A(ox.)}$$

where B = burnup, in $MWD/_{MTM}$

P' = powerdensity in kw per $cm^3$,

$\rho$ = density of the fuel in $kg/cm^3$

A(M) = avg. atomweight of metal in oxide fuel.

t = time in days.

Therefore for each step $\Delta t$ or each average assembly burnupstep $\Delta B_{ass}$,

$$\frac{\Delta B(x,y)}{\overline{\Delta B}_{as}} = P'(x,y) \qquad (5\text{-}9)$$

and at each time t :

$$B(x,y,t) = \overline{\Delta B}_{as}\left[\sum_{\text{all } \Delta t' \text{ intervals}} P'(x,y,t')\right] = \overline{\Delta B}_{as}\int_0^t P'(x,y,t')\,dt' \qquad (5\text{-}10)$$

$$\overline{B}_{as} = \sum \overline{\Delta B}_{as}$$

Thus, knowing the burnupincrement distribution or according to (5-9) the powerdistribution, the 2 dimensional burnupdistribution is obtained from equation 5-10.

3)From the 2D burnupmap B (x,y,t) at time t or avg. assembly burnup $\overline{B}$, the <u>macroscopic</u> two group, thermal GMND X-Sections at each unit cell X, Y, are obtained from the macroscopic X-sections and the 1/V & 1/V grad, versus burnup from LASER.

Stirling's interpolation formula :

$$y(x) = y_i + \frac{y_{i+1} - y_{i-1}}{2} \cdot \frac{x - x_i}{\Delta x} + \frac{y_{i+1} - 2y_i + y_{i-1}}{2}\left(\frac{x - x_i}{\Delta x}\right)^2$$

(where y is the macroscopic X-section $\Sigma$ at burnup B = X, $X_{i+1} - X_i = X_i - X_{i-1} = \Delta X = \Delta B = 2400$ MWD/$_{MTM}$)

and $y_i$ & $x_i$ are the macroscopic X-sections $\Sigma_i$ and burnup $B_i$ at the burnuppoint i in LASER ).

has been programmed for a Wang desk calculator, to obtain accurate macroscopic X-sections at each location X, Y, by quadratic interpolation in 3 LASER data.

Limitations of the method.

Strictly speaking the used procedure is only accurate if the ratios of the fast & epithermal flux to the thermal flux in the $UO_2$ & MIX OXIDE unit cells, are the same as the ratios in the 2 D PDQ-5 diffusiontheory calculation; and if all the microscopic X-sections are flux-independent.

With regard to the first restriction it was found that the ratios of the fast & epithermal flux to the thermal flux in the $UO_2$ unitcell & in the MIX OXIDE cell were respectively : 14.5 an 6.70; whereas in the PDQ-5 calculation they were on the average 11.3 and 6.9. The maximum deviation in the pointwise X, Y burnup will thus be of the order of 5 % in the $UO_2$ and 3 % in the MIX OXIDE, or less since some compensation can be expected.

With regard to the second restriction the Xe-cross-section is flux dependent according to the equation at equilibrium :

$$\Sigma_{a\,XE}(t) = \frac{(\gamma_I + \gamma_X)\,\Sigma_f(t)\,\phi_T(t)}{\phi_X + \phi_T(t)} \qquad \text{(V-11)}$$

where $\gamma_I$ & $\gamma_X$ are the effective yields from fission of Iodine 135 & Xe 135, & $\phi_X = 0.756 \times 10^{13}\ cm^{-2}\ sec^{-1}$.

Since $\phi_T$ is of the order of $2.9 \times 10^{13}$ in $UO_2$ & $1.6 \times 10^{13}$ in the MIX OXIDE, the Xe concentration is on the average, insensitive to the fluxvariations.

The SM-149 equilibrium macroscopic X-section is given by :

$$\Sigma_{a\,SM}(t) = \gamma_P\,\Sigma_f(t) \qquad \text{(V-12)}$$

& is thus independent of the flux.

The fissionproduct microscopic X-section $\sigma_{FP}$ accumulate at a rate of $\sigma_{FP}$ per fissionevent. This X-section is thus given by :

$$\Sigma_{FP} = \sigma_{FP} \int \Sigma_f(t)\,\phi(t)\,dt$$

FIG. V-13 : FRACTION OF TOTAL POWER DUE TO THERMAL NEUTRONS IN A PORTION OF THE PLUTONIUM RECYCLE ASSEMBLY.

| | | | | | | | |
|---|---|---|---|---|---|---|---|
| 0.793 | 0.786 | 0.781 | 0.776 | 0.772 | 0.769 | 0.766 | 0.764 |
| | 0.776 | 0.769 | 0.762 | 0.756 | 0.751 | 0.747 | 0.744 |
| | | 0.759 | 0.749 | 0.738 | 0.726 | 0.718 | 0.715 |
| | | | 0.733 | 0.711 | 0.750 | 0.738 | 0.734 |
| | | | | 0.742 | 0.718 | 0.706 | 0.703 |
| | | | | | 0.699 | 0.690 | 0.688 |
| | | | | | | 0.687 | 0.687 |
| | | | | | | | |

Avg. : .740
Avg. $UO_2$ : .750
Avg. MIX : .715

$\boxed{0.793}$ POWERFRACTION DUE TO THERMAL NEUTRONS (LASER)

and is thus proportional to the burnup; which is accounted for by the model. It is thus observed that for the calculation of unit assemblies during lifetime, the assumptions for the validity of the method are very well satisfied. Only the LASER burnup data, & the PDQ-5 code are thus needed for the calculation of the assemblies during burnup. The drawback evidently is that for each assembly average burnupstep, the 2D burnupmap has to be calculated from Eq.V-10, and the macroscopic 2-groupdata have to be calculated for each of the 34 different unit cells. With the aid of a small deskcalculatorprogram, the complete set-up of one burnupstepproblem for one assembly with PDQ-5 took about 3 to 4 hours.

## 4-3) RESULTS FOR THE BURNUP OF ISOLATED FUEL RODS.

### 4-3)1. Uraniumoxide fuel.

Fig. V-14 shows the thermal neutronspectrum in a fresh $UO_2$ fuel cell & Fig. V-15 shows the thermal neutron spectra in the cell burned to 24000 $MWD/_{MTM}$. Comparison of both spectra reveals that the flux-depressions at the 0.296 eV resonance of PU239 and the 1.06 eV resonance of PU 240 are very pronounced, therefore the self-shielding effects of these resonances become important in irradiated $UO_2$fuels at highburnups & in plutonium recycle fuels, as has been noticed earlier.

Fig. V-16 shows the isotopic fractional absorptionrates as a function of burnup. This figure represents a neutronbalance in the cell excluding leakage. It is seen that about 1.5 % of the absorptions occur in the zircalloy cladding, about about 3 % in the hydrogen of the moderator and about 1 % in the oxygen of the fuel and moderator, and about 94.5 % in the fuel region. The fractional absorptions in the cladding & moderator decrease with burnup.

It is important to note that the U238 & U235 absorptionrate ratios, initially

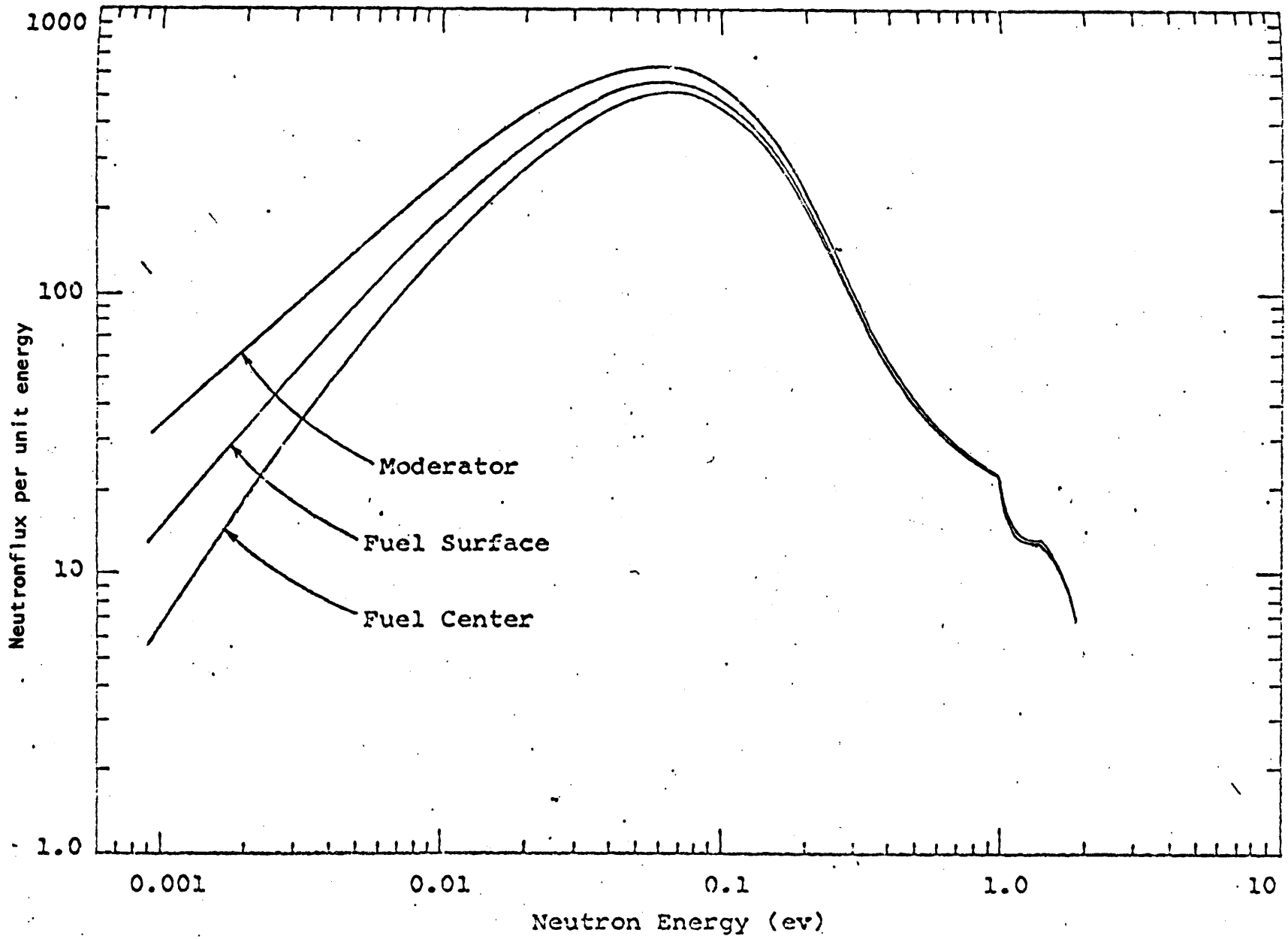


FIG V-14 Thermal neutron spectra in a fresh $UO_2$ fuel cell.

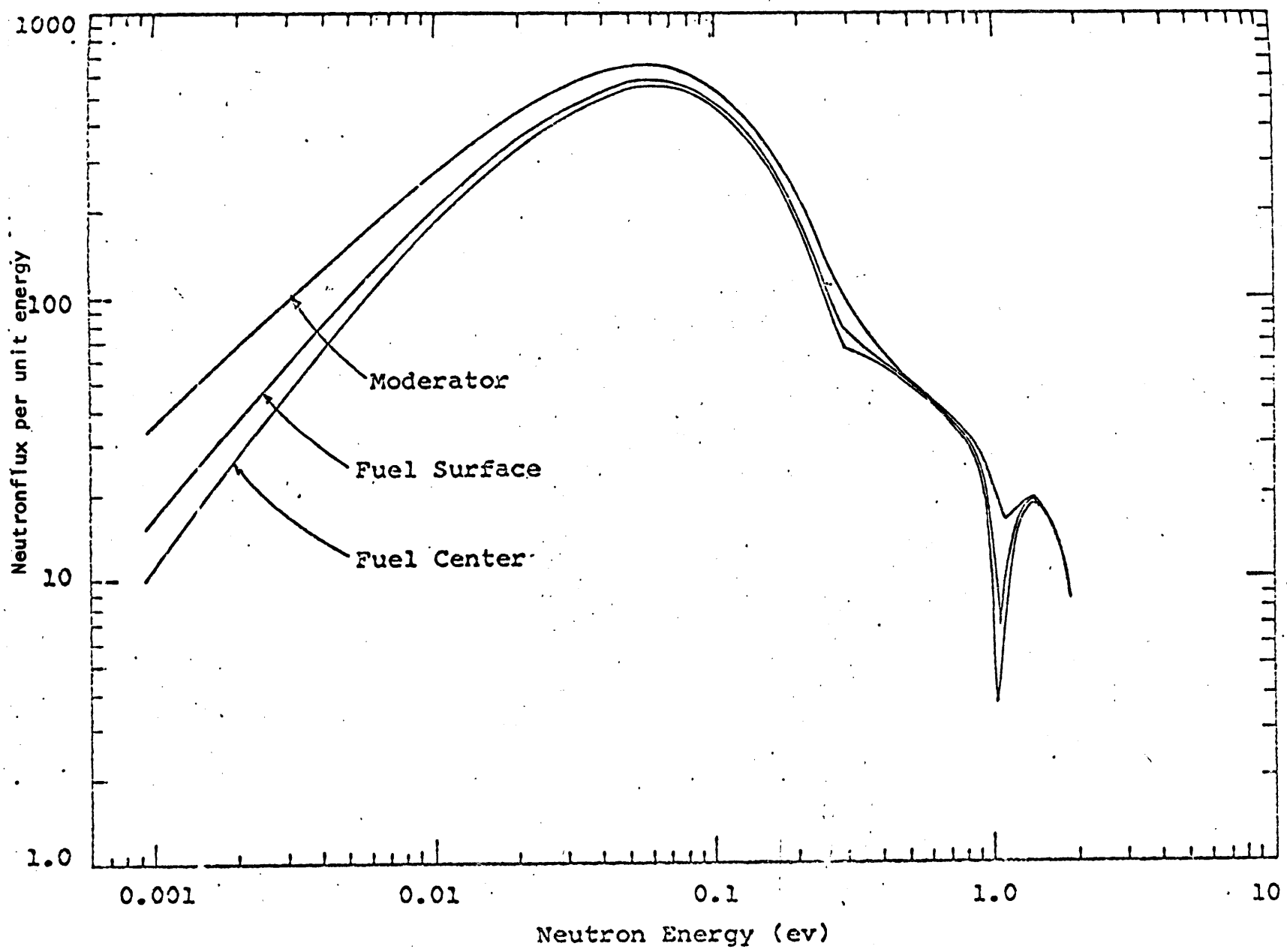


FIG. V-15, Thermal neutron spectra in a depleted $UO_2$ fuel cell.

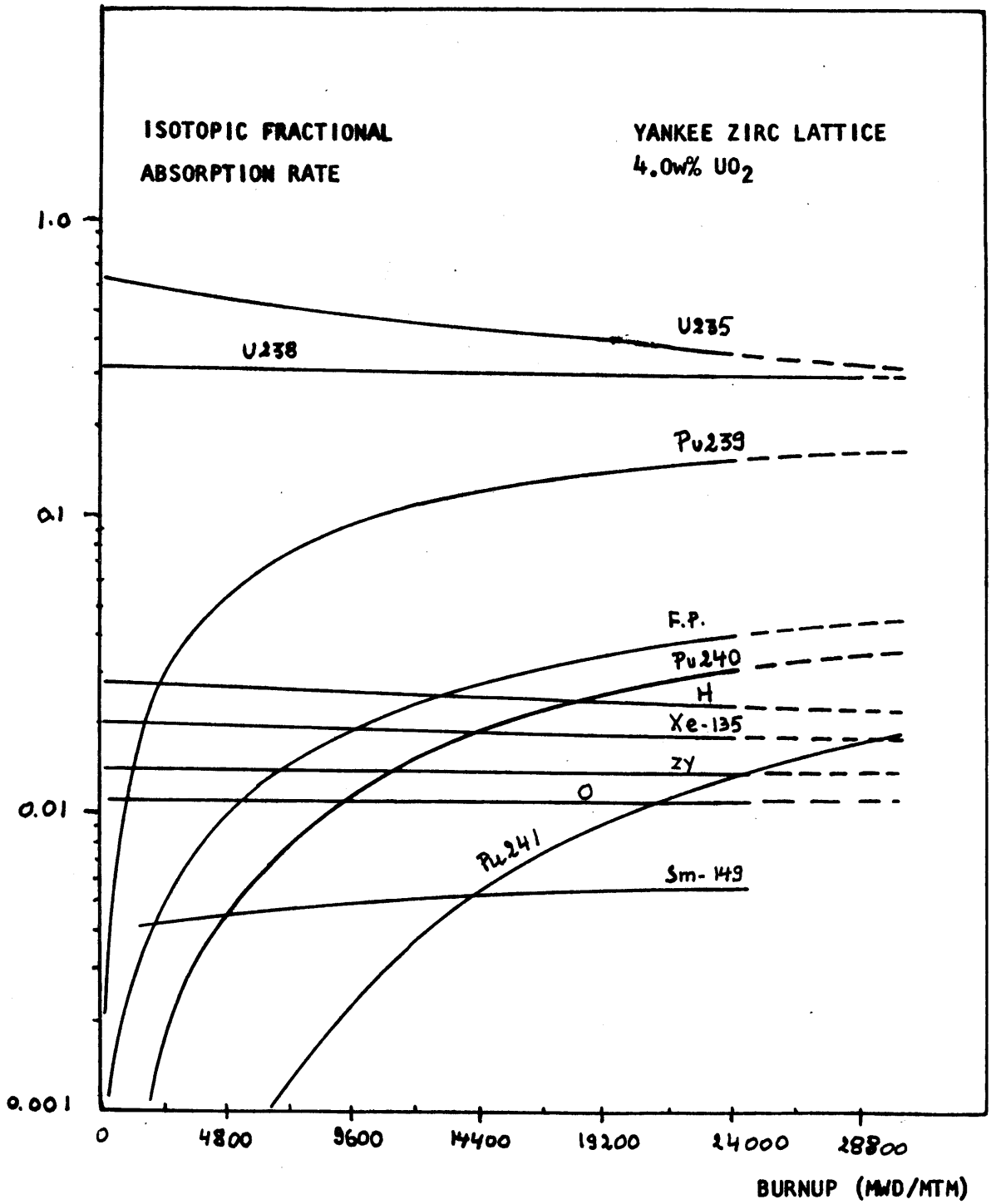


FIG. V- 16 NEUTRON BALANCE IN A $UO_2$ CELL AS A FUNCTION OF BURNUP

responsible for 94.5 % of the absorptions in the cell, are still very important at 24000 $MWD/_{MTM}$, at which they contribute for about 67 % of the absorptions, the rest being taken by mainly the PU239 buildup (about 16%). The contribution of the fissionproducts to the absorptionrate increases nearly linearly with burnup from 0 to about 4.2 % at 24000 $MWD/_{MTH}$.

Fig. V-17, shows the fuel region-averaged isotopic concentrations in an irradiated $UO_2$ fuel. The U238 concentration, per initial U238 atom, which is not shown on the figure changed from an initial 1.0 to 0.9820 at 24000 $MWD/_{MTM}$. The figure shows that this fuel will produce about 7.5 grams of PU fissile (6.5 grams PU-239 an 1.0 grams of PU241) per kg of initial uranium afer burnup of 24000 $MWD/_{MTM}$.

Fig. V-18 shows the plutoniumisotopic composition as a function of burnup. At 24000 $MWD/_{MTM}$ the isotocpic compositions are : 70 % PU239, 16.9 % PU240, 11,2 % PU 241 an 1.8 % PU242. The radial distribution of PU-239 concentrations was noticed to follow the spatial distribution of U238 resonance captures and has a peak at the fuel surface.

The $k_{\infty}$ and $k_{eff}$ of the $UO_2$ unit cell ($B^2 = 0.00071\ cm^{-2}$) are shown on Fig.V-19 The uraniumoxide fuel in an infinite reactor will thus have a k infinity of 1.00 at about 33.600 $MWD/_{MTU}$, whereas the same fuel in a batch loaded Yankee reactor only reaches a burnup of 24000 $MWD/_{MTM}$.

Fig. V-20, shows the variation of the most important macroscopic X-sections versus burnup. It is thus noticed that whereas the absorption X-section increases with burnup & the fast & epithermal fission X-sections decrease, the thermal fission $\Sigma f_2$ & especially the $\nu\Sigma_{f_2}$ are reaching a maximum at about 5000 & 14000 $MWD/_{MTM}$ respectively.

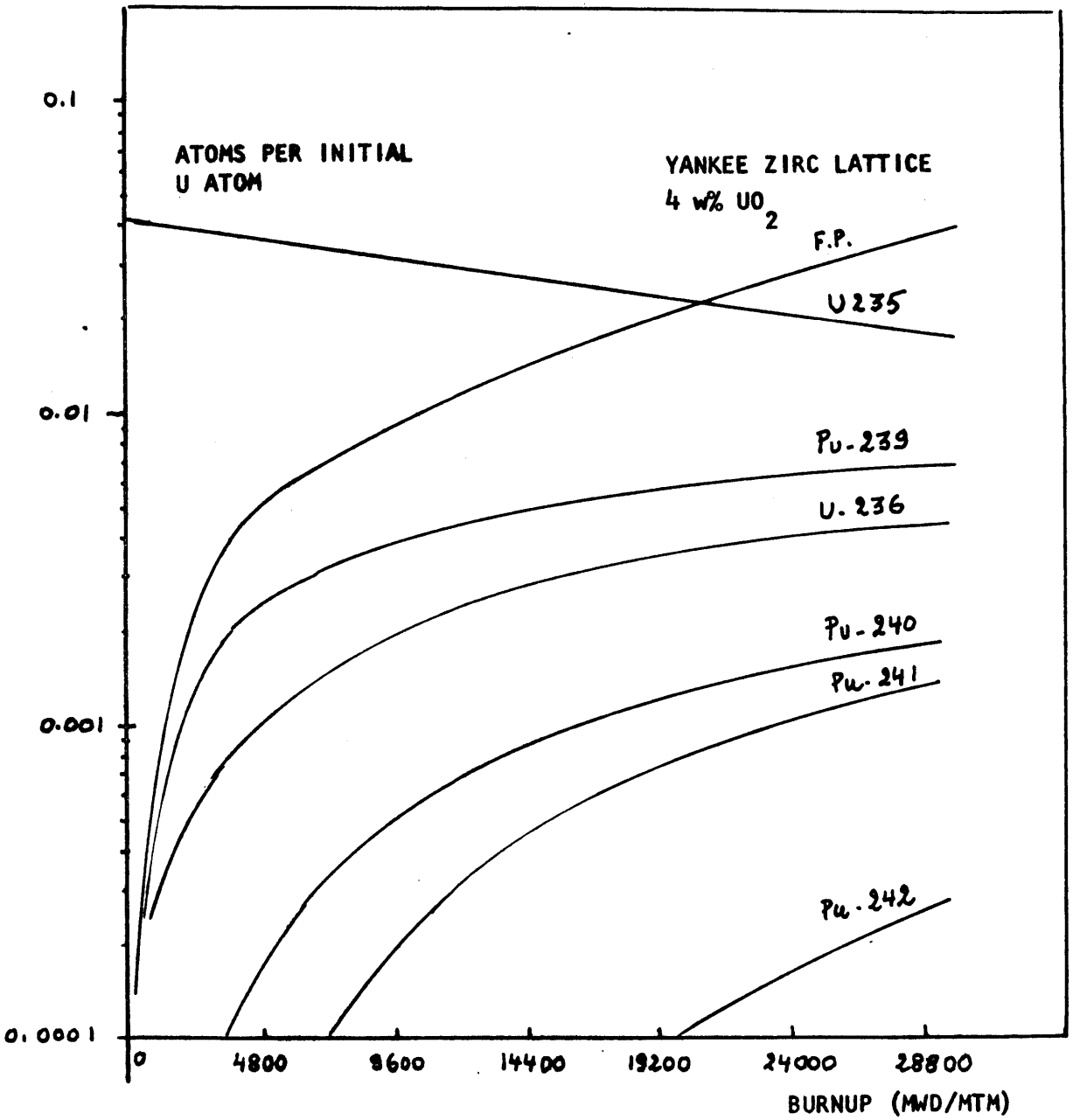


FIG V-17 FUEL REGION AVERAGED ISOTOPIC CONCENTRATIONS IN $UO_2$ VS. BURNUP

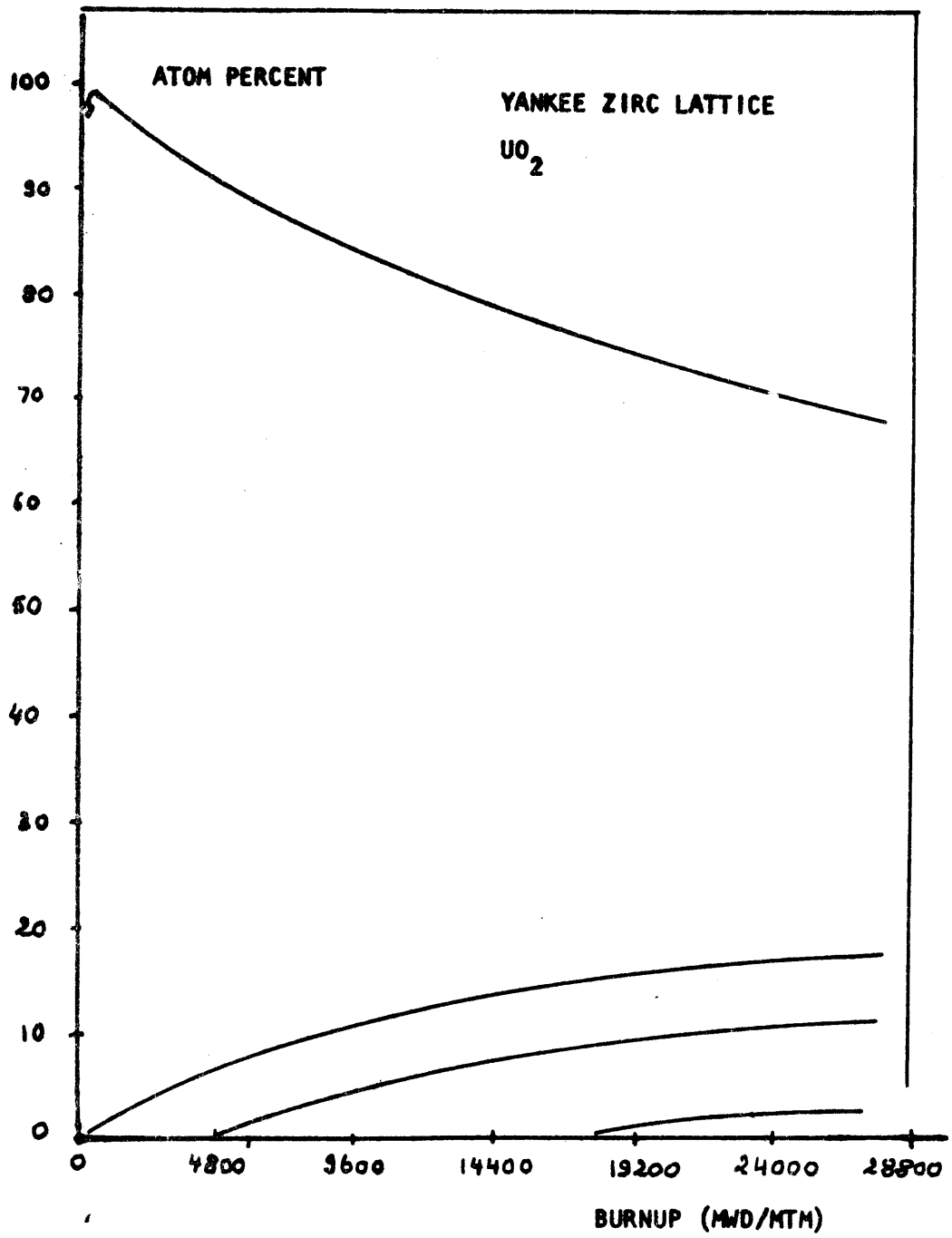


FIG V- 18 CHANGE OF PLUTONIUM ISOTOPIC CONCENTRATIONS IN $UO_2$ FUEL

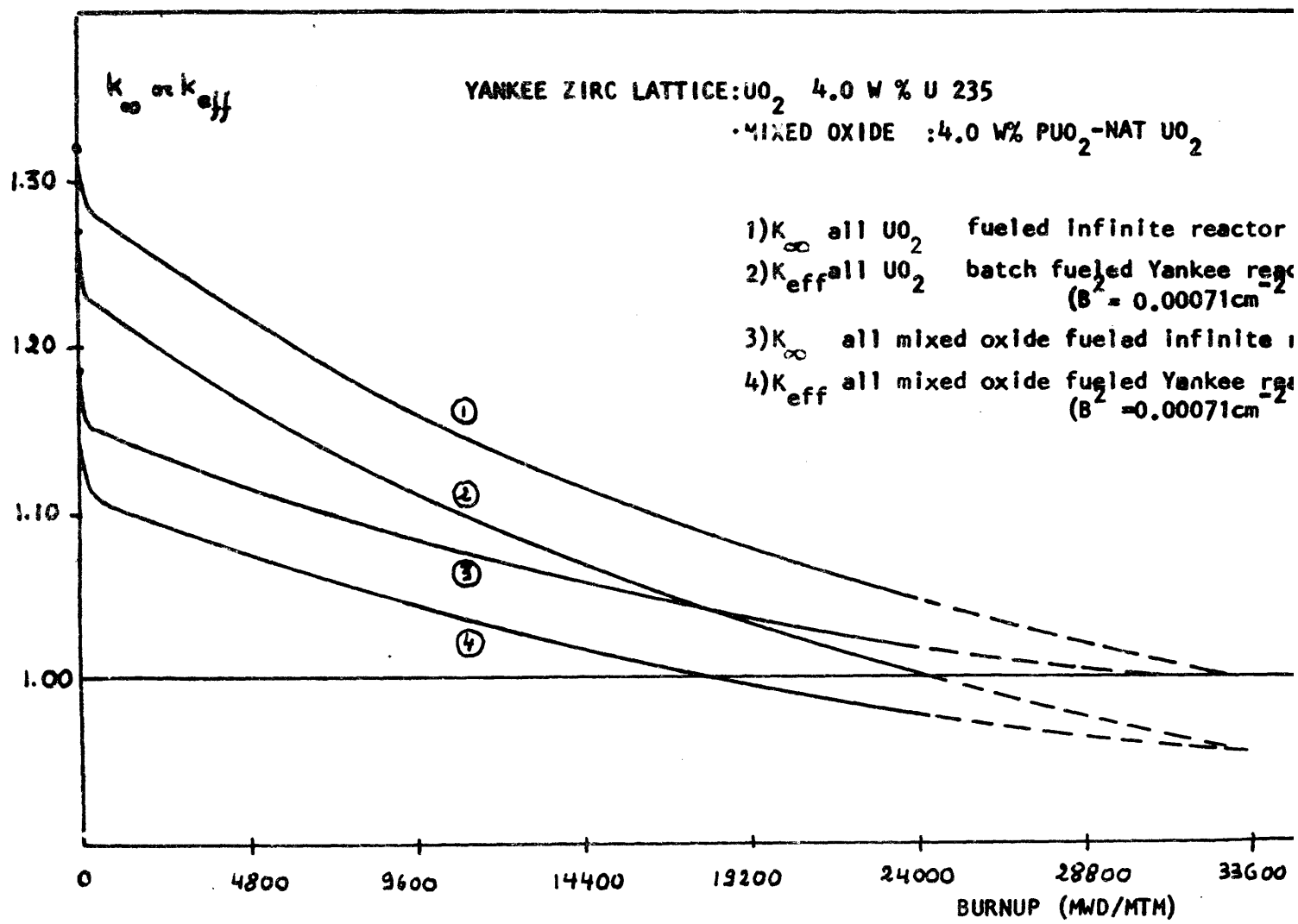


FIG V-19 Variation of $K_\infty$ and $K_{eff}$ with burnup of an all $UO_2$ or mixed oxide fueled Yan Reactor without extra materials)

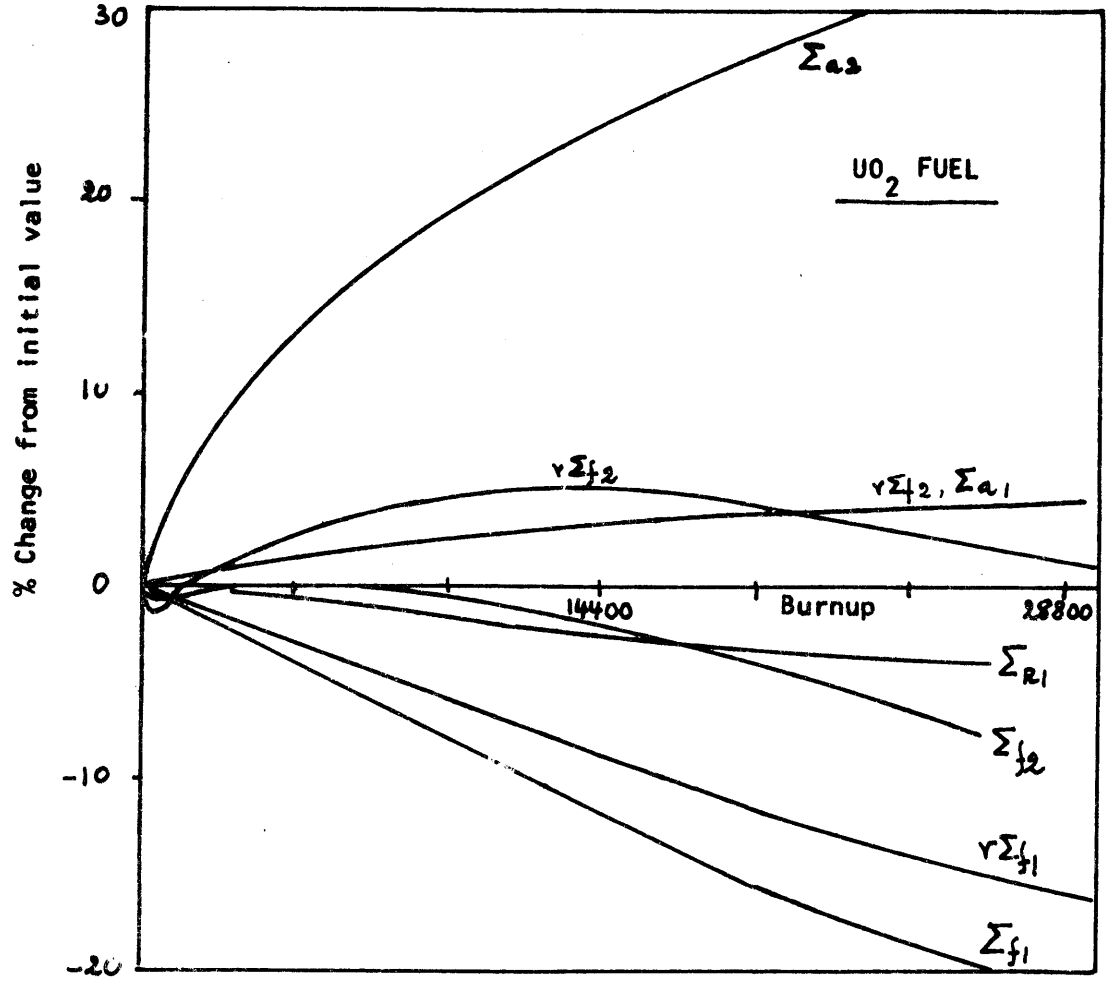


FIG V-20 Variation of the macroscopic X-sections vs.burnup in the $UO_2$ fuel

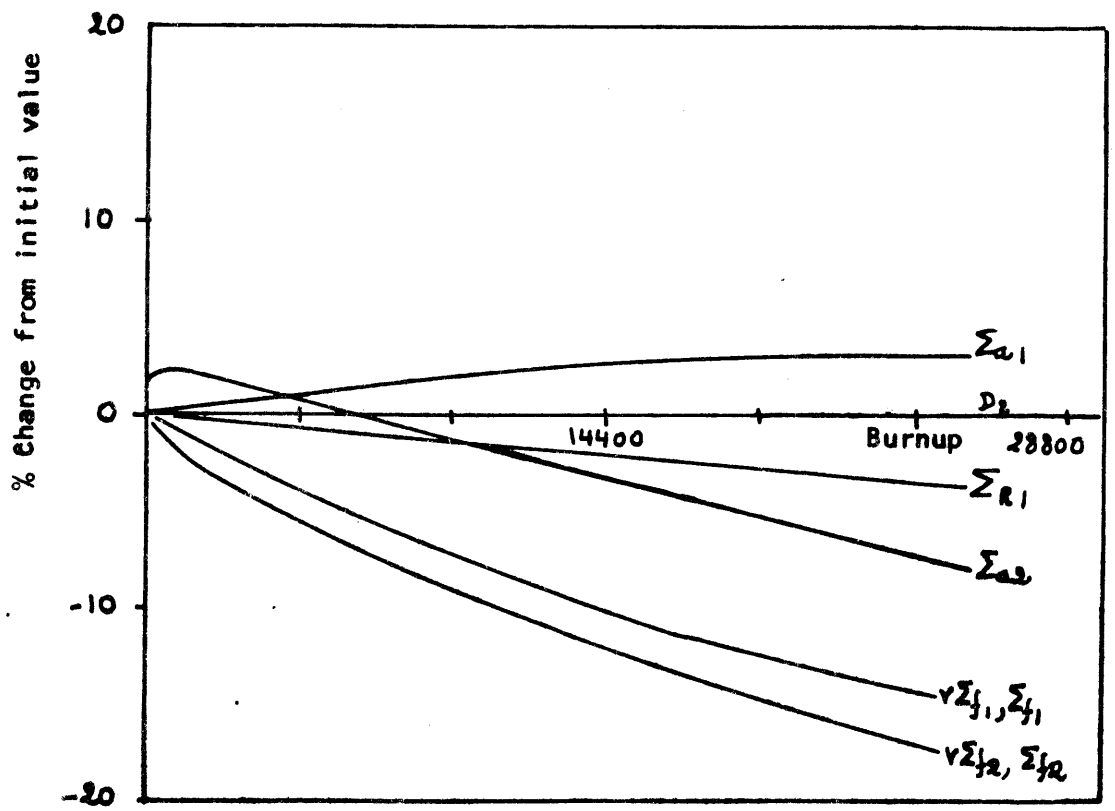


FIG V-26 Variation of the macroscopic X-sections in the mixed oxide

## 4-3)-2. Plutonium Recycle Fuel and Comparison with $UO_2$ fuel.

Fig. V-19 shows the $k_\infty$ and $k_{eff}$ of the MIX-OXIDE unit cell versus burnup. It is thus immediately noticed that the $k_\infty$ and $k_{eff}$ of the MIX-OXIDE fuel is appreciably lower at BOL, but approaches the values of $UO_2$ at very high burnups ($\gtrsim$ 33000 MWD/$_{MTM}$).

In an infinite reactor the MIX OXIDE fuel reaches a burnup of about 31000 MWD/$_{MTM}$, which is only 2000 MWD/$_{MTM}$ lower than the burnup of the $UO_2$ fuel (33000 MWD/$_{MTM}$). In a batch MIX-OXIDE fueled Yankee reactor ($B^2$ = 0.00071 $cm^{-2}$) however the MIX-OXIDE only reaches a burnup of 18200 MWD/$_{MTM}$. The operating time of an all mixed oxide fueled Yankee Reactor at the nominal power of 175 MWe will thus be about 60 % the operating time of a Yankee Reactor fueled with $UO_2$.

This severe reduction is mainly due to the absorptions in the PU240, which counts for 12 % of all absorptions in the MIX-OXIDE cell.

Figs. V-21 and V-22 show the thermal neutron spectra in fresh & depleted MIX-OXIDE fuel. It is noticed, as before that the flux depressions at the PU-239 and PU240 resonances is very severe & much more pronounced than in a high burned $UO_2$ cell, but the spectrum becomes softer with increasing burnup. The spectrum in theMIX OXIDE fuel is also much harder than in the $UO_2$ fuel cell with the same lattice geometry.

The harder spectrum in a plutonium recycle fuel cell is not favorable because the value of $\alpha$ (capture to fission ratio) in PU239 is maximum at 0.3 eV and decreases sharply with increasing neutron-energy.

Therefore the optimum moderation is expected for higher water to fuel ratios than with conventional $UO_2$ fuel. From the comparison with current designs, ( 2 · ), it is thus seen that the Yankee Reactor in particular is very unfavorable for plutoniumrecycle applications, since it has one of the lowest moderator/fuel ratios that exist, and is furthermore one of the smallest commercial reactorcores in operation.

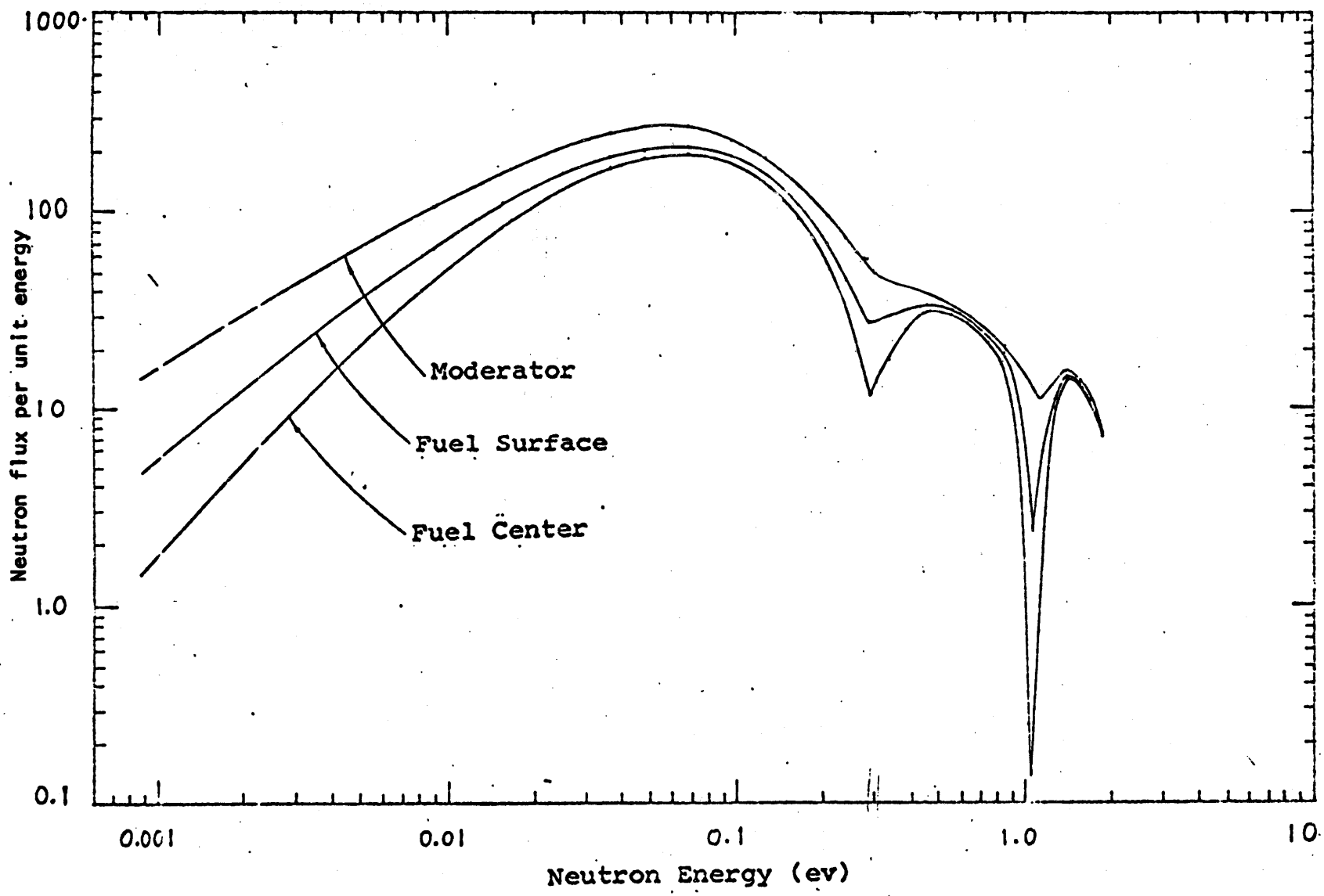


FIG V-21, Thermal neutron spectra in a fresh plutonium recycle fuel cell.

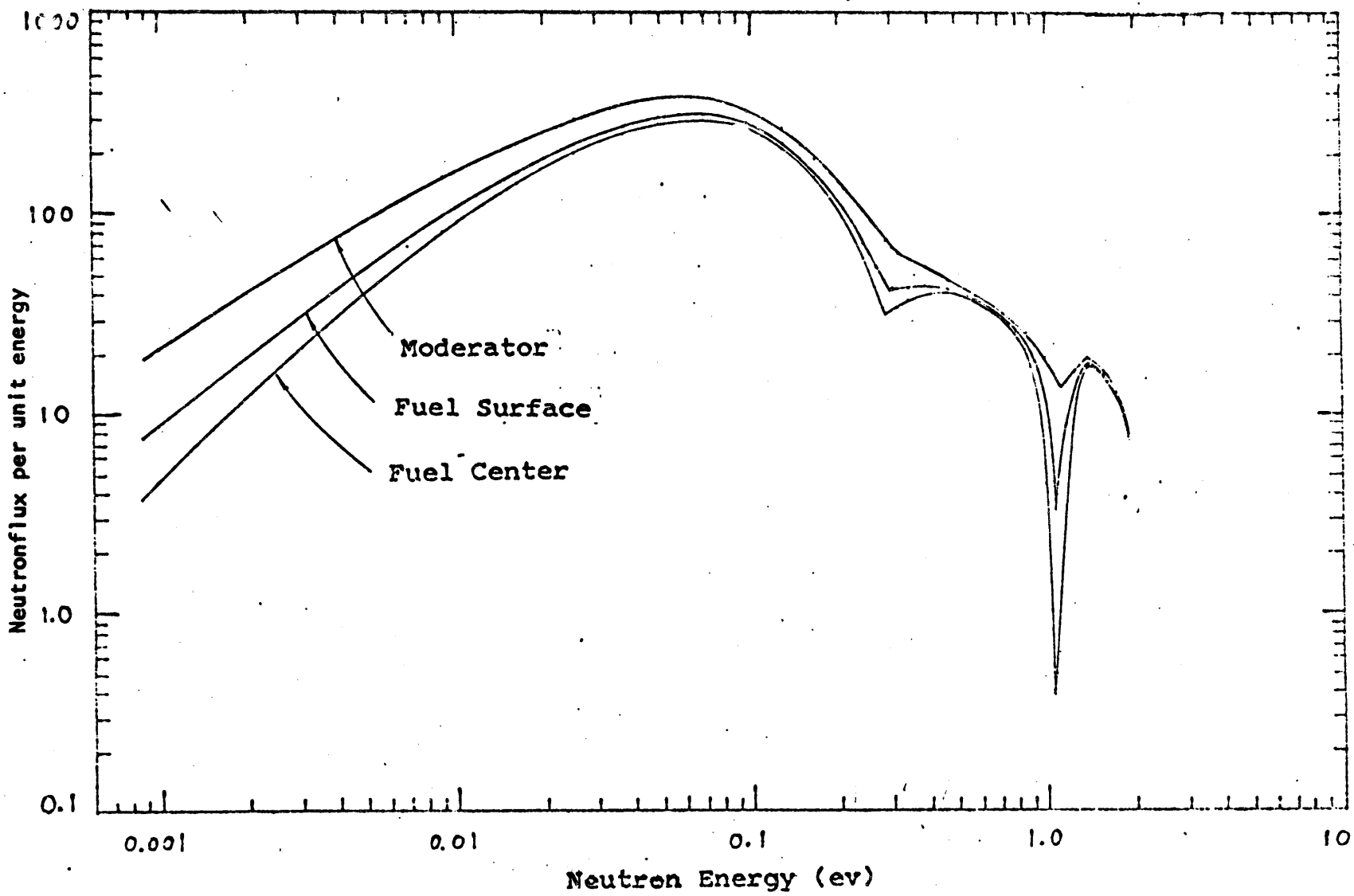


FIG V-22 Thermal neutron spectra in a depleted plutonium recycle fuel cell.

Fig. V-23 shows the isotopic fractional absorptionrates in the plutoniumrecycle fuel cell. The large thermal absorption cross-sections reduce the fractional absorptions in most other isotopes & hardens the spectrum, as compared to the $UO_2$ cell. In the MIX-OXIDE cell e.g. the fractional absorptionrates of the hydrogen & zircalloy clad are reduced to 1.2 %, as are the fissionproducts, & increase with burnup. The same is however also true for control materials (B-10, Cd, Ag etc). Therefore in <u>all</u> MIX-OXIDE fueled reactor the worth of the control materials is reduced, compared to a conventional $UO_2$ fueled reactor.
It is also noticed that the fractional absorption of the PU-isotopes remains much higher than even in (up to 24000 MWD/$_{MTM}$) depleted $UO_2$ fuel. We may therefore expect, as will be shown, that the spectral differences & spectraleffects at $UO_{2/MIX}$ interfaces remain, even at high burnup.
Fig. V-24 shows the fuel region averaged isotopic concentrations in function of burnup. There are little changes in the concentrations of PU240 & PU 241 throughout the lifetime.
Fig. V-25 shows the PU isotopic compositions. At 24000 MWD/$_{MTM}$ the PU isotopic compositions have changed from about 67 % PU239, 18.4 % PU240, 11.8 PU 241 & 2.7 % PU 242, to 54 % PU239, 23.5 % PU240, 16.5 % PU241, 6 % PU 242, at 24.000 MWD/MT.
Fig. V-26 finally shows the variations of the macroscopic X-sections versus burnup; noticle is in contrast to the $UO_2$ fuel that the thermal $\Sigma_{a2}$ decreases with burnup, such as the $\Sigma_{f2}$ & $\nu\Sigma_{f2}$ values.

## 4-3)3. The spectraleffects in the isolated fuel cells and at $UO_2/P_2O$ and $UO_2$/MIX.OX. interfaces versus burnup.

According to the GMND method that we have developed in Chapter IV, the spectraleffects at $H_2O$/FUEL or FUEL/FUEL interfaces can be obtained from unit cell calculations alone.

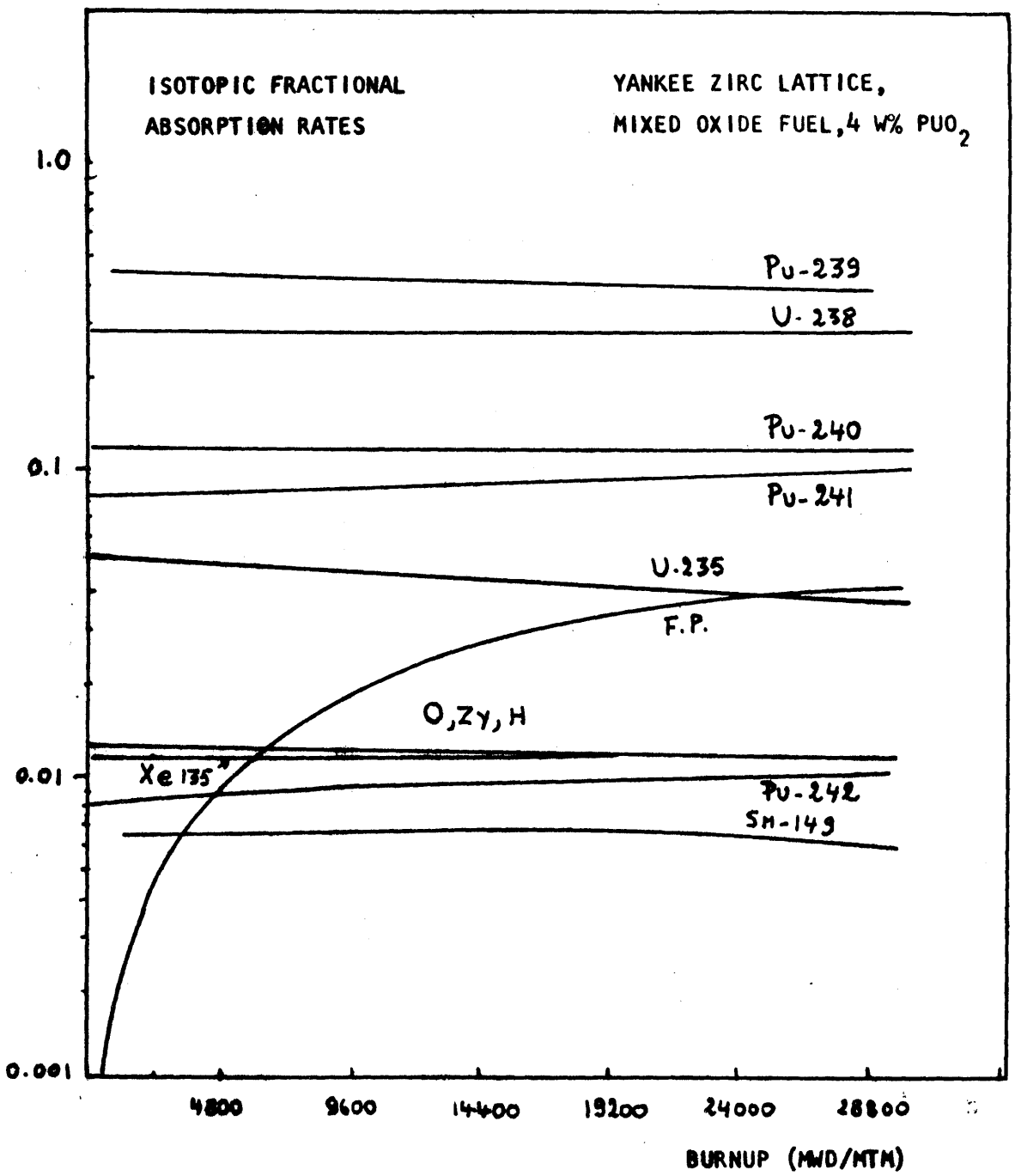


FIG V-23 NEUTRON BALANCE IN MIXED OXIDE FUEL CELL AS A FUNCTION OF BURNUP

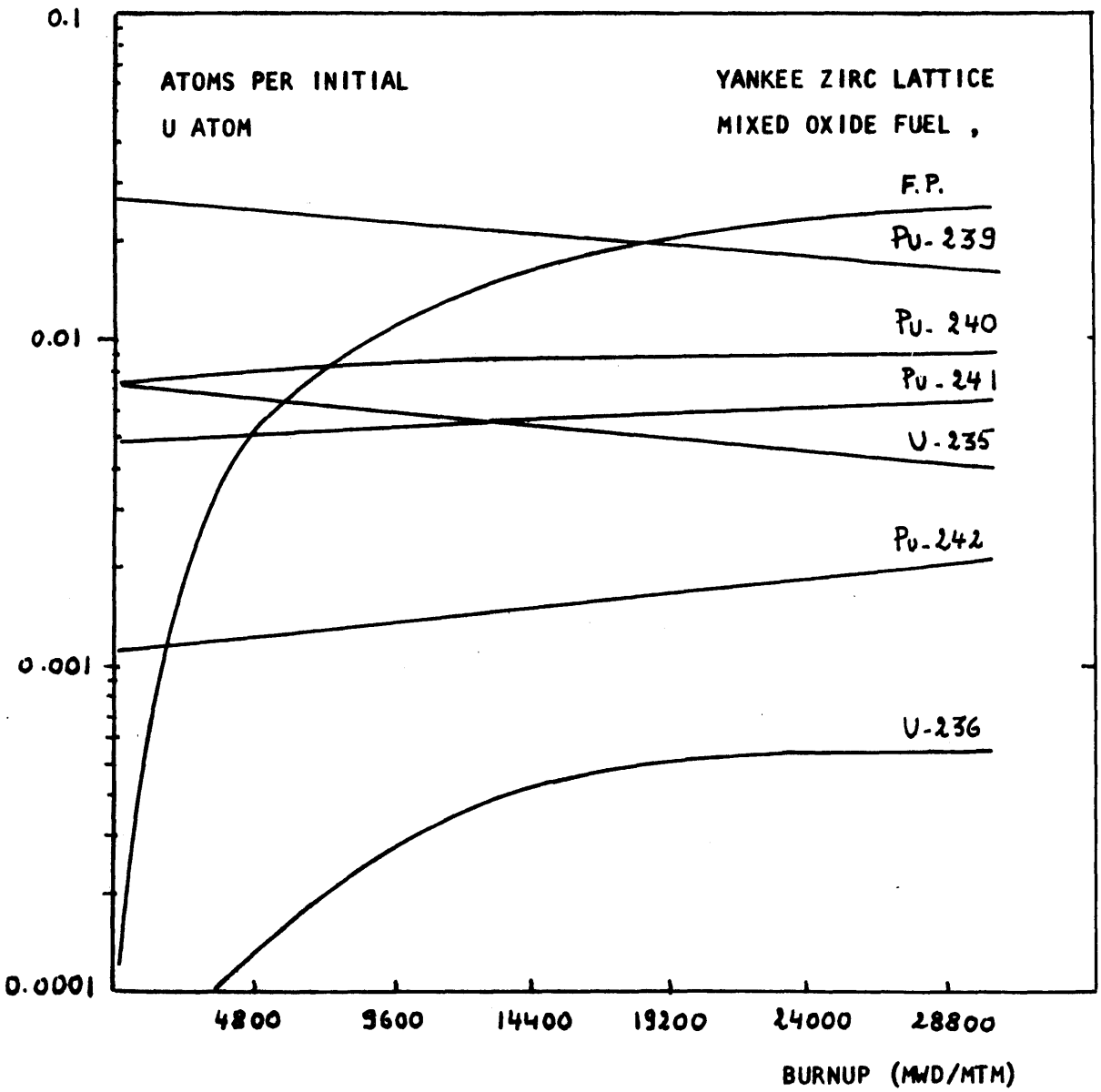


FIG V-24 Fuel Region Averaged Isotopic concentrations ,in the mixed oxide fuel.

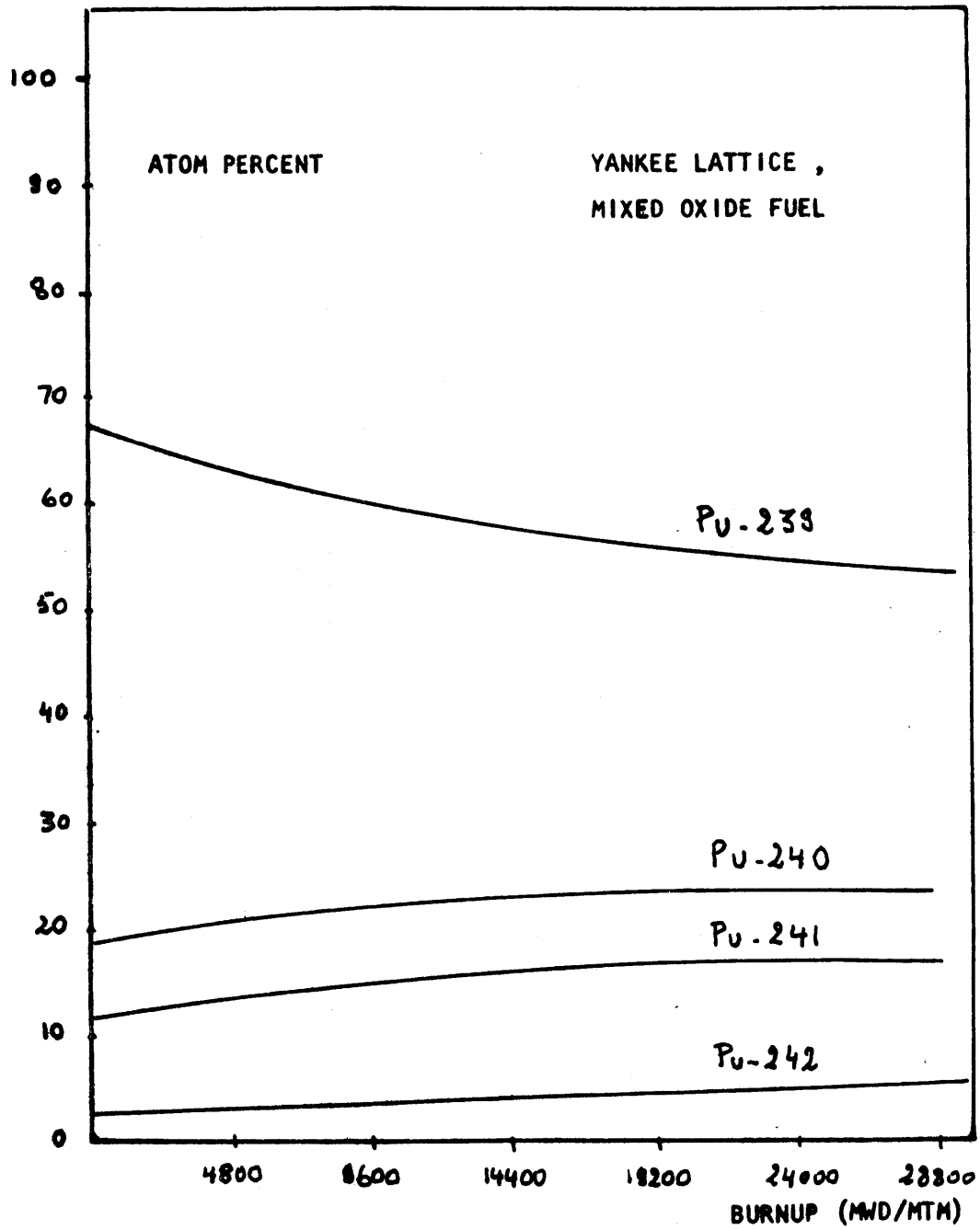


FIG V-25 CHANGE OF PLUTONIUM ISOTOPIC COMPOSITION IN THE MIXED OXIDE FUEL

In particular it is noticed that the % increase or decrease in the power, in the first cells at the interface due to the spectraleffect, at the fuel-fuel interface, is proportional to the $1/V_{GRAD.}$ or inversely proportional to the velocity of the gradientspectrum across the interface. (See Eqs. 4-23 and 4-24 ).

From the knowledge of the fluxes & the isolated cell velocities from LASER the average velocity of the gradientspectrum or the reciprocal has been obtained from :

$$\frac{1}{v_{GRAD}} = \frac{\phi_1/v_1 - \phi_2/v_2}{\phi_1 - \phi_2}$$

in function of the burnup, (which was on the average assumed to be equal in both $UO_2$ & MIX.OXIDE fuel).

The reciprocal of the average $UO_2$ cell & MIX.OXIDE cell thermal neutron velocities has been plotted on Fig. V-27, as well as the reciprocal of the average thermal gradientspectrum velocities at the $UO_2/H_2O$ and $UO_2$/MIX.OXIDE, interfaces.

It is thus noticed that the spectrum in a $UO_2$ fuel cell, only slighltly hardens with burnup, whereas the spectrum in a MIX.OXIDE cell hardens slightly up to 5000 $MWD/_{MTM}$, but softens a little bit at higher burnups.

Both $UO_2$ and mixed oxide fuel cells practicaly retain their own spectrum versus burnup, and do not approach each other even at higher burnups over 30,000 $MWD/_{MTM}$.

With respect to the gradientspectra, it is noticed that the average thermal neutronvelocity of the fluxgradient at the $H_2O$ / $UO_2$ interface increases with burnup, which is evidently due to hardening of the spectrum from the buildup of PU.

At the $UO_2$/ MIX.OXIDE interface the gradientspectrum remains virtually unchanged.

From these results, it may thus be noticed that the spectral-effects at interfaces change only slightly with burnup. Therefore spectraleffects at fresh $UO_2$fuel - burned $UO_2$ fuel interfaces are negligable, but spectraleffects at $UO_2/H_2O$ interfaces

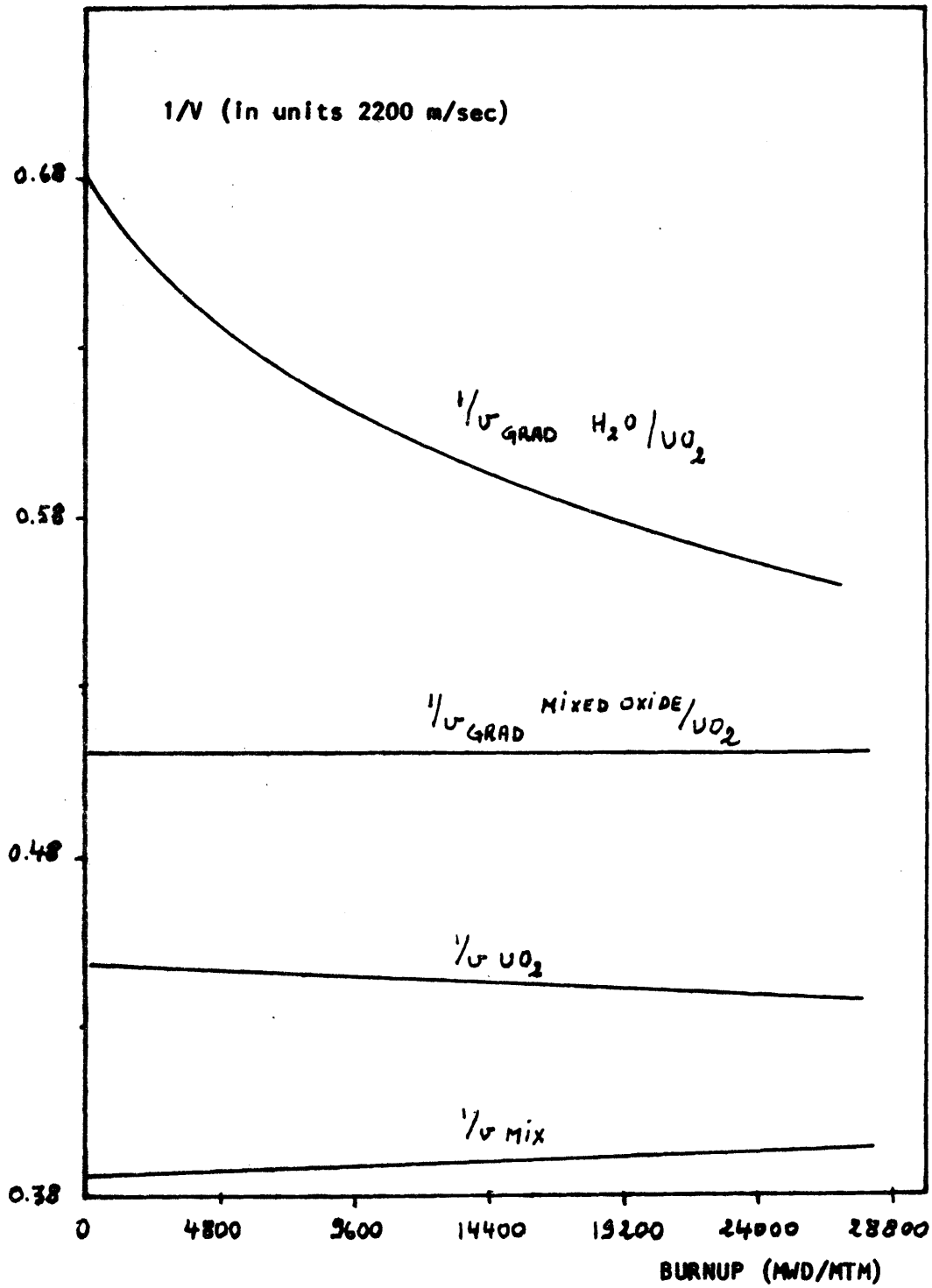


FIG V-27 Variation of the reciprocal avg thermal velocity of the flux and flux gradient at the water and fuels interfaces, versus burnup

and $UO_2$ MIX.OXIDE interfaces will retain their importance, even at high burnups of 33000 $MWD/_{MT}$.

The reason may be found in the fractional absorptionrates of the fuel isotopes, which for $UO_2$ remains rather low for the PU-isotopes & rather high for U238 and U235 even at high burnups. Compared to the $UO_2$ fuel the fractional absorption-rate of the PU-isotopes remains much higher & the associated spectrum remains much harder, in the MIX.OXIDE fuel.

## 4-4) ROD BY ROD BURNUP OF THE CONVENTIONAL & PU-RECYCLE ASSEMBLY.

### 4-4)1. RESULTS FOR THE CONVENTIONAL $UO_2$-ASSEMBLY.

Using the method outlined above a rod by rod burnupstudy of the conventional assembly has been made using the PDQ-5 code, & the GMND X-sections. The results of the first burnupstep of 4800 $MWD/_{MTM}$ are shown on the Figs. 28 & 29. Fig. 28 pictures the rod by rod burnupdistribution for the average assembly burnup of 4800 $MWD/_{MTM}$. The peak burnup is 5400 & the minimum burnup is 4600 $MWD/_{MTM}$.

Using this burnup map, the macroscopic X-sections were calculated, applying Stirling's interpolationformula between LASER results at 2400, 4800 & 6200 $MWD/_{MTM}$; and were inputted in the 34 different rod positions in the PDQ-5 calculation. Fig. 29 shows the powerdistribution in a portion of the $UO_2$-assembly at the avg. assembly-burnup of 4800 $MWD/_{MT}$ compared to the power at BOL, as well as the % increase in power relative to beginning life.

The % changes were obtained from 1/4 assemblymodel, whereas the powerdistribution itself was obtained by applying the % changes on the whole assemblycalculation of sections 3,1-2 . Note that no boron was used for the burnupcalculations. Fig. V-30 shows the powerdistribution & the changes relative to BOL for an average assembly-burnup of 19200 $MWD/_{MTM}$.

FIG. V-28 : BURNUP MAP ROD BY ROD $UO_2$ ASSEMBLY AVG. BU : 4800 MWD/MTM.

| | | | | | | | |
|---|---|---|---|---|---|---|---|
| 5400<br>+12.5% | 5250<br>+9.4 | 5150<br>+7.3 | 5100<br>+6.3 | 5050<br>+5.2 | 5050<br>+5.2 | 5050<br>+5.2 | 5050<br>+5.2 |
| | 5000<br>+4.2 | 4900<br>+2.1 | 4800<br>.0 | 4800<br>.0 | 4800<br>.0 | 4800<br>.0 | 4800<br>.0 |
| | | 4750<br>-1.0 | 4700<br>-2.1 | 4700<br>-2.1 | 4700<br>-2.1 | 4700<br>-2.1 | 4700<br>-2.1 |
| | | | 4650<br>-3.1 | 4650<br>-3.1 | 4600<br>-4.2 | 4600<br>-4.2 | 4600<br>-4.2 |
| | | | | 4600<br>-4.2 | 4600<br>-4.2 | 4600<br>-4.2 | 4600<br>-4.2 |
| | | | | | 4600<br>-4.2 | 4600<br>-4.2 | 4600<br>-4.2 |
| | | | | | | 4600<br>-4.2 | 4600<br>-4.2 |
| | | | | | | | |

Avg. Assy.Burnup = 4800 MWD/MTM
Avg. $UO_2$ Burnup = 4800 Avg. Mix. Oxide Burnup.

Peak BU : 5400
Min. BU : 4600

| | |
|---|---|
| 5400 | BURNUP MWD/MTM |
| +12.5 | ACCUMULATED % BURNUPDIFF/STEP |

$$= \frac{B - \bar{B}}{\Delta B} * 100 \quad (\Delta B = 4800)$$

FIG. V-29 : POWERDISTRIBUTION IN $UO_2$ ASSEMBLY AT AVG. ASSEMBLY BURNUP OF 4800 MWD/MTM.

| | | | | | | | |
|---|---|---|---|---|---|---|---|
| 1.191<br>1.191<br>+0.0 | 1.145<br>1.145<br>+0.0 | 1.124<br>1.124<br>+0.0 | 1.111<br>1.111<br>+0.0 | 1.106<br>1.108<br>+0.2 | 1.103<br>1.104<br>+0.1 | 1.102<br>1.103<br>+0.1 | 1.099<br>1.100<br>+0.1 |
| | 1.093<br>1.092<br>-0.1 | 1.068<br>1.068<br>+0.0 | 1.058<br>1.057<br>-0.1 | 1.052<br>1.051<br>-0.1 | 1.049<br>1.048<br>-0.1 | 1.048<br>1.046<br>-0.2 | 1.047<br>1.045<br>-0.2 |
| | | 1.042<br>1.039<br>-0.3 | 1.031<br>1.030<br>-0.1 | 1.026<br>1.025<br>-0.1 | 1.024<br>1.022<br>-0.2 | 1.021<br>1.019<br>-0.2 | 1.022<br>1.020<br>-0.2 |
| | | | 1.017<br>1.019<br>+0.2 | 1.013<br>1.014<br>+0.1 | 1.004<br>1.006<br>+0.2 | 1.009<br>1.012<br>+0.3 | 1.009<br>1.012<br>+0.3 |
| | | | | 0.998<br>1.001<br>+0.3 | 1.001<br>1.004<br>+0.3 | 1.001<br>1.004<br>+0.3 | 1.002<br>1.004<br>+0.2 |
| | | | | | 1.002<br>1.005<br>+0.3 | 1.003<br>1.006<br>+0.3 | 1.003<br>1.006<br>+0.3 |
| | | | | | | 1.003<br>1.006<br>+0.3 | 1.010<br>1.013<br>+0.3 |
| | | | | | | | |

Avg. Ass%. Burnup = 4800
$k_\infty$ Ass%. = 1.21667
$k_{eff}$ = 1.11717
Av. Assembly Power : 1.000, Avg. $UO_2$ Power : 1.000

| | |
|---|---|
| 1.191 | NORMALISED ROD POWER AT BOP |
| 1.191 | NORMALISED ROD POWER 4800 MWD/MTM |
| +0.0 | % INCREASE |

FIG. V-30 : POWERDISTRIBUTION IN THE $UO_2$ ASSEMBLY AT AN AVG.BURNUP OF OF 19200 MWD/MTM.

| | | | | | | | |
|---|---|---|---|---|---|---|---|
| 1.208 +0.9 | 1.148 +0.3 | 1.126 +0.2 | 1.112 +0.1 | 1.108 +0.2 | 1.105 +0.2 | 1.104 +0.2 | 1.101 +0.2 |
| | 1.093 +0.0 | 1.067 -0.1 | 1.057 -0.1 | 1.051 -0.1 | 1.048 -0.1 | 1.047 -0.1 | 1.046 -0.1 |
| | | 1.041 -0.1 | 1.029 -0.2 | 1.025 -0.1 | 1.023 -0.1 | 1.019 -0.2 | 1.021 -0.1 |
| | | | 1.015 -0.2 | 1.011 -0.2 | 1.003 -0.1 | 1.008 -0.1 | 1.008 -0.1 |
| | | | | 0.997 -0.1 | 1.000 -0.1 | 1.000 -0.1 | 1.001 -0.1 |
| | | | | | 1.001 -0.1 | 1.003 +0.0 | 1.004 +0.1 |
| | | | | | | 1.006 +0.3 | 1.012 +0.2 |
| | | | | | | | |

Avg. Assy Burnup = 19200 MWD/MTM

$k_{\infty}$ assy. = 1.07539, $k_{eff}$ = 0.9964 ($B^2$ = 0.00071 $cm^{-2}$)

| | |
|---|---|
| 1.208 +0.9 | NORMALIZED ROD POWER AT 19200 MWD/MTM % INCREASE RELATIVE TO BOP. |

FIG. V-31 : ROD BY ROD BURNUPDISTRIBUTION AVG. ASSEMBLY BURNUP 28800 MWD/MTM $UO_2$ ASSEMBLY PORTION.

| | | | | | | | |
|---|---|---|---|---|---|---|---|
| 32.57 | 31.45 | 30.85 | 30.55 | 30.40 | 30.35 | 30.30 | 30.30 |
| | 29.95 | 29.70 | 29.00 | 28.80 | 28.80 | 28.75 | 28.75 |
| | | 28.55 | 28.25 | 28.10 | 28.00 | 28.00 | 28.00 |
| | | | 27.90 | 27.80 | 27.75 | 27.70 | 27.70 |
| | | | | 27.65 | 27.60 | 27.60 | 27.60 |
| | | | | | 27.60 | 27.60 | 27.60 |
| | | | | | | 27.60 | 27.75 |
| | | | | | | | |

Avg. Assy.Burnup = 28800 MWD/MTM
Peak : 32.570 MWD/MTM
Min : 27.600 MWD/MTM

32,57 BURNUP IN UNITS 1000MWD/MTM

FIG. V-32 : POWERDISTRIBUTION IN THE $UO_2$ ASSEMBLY AT AN AVG. BURNUP OF 28800 MWD/MTM.

| | | | | | | | |
|---|---|---|---|---|---|---|---|
| 1.191<br>+0.2 | 1.146<br>+0.1 | 1.125<br>+0.1 | 1.111<br>+0.0 | 1.107<br>+0.1 | 1.103<br>+0.0 | 1.102<br>+0.0 | 1.099<br>+0.0 |
| | 1.093<br>+0.0 | 1.065<br>-0.3 | 1.058<br>+0.0 | 1.052<br>+0.0 | 1.049<br>+0.0 | 1.048<br>+0.0 | 1.047<br>+0.0 |
| | | 1.042<br>+0.0 | 1.031<br>+0.0 | 1.026<br>+0.0 | 1.024<br>+0.0 | 1.020<br>-0.1 | 1.022<br>+0.0 |
| | | | 1.016<br>-0.1 | 1.012<br>-0.1 | 1.003<br>-0.1 | 1.009<br>+0.0 | 1.009<br>+0.0 |
| | | | | 0.998<br>+0.0 | 1.001<br>+0.0 | 1.001<br>+0.0 | 1.002<br>+0.0 |
| | | | | | 1.002<br>+0.0 | 1.004<br>+0.1 | 1.004<br>+0.1 |
| | | | | | | 1.006<br>+0.3 | 1.013<br>+0.3 |
| | | | | | | | |

Av. Assy. Burnup = 28800

$k_\infty$ Assy. = 1.02062

$k_{eff}$ = 0.9451

| | |
|---|---|
| 1.191<br>+0.2 | NORMALIZED ROD POWER AT 28800 MWD/MTM<br>% INCREASE RELATIVE TO BOL |

FIG. V-33 : K-INFINITY MAP $UO_2$ ASSEMBLY AT AVG. ASSEMBLY BU : 28800 MWD/MTM.

| | | | | | | | |
|---|---|---|---|---|---|---|---|
| 1.004 | 1.009 | 1.012 | 1.013 | 1.014 | 1.014 | 1.014 | 1.014 |
| | 1.016 | 1.017 | 1.020 | 1.021 | 1.021 | 1.021 | 1.021 |
| | | 1.022 | 1.023 | 1.023 | 1.024 | 1.024 | 1.024 |
| | | | 1.024 | 1.026 | 1.026 | 1.027 | 1.027 |
| | | | | 1.027 | 1.027 | 1.027 | 1.027 |
| | | | | | 1.027 | 1.027 | 1.027 |
| | | | | | | 1.027 | 1.026 |
| | | | | | | | |

Av. Assy. Burnup = 28800 MWD/MTM

$k_{\infty}$ Assy. = 1.0206

$k_{eff}$ = 0.9451

1.004 K-INFINITY.

Fig. V-31 shows the rod by rod burnup distribution for an average assembly burnup of 28800 $MWD/_{MTM}$; whereas Fig. V-32 pictures the powerdistribution & changes relative to BOL. In the $k_\infty$ the extra-regions other than fuel were excluded.

Fig. V-33 shows the values of $k_\infty$ ineach unit cell for an avg. burnup of 28800 $MWD/_{MTM}$ as obtained with PDQ-5.

From the results it is thus seen, in contrast to what expected, that the local powerpeakingfactor increases with burnup to a certain maximum increase of about 1 % after which it decreases again. The reason may probably be found in the build-up of PU 239, which increases $\Sigma_{a2}$ which levels off at higher burnups, but also increases $\nu\Sigma_{f2}$ to a maximum value (Fig.V-20). On the whole the powerdistribution in a $UO_2$-assembly changes by about 0.2 %, nearly no flattening is observed.

From Fig. 32 it is thus observed that the local powerdistribution in the assembly does not follow the $k_\infty$, but rather a complex relationship between macroscopic parameters where $\Sigma_{f2}$ & $\nu\Sigma_{f2}$ & $\Sigma_{a2}$ are playing important roles.

It was also observed that the $k_\infty$ of the assembly (excluding extra regions other than fuel) follows very closely the $k_\infty$ of a unit cell, which is not surprising because of the nearly linear behaviour of $k_\infty$ versus burnup. The avg. $k_\infty$ of an assembly & the inventories are insensitive to the local powerdistributions & the unit cell values can be used with very good confidence.

Fig. V-40 curves 1 & 3 show the variations of $k_\infty$ & $k_{eff}$ versus burnup of the conventional assembly. The $k_\infty$ curve is without extra materials, (SS can, zirc follower, instrumentation cell, $H_2O$ gap), whereas the $k_{eff}$ curve includes these extra materials.

From comparison with Fig. 19 , it is thus noticed that the Batch loaded Yankee reactor fueled with $UO_2$ assemblies reaches a burnup of 19,050 $MWD/_{MTM}$ (compared to 24,000 $MWD/_{MTM}$ without the extra materials). The extra-materials account for roughly 51 mk at 4800 $MWD/_{MT}$ and 39 milli- k at 19,200 $MWD/_{MT}$. The influence is thus substantial.

## 4-4)2. RESULTS FOR THE PU-RECYCLE ASSEMBLY & COMPARISON WITH THE $UO_2$ ASSEMBLY.

Figs. V-34 to 39 show the powerdistribution in the PU-recycle assembly, using the conventional 4 w/o U235 $UO_2$ fuel & the base case mixed oxide fuel (4.0 w/o PU $O_2$-$UO_2$ (nat); 19 a/o PU240), at different avg. assembly burnups. (BOL, 4800, 9600, 19200 and 28800 $MWD/_{MTM}$).

It is thus noticed that :

1) There is a shift in peakpowerposition versus burnup from the peak in the MIX OXIDE region (location D-6) to the peak in the $UO_2$ region at lacation A-1.
2) There is a sizeble change in the peakpower versus burnup, especially in the mixed oxide region.
3) There is a considerable powerflattening, especially in the mixed oxide, but also in the $UO_2$ at the boundary of the $MIX/_{UO_2}$ .
4) Although there is a flattening in the peak $UO_2$ location, the flattening is not so substantially in the MIX.OXIDE. This peak further decreases with burnup, reaches a min. at about 9600 $MWD/_{MTM}$ after which it increases, but decreases definitively after 19200 $MWD/_{MTM}$.
   In the mix.oxide peak, there is a definite monotonuous decrease in peakpower versus burnup.
5) The mix.oxide accumulates approximately 3.5 % more burnup than the $UO_2$.
6) From Fig. V-40 it is noticed that the $k_\infty$ of the PU-recycle assembly (excluding extra materials, reaches a burnup of about 33,000 $MWD/_{MT}$ at the same point

as the conventional assembly. A batch fueled Yankee reactor with PU-recycle assemblies, only reaches about 15400 $MWD/_{MTM}$ (extra materials included).

Comparison of the Conventional & PU-recycle unit-assemblies.

1) Comparing the variation of $k_{\infty}$ and $k_{eff}$ with burnup of a batch fueled Yankee Reactor with conventional & plutonium-recycle assemblies, it is noticed that whereas the conventional & PU-recycle infinite reactors both reach end of life at about 33.000 $MWD/_{MTM}$, the batch fueled Yankee reactor reaches 19050 $MWD/_{MTM}$ with conventional assemblies, whereas the same reactor fueled with plutoniumrecycle assemblies with the proposed design only attains 15400 $MWD/_{MTM}$. The cycletime of the batch reactor with the proposed recycle assemblies is thus about 81 % of the cycletime of a conventional reactor. From inexpensive CELL-code ( 9 ) calculations it has been estimated that the burnup of mixed oxide fuel increases with about 4000 $MWD/_{MT}$ per weight percent of $PUO_2$. A fuel of about 4.5 to 5.0 w/o $PUO_2$ (or 3.5 to 4.0 % PU fissile) in the mixed oxide would therefore be necessary in order to achieve the same batch lifetime as with conventional $UO_2$ (4.0 w/o U235) fuel assemblies. An as we have seen in section 3 this would increase the localpowerpeaking-factor in the plutoniumrecycle assemblies.

2) Whereas the unit assembly powerdistribution in conventional assemblies remains nearly unchanged with burnup, the powerdistribution in a plutoniumrecycle assembly flattens considerably with burnup.

3) The local powerpeakingfactor at beginning of life is about 2 % higher in a PU-recycle assembly of the proposed design; and is located in the mixed oxide region.

4) Whereas the local powerpeakingfactor in a conventional assembly increases by

about 1 % with burnup, the local powerpeakingfactor in a plutoniumrecycle assembly decreases by about 2 % (Fig. V-41)

There is furthermore a shift in the location of the powerpeak from the mixed oxide to the $UO_2$ region (Fig. V-41).

4-4)3. COMPARISON WITH WESTINGHOUSE RESULTS FOR LARGE PWR'S.

For the purpose of comparison of our results for the Yankee-reactor & Westinghouse results for large PWR'S the Figs. V-42 and V-43 from reference are shown.

The layout of the PU-recycle assembly consisting of 5 different mixed oxide fuels (3.2 - 3.5 - 3.8 - 4.2 and 4.6 w/o PU $O_2$) in order to flatten the power was pictured on Fig.

From these results it is thus observed that :

1) in Yankee assemblies the local powerpeakingfactor is 1.191 for the $UO_2$ assembly & 1.210 for the plutoniumrecycle assembly. In the W-design, the local powerpeakingfactor in the $UO_2$ assemblies is 1.101, and is 1.093 in the PU-recycle assembly. Therefore in Yankee assemblies there seems to be no need for several PU-enrichments to flatten the power.
2) In the W -design there is also a shift in the peakrod positions versus burnup; and a sizable change in power (10 %) with burnup in the uraniumfuel-rods at the boundary between fuel regions.
3) The plutonium region accumulates more burnup than the uraniumregion in both designs.

FIG.V-34 : POWERDISTRIBUTION IN THE PLUTONIUM RECYCLE ASSEMBLY AT 4800 MWD/MTM AVG. BURNUP.

| | | | | | | | |
|---|---|---|---|---|---|---|---|
| 1.200<br>1.185<br>-1.3 | 1.135<br>1.121<br>-1.2 | 1.106<br>1.096<br>-0.9 | 1.085<br>1.077<br>-0.8 | 1.069<br>1.062<br>-0.6 | 1.057<br>1.052<br>-0.4 | 1.049<br>1.049<br>-0.0 | 1.045<br>1.044<br>-0.1 |
| | 1.083<br>1.072<br>-1.0 | 1.050<br>1.044<br>-0.6 | 1.023<br>1.020<br>-0.3 | 0.999<br>1.000<br>+0.1 | 0.978<br>0.981<br>+0.3 | 0.964<br>0.967<br>+0.3 | 0.958<br>0.962<br>+0.4 |
| | | 1.008<br>1.008<br>+0.0 | 0.969<br>0.973<br>+0.4 | 0.925<br>0.934<br>+0.9 | 0.880<br>0.890<br>+1.1 | 0.855<br>0.867<br>+1.3 | 0.848<br>0.861<br>+1.4 |
| | | | 0.908<br>0.917<br>+0.9 | 0.825<br>0.838<br>+1.4 | 1.210<br>1.152<br>-4.7 | 1.146<br>1.113<br>-3.1 | 1.131<br>1.105<br>-2.6 |
| | | | | 1.166<br>1.128<br>-3.8 | 1.048<br>1.052<br>+0.4 | 1.000<br>1.022<br>+2.2 | 0.988<br>1.019<br>+3.1 |
| | | | | | 0.971<br>1.019<br>+4.8 | 0.942<br>0.976<br>+3.4 | 0.935<br>0.973<br>+3.8 |
| | | | | | | 0.929<br>0.963<br>+3.4 | 0.935<br>0.969<br>+3.4 |
| | | | | | | | |

Avg. Assy. Burnup = 4800
Avg. $UO_2$ Burnup = 4730 Avg.Mix. Oxide Burnup = 4950

Peak $UO_2$ 4800 : 1.210
BOL : 1.152
Peak Mix 4800 : 1.200
BOL : 1.185

$k_\infty$ Assy. = 1.17792, $k_\infty$ $UO_2$ = 1.21802, $k_\infty$ MIX = 1.11411

$k_{eff}$ = 1.0963

Avg. Assembly Power : 1.000
Avg. $UO_2$ Power = .987 Avg. Mix. Oxide Power = 1.031

| | |
|---|---|
| 1.200 | NORMALIZED ROD POWER AT BOP |
| 1.185 | NORMALIZED ROD POWER 4800 |
| -1.3 | % INCREASE RELATIVE TO BOP. |

FIG. V-35 : POWERDISTRIBUTION IN THE PLUTONIUMRECYCLE ASSEMBLY AT 9600 MWD/MTM AVG.

| | | | | | | | |
|---|---|---|---|---|---|---|---|
| 1.156<br>-3.7 | 1.111<br>-2.1 | 1.085<br>-1.5 | 1.074<br>-1.0 | 1.064<br>-0.5 | 1.057<br>-0.0 | 1.052<br>+0.3 | 1.049<br>+0.4 |
| | 1.071<br>-1.1 | 1.047<br>-0.3 | 1.028<br>+0.5 | 1.014<br>+1.5 | 0.998<br>+2.0 | 0.988<br>+2.4 | 0.984<br>+2.6 |
| | | 1.017<br>+0.9 | 0.993<br>+2.7 | 0.966<br>+4.1 | 0.928<br>+4.8 | 0.905<br>+5.0 | 0.900<br>+5.2 |
| | | | 0.945<br>+3.7 | 0.885<br>+5.3 | 1.126<br>-7.0 | 1.088<br>-5.4 | 1.080<br>-5.0 |
| | | | | 1.108<br>-5.8 | 1.055<br>+0.7 | 0.990<br>-1.0 | 0.985<br>-0.3 |
| | | | | | 0.982<br>+1.1 | 0.937<br>-0.5 | 0.932<br>-0.3 |
| | | | | | | 0.920<br>-0.9 | 0.927<br>-0.8 |
| | | | | | | | |

Avg. Assy. Burnup = 9600
Avg. $UO_2$ Burnup = 9470 Avg.Mix Oxide Burnup = 9900

Peak $UO_2$ 9600 : 1.156
BOL : 1.200

Peak Mix 9600 : 1.126
BOL : 1.210

$k_\infty$ Assy. = 1.13226, $k_\infty$ $UO_2$ = 1.16097, $k_\infty$ Mix = 1.08269
$k_{eff}$ = 1.0457

Avg. Assembly Power : 1.000
Avg. $UO_2$ Power : 1.000 Avg. Mix Oxide Power : 1.000

| | |
|---|---|
| 1.156 | NORMALIZED ROD POWER AT 9600 MWD/MTM |
| -3.7 | % INCREASE IN POWER AT 9600 MWD/MTM, (Relative to Bop) |

Fig. V-36 : POWERDISTRIBUTION IN THE PLUTONIUMRECYCLE ASSEMBLY AT 19200 MWD/MTM AVG.

| | | | | | | | |
|---|---|---|---|---|---|---|---|
| 1.185<br>-1.3 | 1.119<br>-1.4 | 1.095<br>-1.0 | 1.076<br>-0.9 | 1.064<br>-0.4 | 1.058<br>+0.1 | 1.053<br>+0.4 | 1.049<br>+0.4 |
| | 1.067<br>-1.6 | 1.038<br>-1.2 | 1.019<br>-0.4 | 1.002<br>+0.3 | 0.989<br>+1.1 | 0.978<br>+1.4 | 0.976<br>+1.8 |
| | | 1.006<br>-0.2 | 0.976<br>+0.7 | 0.927<br>+0.2 | 0.914<br>+3.4 | 0.897<br>+4.2 | 0.890<br>+4.3 |
| | | | 0.932<br>+2.4 | 0.869<br>+4.4 | 1.112<br>-8.7 | 1.085<br>-5.7 | 1.080<br>-5.1 |
| | | | | 1.097<br>-6.7 | 1.018<br>-3.0 | 1.011<br>+1.1 | 1.008<br>+2.0 |
| | | | | | 1.010<br>+3.9 | 0.969<br>+2.7 | 0.964<br>+2.9 |
| | | | | | | 0.953<br>+2.5 | 0.961<br>+2.6 |
| | | | | | | | |

Avg. Assy. Burnup = 19200
Avg. $UO_2$ Burnup = 19.10 Avg. Mix Oxide Burnup = 19.5

Peak $UO_2$ 19.2 = 1.185
BOP = 1.200
Peak Mix 19.2 = 1.112
BOP = 1.210

$k_\infty$ Assy. = 1.06244
$k_\infty$ $UO_2$ = 1.07694 $k_\infty$ Mix = 1.03642

$k_{eff}$ = 0.9844

Avg. Assembly Power : 1.00
Avg. $UO_2$ Power = .994 Avg. Mix Oxide Power = 1.014

| | |
|---|---|
| 1.185 | NORMALIZED ROD POWER AT 19200 MWD/MTM |
| -1.3 | % INCREASE ROD POWER AT 19200 MWD/MTN (relative to BOP) |

FIG. V-37 : POWERDISTRIBUTION IN THE PU-RECYCLE ASSEMBLY AT 28800 MWD/MTM.

| | | | | | | | |
|---|---|---|---|---|---|---|---|
| 1.164<br>-3.2 | 1.103<br>-3.0 | 1.082<br>-2.4 | 1.063<br>-2.2 | 1.054<br>-1.5 | 1.048<br>-0.9 | 1.043<br>-0.6 | 1.039<br>-0.6 |
| | 1.053<br>-2.8 | 1.039<br>-2.1 | 1.011<br>-1.2 | 0.996<br>-0.3 | 0.986<br>+0.8 | 0.976<br>+1.2 | 0.974<br>+1.6 |
| | | 0.998<br>-1.0 | 0.975<br>+0.6 | 0.948<br>+2.3 | 0.920<br>+4.0 | 0.906<br>+5.1 | 0.901<br>+5.3 |
| | | | 0.935<br>+2.7 | 0.873<br>+4.8 | 1.100<br>-9.2 | 1.088<br>-5.5 | 1.081<br>-4.8 |
| | | | | 1.094<br>-6.8 | 1.081<br>+3.2 | 1.029<br>+2.9 | 1.027<br>+3.9 |
| | | | | | 1.030<br>+5.9 | 0.992<br>+5.0 | 0.988<br>+5.3 |
| | | | | | | 0.948<br>+1.9 | 0.940<br>+5.0 |
| | | | | | | | |

Avg. Ass. Burnup = 28.8
Avg. $UO_2$ Burnup = 28.5 Avg. Mix Oxide Burnup = 29.5

Peak $UO_2$ 28.8 : 1.164
BOL : 1.200
Peak Mix 28.8 : 1.100
BOL : 1.210

$k_\infty$ Assy. = 1.01416, $k_\infty$ $UO_2$ = 1.1210, $k_\infty$ MIX = 1.00185
$k_{eff}$ = 0.9408 (including extra)

Avg. Assembly Power : 1.00
Avg. $UO_2$ Power = 0.989 Avg. Mix Oxide Power = 1.026

| | |
|---|---|
| 1.164 | NORMALIZED ROD POWER AT 28800 MWD/MTM |
| -3.2 | % INCREASE ROD POWER AT 28800 MWD/MTM (relative to BOL) |

FIG. V-38 : BURNUPDISTRIBUTION IN THE PU-RECYCLE ASSEMBLY AVG. BURNUP. 28800 MWD/MTM.

| | | | | | | | |
|---|---|---|---|---|---|---|---|
| 32.90 | 31.90 | 30.85 | 30.70 | 30.35 | 30.05 | 30.00 | 30.05 |
| | 30.60 | 29.70 | 29.05 | 28.80 | 28.15 | 28.20 | 27.90 |
| | | 28.75 | 28.05 | 27.00 | 26.40 | 25.55 | 25.55 |
| | | | 26.70 | 25.20 | 32.65 | 30.90 | 30.65 |
| | | | | 31.45 | 28.85 | 27.85 | 27.55 |
| | | | | | 27.15 | 26.35 | 26.30 |
| | | | | | | 26.30 | 26.35 |
| | | | | | | | |

Avg. Assy. Burnup = 28.8 (in units 1000 MWD/MTM)
Avg. $UO_2$ Burnup = 28.7 Avg. Mix Oxide Burnup = 28.90

Max. $UO_2$ BU : 32.90
Min. $UO_2$ BU : 25.20
Max. Mix BU : 32.65
Min. Mix BU : 26.30
$k_\infty$ assy. = 1.01416, $k_\infty$ $UO_2$ = 1.02100, $k_\infty$ Mix = 1.00185

32.90 BURNUP IN 1000 MWD/MTM.

FIG. V-39 : K-INFINITY MAP FOR THE PU-RECYCLE ASSEMBLY AT 28800 MWD/MTM.

| | | | | | | | |
|---|---|---|---|---|---|---|---|
| 1.003 | 1.007 | 1.012 | 1.012 | 1.014 | 1.015 | 1.016 | 1.015 |
| | 1.013 | 1.017 | 1.020 | 1.021 | 1.024 | 1.024 | 1.026 |
| | | 1.022 | 1.025 | 1.030 | 1.033 | 1.038 | 1.038 |
| | | | 1.032 | 1.039 | 0.990 | 0.995 | 0.996 |
| | | | | 0.994 | 1.002 | 1.005 | 1.006 |
| | | | | | 1.007 | 1.010 | 1.010 |
| | | | | | | 1.010 | 1.010 |
| | | | | | | | |

$k_\infty$ Assy. = 1.01416, $k_\infty$ $UO_2$ = 1.0210, $k_\infty$ Mix = 1.00185

1.003 K-INFINITY

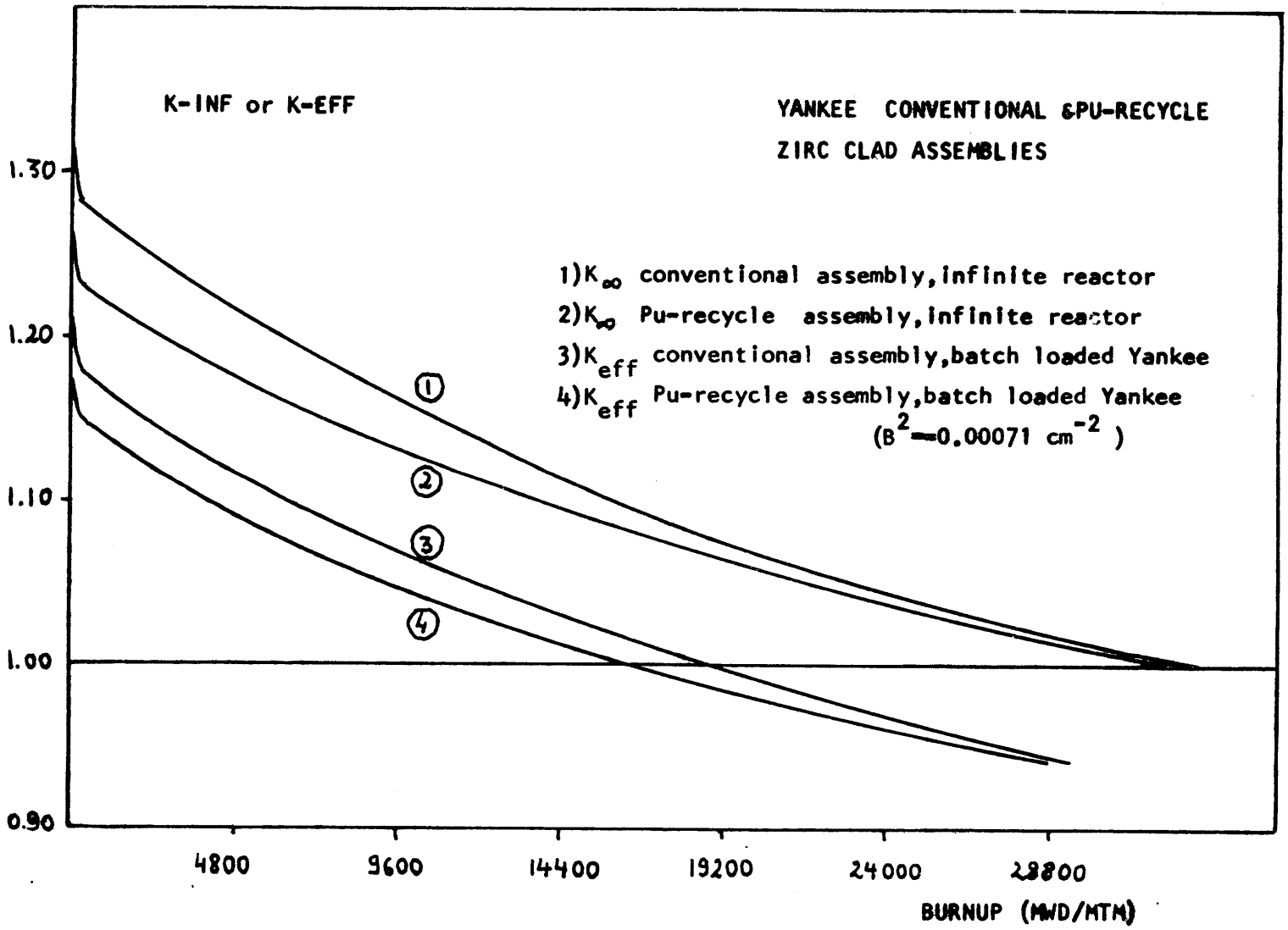


FIG V-40 COMPARISON OF K-INF AND K-EFF VS BURNUP FOR THE CONVENTIONAL &PU-RECYCLE ASSEMBLIES (K -inf without extra materials,K-eff with extra materials and buckling)

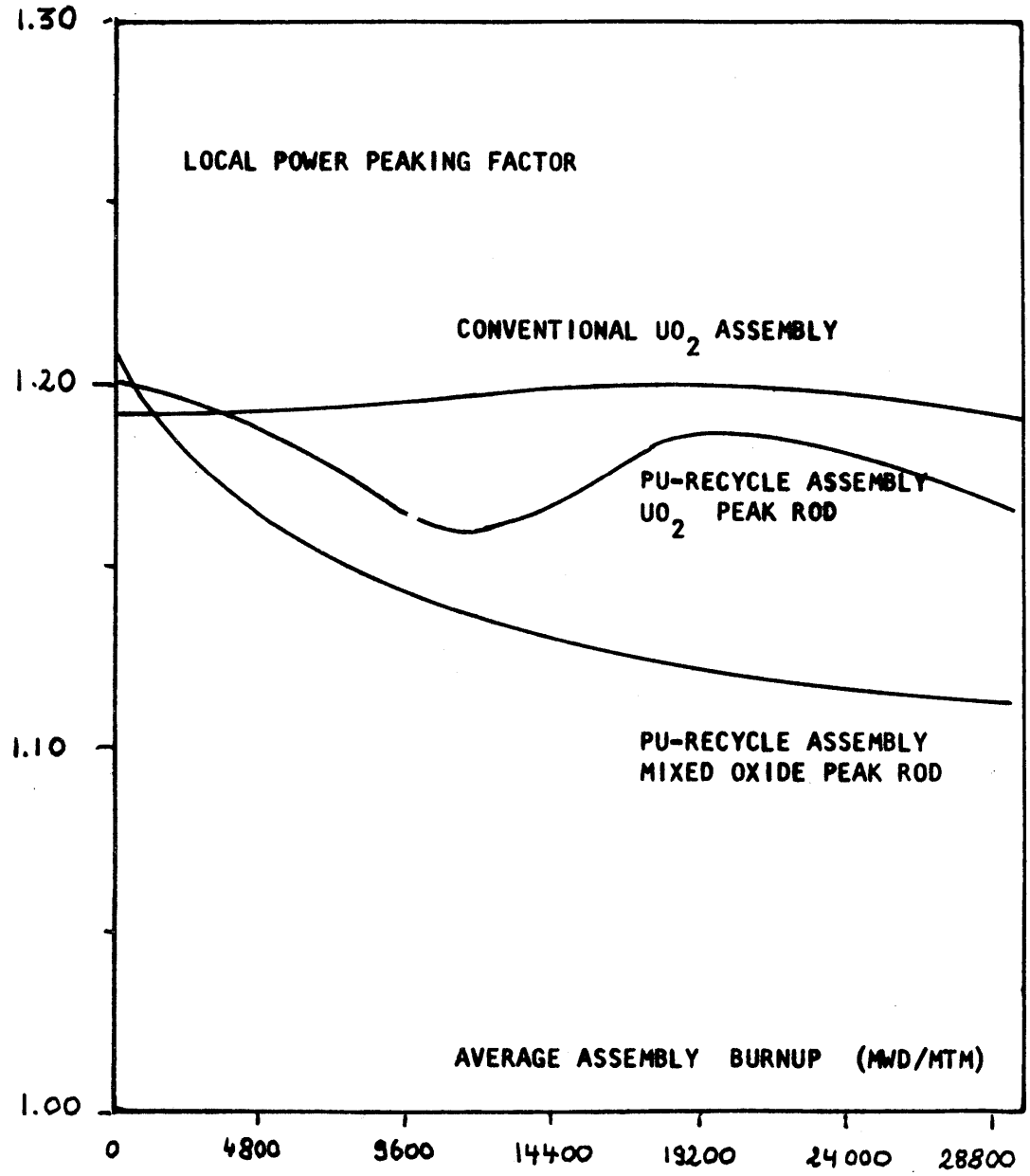


FIG V-41 LOCAL POWER PEAKING FACTORS IN THE CONVENTIONAL AND PU-RECYCLE ASSEMBLIES VS BURNUP

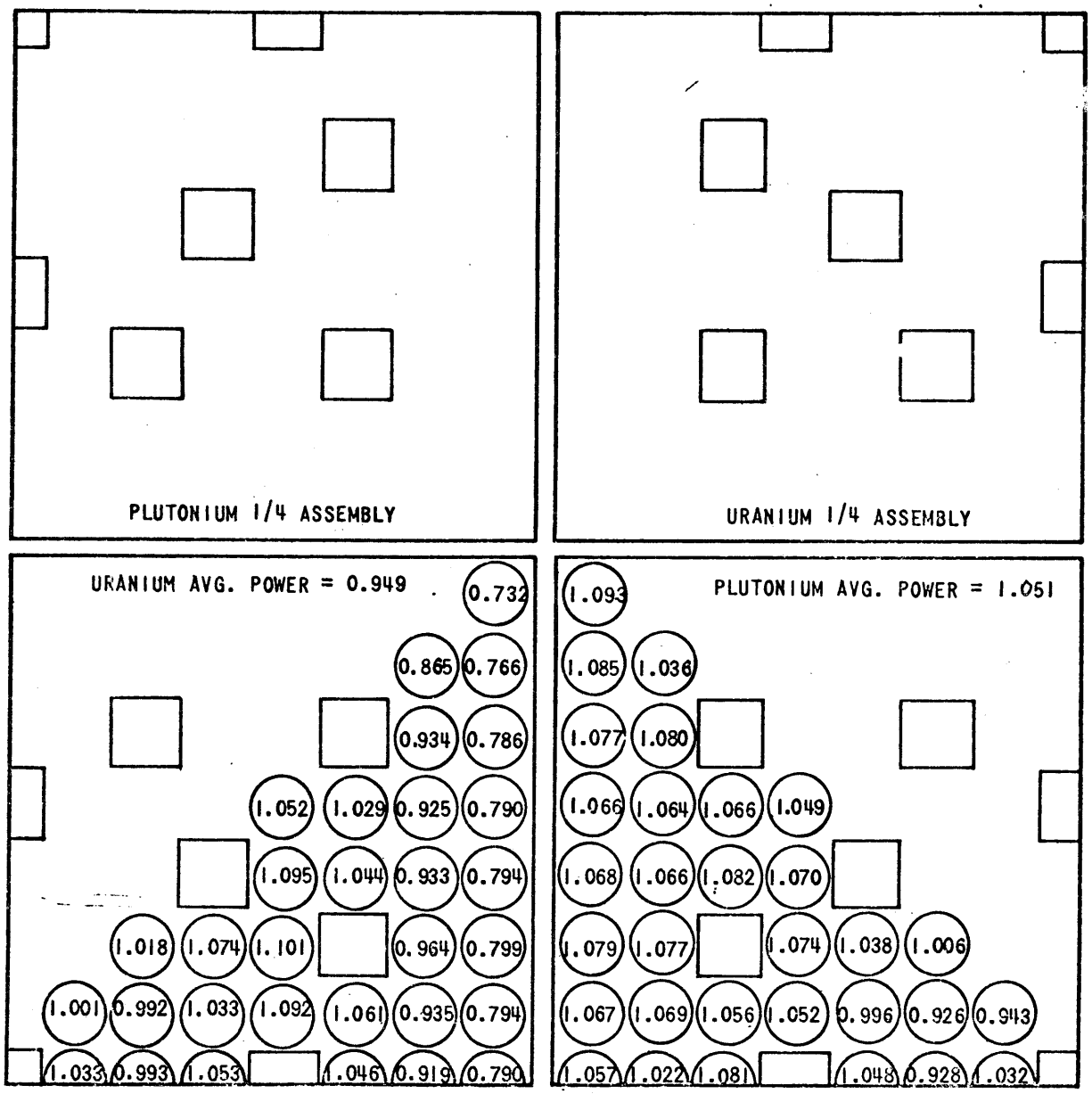


Figure V-42, Unit Assembly Power Distribution at the Beginning-of-Life for a Discrete Assembly Concept

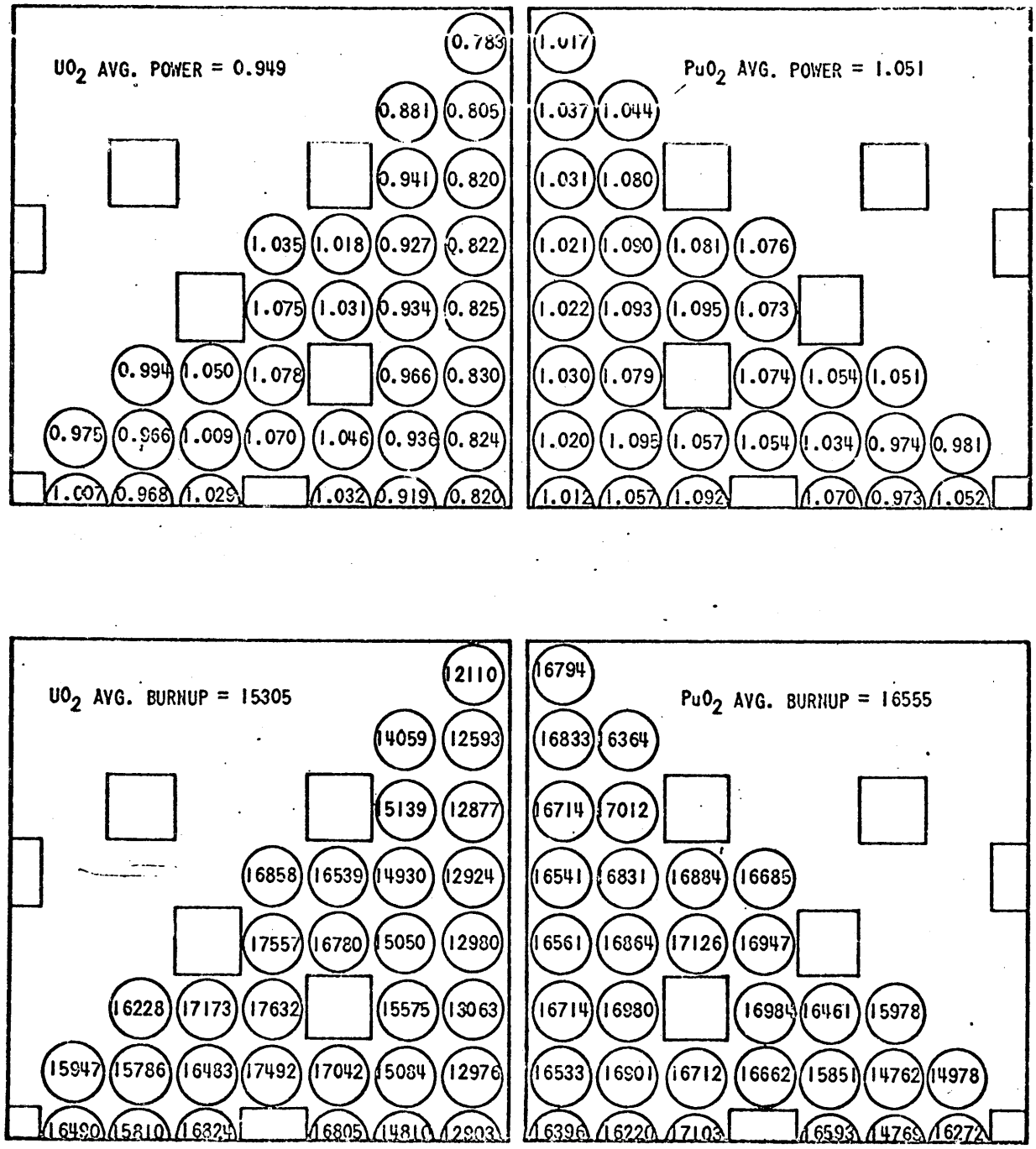


Figure V-43. Unit Assembly Power Distributions at the End-of-Life for a Discrete Assembly Concept

# CHAPTER VI : THE CALCULATION OF POWERGRADIENTS AND POWERDISTRIBUTION INSIDE THE PEAK RODS OF CONVENTIONAL & PU-RECYCLE-ASSEMBLIES.

## VI - 1 : INTRODUCTION.

Steep powergradients have been noticed in the plutoniumrecycle assembly. It is therefore useful to calculate these gradients inside the rods in both PU-recycle and conventional assemblies during normal operation and at beginning of life.

Powergradients & non-uniform powerdistributions are important for the mechanical design of fuel assemblies & fuel elements. Due to the non uniform cladding & fuel temperatures a permanent bending moment will exist on the fuel pins, which causes them to bow. Also for the thermal & hydraulic analysis, these gradients are important since they create circumferential hot spots in the cladding and produce a non uniform heat flux.

A succesful attempt has been made to calculate the non uniform powerdistribution (including spectraleffects) in a simple manner and to correlate the obtained X, Y powerdistribution inside a pin with a formula of the type :

$$P(r,\theta) = f\left(a + b\,\frac{r}{R}\cos\theta\right) e^{\xi_i\left(\frac{r}{R}\right)^2} + (1-f)$$

This expression is more convenient for the type of cylindrical geometry & greatly simplifies the thermal calculations performed in Chapter VII.

## VI - 2 : DESCRIPTION OF THE CALCULATIONMETHOD.

The accurate calculation of the powerdistribution inside the fuel pins in a cluster of rods is very complex.

An accurate calculation would require the solution of 2 dimensional transport-equations with many thermalgroups, an $S_N$ order of 16 and about 4900 meshpoints. Although such calculations, in a simplified way, have been made occasionaly on

small 7 or 9 rod clusters for pressure tube light water moderated reactors, ( 45 , 46 ), they are not practicle, as the authors in refs. 45 point out. The basic difficulty is the need for 2 dimensional transport-theory codes since the spectrumeffects can be accounted for by superposition of THERMOS results on the 2D transporttheory calculation ( 46 ). For such pressure tube clusters, were the coolant is air, only transporttheory calculations have been reported. In the case of PWR or BWR assemblies, cooled and moderated by water, transport-theory may be replaced by diffusiontheory, as shown further. By making a fixed source, 1 thermal group calculation on the most interesting portions of the assemblies, the powerdistribution calculation in the fuel pins with the PDQ-5 code can be made inexpensively and straightforward. The method that was developed for the calculation of the powerdistribution inside the fuel pins in the assemblies, consits of the following steps :

1) From a THERMOS-<u>cylindrical unit cell</u> calculation, the region averaged thermal macroscopic cross-sections for the fuel & homogenized clad & water are obtained.

At the same time a basic spatial spectralcorrectionfactor, defined as :

$$s^{u}(r) = \frac{\Sigma_f^{u}(r/R)}{\overline{\Sigma}_f^{u}}$$

is also calculated from THERMOS. It has been found (see section 3) that this spectral correctionfactor can be expressed by a simple formula :

$$s^{u}(r) = A\, e^{\xi_s^{u}(r/R)^2} \qquad (6-1)$$

Therefore only 2 points are necessary to calculate $\xi_s^{u}$ or $s(r)$ from :

$$\xi_s^{u} = \ln \frac{s(R)}{s(0)}$$

2) Using the thermal macroscopic parameters a 2 dimensional X-Y PDQ-5 fine mesh (50 X 50 or 70 X 70) fixed source calculation is made, and the power-distribution $P_i^{Th}$ (X,Y) in each fuel pin i of a cluster of 9 or 49 rods is obtained. A unit cell of 10 X 10 = 100 meshpoints with 8 X 8 -12 = 52 meshpoints in the fuel has been used in this study.

3) From a THERMOS-slab model calculation spatial spectrumcorrectionfactors $s^P(X)$ are obtained in the peak slabs at the $H_2O$ gap or $MIX/_{UO_2}$ interface.

These factors are calculated from :

$$s^P = \frac{\Sigma_f^P (x/L)}{\Sigma_f^U (x/L)}$$

were $\Sigma_f^P(X/_L)$ is the macroscopic fission section in the peak rod at the normalised distances $X/_L$, and $\Sigma_f^U(X/_L)$ is the same factor but in an unperturbed cell.

It has been assumed that this spectrumcorrectionfactor $S^P$ can be expressed by a simple formula :

$$s_i^P = a_i + b_i \frac{r}{R} \cos\theta \qquad (6\text{-}2)$$

were $\theta$ = is the angle, from the symmetryline to the point involved at distance $\frac{r}{R}$ from the center of the fuel pin.

4) The obtained powerdistribution from thermal neutrons $P_i^{Th}$ (X, Y) in the peak gradient pin is then correlated to a general formula suggested by Palmedo ( 47 )

$$T_i^{th}(r,\theta) = \left( c_i + d_i \frac{r}{R} \cos\theta \right) \exp \xi_i' \left(\frac{r}{R}\right)^2 \qquad (6\text{-}3)$$

which was found to describe the powerdistribution reasonably well even in our assemblies.

5) The total powerdistribution inside the pin i, including the flat fast & epithermal power and all the thermal spectraleffects, is finally obtained from superposition of all effects according to the equation (6-4)

$$P_i(r,\theta) = f_i\left(a_i + b_i \frac{r}{R}\cos\theta\right)\exp \xi_s^{u}\left(\frac{r}{R}\right)^2 + (1-f_i)\left(c_i + d_i \frac{r}{R}\cos\theta\right)\exp \xi_i'\left(\frac{r}{R}\right)^2 \qquad (6\text{-}4)$$

Eq. 6-4 can be simplified by the observation that the $b_i$ and $d_i$ factors are small : therefore :

$$\frac{P_i(r,\theta)}{P_{i\,AVG}} = f_i N_i\left(1 + q_i \frac{r}{R}\cos\theta\right)\exp \xi_i\left(\frac{r}{R}\right)^2 + (1-f_i) \qquad (6\text{-}5)$$

were $\frac{r}{R}$ = normalised distance (R=radius of the fuel pin)

$f_i$ = fraction of the total average pin power coming from thermal neutrons at location i (as determined from previous unit-cell homogenized 2 group PDQ calculations)

$\theta$ = angle from the symmetryline to the point involved

$q_i = b_i/a_i + d_i/c_i$

$\xi_i = \xi_i' + \xi_s^{u}$

Ni = normalisationfactor

such that $$\int_0^{2\pi}\int_0^{R} P_i(r,\theta)\, r\,dr\,d\theta \Big/ P_{i\,AVG}\,\pi R^2 = 1$$

from (6-5) the normalisationfactor is thus also given by (after performing the double integration)

$$N_i = 1 \Big/ (\exp \xi_i - 1)/\xi_i \qquad (6\text{-}6)$$

(Since $\xi_i$ is usually small $N_i$ is close to unity).

## VI-3 EVALUATION OF THE METHOD BY COMPARISON WITH THERMOS.

The method described above has been evaluated by comparison with the more rigorous THERMOS-35 thermal group integral transporttheory program. The figures VI-1, A, B and C show the results of the calculations.

Fig. VI-1,A pictures the powerdistribution in a cylindrical fuel element as calculated by THERMOS on a cylindrical unit cell (heavy line). The dotted line shows the uncorrected powerdistribution as calculated with PDQ-5. It is noticed that the uncorrected powerdistribution is heavily in error. After applying the spectralcorrectionfactors (Eq. 6-1), the powerdistribution as calculated with our method is in excellent agreement with the THERMOS calculation. A PDQ-5 calculation of an X-Y unit cell also gives excellent results, as the * points indicate.

After these encouraging results a more difficult arrangement of 4 slabs (2 $UO_2$ slabs and 2 mixed oxide slabs) at the $UO_2$/MIX. interface have been calculated with THERMOS & our method.

Fig. VI-1,B shows the normalised powerdistribution in the peak MIX.OXIDE slab as calculated with THERMOS and our method. (after applying the $S_X$ spectralcorrectionfactors) and Fig. VI-1,C shows the same results for the $UO_2$ slab at the interface. It is noticed that in this case the agreement is not as good, but the errors are still within the $\pm$ 3 % error claimed for experimental accuracy ( 47 ). The agreement between our method & THERMOS on a gradient-factor defined as the ratio of the peak power at surface to the minimum power at the surface is about 1 %.

Noticible is that the gradient in the $UO_2$ slab is small & opposite to what expected. Therefore in all our further calculations, spectrumcorrection-factors $S^P$ for the $UO_2$ pin next to the Mixed oxide have been neglected, since they make the results worse.

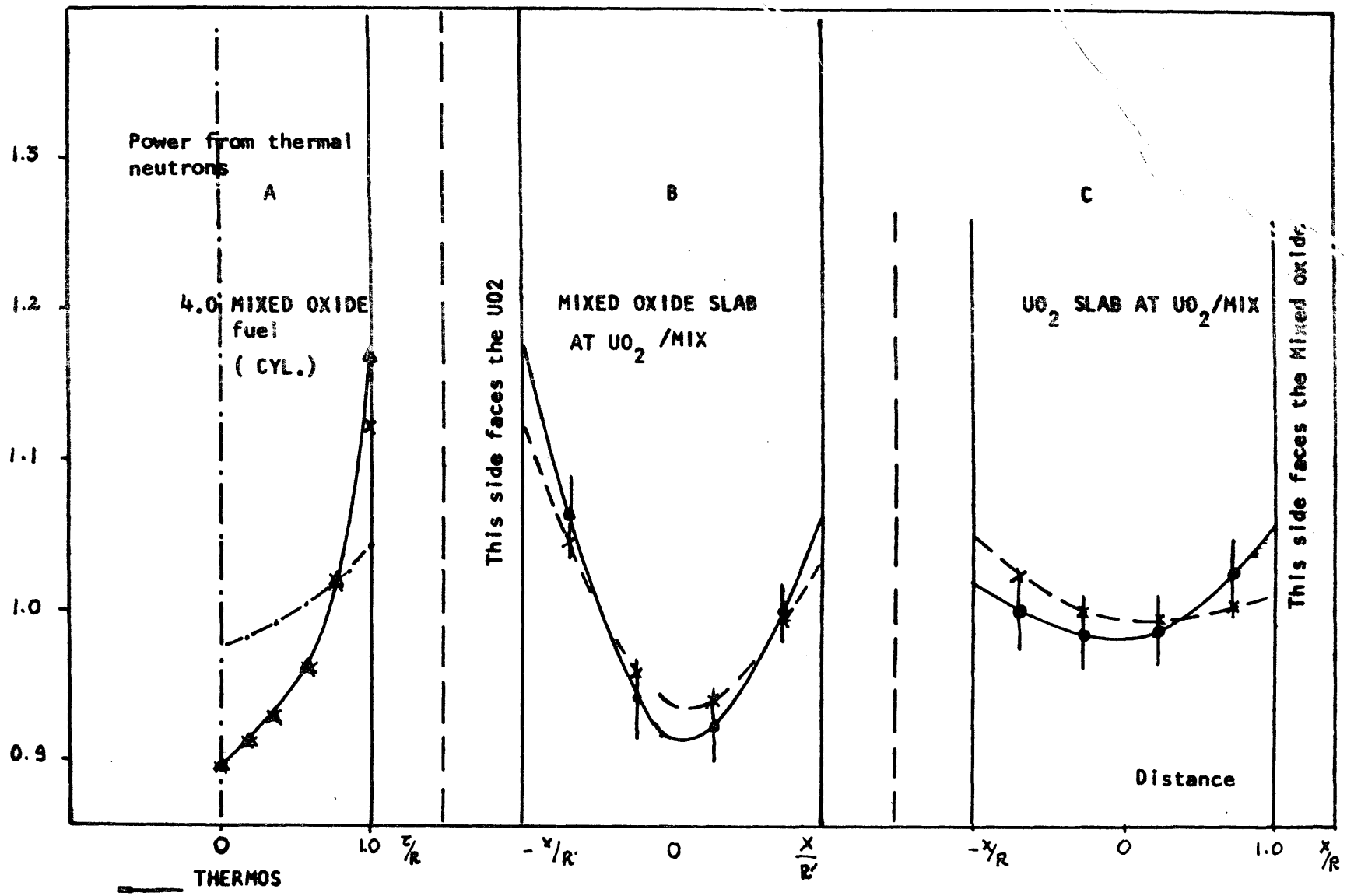


THERMOS

△ Corrected cylindrical PDQ calculation

—X— Corrected X Y PDQ calculation

—•— Uncorrected PDQ calculation

FIG VI-1 COMPARISON THERMOS AND CORRECTED ONE GROUP DIFFUSION THEORY

In summary it may be concluded that the basics of the simple method are adequate for the calculation of the powerdistribution inside the pins. The accuracy of the method is nearly as good as the accuracy of 3 % claimed for the experimental determination of the power inside the rods using a fuel activationtechnique.

## VI -4) RESULTS FOR THE CONVENTIONAL & PU-RECYCLE ASSEMBLIES.

### 4)-A SPECTRUM CALCULATION RESULTS.

Four THERMOS calculations were made to determine the spectrum correctionfactors $S^P$ at the $H_2O/UO_2$ interface, $UO_2$/MIX interface and the unperturbed spectralcorrectionfactors $S^U$ (r) in cylindrical $UO_2$ and mixed oxide unit cells. The geometry for the $H_2O/UO_2$ interface calculation consisted of a 1 dimensional slab model of the zirc follower, watergap, can and 3 fuel slabs of $UO_2$, inbedded in $H_2O$. Four slabs (2 slabs $UO_2$ & 2 slabs MIX.OXIDE) were taken for the $UO_2$/MIX interface calculation.

Fig. VI-2 shows the spectralcorrectionfactors $S^P$ in the peak slabs at the $H_2O/UO_2$ and MIX/$UO_2$ interfaces, at various normalized positions in the peak slabs. As seen there is a linear variation of the $S^P$ factor versus normalized distance given by :

$$S^P = 1 + 0.04\ x/L$$

(It is only by chance that the correctionfactors are the same in both cases). The linear variation is more or less expected, since it had been observed that the spectraleffects decay exponentially away from the interface, in the small peak slab the exponential with a decay constant of about 2 unit cells, is nearly linear.

Because a real fuel pin is cylindrical a reasonable assumption for the variation of the spectrum correctionfactor $S^P$ in the peak $UO_2$ pin at the $H_2O/UO_2$ and the

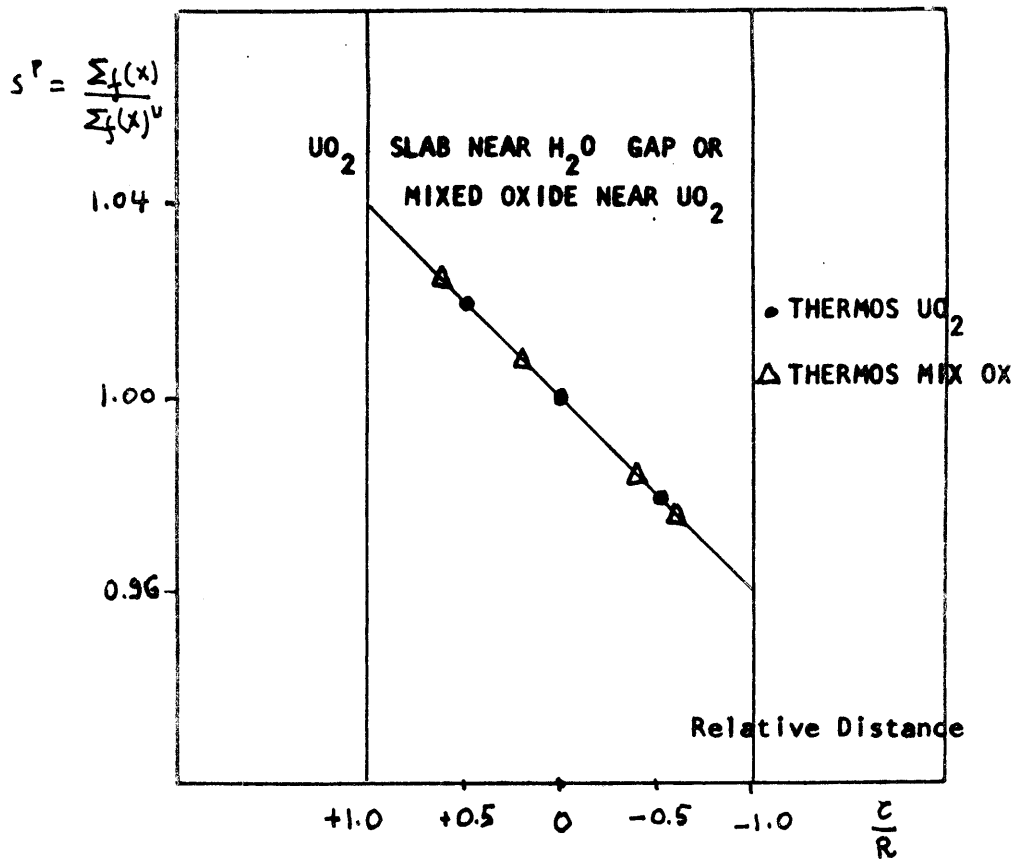


FIG VI-2 PERTURBED SPECTRAL CORRECTION FACTORS

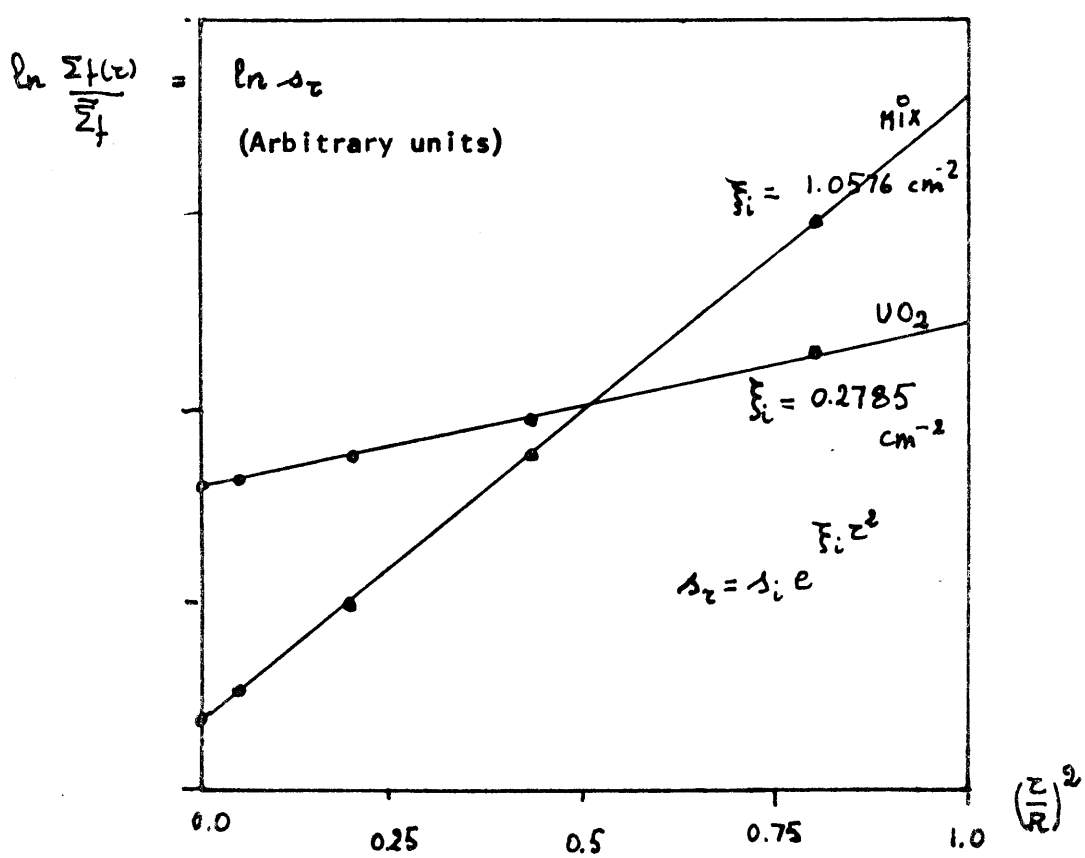


FIG VI-3 SPECTRAL CORRECTION FACTORS IN THE UNPERTURBED CYLINDRICAL PINS

peak MIX.OXIDE pin at the $UO_2$/MIX is ;

$$s_i^p(r,\theta) = 1 + 0.04\left(\frac{r}{R}\right)\cos\theta \qquad (6-8)$$

were the $\theta$ angle is taken from the symmetry line in the direction of the peak to the line from the center of the pin to the point at a normalized distance $\frac{r}{R}$ from the center.

Note that eq. (6-8) is consistent wit eq.(6-7) for $\theta = 0^o$ and $\theta = 180^o$ and the slabresults of Fig. VI,2.

Fig. VI-3 pictures the variation of the spectralcorrectionfactors S(r) in the unperturbed $UO_2$ and Mixed oxide cylindrical fuel elements, as calculated with THERMOS on a cylindrical unit-cell model.

The ln S(r) has been plotted in fuction of $(r/R)^2$, and it is noticed that there is a perfect linear relationship. The S (r) factor may thus be expressed by :

$$s(r) = A \exp \xi_U^s \left(\frac{r}{R}\right)^2 \qquad (6-9)$$

From the results the $\xi_U^s$ factors were found to be :

$$(UO_2)\ \xi_U^s = 0.044 \qquad (6-10)$$

$$(Mix)\ \xi_U^s = 0.167 \qquad (6-11)$$

It is thus also noticed that the spectrum varies much stronger in a mixed oxide fuel pin than in a uraniumoxide fuel pin.

## 4)-B UNCORRECTED X-Y POWERDISTRIBUTIONRESULTS.

### Description of the model.

Using the thermal macroscopic cross-sections obtained from the THERMOS unit cell calculations, two dimensional X-Y powerdistributioncalculations were made with the PDQ-5 code on portions of the conventional and PU-recycle assembly.

Large savings in computortime (about a factor of 30) was realised by using 1 thermal group and a flat fixed source in water. Since the powergradients inside the rods are smaller than the overall gradients from rod to rod and damp out about three fuel pins from the $H_2O/UO_2$ or $MIX/UO_2$ interface, only portions of the assembly were considered. A cluster of 9 $UO_2$ rods at the cruciform watergap, and a cluster of 36 $UO_2$ and mixed oxide rods were therefore calculated, with the geometrical lay-out pictured on Figs.VI-4 and VI-5. As seen on the figures, a unit cell had been described by 12 X 12 = 144 meshpoints, and the cylindrical fuel rod by an X-Y model of 8 X8 - 3X4 = 52 meshpoints. The total size of the problem was 51 X 51 = 2601 meshpoints for the 9 rod cluster in the corner of the assemblies and 70 X 70 = 4900 meshpoints for the 36 rod cluster in the center of a plutoniumrecycle assembly. The $UO_2$ rods were of the usual 4.0 w/o U235 type & the Mixed oxide rods were of the proposed 4.0 w/o PU $O_2$ - nat $UO_2$ (19 a/o PU 240) type. The total CPU time for such a large size problem was only $\pm$ 1 min. for the 9 rod cluster & $\pm$ 2 min. for the 36 rod cluster. The rather small CPU time & low cost (about 20 $ per run) is mainly due to the selection of the 1 thermalgroup & fixed source model, which is adequate for our purpose since the epithermal & fast fluxes inside the fuelrods (& even over the whole clusters) are very flat. It is estimated that about 10 to 20 outer iterations would have been necessary to calculate a 2-group, $k_{eff}$ calculation of the same size. The estimated computorcost would have been about 2 X 15 X 20 = 600 $ instead of 20 $ as with our model. A transport-theory calculation of about the same size and S-12 approximation to reduce streaming effects would cost about $(12)^2$ = 144 times more. The numbers speak for themselves.

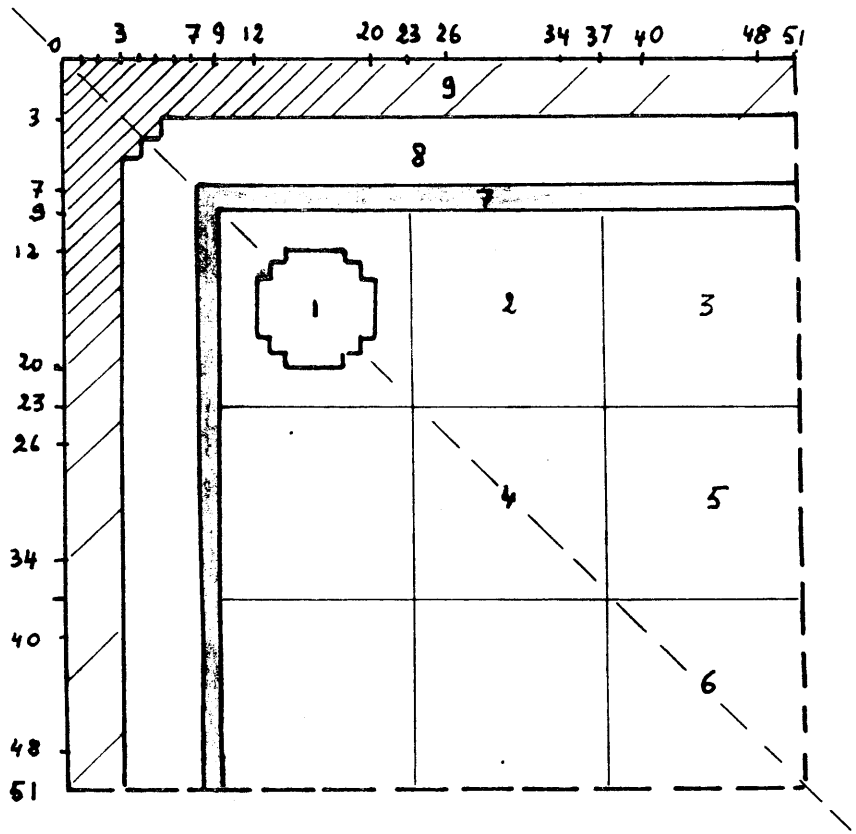


FIG VI-4 GEOMETRICAL AND COMPOSITION LAY OUT OF THE 9 ROD CLUSTER AT THE CRUCIFORM WATER GAP

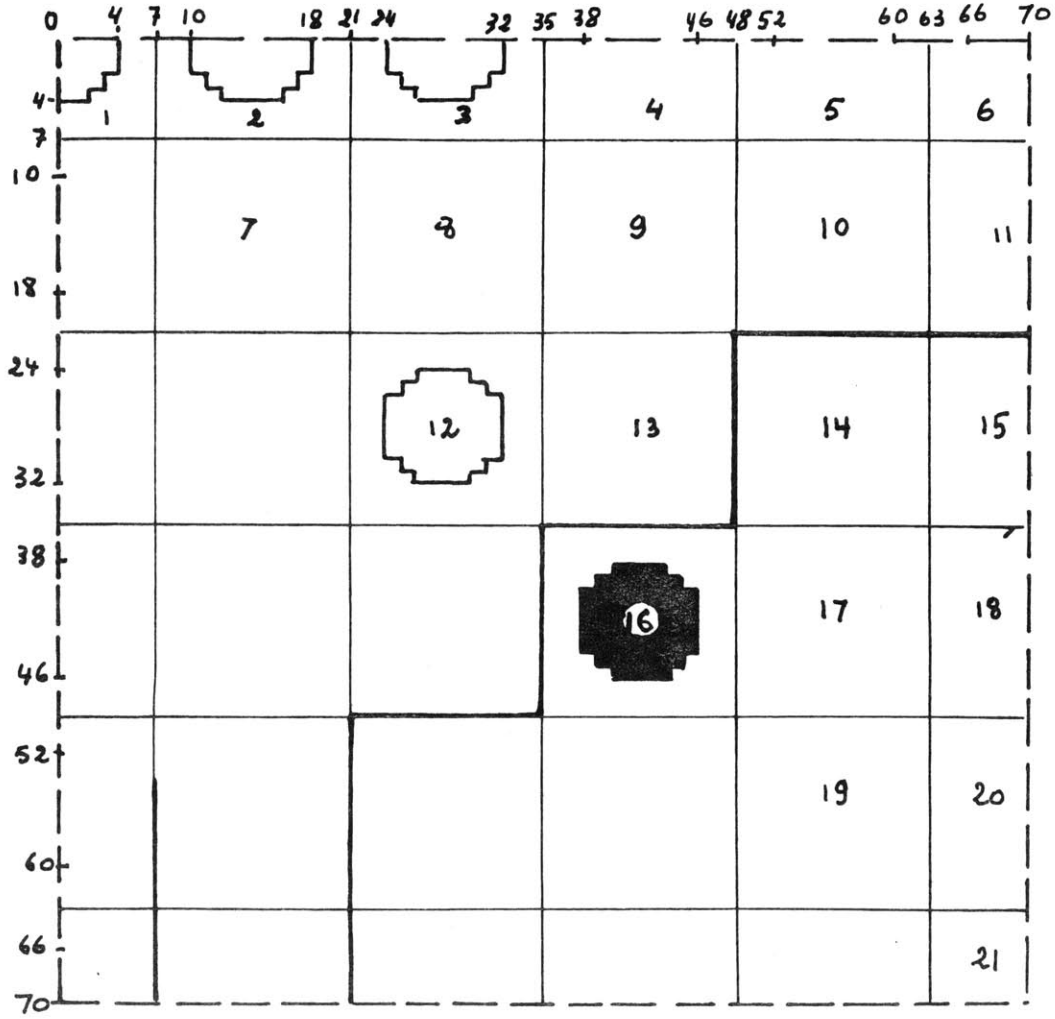


FIG VI-5 GEOMETRICAL AND COMPOSITION LAY OUT OF THE 36 $UO_2$ & MIXED OXIDE ROD CLUSTER

Results :

Fig. VI-6 shows the 2 dimensional map of a gradient-factor G.F., defined as the max/power at the surface of the fuel rod to the minimum power at the fuel rod, as determined from the uncorrected PDQ-5 results.

It is noticed that the uncorrected gradients in the $UO_2$ cluster at the cruciform watergap are much less than the gradients in the peak mixed oxide pins in the 36 rod cluster. It is also important to notice that the gradients in all the mixed oxide pins at the boundary of the interface are about the same, but is maximum for mixed oxide pin number 2.

Also shown on the figures is the direction from the min. to maximum circumferential powervalues. They are thus the directions in which the fuel pins will bow.

For comparison reasons, the gradientfactors have also been multiplied with the spectrum correctionfactor $S^P$. It is thus noticed that the spectralcoupling effects are responsible for about 80 % of the gradients in the peak $UO_2$ rods at the watergaps and for about only 25 % in the peak mixed oxide rods.

It is also observed that gradient-effects will be about 150 % worse in aPU-recycle assembly compared to a conventional assembly & the peak gradients are found in the peak mixed oxide pins.

The Figures VI-7 and 8 are showing the uncorrected X-Y powerdistribution in the uranium oxide pins 1 and 3 of the 9 rod cluster at the cruciform watergap of a conventional or PU-recycle assembly. They are obtained directly from PDQ-5 after normalisation of the average pin powerdensity to unity. The powerdistribution does not include the unperturbed spectralcorrectionfactor S(r) and the perturbed factor $S^P(r,\theta)$, and gives only the power from thermal neutrons.

The asymptotic $UO_2$ pin 9 was found to follow an exp. $\left[\xi'\left(\frac{r}{R}\right)^{\ell}\right]$ — law;

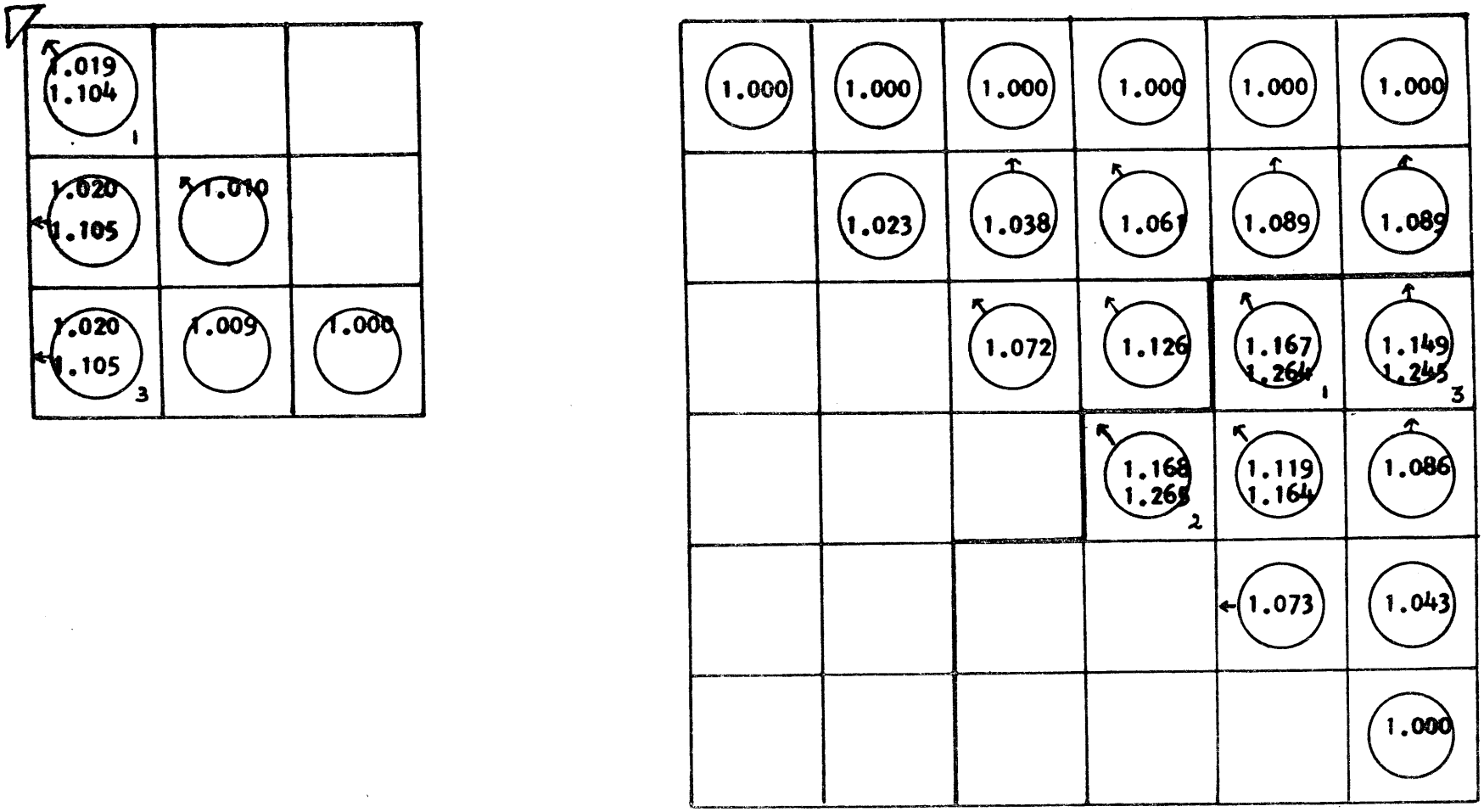


FIG VI-6 GRADIENT FACTOR DISTRIBUTION & BOWING DIRECTIONS IN THE 9ROD CLUSTER IN THE CORNER OF THE ASSEMBLIES, AND IN THE 36 ROD CLUSTER IN A PLUTONIUM RECYCLE ASSEMBLY (PDQ-5 UNCORRECTED RESULTS)

PEAK $UO_2$ ROD AVG. POWER 1.00 PIN # 1.

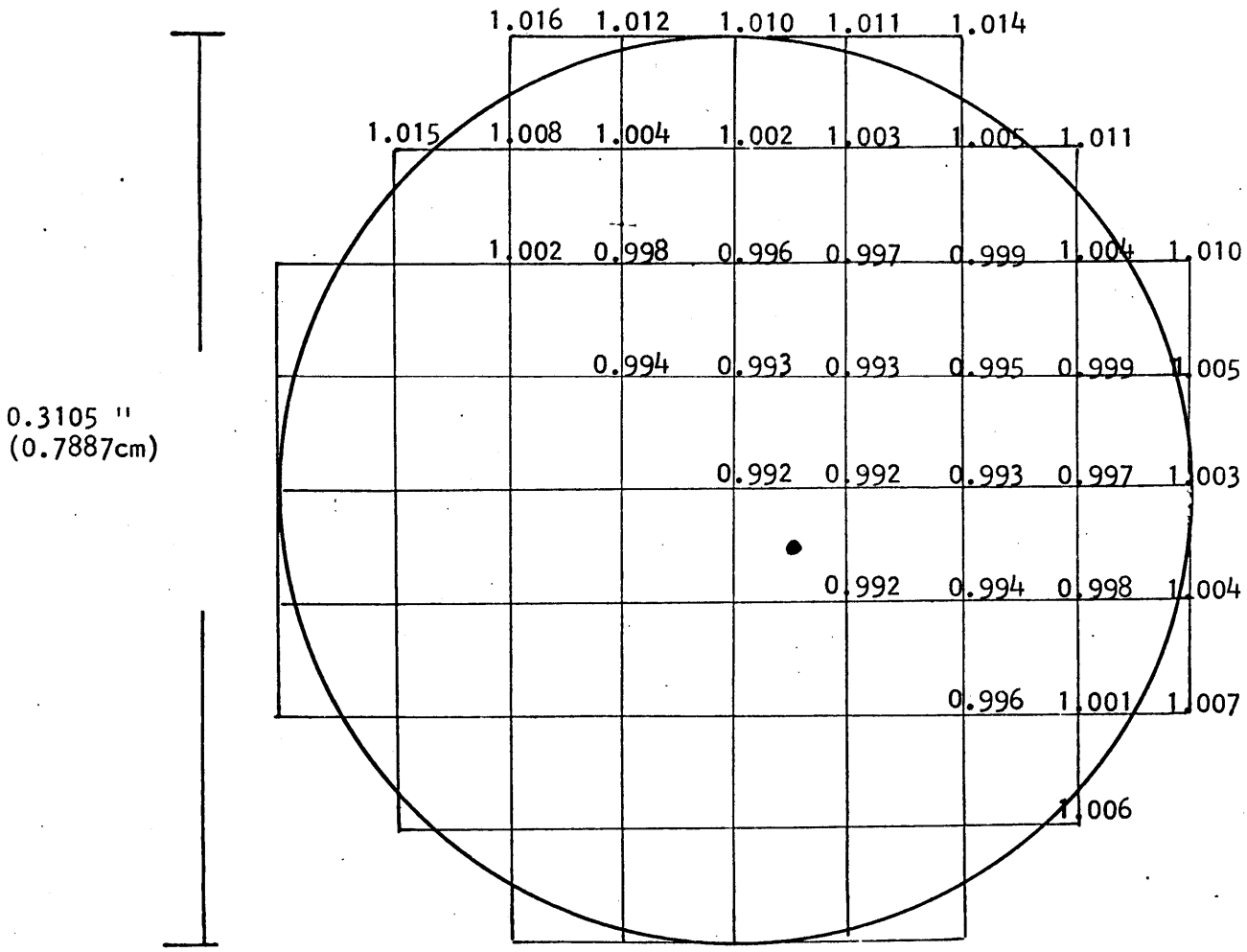


FIG. VI-7 : Uncorrected X - Y powerdistribution in the peak $UO_2$ pin number 1, in the 9 rod cluster at the cruciform watergap (conventional & PU-recycle assembly).

$UO_2$ region Avg. Power 1.00 Pin # 3.

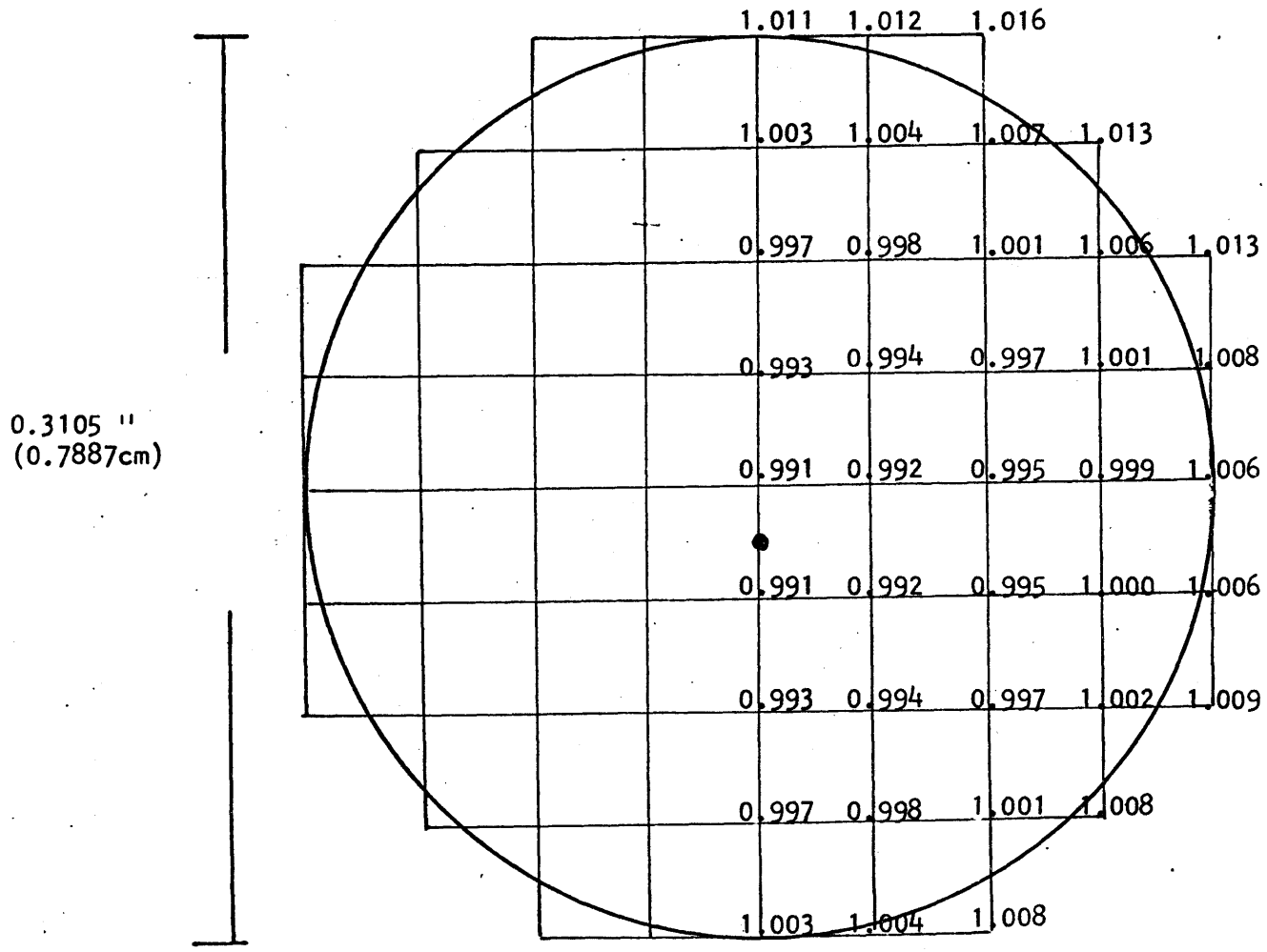


FIG. VI-8 : Uncorrected X-Y powerdistribution in $UO_2$ pin number 3, in the 9 rod cluster at the cruciform watergap.

and the $\xi$ factor was found to be 0,016 (6-12).

The figures 9 to 11 picture the uncorrected X-Y powerdistribution in the mixed oxide pins number 1, 2 and 3. The pins 2 & 3 are having a symmetryline at 45 $^{o}$ and 90$^{o}$ respectively, in which directtion the fuel pins will bow. The peak mixed oxide pin number 1, does not have a symmetry, as seen from Fig, 9. The gradients may be thought of as coming from a 0$^{o}$ and 90$^{o}$ line with different strength. Since the 90$^{o}$ line gives somewhat larger gradient , the vector result of bow-driving forces will be around the 50 to 60$^{o}$line. Note that all the peak mixed oxide pins have about the same gradient-factor & about the same skewed distribution. Therefore instead of analysing the peak pin number 1, we will analyse the pin number 2. In view of its symmetry & the fact that easy formulas exist makes the problem of one order of magnitude simplier. The asymptotic mixed oxide pin was also observed to follow a law esp. $\xi' \left(\frac{r}{R}\right)^2$ and the factor was found to be $\xi'_{MIX} = 0.0524$ (6-13).

The X-Y PDQ calculations are not practicle to work with, therefore it was tried to correlate the uncorrected X-Y results in the regular peak $UO_2$ and mixed oxide pins with a formula of the type:

$$P'_i(r,\theta) = \left(p_i' + q_i' \frac{r}{R} \cos\theta\right) \exp \xi_i' \left(\frac{r}{R}\right)^2 \qquad (6\text{-}14)$$

It was found that the uncorrected powerdistribution in the peak $UO_2$ pin could be expressed by the formula (6-14)

$$P'_{UO_2}(r,\theta) = \left(0.9914 + 0.0056 \frac{r}{R} \cos\theta\right) \exp 0.016 \left(\frac{r}{R}\right)^2 \qquad (6\text{-}14)$$

and the uncorrected powerdistribution in the regular peak mixed oxide pin (number 2) by the formula (6-15)

$$P'_{Mix}(r,\theta) = \left(0.980 + 0.0765 \frac{r}{R} \cos\theta\right) \exp 0.0524 \left(\frac{r}{R}\right)^2 \qquad (6\text{-}15)$$

MIX. OXIDE PEAK PIN # 1 Ag. power 1.00

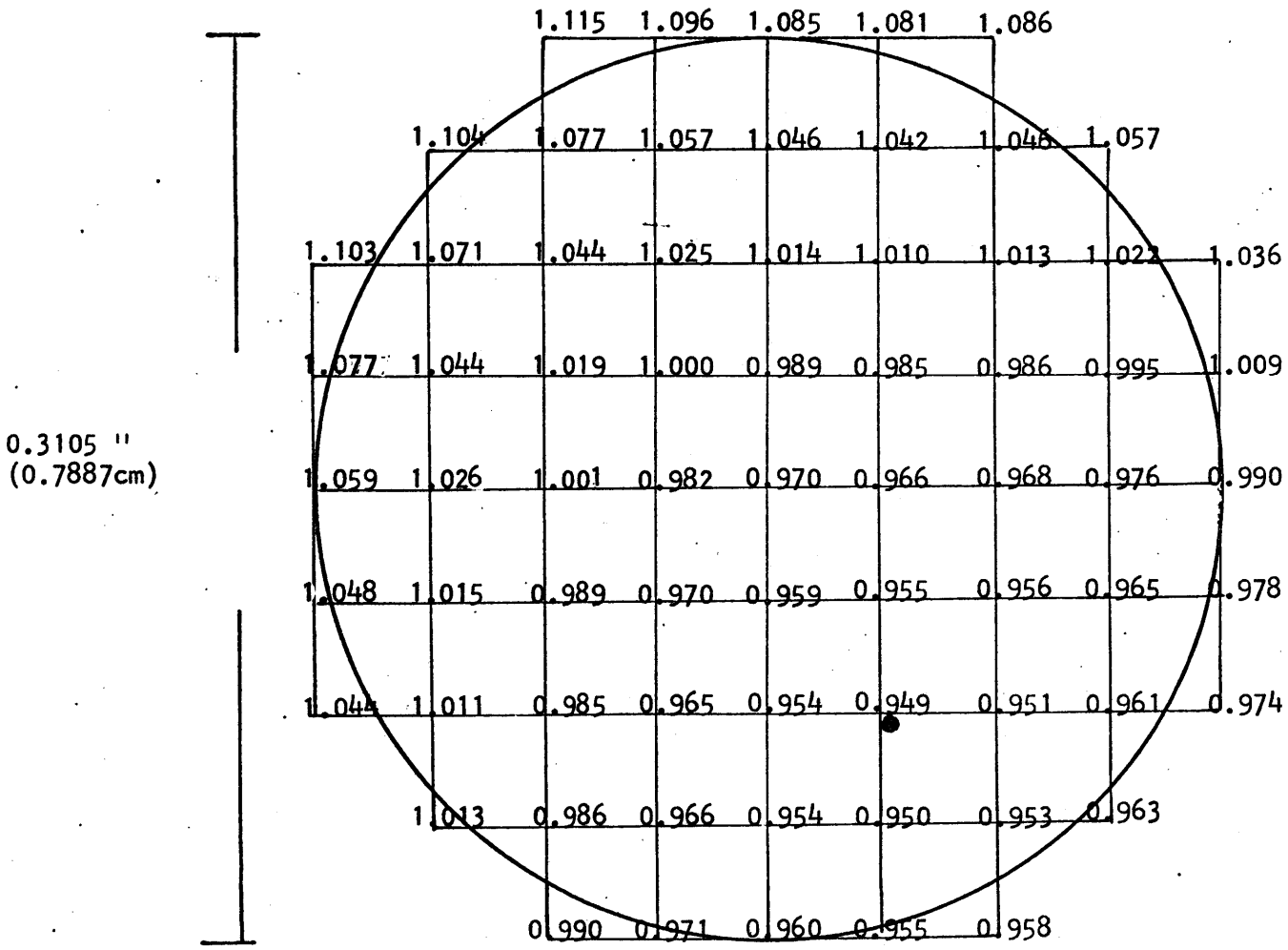


FIG. VI-9 : Uncorrected X-Y powerdistribution in the peak Mixed oxide pin number 1, in the 36 rod cluster in the center of a plutoniumrecycle assembly.

MIX OXIDE PIN # 2.

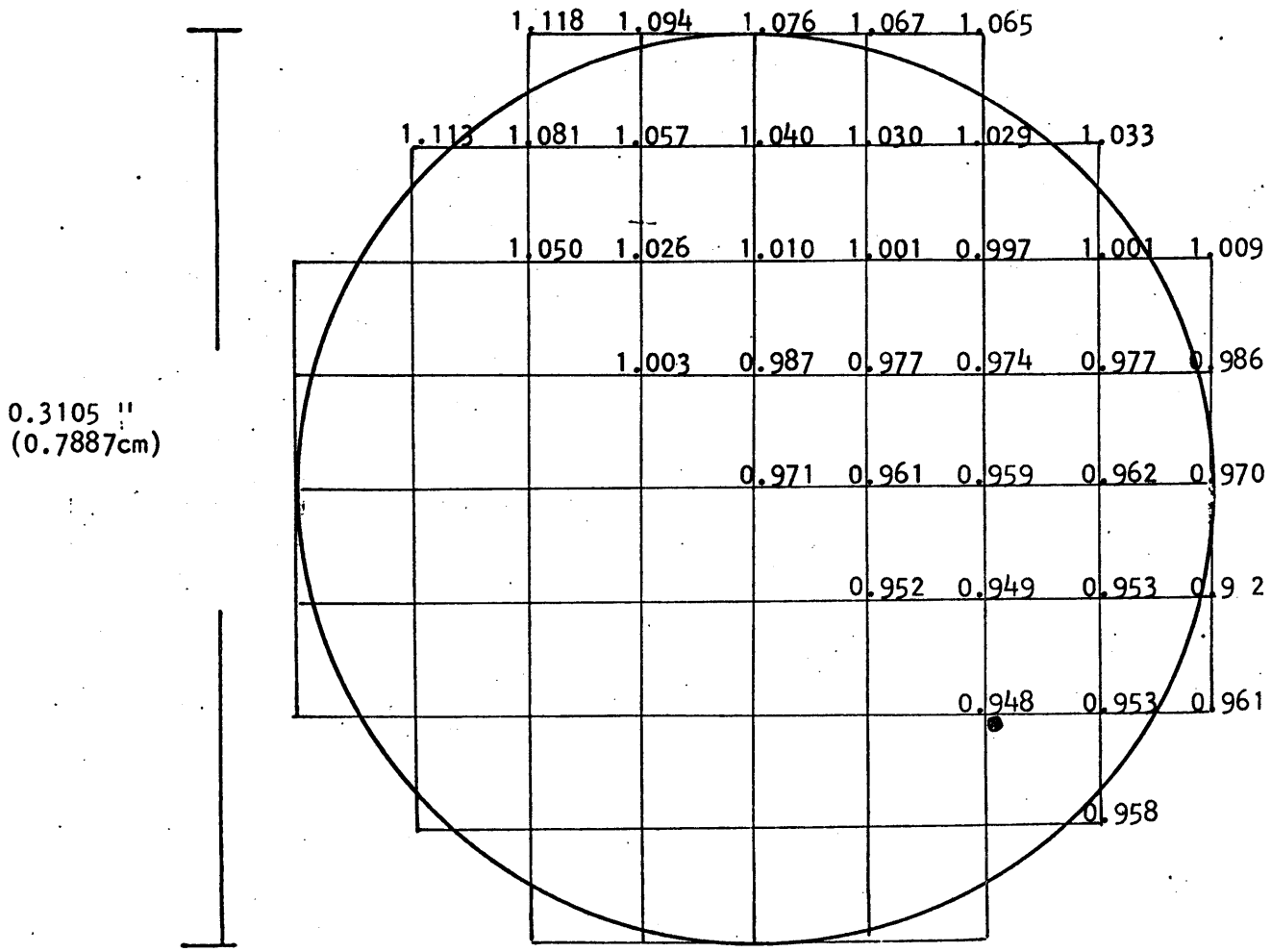


FIG. VI-10 : Uncorrected X-Y powerdistribution in the mixed oxide pin number 2 in the 36 rod cluster in the center of a PU-recycle assembly.

MIX OXIDE PIN # 3.

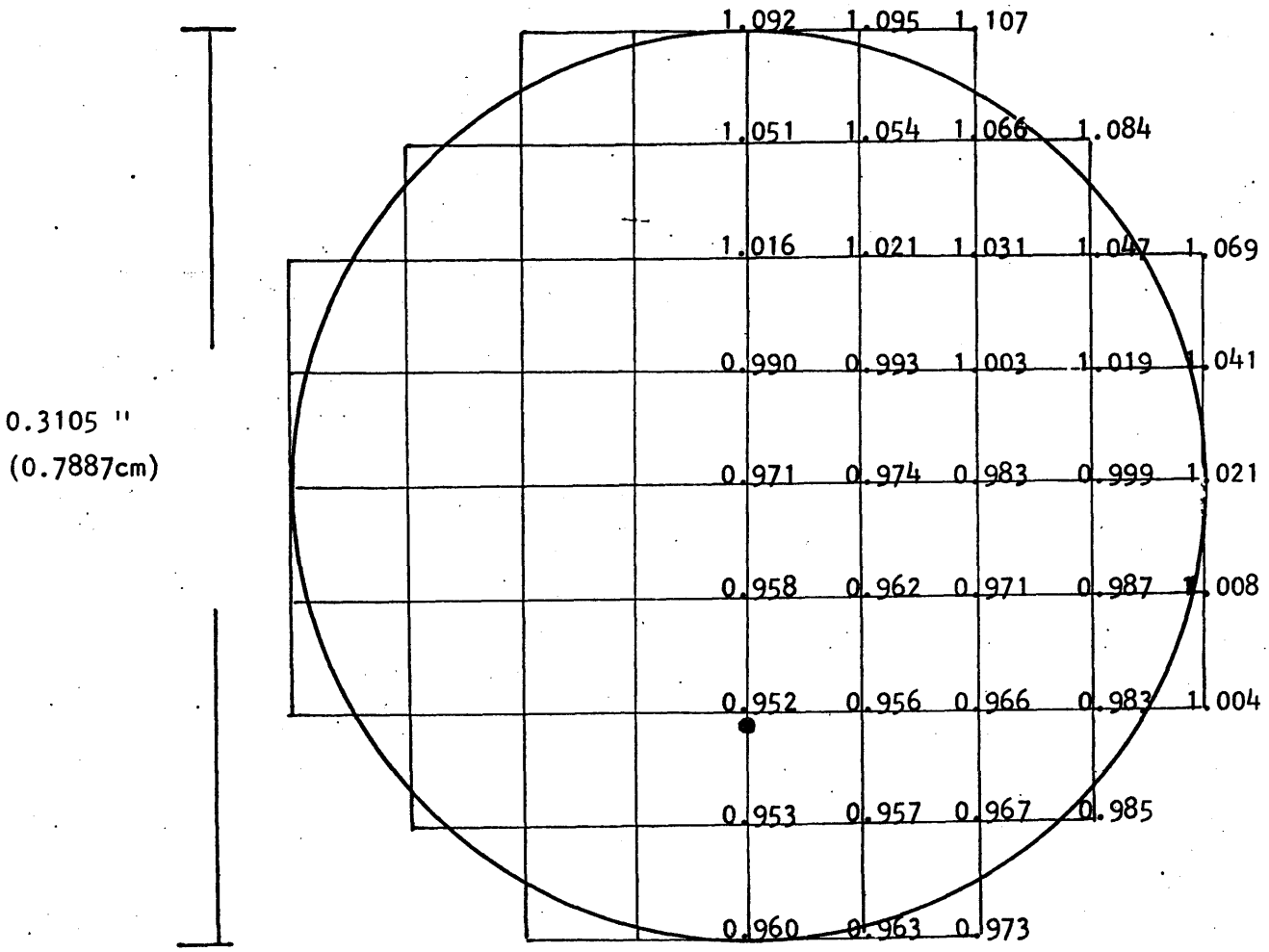


FIG. VI-11 : Uncorrected X-Y powerdistribution in the mixed oxide pin number 3 in the 36 rod cluster in the center of a Pu-recycle assembly.

The deviations between the powerdistribution as calculated with this correlation & the PDQ X-Y results were maximum o.3 % for the $UO_2$ pin and 0.1 % for the mixed oxide pin. These conservative fits were obtained from correlation of the circumferential powerdistribution at the edge (r = R) with the formula a + b , cos$\theta$ and the correlation of the unperturbed variation exp. $\xi' \left(\frac{r}{R}\right)^2$.

Note that the circumferential powerdensity in the mixed oxide pin varies 10 X more than in a uraniumoxide pin and that the dip in the powerdensity is much more pronounced also.

The total powerdistribution in the peak regular $UO_2$ and mixed oxide pins.

By superposition of all the results it is now possible to obtain simple 2 dimensional r,$\theta$ expressions for the total power, including the assumed flat fast & epithermal parts and all the spectraleffects.

Combining the equations & values 6-8, 6-9, 6-10 and 6-14, we get for the total powerdistribution in the peak $UO_2$ pin :

$$P^{tot}_{UO_2}(r,\theta) = f_{UO_2} N' \left(0.9914 + 0.0056 \frac{r}{R} \cos\theta\right) \exp 0.016 \left(\frac{r}{R}\right)^2 \times 0.9796 \times \exp 0.044 \left(\frac{r}{R}\right)^2 \times \left(1 + 0.04 \frac{r}{R} \cos\theta\right) + \left(1 - f_{UO_2}\right) \quad 6\text{-}16$$

From Fig. V- 6 showing the fraction of power due to thermal neutrons in the peak $UO_2$ cell, f is found to be 0.8.

After simplification of (6-16) & normalisation such that the average powerdensity from thermal neutrons is 0.8 we get :

$$P^{tot}_{UO_2}(r,\theta) = \left\{0.80 \times 0.9796 \left[0.9914 + 0.045 \frac{r}{R} \cos\theta\right] \exp 0.060 \left(\frac{r}{R}\right)^2\right\} + 0.20 \quad (6\text{-}17)$$

or $P^{total}_{UO_2}(r,\theta) = \left\{(0.777 + 0.0353 \frac{r}{R} \cos\theta) \exp 0.060 \left(\frac{r}{R}\right)^2\right\} + 0.2$ (6-18)

Combining the values and eqs. (6-8), (6-9), (6-11) and (6-15), using the fraction

of power due to thermal neutrons in the peak mixed oxide rod f = 0.75 (Fig. V- 13 ) & after simplification in the same way as above we get for the regular peak mixed oxide pin :

$$P^{tot}_{Mix}(r,\theta) = 0.75 \times 0.9126\left[0.980 + 0.1157\,\frac{r}{R}\cos\theta\right] * \exp 0.2194\left(\frac{r}{R}\right)^2 + 0.25 \qquad (6\text{-}19)$$

$$\text{or}\quad P^{tot}_{Mix}(r,\theta) = \left\{\left[0.671 + 0.0792\,\frac{r}{R}\cos\theta\right]\exp 0.2194\left(\frac{r}{R}\right)^2\right\} + 0.25 \qquad (6\text{-}20)$$

The figures VI-12 and 13, show the normalised total corrected 2 dimensional powerdistributions inside the regular peak $UO_2$ and mixed oxide pins; compared to the total powerdistributions in an unperturbed fuel rod. For clarity the powerdistributions of the peak $UO_2$ & regular peak MIX.OX. at the 0-180° plane & the unperturbed 90° plane are also shown in one dimension on the Figure VI-14.

5) <u>CONCLUSIONS</u>.

A simple method has been developed for the calculation of the powerdistribution inside the peak $UO_2$ pin at the corner of a conventional and PU-recycle assembly, and inside the peak regular mixed oxide pin,

The two dimensional total normalised powerdistributions can be expressed by the formulas :

$$P^{tot}_{UO_2}(r,\theta) = \left(0.777 + 0.0353\,\frac{r}{R}\cos\theta\right)\exp\left(0.06\left(\frac{r}{R}\right)^2\right) + 0.2$$

for the peak $UO_2$ pin

and by

$$P^{tot}_{Mix}(r,\theta) = \left(0.671 + 0.0792\,\frac{r}{R}\cos\theta\right)\exp\left(0.2194\left(\frac{r}{R}\right)^2\right) + 0.25$$

for the regular peak mixed oxide rod.

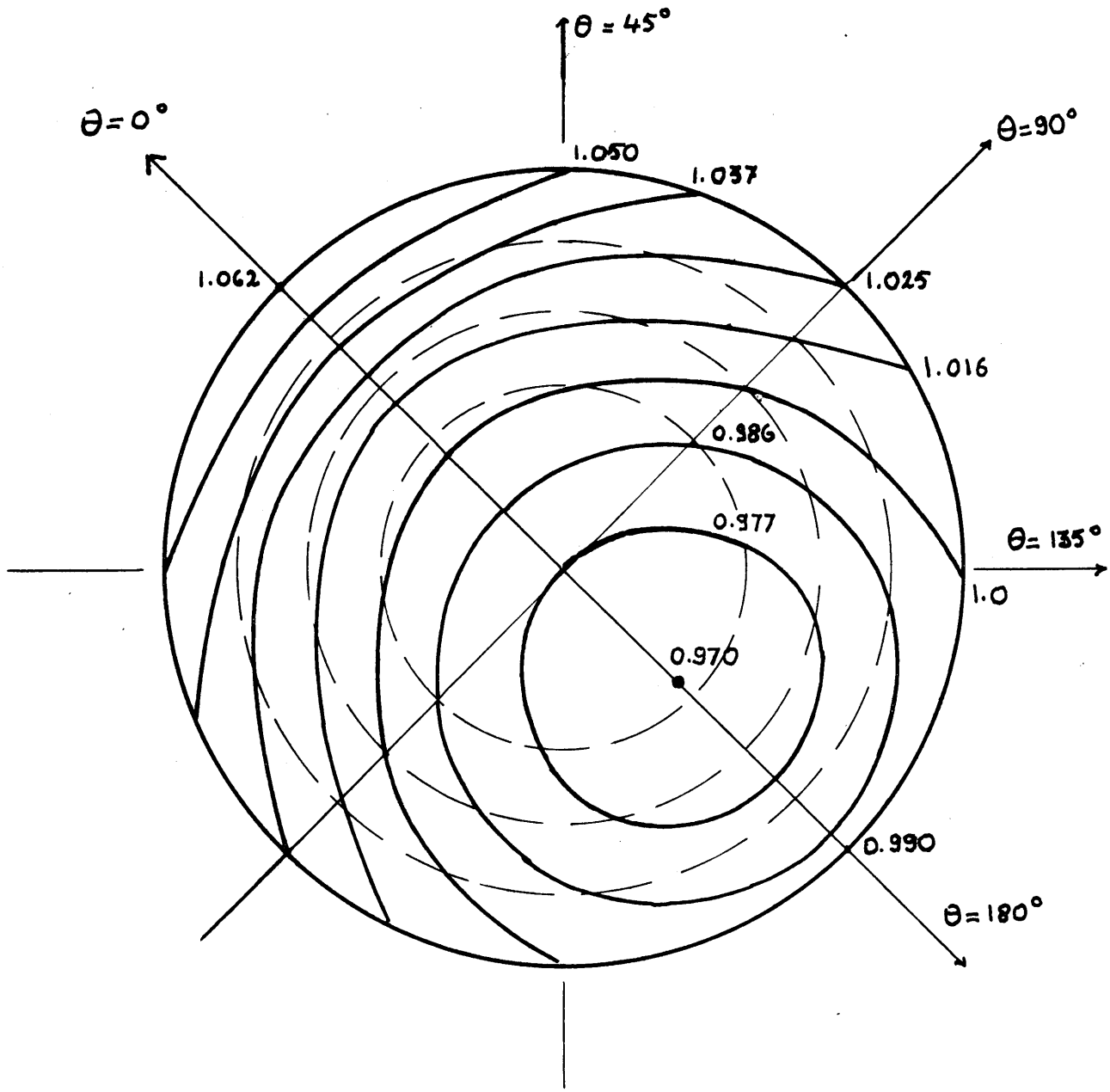


FIG VI-12 CORRECTED TOTAL POWERDISTRIBUTION IN THE PEAK $UO_2$ ROD (COMPARED TO THE NORMAL POWERDISTRIBUTION-DASHED CIRCLES)

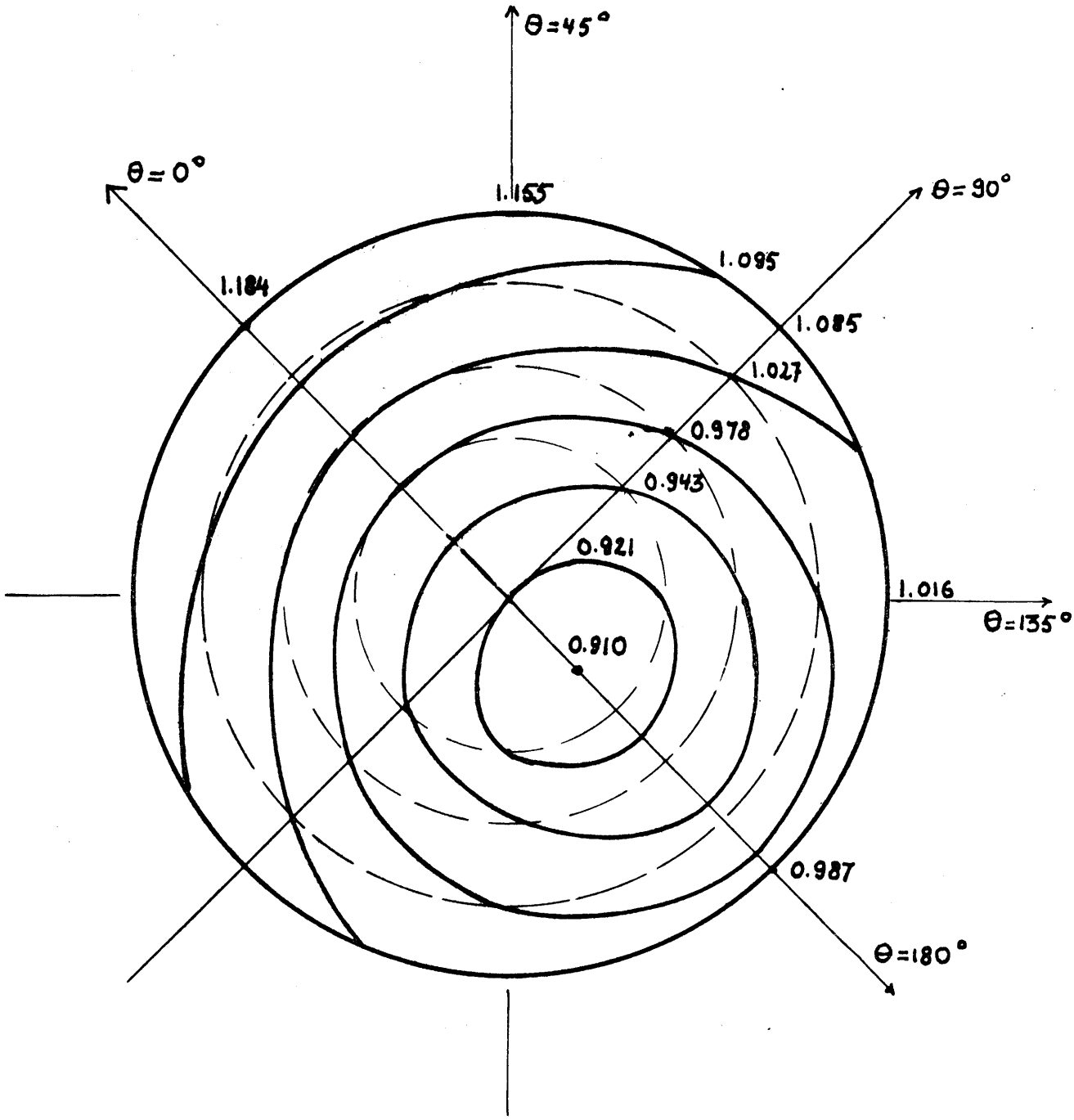


FIG VI-13 CORRECTED TOTAL POWERDISTRIBUTION IN THE PEAK MIXED OXIDE ROD (COMPARED TO THE NORMAL POWERDISTRIBUTION-DASHED CIRCLES)

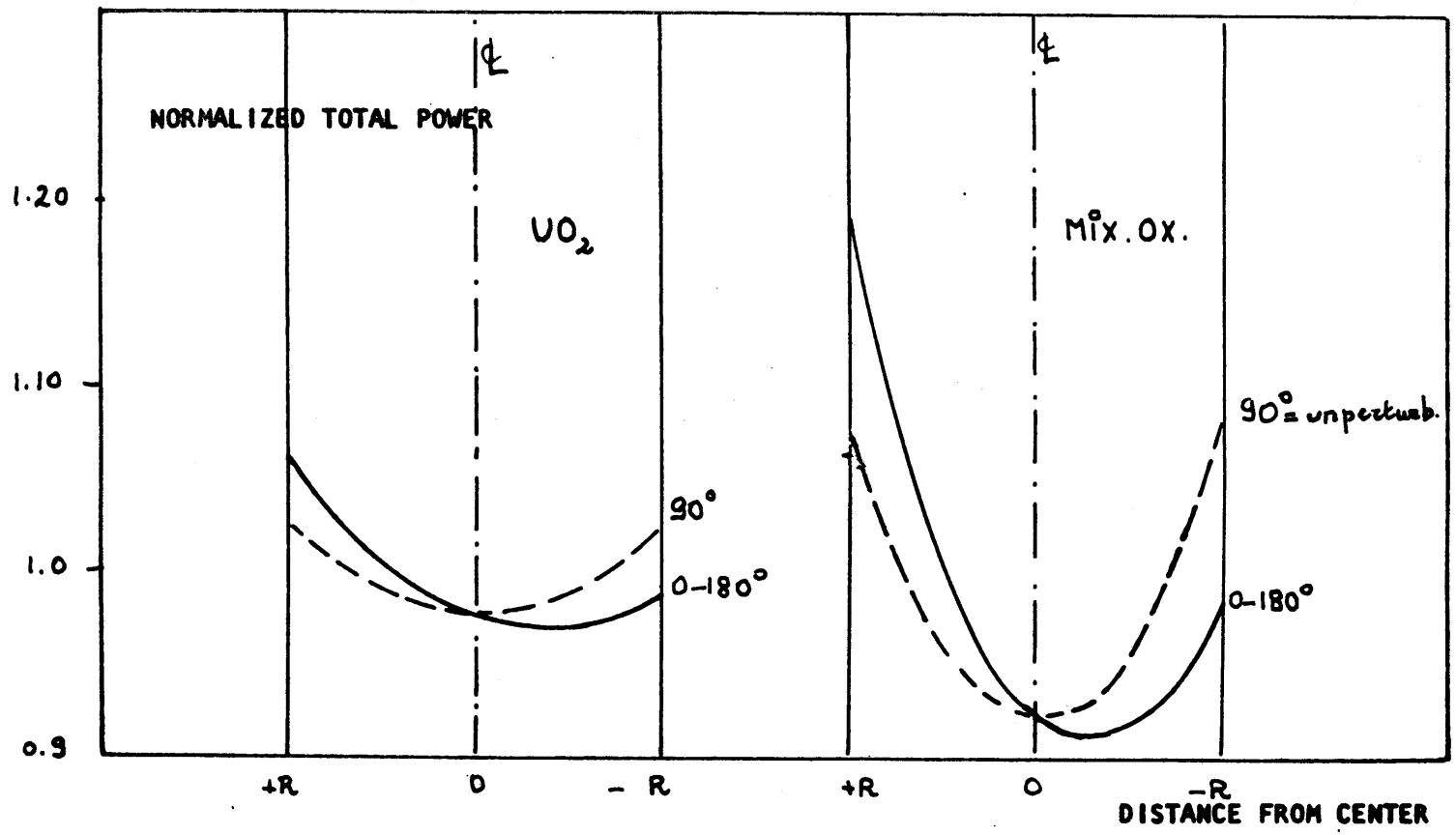


FIG VI-14 COMPARISON OF THE POWERDISTRIBUTIONS, IN THE 0-180° PLANE, IN THE PEAK $UO_2$ AND PEAK MIXED OXIDE RODS

where $\Theta$ = the angle from the direction of the center to the hot powerspot ($\Theta = 0^{o}$) to the direction of the center to the point at a normalised distance r/R ($\Theta = \vartheta^{o}$).

(R= fuel rod radius = 0.3975 cm in our case.)

The real peak mixed oxide rod does not follow this simple law since there is no symmetry in the powerdistribution. This rod is very difficult to analyse due to the large uncertainties in the spectralcorrectionfactor and the need for elaborate codes such as HEATING, for the thermal analysis of this pin. It has however been observed that the gradientfactor, defined as the ratio of the max.power at the surface of the pin to the min.power, of the peak rod is the same as the gradientfactor of the symmetric rod next to it, for which the formula applies. Therefore the assumption of the formula (6-19) applied to the real peak rod, should not lead to large errors.

In general it has been found that powergradients in the plutoniunrecycle assembly are much larger an the mixed oxide pins at the $UO_2$/MIX interface than in the $UO_2$ rod in the corner of the conventional & PU-recycle assembly.

Particular attention has thus to be paid to these effects for plutoniumrecycle applications, as well in graded as discreet assemblies.

It must be noted that the calculations were performed at beginning of life and for normal operation. With burnup, it may be expected that the peak $UO_2$ pin will behave more as a mixed oxide pin due to the build-up of plutonium. The gradienteffect at the watergap will be affected somewhat but not too much.

In abnormal situations, such as e.g. with the insertion of the cruciform control rods, large gradiensts in the cor ner $UO_2$ pin will exist of the same magnitude as in the mixed oxide pins. Although for the mechanical design, this evaluation is important, the gradient $UO_2$pin will not be at the hot spot, and is therefore of less importance unless the bowing of the rod is so large that the rods nearly touch the can.

# CHAPTER VII : THERMAL HYDRAULIC EVALUATION OF CONVENTIONAL AND PU-RECYCLE ASSEMBLIES.

## VII-1) INTRODUCTION : THERMAL HYDRAULIC CHARACTERISTICS.

The nuclear design aspects of the assemblies and the core are important for the determination of powerdistributions, powerpeakingfactors and fuel management characteristics. The thermal-hydraulic evaluation has its primary objective to assure that the core can meet normal steady state and transient performance requirements without exceeding design limits. Complete thermal-hydraulic analysis in steady state & transient is quite complex, and elaborate computer programs are presently being used by manufacturers and utilities. These codes are however slowly coming in the public domain and many special proprietary design informations (e.g. on spacers & experiments) are still hard to come by.

Because computerprograms such as THINC II ( 48 ), or COBRA & FLASH for some of the thermal-hydraulic analysis & fortransientanalysis were not available, the thermal hydraulic evaluation has been performed by comparison of PU-recycle assemblies to existing data for conventional assemblies, and a conservative approach was taken to evaluate the in core performance of the peak mixed oxide pin relative to the peak corner $UO_2$ pin in the PU-recycle assemblies.

Special emphasis has been put on the calculation of a more refined engineering heat flux hot channelfactor taking the nuclear non-uniformpowerdistributions in account, which were determined in the previous chapter.

A summary of the thermal hydraulic parameters is given in Table VII-1 as determined at the YAEC. ( 49 ) for the analysis of core 10.

Estimated values for a peak mixed oxide pin, with similar nuclear heat fluxpeakingfactors as the peak $UO_2$ rod are also included.

## VII -2) HOT CHANNEL FACTORS.

Hot channel factors are divided in two basic groups :nuclear & engineering

hot channel factors. Nuclear hot channel factors can vary from core to core design; and the predicted values are less than the design peaking factors which are set to assure that the core design limits in steady state & transient operation are not exceeded. The engineering factors usually do not vary much, unless mechanically new assemblies are designed .

New concepts such as plutonium recycle in which the mixed oxide pin may be the peak pin has an effect, however for the peak $UO_2$ pin in the corner, the same engineering factors can probably be used with good confidence.

The total hotchannelfactors are the ratios of the maximum values in the core to the core average values, and are thus divided into the nuclear and engineering components but may on their turn be divided in subfactors which account for specific hot spot effects. E.g. most of the work has been centered on the determination of a method for the calculation of nuclear local powerpeaking-factors, which on its turn can be divided in a nuclear spectral-effect HCF.

Two basic quantities are of fundamental interest & principly used in reactor design and performance evaluation:

The total heat flux hotchannelfactor, which is the ratio of the mamixmum heat flux at a certain outer cladding spot in the reactor to the average core value; and the total enthalpy rise hotchannelfactor, which is the ratio of the enthalpy rise in the hot coolant channel to the core average enthalpy rise.

A further classification of engineering hot channelfactors is a deterministic & statistical HCF. The deterministic HCF. accounts for all physical effects that exist in the peak pin which are not random in nature. The statistical factors take into account random effects which can cause hot spots, and are treated in a statistical manner, based on usually a large number of data.

The nuclear heat flux factor is the ratio of the maximum heat flux in a fuel rod, to the core average heat flux. The nuclear enthalpy rise factor is the ratio of the axial distance averaged heat flux in a channel enclosed by four or less fuel rods, to the core average heat flux. Only the average of the radial

nuclear hot channelfactors of the rods adjacent to the channel has to be taken. All nuclear hot channelfactors are based on nominal dimensions and nominal pellet and enrichment specifications.

Engineering factors account for the physical differences between the hot channel and a nominal channel, other than those differences due to nuclear effects. Thus the circumferential heat flux in the peak rod, at the outside of the fuel pellet could be classified as a nuclear hot channelfactor, whereas the heat flux HCF leaving the cladding surface could be classified as an engineering factor. This convention has however not been used for practicle reasons.

2)-1 Nuclear Factors.

The nuclear heat flux factor relates the peak heat flux in the core to the core average heat flux. The nuclear heat flux factor is primarely used for three important calculations : the maximum cladding temperatures, the departure of nuclear boiling ratios (DNBR) , and the fuelcenterline temperature. It should therefore be noted that this core average heat flux is reduced by a fraction (normally 2.7% in PWR's) from that obtained from total core power and total heat-transfer area to account for the fact that some heat is released directly in the coolant and reactor internals. (gamma heating & neutron slowing down).

For the calculation of the fuel centerline temperature, a flat power inside the rods is usually assumed. As determined in this study, the linear powerrating should besides of the appropriate engineering & nuclear heat flux hotchannel-factors, also be multiplied with a reducing engineering hot channelfactor due to non-uniform heat generation. This factor is especially important for mixed oxide rod since the heat generation is much more non-uniform. No circumferential nuclear heat flux HCF should be used for this application.

Design values of 3.11 and 2.74 for the nuclear heat flux HCF were established by the YAEC for the stainless steel clad fuel and zircalloy clad fuel. Design values of 2.06 and 1.88 were established for the enthalpyrise factor. These design factors were established on the basis of the results of a loss-of-flow accident analysis ( 49 ).

2)-2 Engineering Heat Flux Factor.

The effect on local heat flux of deviations of nominal design dimensions and specifications is accounted for by the engineering heat flux factor. Design variables that contribute to this factor are fuel density, fuel enrichment, pellet diameter and clad outside diameter. Manufacturing data associated with these variables were analysed statistically to obtain the engineering heat flux factor. Values of 1.03 and 1.04 were obtained for the stainless steel & zircalloy fuels respectively.

A deterministic circumferential heat flux peaking factor has been introduced in our study to account for the local variations of the heat flux arround the pellet & cladding due to non-uniform powergradients in the peak pins.

The conduction of the cladding attenuates these circumferential variations such that the heat fluxvariations leaving the cladding surface is less than the variations from the pellet.

An engineeringfactor for the heat flux at the pelletsurface was found to be 1.024 for the $UO_2$ & 1.064 for the mixed oxide zircalloy pins. Due to attenuation in the cladding the outercladding heat flux was found to be 1.012 for the zircalloy $UO_2$ rods and 1.038 for the future zircalloy mixed oxide rods.

The total engineering Heat flux hot channel factor thus becomes 1.052 & 1.080 for the zirc $UO_2$ and mixed oxide rod respectively.

TABLE 7-1 : Core 10 Thermal-Hydraulic Parameters at Full Power (from Ref 49 )

General Characteristics

| | Stainless Steel | Zircalloy |
|---|---|---|
| Total Heat Output, MWt | 600 | |
| Total Heat Output, BTU/hr | $2048 \times 10^6$ | |
| Fraction of Heat Generated in Fuel | .973 | |
| Pressure - Nominal, psig | 2000 | |
| Pressure - Minimum Steady State, psig | 1925 | |
| Pressure - Maximum Steady State, psig | 2075 | |
| Nominal Coolant Inlet Temperature, $^oF$ | 510 | |
| Design Inlet Temperature, $^oF$ | 514 | |
| Nominal Vessel Outlet Temperature, $^oF$ | 552 | |
| Nominal Core Bulk Outlet Temperature, $^oF$ | 556 | |
| Total Coolant Flow Rate, lb/hr | $40.6 \times 10^6$ | |
| Heat Transfer Flow Rate, lb/hr | $36.4 \times 10^6$ | |
| Nominal Channel Hydraulic Diameter, in. | .327 | .399 |
| Average Mass Velocity, lb/hr-ft$^2$ | $2.67 \times 10^6$ | $2.37 \times 10^6$ |
| Average Coolant Velocity in Core, ft/sec | 15.5 | 13.8 |
| Core Pressure Drop, psi | 17 | |
| Vessel pressure Drop, psi | 35 | |
| Average Heat Flux, BTU/hr-ft$^2$ | 129,000 | 153,000 |
| Assembly Heat Transfer Area, ft$^2$ | 203 | 171 |
| Average Film Coefficient, BTU/hr-ft$^2$-$^oF$ | 6670 | 5820 |
| Aveeage Film Temperature Difference, $^oF$ | 19.3 | 26.3 |
| Average Linear Rod Power, kw/ft | 3.36 | 4.28 |
| Specific Power, kw/kgU | 28.1 | 28.3 |
| Power Density, kw/liter | 89.3 | 90.1 |
| Average Core Enthalpy Rise, BTU/lb | 56.3 | |

Design Heat Flux Factors

| | Stainless Steel | Zircalloy |
|---|---|---|
| Nuclear Heat Flux Factor | 3.11 | 2.74 |
| Engineering Heat Flux Factor | 1.03 | 1.04 |
| Total Heat Flux Factor | 3.20 | 2.85 |

Design Enthalpy Rise Factors

| | Stainless Steel | Zircalloy |
|---|---|---|
| Nuclear Enthalpy Rise Factor | 2.06 | 1.88 |
| Engineering Enthalpy Rise Factor | 1.26 | 1.19 |
| Total Enthalpy Rise Factor | 2,60 | 2.24 |

Table 7-1 Continued : Hot Channel and Hot Spot Parameters & Comparison.

| | Design | | Core X predicted | | Estimation for a plutonium recycle assembly - peak MIX *. |
|---|---|---|---|---|---|
| | Stainless | Zircalloy | Stainless | Zircalloy | |
| Maximum Heat Flux, BTU/hr-ft$^2$ | 412,800 | 436,000 | 309,600 | 335,000 | 345,000 |
| Maximum linear Rod Power, kw/ft | 10.8 | 12.2 | 8.07 | 9.38 | 9.38 |
| Maximum $UO_2$ temperature ($^oF$) | 3100 | 3400 | 2350 | 2700 | 2630 |
| Maximum clad Surface Temp. ($^oF$) | 647 | 647 | 642 | 642 | 642 |
| (Jens-Lottes) | | | 645 | 645 | 645 |
| (Thom et al) | | | | | |
| Hot Channel Outlet Temperature ($^oF$) | 624 | 611 | 605 | 594 | 584 |
| Hot Channel Outlet Enthalpy, BTU/lb | 650 | 630 | 622 | 606 | 593 |
| Maximum W-2 DNB ratio : | 2.11 | 2.05 | 2.93 | 2.87 | 3.00 |
| Minimum W-3 DNB ratio : | 3.62 | 2.80 | - | - | - |

* Estimated as if a conventional zircalloy clad peak assembly is replaced by a plutoniumrecycle assembly - only the values for the peak mixed oxide rod are given. The values for the peak $UO_2$ are assumed to be the same as for a conventional assembly.

2)-3. Statistical Enthalpy Rise Factor.

The statistical enthalpyrise factor accounts for the effects of deviations in fuel fabrication from nominal dimensions or specifications on the enthalpyrise in the hot channel.

Tolerence deviations (averaged over the length of the four or one fuel rod that enclose the hot channel) for fuel density, enrichment, pellet diameter, clad outside diameter, and rod pitch and bowing are taken by this factor. Manufacturing data associated with these variables was analysed statistically to obtain the statistical enthalpyrisefactor. Values of 1.20 and 1.10 were obtained for the stainless steel and zircalloy fuels respectively.

Because of the powergradients inside the rods it seems that the bowingeffects should be treated deterministically. Since larger circumferential heat flux variations were noticed in the peak mixed oxide rod, one should be inclined to accept a higher bowing factor. It has however been found that the coolant varies in an opposite way, such that the overall circumferential cladding temperature is rather flat. Therefore it seems not necessary to include a higher bowing effect in the mixed oxide rods, the more that these rods are in the middle of the assembly and one channel is surrounded by 4 rods, compared to a peak corner $UO_2$ rod which will bow toward the can and produces a higher effect.

2)-4. Lower Plenum Flow Distribution Factor.

This subfactor was determined at YAEC by comparing an experimentally measured inlet flowdistribution in a 1/12 model ( 50 ).

It was concluded that the maximum increase in the enthalpy rise of the hottest assembly was less than 5 %. Therefore a value of 1.05 was chosen for the lower plenum factor.

2)-5. Flow Mixing Factor.

The enthalpy-rise in a hot channel is decreased in part by mixing of the coolant in the hot channel with coolant in the surrounding channels.
Flow mixing between adjacent channels occurs because of random flow fluctuations in turbulent flow superimposed on the axiai velocity of the fluid. This lateral eddy diffusion (perpendicular to the dominant flow direction) results in heat transport from cold coolant to the warm cooland and vice versa. There is no net transfer of fluid from one location to another, but there is a net transport of heat. The eddy transport can be increased by increasing the turbulence in the subchannels. One possibility comes from the spacers which are claimed to have very beneficial effects.
For the stainless steel assemblies, the flow mixing in a rod bundle has been tested by Westinghouse ( 51 ). A conservative value of 0.95 was found.
For the zircalloy clad assemblies, calculations made to determine the enthalpy rise in 25 parallel channels ( 49 ). The heat balance equations for the fluid were applied to each channel. To determine the hot channel mixing factor, two cases were considered - one with no mixing and one with mixing based on data obtained by Rowe ( 52 ). The ratio of the hot channel enthalpy-rise with mixing to the hot channel enthalpyrise without mixing ($\beta = 0$) was found to be 0.94.
Because of the somewhat larger Reynolds number in the center of the bundle, it may be anticipated that the mixing factor for the hot mixed oxide channel will not be less than for the peak $UO_2$ channel. Therefore the same mixing hot channelfactor should also apply for the peak mixed oxide channel.

2)-6. The Flow-Redistribution Factor.

The flow-redistribution is very important for the evaluation of the engineering enthalpyrise hotchannel factor. Its calculation, such as the

mixing factor is complicated because of the need for rather elaborous codes solving the mass-balance, energy & fluid momentum equations in a large number of channels simultaneously.

This complex interaction is however very beneficial. Attemps to use more simple methods failed and yielded much larger flow redistributionfactors as the ones calculated with thermal hydraulic analysis codes and conservative assumptions.

## 2 - 7) COOLANT FLOW IN THE YANKEE REACTOR.

A layout of the Yankee Reactor was given on Fig. I-2 . Coolant enters the reactor through four nozzles located $90^{o}$ apart at the same elevation near the top of the vessel.

In the reactorvessel the coolant is distributed as follows : 1 % of the total coolant flow entering through the vessel inlet nozzles is bypassed up through holes in the guide tube hold-down plate & support plate to cool the reactor vessel head. The remaining 99 % of the coolant cools the core baffle and thermal shield as it flows down. In the core, 90 % of the total design coolant flow is conservatovely estimated to be available for heat transfer purposes. The rest of the coolant flows through passages around the control rods and adjacent to the core baffle.

From pressure drop and coolant flowrate data from previous cores, and from data of zircalloy clad fuel assemblies and the main coolant pump delivery characteristic curve the YAEC calculated total coolant flowrate is $40.6 \times 10^{6}$ lb/hr, while the calculated heat transfer flowrate is $36.4 \times 10^{6}$ lb/hr.

Pressure Drop & Cooland Velocity.

At the total flowrate of $40.6 \times 10^{6}$ lb/hr the total pressure drop across the reactor from inlet to outlet nozzles was calculated by YAEC to be 35 psi.

The calculated pressure drop across the core, including the support plates, is 17 psi. The average coolant velocity along the fuel rods is 15.5 and 13.8 fps for the stainless steel and zircalloy clad fuel respectively.

The total pressure drop across a core or a reactor vessel is often expressed as :

$$\Delta p_{core} = K_{core} \frac{\rho V^2}{2 g_c} \qquad \Delta p_{vessel} = K_{vessel} \frac{\rho V^2}{2 g_c}$$

V = average velocity inside the core

$\rho$ = average density in the core

$g_c$ = conversionfactor.

The K values for the SS-clad assembly Yankee Reactor are :

$K_{core} = 15$, $K_{vessel} = 34$.

Three Loop Operation.

Three loop operation characteristics were also calculated by YAEC for core 10. Results of loss-of-flow accident analysis ( 49 ) indicate that nominal 3-loop power should be limited to 75 % of the fuel power. The total 3 loop coolant flowrate is 78 % of the four loop flow rate. The maximum temperatures, heat fluxes and other data, were for this mode found to be more conservative in these conditions than 4-loop operation.

## VII-2) THE THERMAL-HYDRAULIC MODEL.

### 2)-1. THE FLOWDISTRIBUTION IN THE ASSEMBLIES.

The basic parameters needed for the thermal evaluation of the assemblies and the core, is the flow distribution in the coolant subchannels of the assembly. (Fig. VII-1). Because of the different heat flux going into the channels, the physical properties of the coolant are also affected by the nuclear calculations, thus the power generated by each rod. The fact that the subchannels are not separated from neigbours such that flow diversion or redistributions will exist between channels as the pressures try to equalize, and the presence of turbulent

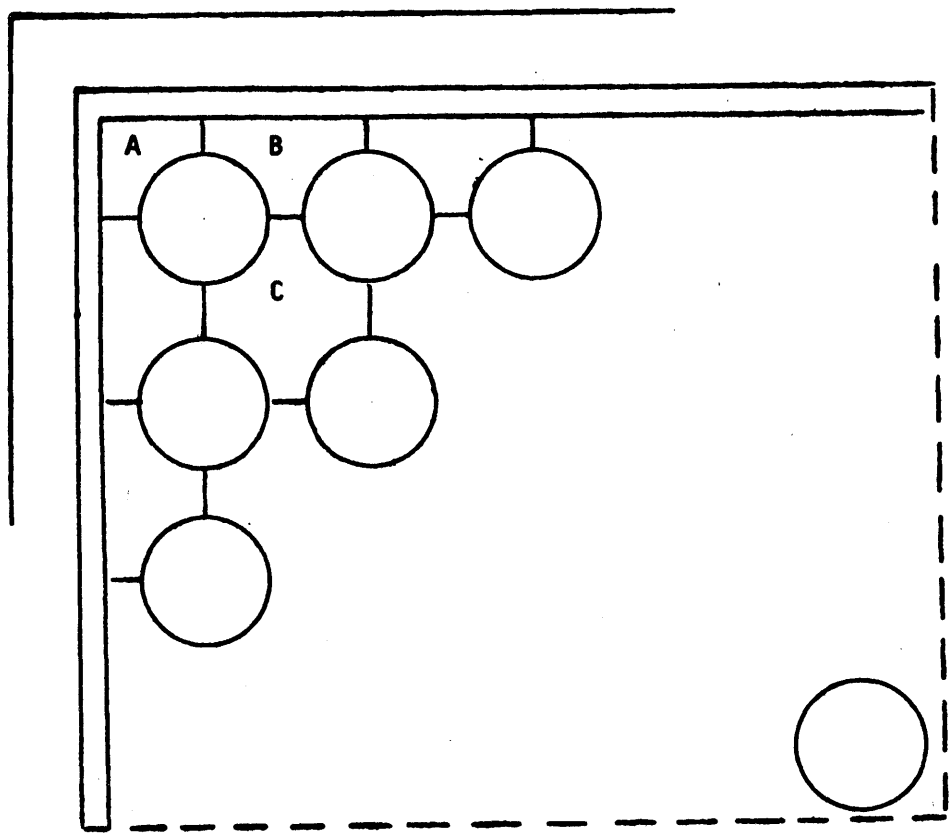


FIG VII-1 DIFFERENT COOLANT CHANNELS IN THE ZIRC CLAD ASSEMBLIES

cross-flow mixing which exchanges only the heat between channels, makes the analysis complicated. The general equations for the solution of the thermal-hydraulic behaviour of the different coolant channels in the assembly according to the "pressure gradient model" are given by ( 18 ) :

Calling i the channel of interest, e.g. the hot channel, the equations that govern the thermal-hydraulic behaviour of the coolant in channel i are given by :

Continuity :

$$\frac{dm_i}{dx} = -\sum_{j=1}^{N} \omega_{ij} \qquad j = 1,2,3 \cdots N \qquad (7-1)$$

Energy-balance :

$$m_i \frac{dh_i}{dx} = q'_i + \sum_{j=1}^{N} \omega'_{ij}(h_j - h_i) - \sum_{j=1}^{N} \begin{Bmatrix} 0 \text{ if } \omega_{ij} \geq 0 \\ \omega_{ij}(h_j - h_i) \quad \omega_{ij} < 0 \end{Bmatrix} \qquad (7-2)$$

Axial Momentum :

$$-\left[1 + \frac{1}{g_c}\left(\frac{m_i}{A_i}\right)^2 \frac{\partial v_i}{\partial p}\right]\frac{dp}{dx} = \frac{1}{g_c}\left(\frac{m_i}{A_i}\right)^2 \left[\frac{f_i \phi_i}{2\rho_f D_i} + \frac{\partial v_i}{\partial h} \cdot \frac{dh_i}{dx}\right]$$

$$+ \rho_i \cos\theta + \frac{1}{g_c A_i} \sum_{j=1}^{N} f_T \omega'_{ij}(u_i - u_j) + \frac{1}{g_c A_i} \sum_{j=1}^{N} \begin{Bmatrix} \omega_{ij} u_i (f_D - 2) \text{ if } \omega_{ij} > 0 \\ \omega_{ij}(f_D u_i - 2u_j) \text{ if } \omega_{ij} < 0 \end{Bmatrix} \qquad (7-3)$$

Transverse momentum :

$$P_i - P_j = C_{ij}\, \omega_{ij} |\omega_{ij}| \qquad (7-4)$$

Where i refers to the channel of interest an

j = 1 → N are the adjacent channels surrounding i.

$\frac{mi}{Ai}$ = mass velocity ($lb/_{hr\ ft^2}$)

X = axial distance : (ft)

$W_{ij}$ = diversion cross-flow mass velocity per unit axial length ($lb/_{hrft^3}$) or $W'_{ij}$ turbulent cross-flow

p = pressure (psi)

A i = flow area ($ft^2$)

$h_i$ = enthalpy (BTU/lbm)

v' = equivalent specific volume ($ft^3$/lb) in single phase flow = v = $1/\rho$ ( $\rho$ density)

$g_e$ = conversionfactor = $4.17 \times 10^8$ lbm/lbf $hr^2$

$D_i$ = hydraulic diameter

$f_i$ = Darcy-Weisbach frictionfactor

$$( f = \frac{0184}{Re^{0.2}} )$$

$\emptyset_i$ = 2 phase flow friction multiplier = 1.0 for simple phase flow.

$f_t$ , $f_D$ = turbulent & diversion parameters.

$C_{ij}$ = loss funtion

u = momentumvelocity = $\frac{mv'}{A}$

$q'_i$ = linear heat rate in the channel i.

The equations describe completely the flow & enthalpy in channel i, taking coupling due to mixing & flow diversion between other channels into account, as well as the interaction of the fluid properties with the heat generated in the channel & the enthalpy & pressure at each axial distance X. The equations are solved with computer programs such as the COBRA series ( 18 , 19 ). The various computorcodes that exist for the solution of the thermal-hydraulic equations of a large number of channels simultaneously differ primarely in the manner in which diversion cross-flow is treated and the mathematicel procedure used to solve the set of non-linear equations. In COBRA, the diversion cross-flow is determined by the pressure gradient ($p_i$ -$p_j$) between the adjacent channels.

The Westinghouse THINC II code ( [48] ) however assumes that no significant pressure drops exist between subchannels. The cross-flows are then determined as those required to provide a laterally uniform pressure at each axial position, subject to an inlet flowdistribution.

The fact that the different subchannels are not isolated has a large effect on the flowistribution hot channel factor.

With the assumptions that the pressure drop across each isolated channel as pictured in Table7-1& on Fig, 7-1 is the same, & that the sum of the flowrates in the subchannels equals the average assembly flowrate, the flowdistribution factor may be written as :

$$F^{E}_{\Delta h}\,(\text{redistrib.}) \cong \frac{A_{av}}{A_i}\left(\frac{D_{av}}{D_i}\right)^{2/3} \qquad (7\text{-}5)$$

where $A_{av}$ = average cross-section for the flow of the average channel

$A_i$ = cross-section of the hot channel.

$D_{av}$ = average hydraulic diam.

$D_i$ = hydraulic diameter of the hot channel.

The flowredistribution obtained with such an isolated channel was found to be 1.38. Compared to a typical value of 1.05 obtained with thermal hydraulic codes. The need for thermal hydraulic codes is thus remarkably.

Since the mixed oxide peak rod is located in the middle of the assembly, one may expect that the flowdistributionfactor is relatively unimportant & a value of 1.00 can probably be used.

## 2)-2. THE EFFECT OF NON UNIFORM HEAT GENERATION IN THE PEAK $UO_2$ AND MIXED OXIDE PINS, AND ASSOCIATED HOT-CHANNELFACTORS.

### 2)-2 A) THEORETICAL CONSIDERATIONS.

Assuming a uniform coolant temperature & het-transfercoefficient around the pin, and a non-uniform heat generation in the pin described by en equation of the form :

$$q'''/q'''_{AV} = f\left(a_1 + b_1 \frac{r}{R}\cos\theta\right)\exp\left[\xi\left(r/R\right)^2\right] + (1-f) \qquad (7\text{-}6)$$

With the consideration that the $\xi$ factor is only of the order of magnitude of 0.15, and that the exponential term may be expanded, eq (7- 6) can be simplified to :

$$q'''/q'''_{av} = A_1 + A_2\left(\frac{r}{R}\right)^2 + A_3\frac{r}{R}\cos\theta + A_4\left(\frac{r}{R}\right)^3\cos\theta \qquad (7\text{-}7)$$

Nysing (Ref. 53 ) has developed simple formulas, for the heat flux, cladding temperatures & fuel temperature vararions of fuel elements by solving the equations (7- 8) & (7-9 )

$$\frac{\partial^2 T}{\partial r^2} + \frac{1}{r}\frac{\partial T}{\partial r} + \frac{1}{r^2}\frac{\partial^2 T}{\partial \theta^2} + \frac{q'''(r,\theta)}{\lambda_f} = 0 \qquad (7\text{-}8)$$

for the fuel and,

$$\frac{\partial^2 T}{\partial r^2} + \frac{1}{r}\frac{\partial T}{\partial r} + \frac{1}{r^2}\frac{\partial^2 T}{\partial \theta^2} = 0 \qquad (7\text{-}9)$$

for the cladding.

After solving the eqs. (7- 8) - (7- 9) with (7- 7) & applying the boundary conditions, Nysing obtains for the fuel temperature at each point : r, $\theta$

$$T = a_0 - Nu_g\left(T_R - T_i\right)_{av}\left[\frac{A_1}{2}\left(\frac{r}{R}\right)^2 + \frac{A_2}{8}\left(\frac{r}{R}\right)^4 + \frac{A_3}{4}\left(\frac{r}{R}\right)^3\cos\theta + \frac{A_4}{12}\left(\frac{r}{R}\right)^5\cos\theta\right] + k_1\frac{r}{R}\cos\theta \qquad (7\text{-}10)$$

and for the <u>temperature</u> at each point r, $\theta$ in the <u>cladding</u> :

$$T = T_b + \Delta T_{av} - Nu_h \Delta T_{av} \ln \frac{r}{r_o} + m \Delta T_{av} \frac{k\, Nu_h}{\frac{1+Nu_h}{1-Nu_h} - k^2} *$$

$$* \left[ \frac{r}{R_o} + \frac{1+Nu_h}{1-Nu_h} \left(\frac{r}{R_o}\right)^{-1} \right] \cos\theta \qquad (7\text{-}11)$$

The temperature at the inner cladding surface becomes :

$$T_i = T_b + \Delta T_{av} - Nu_h \Delta T_{av} \ln k + mb\, \Delta T_{av} \frac{Nu_h (Nu_g + 1)}{Nu_g} \cos\theta \qquad (7\text{-}12)$$

and at the outer cladding surface :

$$T_o = T_b + \Delta T_{av} + 2m \Delta T_{av} \frac{k\, Nu_h}{1 + Nu_h + k^2 (Nu_h - 1)} \cos\theta \qquad (7\text{-}13)$$

For the heat fluxes at the fuel surface Nysing obtains in a dimensionless form :

$$F^{E}_{q''_i}(\theta) = \frac{q''_i}{q''_{i\,av}} = 1 + m \cos\theta \qquad (7\text{-}14)$$

and for the heat flux at the outer cladding surface

$$F^{E}_{q''_o}(\theta) = \frac{q''_o}{q''_{o\,av}} = 1 + m \frac{k\, Nu_h}{1 + Nu_h + k^2 (Nu_h - 1)} \cos\theta \qquad (7\text{-}15)$$

where

$$a_o = \Delta T_{av} \left[ \frac{1}{D} \left( \frac{1}{2} A_1 Nu_g + \frac{1}{8} A_2 Nu_g + 1 \right) - Nu_h \ln k + 1 \right] + T_b \qquad (7\text{-}16)$$

with D given by $$D = \frac{\Delta T_{av}}{(T_R - T_i)_{av}} = \frac{\alpha_{g\,av}}{\alpha_{ou}} \cdot k \qquad (7\text{-}17)$$

$$k_1 = \frac{\Delta T_{av}\, Nu_g}{D \left[ 1 + \lambda_f / \lambda_{cl} \cdot b \right]} \left[ \frac{A_3}{4} \left( \frac{Nu_g + 3}{Nu_g + 1} + 3 \frac{\lambda_f}{\lambda_{cl}} b \right) + A_4/12 \left( \frac{Nu_g + 5}{Nu_g + 1} + 5 \frac{\lambda_f}{\lambda_{cl}} b \right) \right] \qquad (7\text{-}18)$$

with b given by :

$$b = \frac{1 + Nu_h - k^2 (Nu_h - 1)}{1 + Nu_h + k^2 (Nu_h - 1)} \cdot \frac{Nu_g}{Nu_g + 1} \qquad (7\text{-}19)$$

$$m = \frac{3 A_3 + 2 A_4}{6 \left( 1 + (\lambda_f / \lambda_{cl}) b \right)} \cdot \frac{Nu_g}{Nu_g + 1} \quad ; \quad T_R - T_i = \frac{R^2 q'''_{av}}{2\, Nu_g\, \lambda_f} \qquad (7\text{-}20)$$

<u>The following notations have been used</u> :

$k$ = ratio of inner to outer clad radius (Ri/Ro)

$q''_i$ = local radial heat flux at fuel surface on interior of cladding ($W/m^2$ or $BTU/_{hr\ ft^2}$)

$q''_{av}$ = averaged " "

$q''_o$ = local radial heat flux at outer cladding surface.

$q''_{oav}$ = averaged " "

$q'''$ = local heat generation in fuel ($W/_m3$ or $BTU/hr\ ft^3$)

$q'''_{av}$ = average " "

$r$ = radial distance of fuel rod center (m or ft)

$R$ = radius or fuel pellet (m or ft)

$R_i$ = inner cladding radius (m or ft)

$R_o$ = outer " "

$T$ = temperature in fuel or cladding ($^oC$ or $^oF$)

$T_b$ = bulk coolant temperature ($^oC$ or $^oF$)

$T_R$ = temperature at fuel surface ($^oC$ or $^oF$)

$T_i$ = temperature at inner cladding surface ($^oC$ or $^oF$)

$T_0$ = " at outer cladding surface.

$T_{oav}$ = average temperature et outer cladding suface.

$\Delta T_{av}$ = "average " difference between outer cladding surface temperature and bulk coolant Temperature given by : $q''_{oav}/\alpha_{oav}$ or $q''_{oav}/\alpha_{ou}$

$\alpha_o$ = local heat transfercoefficient at outer cladding surface ($W/M^2\ ^oC$ or $BTU/_{hr\ ft^2\ ^oF}$)

$\alpha_{oav}$ = average " " " " "

$\alpha_{ou}$ = heat transfer coefficient at quter cladding surface in the case of a uniform heat-transfer coefficient distribution.

$\alpha_g$ = local gap heat transfercoefficient ($W/_m{}^2\,{}^oC$)

$\alpha_{gav}$ = average " " "

$\alpha_{gu}$ = gap heat transfercoefficient for uniform contact resistance ($W/_M{}^2\,{}^oC$)

$\lambda_f$ = thermal conductivity of fuel ($W/_m\,{}^oC$ or $BTU/hr/_{ft}\,{}^oF$)

$\lambda_{cl}$ = thermal conductivity of cladding

$\theta$ = angle (radians)

$Nu_g$ = dimensionless heat transfer number representing $\alpha_{gav}\,R/\lambda_f$ or $\alpha_{gu}\,R/\lambda_f$

$Nu_h$ = dimensionless heat transfer number representing $\alpha_{oav}\,Ro/\lambda_{cl}$ or $\alpha_{ou}\,Ro/\lambda_{cl}$.

In the case that radial cracks appear in the fuel ,fuel periferal conduction (assuming no radiation-heat transfer) cannot take place and m becomes :

$$m^* = \frac{2}{3}\,A_3 + \frac{2}{5}\,A_4 \qquad (7\text{-}21)^*$$

## 2-2.B) RESULTS OF NUMERICAL CALCULATIONS OF THE EFFECTS OF NON-UNIFORM HEAT GENERATION.

Using the in-rod powercorrelation for the peak $UO_2$ & peak mixed oxide pins, developed in chapter 6, the $A_i$ factors were found to be :

| | peak $UO_2$ pin : | peak Mixed oxide pin : |
|---|---|---|
| $A_1$ | 0.9769 | 0,92076 |
| $A_2$ | 0.04662 | 0.14716 |
| $A_3$ | 0.0353 | 0.08504 |
| $A_4$ | 0.00212 | 0.0187 |

The m factors of the heat flux hotchannelfactors were calculated, assuming :

1) $\theta$ conduction in the fuel

2) assuming no $\theta$ conduction in the fuel (radial cracks).

3) assuming no conduction in the fuel $\lambda_f = 0$.

The effect of the gapconductance or $Nu_g$ factor was also investigated by taking $\alpha_g = \infty$, $\alpha_g = 1400$ and $\alpha_g = 700$ BTU/hr ft$^2$ $^oF$ .

The results of the calculations for the circumferential <u>heat flux</u> hot channel-factors are shown in Table 7-2 picturing the maximum HCF at the hot spot $\theta = 0$, for various situations, and on Fig. 7-2 picturing the HCF, in function of the angle $\theta$ around the pin, in the recommended cases.

From these results it is observed that the variation of the heat flux around the pin due to a non uniform heat generation is about 3 times more important in the mixed oxide pin than in the $UO_2$ pin. The maximum values are obtained in the assumption that there are radial cracks in the fuel and no possible conduction in the fuel, and a perfect contact clad-fuel ($Nu_g$ or $\alpha_g = \infty$ )

It is observed that the attenuation due to $\theta$-conduction in the cladding is about 50 % for the $UO_2$ and 59 % for the mixed oxide fuel. The effect of the fuel condictivity $\lambda_f$ is rather small, the maximum effect is obtained for zero conduction in the fuel.

The influence of the gapconductivity is much stronger. The better the heat transfer cladding-fuel, the larger the hotchannelfactor becomes. An attenuation of about 87 % is due to this effect.

A conservative HCF value of 1.024 for the innercladding surface heat flux and 1.012 for the outer surface heat flux should be used for the peak $UO_2$ pin, and a value of 1.064 an 1.038 for the peak mixed oxide pin.

Table 7-2 HYDRAULIC DIAMETERS AND FLOWAREAS FOR THE DIFFERENT CHANNEL TYPES.

| CHANNEL TYPE | FLOW AREA ($in^2$) | HYDRAULIC DIAMETER (in) |
|---|---|---|
| Corner A (1/4) | 0.03402 | 0.1749 |
| periferal B (1/2) | 0.06241 | 0.2395 |
| internal C (1) | 0.11405 | 0.3972 |
| Average Assembly (Type B) | 28,094 | 0.370 |

Table 7-3 Maximum HCF $F_{q''}^{n.v}$ ($\theta$ =0) for the heat flux at outer-and inner cladding surface, in the peak $UO_2$ and peak mixed oxide pins for various situations of non-uniform heat generation.

| CASE | PEAK $UO_2$ | | PEAK MIXED OXIDE. | |
|---|---|---|---|---|
| | $F_{q''_i}^{nu}$ ($\theta$=0) | $F_{q''_o}^{nu}$ ($\theta$ =0) | $F_{q''_i}^{nu}$ ($\theta$ =0) | $F_{q''_D}^{nu}$ ($\theta$ =0) |
| 1) with radial cracks no conduction in fuel, $Nu_g = \infty, \lambda_f \neq 0$ | 1.024 | 1.012 | 1.064 | 1.038 |
| 2) $\lambda_f$ =0 $Nu_g = \infty$ | 1.018 | 1.009 | 1.049 | 1.029 |
| 3) $\lambda_f \neq 0, Nu_g = \infty$ | 1.018 | 1.009 | 1.047 | 1.028 |
| 4) $\lambda_f \neq 0, Nu_g = 6.76$ | 1.015 | 1.008 | 1.042 | 1.025 |
| 5) $\lambda_f \neq 0, Nu_g$ 3.88 | 1.014 | 1.007 | 1.038 | 1.022 |
| RATIO $(F_{q_o''}-1)/(F_{q_i''}-1)$ | 0.49 | | 0.59 | |
| RATIO $(F_{q_i''}^{Mix}-1)/(F_{q_i''}^{UO_2}-1)$ | | 2.7 | | |

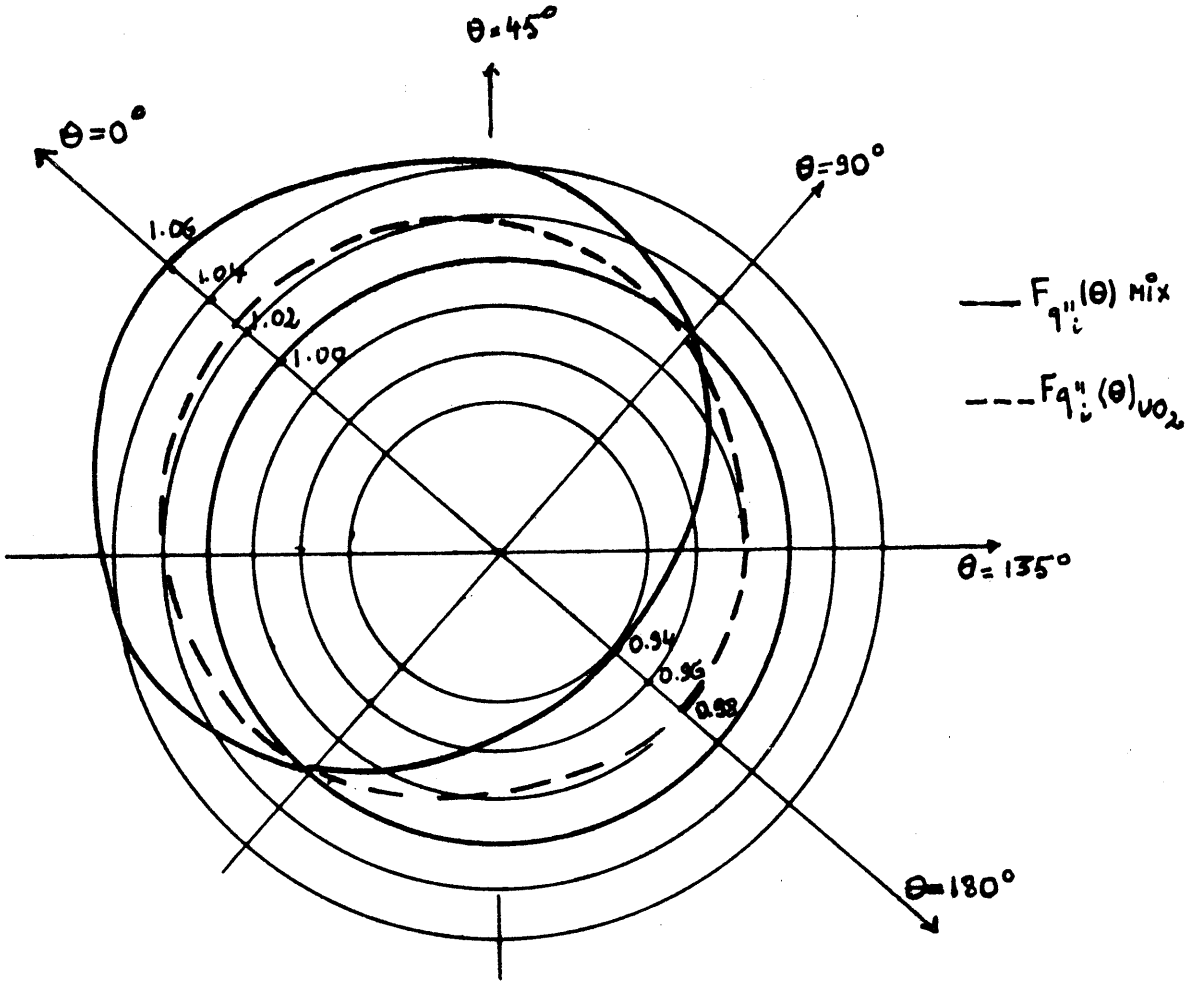


FIG VII-2 R-θ VARIATION OF THE CIRCUMFERENTIAL INNER CLAD HEAT FLUX, IN THE PEAK $UO_2$ AND PEAK MIXED OXIDE PINS

## 2)-2C) THE EFFECT OF THE NON-UNIFORM POWERGENERATION INSIDE THE $UO_2$ AND MIXED OXIDE PINS ON THE FUEL CENTERLINE TEMPERATURE

Although Nysing has developed formulas for the calculation of the temperature field inside the fuel, with non-uniform powergeneration they are very unpracticle to work with. Furthermore it has been found that the influence of the "skewed" powergradient was negligible and of the order $1^{o}F$. The infuence of the $e^{\xi_i r^2}$ type variation of the power inside the pin was found to be much more important. Therefore a more simple & more accurate formula has been developed for the calculation of the maximum centerline temperatures, taking the $e^{\xi_i r^2}$ variation into account, and the change of the fuel conductivity $\lambda_f$ with temperature.

The heat balance equation at the hot spot of the fuel pin can be written in a more generalized form as :

$$\frac{1}{r}\frac{d}{dr}\left[r\lambda_f \frac{dT}{dr}\right] = -q'''_{av}(r)\, F_z^N F_r^N \qquad (7\text{-}22)$$

$$q'''_{av}(r) = q'''_{av}\, a_1\, e^{\xi_1 (r/R)^2} \cong q'''_{av}\left[A_1 + A_2\left(\frac{r}{R}\right)^2\right] \qquad (7\text{-}23)$$

Integrating the equation (7-22) with (7-23) gives :

$$\int_{T_s}^{T_{MAX}} \lambda_f(T)\, dT = q'''_{av}\, F_z^N F_r^N \left[\frac{A_1}{4}R^2 + \frac{A_2}{16}R^2\right]$$

or with $q'''_{av}\,\pi R^2 = q'_{av}$ (linear heat rate).

$$\int_{T_s}^{T_{MAX}} \lambda_f(T)\, dT = F_z^N F_r^N \frac{q'_{av}}{4\pi}\left[A_1 + \frac{A_2}{4}\right] \qquad (7\text{-}24)$$

If a flat power inside the fuel pin is assumed :

the average volumetric heat rate would be :

$$\bar{q}'''_{av} = q'''_{av} \int_0^R \left[A_1 + A_2\left(\frac{r}{R}\right)^2\right] 2\pi r\,dr \Big/ \int_0^R 2\pi r\,dr = q'''_{av}\left(A_1 + \frac{A_2}{2}\right)$$

Because of the normalisation $A_1 + \frac{A_2}{2} = 1.0$

Therefore due to the parabolic variation of the heatrate inside the pin, the linear heat rate $q'_{av}$ has to be reduced by a factor

$$F_{q'}^{n.u} = \frac{A_1 + A_2/4}{A_1 + A_2/2} \qquad (7\text{-}25)$$

With this defined hotchannelfactor which takes into account that the powerdistribution is not flat, the equation (7-24) can be written as :

$$\int_{T_s}^{T_{MAX}} \lambda_f(T)\,dT = F_z^N F_r^N F_{q'}^{n.u.} \frac{q'_{av}}{4\pi} \qquad (7\text{-}26)$$

Where the constants $A_1$, $A_2$ can be obtained from a LASER calculation on a regular unit cell.

Using the values found in our case these hotchannelfactors were found to be for the $UO_2$ mixed oxide pin (Table 7-4).

<u>Table 7-4</u> ; Linear heat rate HCF, for the $UO_2$ & mixed oxide pins, which have to be applied on the limits for fuel centerline temperature at BOL.

| $F_{q'}^{n.u}$ $(UO_2)$ | $F_{q'}^{En.u.}$ (MIXED OXIDE) | $\frac{F_{q'}^{n.u}(UO_2)}{F_{q'}^{n.u.}(MIX)}$. |
|---|---|---|
| 0.988 | 0.963 | 1.026. |

It is thus observed that due to more pronounced variation of the power inside a mixed oxide pin about 3 % more power can be allowed in the mixed oxide pin, relative to the $UO_2$ pin, to get fuel centerline melting at beginning of life.

## 2)-3. THE NUCLEAR ENTHALPY RISE HOTCHANNELFACTOR OF THE PEAK $UO_2$ PIN COMPARED TO THE PEAK MIXED OXIDE PIN.

Since the nuclear enthalpyrise HCF is related to the peak coolant channel; its value may differ from the total nuclear radial powerpeakingfactor in the peak pin. For the peak $UO_2$ channel which is located isolated in the corner, the radial nuclear powerpeaking factor is also the nuclear enthalpy HCF. For the peak mixed oxide pin, the situation is completely different. Assuming that the radial nuclear HCF (no local peaking) for the peak mixed oxide pin in the core is about the same as for its adjacent neighbours, the ratio of the nuclear enthalpy riseHCF associated with the hottest coolant channel, surrounded by four rods, to the nuclear total radial HCF.(including local peaking) can be obtained from the unit assemblycalculations pictured on the Figures 5-7 & 5-9 .

Conservative values of 1.000 and 0.91 were obtained for the ratios of the nuclear enthalpyrise HCF & the nuclear radial (total) HCF for the $UO_2$ pin & mixed oxide pin respectively. It is thus noticed that the fact that the peak mixed oxide rods are surrounded by low power $UO_2$ & other mixed oxide rods is very beneficial. Fig. 7-3 shows the ratios in different channels around the peak $UO_2$ pin & peak mixed oxide pin. It is also noticed that the hot coolant mixed oxide channel at the peak pin is located towards the mixed oxide region.

The periferal variations of the bulk coolant temperatures around the peak mixed oxide pin are opposite to the periferal variations of the heat flux. It has been calculated that if no mixing occurs these opposite combined effects result in a virtually constant cladding temperature around the pin.

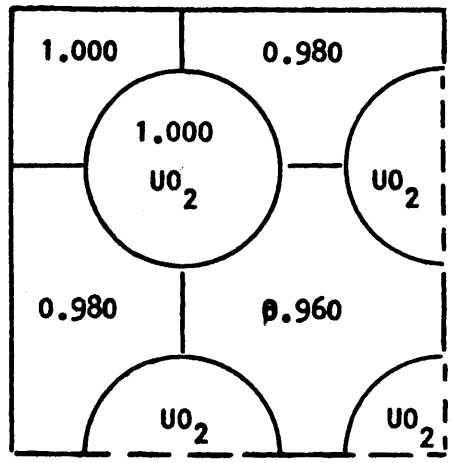


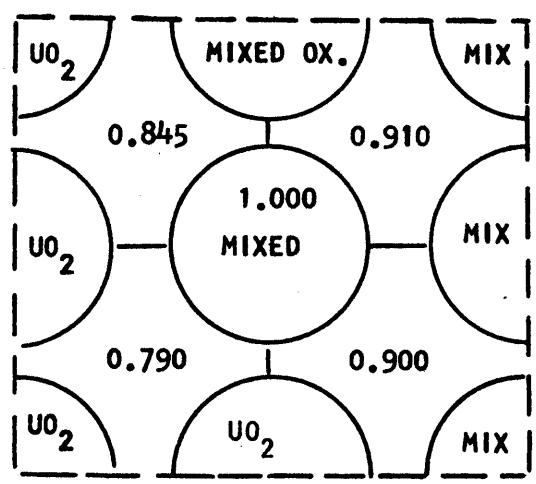


FIG VII-3 RATIOS OF THE NUCLEAR ENTHALPY RISE HOT CHANNEL FACTOR TO THE NUCLEAR PEAK FACTOR IN THE PEAK ROD, (PEAK $UO_2$ AND PEAK MIXED OXIDE )

## 2)-4 : MAXIMUM TEMPERATURES.

### MAXIMUM CLADDING TEMPERATURES.

The maximum cladding temperatures can be calculated from :

$$T_{cl} = T_{c\,in} + \frac{\Delta T_{cav}^{max}}{2}\left(1 + \sin\frac{\pi}{H} z_m\right) F^{E}_{\Delta t_c} F^{N}_{tz} + \Delta T_{f_{av}} F^{N}_{z} F^{N}_{tz} F^{E}_{\Delta t_f} \cos\frac{\pi}{H} z_m$$

where $T_{cav}^{MAX}$ = average outlet coolant temperaturerise
$= q'_{av}\, H/_{\overline{cp}} \cdot Mav$

$T_{fav}$ = average filmdroptemp.rise = $q''\,av/_{c_p Mav}$
($q''_{av}$ = average heat flux)

& the plan of max. cladding Temperature :

$$\text{tg}\ \frac{\pi}{H} z_m = \frac{\alpha_{av} D_{co}}{c_p M_{av}} F^{E}_{\alpha} F^{E}_{M}$$

(usually $Z_m$ = 1/3 from top).

where $D_{co}$ = outer cladding diameter.

A more conservative & realistic approach is to assume some local boiling at the place of maximum heat flux(center). In this case the maximum cladding surface temperature is given by the Jens-Lottes equation : ( 54 )

$$T_W = T_{SAT} + 60\left[\frac{q''}{10^6}\right]^{0.25} \cdot \exp\left(-P/900\right) \qquad (7\text{-}27)$$

where $T_W$ = wall temperature ($^oF$)

$T_{sat}$ = saturation temperature ($^oF$) of the coolant at pressure P (psia)

$q''$ = local heat flux $BTU/_{hr\ ft^2}$

The correlation appears to hold for all geometries and both local and bulk boiling. The correlation of Jens and Lottes appears to have been preferred by most workers in the field.

More recently, there has been concern that the temperature differences predicted by the Jens-Lottes correlation are too low at high pressures. Thom et al ( 55 ) concluded that their extensive data for pressures from 750 to 2000 psia were best correlated by :

$$(T_W - T_{Sat}) = 72 \left( \frac{q''}{10^6} \right)^{0.5} \exp\left(- \frac{P}{1260}\right) \qquad ( 7\text{-}28 ).$$

The temperature differences predicted by this correlation tend to be higher, than those obtained from the Jens-Lottes equation.

During the loss-of-Coolant Accident Analysis, in which a hypothetical double ended rupture of the main coolant pipe is postulated, the core goes through several regimes such as; subcooled blowdown, saturated blowdown, and a dry period ( 56 ). The heat transfercorrelations that are used during the boiling & dry period crisis are given in refs. 56 and 49 .

It is important to notice that the heat transfercoefficient, except for the subcooled water with local boiling regime is dependent on the heat flux, flow rate and quality of the steam.

Since for equal factors, the circumferential engineering heat flux factor in the mixed oxide is larger than for the $UO_2$, the cladding temperatures on the mixed oxide are higher if the heat transfer coefficient is independent of the flow rate & enthalpy-rise effects (quality).

In most cases however the heat-transfer coefficient also depends strongly on the quality & flowrate which, in view of the lower nuclear enthalpyrise hot-channelfactor for the peak mixed oxide & the maybe somewhat lower flowredistribution factor, will be higher for the mixed oxide, thereby reducing the cladding temperatures.

Without more detailed analysis, also by taking powergeneration after shutdown in the $UO_2$ fuel & mixed oxide fuel in account (including fission product decay

heat and heat from heavy isotope decay), it is however impossible to predict which peak will be the most limiting in a loss-of-coolant accident.
Because of the beneficial location of the mixed oxide rod one should be inclined to allow a much higher design limit for that pin.
However after shutdown, the fissionproduct $\beta$ and $\gamma$ ray release of the mixed oxide rod is different than for the $UO_2$ rod.
Furthermore detailed nuclear assembly calculations in which the nuclear calculations are strongly coupled with the thermal-hydraulics, will be necessary to evaluate the <u>design</u> limits of a peak mixed oxide rod versus a $UO_2$ rod.
The normal core values may be much lower than the design limits however.
The <u>inside cladding temperature</u> can be calculated from :

$$T_{ci} = T_w + \frac{3413\ q'\ t}{4\pi \bar{D}\ k_c} \qquad (7\text{-}29)$$

where q' = linear heat rate, KW/ft.

$k_c$ = thermal conductivity of the clad, 9.5 BTU/$_{hr\ ft}$-$^oF$ for zircalloy at 680 $^oF$.

t = cladding thickness (inches)

$\bar{D}$ = clad mean diameter (inches).

<u>The pellet surface temperature</u> is calculated from $T_s = T_{ci} + q''/_{Hgap}$

q'' = heat flux at the pellet surface BTU/hr ft$^2$ $^oF$

$H_{gap}$ = fuel gap conductance ,BTU/hr ft$^2$ $^oF$

$H_{gap}$ can be calculated from the Ross and Stoute Equation as modified by Rich ( 57 )

$$H_{gap} = 1000 + 2954\ E \qquad (7\text{-}30)$$

where E = interference clad strain (%)

$$\frac{E}{100} = \frac{D_f - D_i}{\bar{D}} \quad \text{for } D_f > D_i \qquad E = 0 \text{ for } D_f \leq D_i \qquad (7\text{-}31)$$

where $D_f$ = fuel pellet outside diameter (hot)

$D_i$ = clad inside diameter (hot)

$\bar{D}$ = clad mean diameter (hot)

The <u>fuel centerline temperature</u> can be calculated from the equation (7-26 ) in which the thermal conductivity formula from Lyons may be used where :

$$\lambda_f = \frac{1}{3.384 + 0.02615\,T} + 4.788 \times 10^{-13}\,T^3 \ (\text{Watts}/_{\text{cm}}\ {}^{o}\text{C})$$

& T is in $^{o}$ K.

The conductivity integral $\int \lambda_f\,(T)\,dT$ is then given by :

$$\int_{T_s}^{T_{MAX}} \lambda_f(T)\,dT = 38.24 \ln \frac{1 + 0.007728\,T_{MAX}}{1 + 0.007728\,T_s} + 1.197 \times 10^{-13}\left(T_{MAX}^4 - T_s^4\right) = \frac{q'_{HOT}}{4\pi} F_{q'}^{n.u}$$

(q' in Watt/cm)

Or directly from q', Ts and Fig. 7-4 , showing the thermal conductivity integral of $UO_2$ versus temperature (in $^{o}$F, q' in KW/ft ) based on Westinghouse conductivity data. ( 58 ).

## 2)-5 DEPARTURE FROM NUCLEATE BOILING.

The margin to departure from nucleate boiling (DNB, in which a fuel rod is blanketted by low conductivity vapor), is very important for the evaluation of the probability for clad failure during a nucleate boiling crisis. The DNBR is defined as the ratio of the heat flux required to produce departure from nucleate boiling at specific local coolant conditions to the actual local heat flux. The DNBR is minimum in the peak coolant channel at the peak pin & reaches a complete minimum somewhere along half of the core length or close to the max.

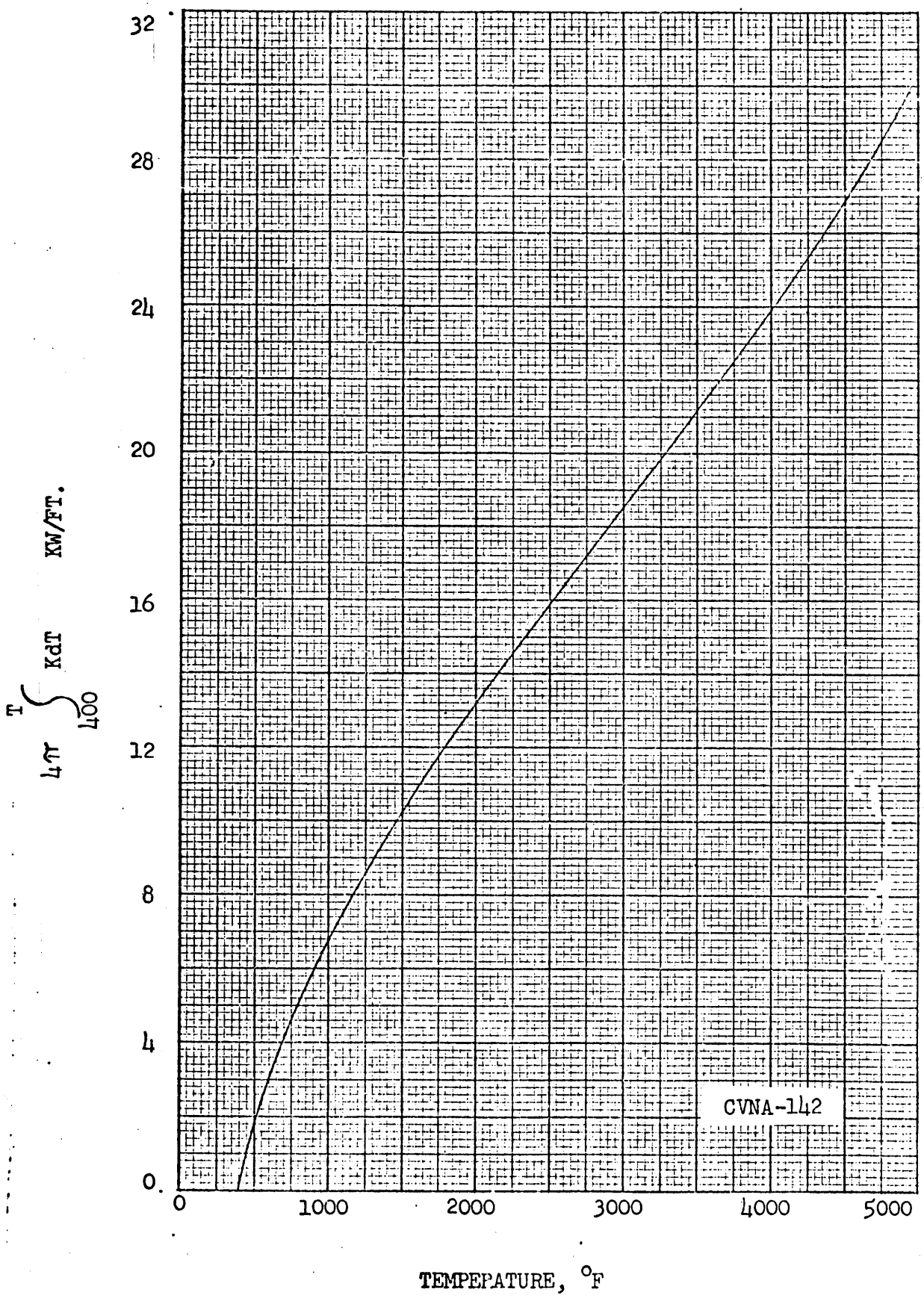


| YANKEE NUCLEAR POWER STATION | THERMAL CONDUCTIVITY INTEGRAL OF $UO_2$ VERSUS TEMPERATURE | FIGURE VII-4 |
|---|---|---|

heat flux. At this complete minimum the departure of nucleate boiling for the core is evaluated & called the MDNBR (minimum departure from nucleate boiling ratio)

The MDNBR is dependent on :

- the coolant inlet conditions
- the powerlevel
- the nuclear powerdistribution
- the analytical methods used to predict local coolant flow & coolant conditions (enthalpy, quality)
- the correlation used to predict DNB heat flux.

Tong ( 59 ) has emphasized the need for the evaluation of assembly-flow & peak channel enthalpy conditions, used with single channel DNB correlations.

The knowledge of these flowconditions & enthalpy in the hot channel, at each axial position & the knowledge of the design heat flux shapeaxially is needed in the first place to evaluate the MNBR. The approach in design is to select core operating conditions and models in such way that there is very small probability that the actual hot channel conditions are worse than the calculated conditions used as an input to the DNB correlation.

Based on large amounts of experimental data Westinghouse has developed DNB heat flux correlations applicable in several situations.

The W-2, DNB heat flux correlation for <u>the subcooled region</u>, & obtained from uniform flux data is given by :

( & is used when the subcooled quality is lower than - 15 %, (at which W-3 correlation is inapplicable).

$$q''_{DNB} = (0.23 \times 10^6 + 0.094G)(3.0 + 0.01\,\Delta T_{sub})(0.435 + 1.25\,e^{-0.0093\frac{L}{D_e}})$$

$$*(1.7 - 1.4\,e^{-a})$$

$$a = 0.532\left(\frac{H_{sat} - H_{in}}{H_{fg}}\right)^{3/4}\left(\frac{\rho_l}{\rho_v}\right)^{1/3} \qquad (7\text{-}32)$$

$q'_{DNB}$ = DNB heat flux, BTU/hr $ft^2$

G = coolant mass velocity (lb/hr -$ft^2$)

$\Delta T_{Sub}$ = Subcooling $^oF$.

L = heated channel length, ft

$D_c$ = equivalent channel diameter (ft)

$H_{SAT}$ = specific enthalpy of the saturated liquid BTU/lb.

$H_{in}$ = inlet enthalpy (BTU/lb

$H_{fg}$ = latent heat of vaporization BTU/lb.

$\rho_\ell$ = density of the saturated liquid lb/$ft^3$

$\rho_v$ = density of the saturated vapor lb/$ft^3$.

The DNB heat flux is interpreted either as the local DNB flux with the corresponding enthalpy, or as the average DNB flux up to a point, with the enthalpy at that point (exit usually). The most conservative interpretation is used. The formula correlates the existing uniform flux data within 20 %, at a probability of 95 %. A DNBR of 1.25 means that there is 95 % of probability that DNB will not occur.

In the quality region, the older W-2 correclation is :

$$H_{DNB} = H_{in} + 0{,}529\,(H_{Sat} - H_{in}) + (0.825 + 2.36\,\exp^{-204\,D_e})$$

$$H_{fg}\,\exp\left(-1.5\,\frac{G}{10^6}\right) - 0.41\,H_{fg}\,\exp\left(-0.0048\,\frac{L}{D_e}\right)$$

$$-1.12\,H_{fg}\,\frac{\rho v}{\rho l} + 0.548\,H_{fg} \qquad (7-33)$$

This equation correlates about 1000 data points within 25 % for a pressure range from 800 to 2750 psia at a probability level of 95 %. The data scattering is reduced to 20 % for 2000 psia, i.e.a DNBR of 1.25 for the full range and 1.20 for 2000 psia means that there is 95 % probability that DNB will not occur. The new improved W-3 correclation, (appendix A ) is used if the data are within the range of applicability (-15 to + 15 % quality).

It should be noted that in the regular W-3 correlations A-1 & A-2, the actual hot channel geometric condition (corner of the assembly) falls outside the range of heated to wetted perimeter ratio. This hot channel has unheated walls, & the conservative correlation A-3 developed for a single channel with unheated walls should be used. Since the R.H.S. factor in equation A-3, with $X = \infty$ and $D_h = 0.399$ in reduces to 0.81, the DNB flux using the W-3 correlation with unheated walls reduces the usual DNB heat flux by about 80 %. Since the W-3 correlation (with non uniform heat flux) was used, a more conservative MDNBR design limit would be 2.24 instead of 2.80. The core DNBR however should also been evaluated with this procedure. It is however noticed that the W-2 correlation is still the most conservative even if the cold wall W-3 correlation is used.

The effect of the non-uniform heat flux can be accounted for by the W-3, formula A-2 & its F factor. This factor is low in the subcooled region & the critical heat flux determines mostly the boiling crisis. For larger qualities the F factor is larger and the average heat flux or enthalpy rise mostly determines the boiling crisis.

The effect of the axial powerpeaks in the fuel rods at the top & bottom reflector has also been investigated since it was noticed from 2 dimensional r, Z calculations of a Pu-recycle assembly that the axial powerpeaking at the reflector was much larger in the mixed oxide. The top & bottompowerpeakfactor (with all rods out) defined as the actual powerpeak at top & bottom to the extrapolated chopped cosine value was 1.92 for the $UO_2$ fuel and 2.46 for the mixed oxide fuel (the extrapol. length $H_e$ to active core length ratio was 1.079). It was found that the DNB ratios at these high quality locations were not worse than the MNBR that occured near the max.heat flux, half away in the core.

The extra axial powerpeaking in the mixed oxide fuel, does not seem to be limiting & the local heat flux seems much more important than the enthalpy even for a

large range of exit qualities.

In certain transient situations where the exit quality is higher, the MDNBR for the mixed oxide pin could occur at 2 locations, at the exit of the channel and at the usual location between the exit and the maximum heat flux.

## VII-3 SUMMARY OF CALCULATED HOT CHANNEL FACTORS FOR THE UNITY CONVENTIONAL AND PU-RECYCLE ASSEMBLIES.

A summary of the calculated hot channel factors for the unit assemblies are given on Table VII-5. The engineering heat flux factor, the statistical enthalpy rise factor and the flow mixing factor, determined at YAEC for a conventional assembly, were assumed to be identical for Pu-recycle applications. The flowredistribution factor of 1.05 was also assumed for the peak $UO_2$ pin and 1.00 for the mixed oxide pin.

TABLE VII-5 SUMMARY HOT CHANNEL FACTORS OF THE UNIT ASSEMBLIES.

| | CONVENTIONAL $UO_2$ ASSEMBLY | PLUTONIUM RECYCLE ASSEMBLY. PEAK $UO_2$ | PEAK MIX.OXIDE |
|---|---|---|---|
| | 4w/oU235-$UO_2$ | 4 w/oU235-$UO_2$ | 4 w/o $PUO_2$ - nat $UO_2$ |
| **Heat Flux Factors.** | | | |
| Nuclear Heat Flux | 1.19 | 1.20 | 1.21 |
| Engineering Heat Flux | 1.04 (1) | 1.04 | 1.04 |
| Circumferential Heat Flux Factor. | 1.01 | 1.01 | 1.04 |
| Total Heat Flux Factor (unit-assembly) (3) | 1.25 | 1.26 | 1.31 |
| **Enthalpy rise Factors.** | | | |
| Statistical Enthalpy Rise | 1.10 (1) | 1.10 | 1.10 |
| Flow Mixing Factor | 0.94 (1) | 0.94 | 0.94 |
| Flow Redistribution | 1.05 (1)(2) | 1.05 | 1.00 |
| Total Engineering | 1.09 | 1.09 | 1.03 |
| Nuclear Enthalpy Rise | 1.19 | 1.20 | 1.10 |
| Total Enthalpy Rise (4) Factor (unit assembly) | 1.30 | 1.31 | 1.13 |

(1) From Yankee - thermal hydraulic calculations - core 10.
(2) core 10 value is 1.10, (both stainless and Zirc assemblies are present, the zirc assemblies have a higher flow resistance, 1.05 estimated.
(3) without radial and axial power peaking factors.
(4) without radial power peaking factor and lower plenum factor of about 1.05.

Table VII-6 ESTIMATED PLUTON. RECYCLE CORE HOT CHANNEL FACTOR RATIOS $F^{UO_2}/F_{MIX}$.

| Heat Flux Factor ratios : | $F^{UO_2}/F_{MIX}$ |
|---|---|
| Nuclear | 1.00 |
| Engineering | 1.00 |
| Circumferential | 0.97 |
| Total | 0.97 |
| | |
| Enthalpyrise Ratio's. | |
| Statistical | 1.00 |
| Lower plenumfactor | 1.00 |
| flow mixing factor | 1.00 |
| Flow redistribution | 1.05 |
| Total engineering | 1.05 |
| Nuclear enthalyrise | 1.09 |
| Total enthalpyrise | 1.14 |
| | |
| RATIOS ESTIMATED MDNBR. | |
| MDNBR | 1.05 |
| RATIOS FUEL & TEMPERATURES. | |
| fuel & temperature ratio : | 1.026 |

## VII-4 : CONCLUSION.

In this Chapter an analysis was made of the circumferential heat flux variations in a peak $UO_2$ and mixed oxide pin. An engineering hotchannelfactor for the circumferential outer clad heat flux was calculated to be 1.012 and 1.038 for the $UO_2$ & mixed oxide respectively. Due to the more non-uniform powergeneration in the mixed oxide fuel, the linear powerrrating in the peak mixed oxide fuel, to obtain the same maximum fuel centerline temperature as a peak $UO_2$ pin, can be increased by 2.6 %. Estimations of other hotchannelfactors, based on extrapolations of more detailed calculations performed at YAEC, have been made, which indicate that the ratio of the total heat flux HCF of the peak $UO_2$ pin to the peak mixed oxide pin is 0.96 and for the total enthalpyrise HCF ratio 1.14. The estimated conservative ratio of the MDNBR is about 1.05, conservatively, which indicate that at least 5 % more power could be allowed in the mixed oxide rods to get the same probability of cladding failure in a nucleate boiling crisis. More refined calculations using steady state & transient thermal-hydraulic computerprograms will be necessary to establish how much more power could be allowed in a peak mixed oxide pin, relative to a peak $UO_2$ pin in a conventional assembly.

This will however require knowledge of the complete nuclear analysis of the plutonium recycle core, the knowledge of decay heat from fissionproducts (which will probably be higher in mixed oxide fuel) and a coupling of thermal hydraulic accident conditions in the plutonium recycle assembly with detailed nuclear unit assembly calculations.

## Appendix A : W-3 DNB HEAT FLUX CORRELATIONS.

### 1) W-3 UNIFORM FLUX DNB CORRELATION FOR SINGLE CHANNEL WITH ALL WALLS HEATED :

$$\frac{q''_{DNB,EU}}{10^6} = \left\{(2.022 - 0.0004302\,p) + (0.1722 - 0.0000984\,p) * \exp\left[(18.177 - 0.004129\,p)\,X\right]\right\} * \left[(0.1484 - 1.596\,X + 0.1729\,X\;X)\,G/_{10^6} + 1.037\right] * \left[1.157 - 0.869\,X\right] * \left[0.2664 + 0.8357\exp(-3.151\,D_e)\right] * \left[0.8258 + 0.000784\,(H_{sat} - H_{in})\right] \qquad \text{(EQ.A-1)}$$

The heat flux q'' is given in $BTU/_{hr\ ft^2}$, and the units and ranges of the parameters of the data used in developing this correlation are :

$1000 \leq p \leq 2300$ psia

$10^6 \leq G \leq 5.0 \times 10^6\ lb/_{(hr\ ft^2)}$

$0.2 \leq D_e \leq 0.7$

$-0.15 \leq X_{loc} \leq +0.15$

$H_{in} \geq 400$ BTU/lb

$10 \leq L \leq 144$ in

$0.88 \leq \dfrac{\text{Heated perimeter}}{\text{wetted perimeter}} \leq 1.0$

### 2) W-3 Non-uniform Flux DNB correlation for Single Channel with all Walls Heated.

$q''_{DNB,N} = q''_{DNB,EU}/F$ ($q''_{DNB,N}$ = DNB heat flux for non uniformly heated channel)

$$F = C / q''_{local} \times \left(1 - \exp(-C.\ell_{DNB,EU})\right) \times \int_0^{\ell_{DNB}} q''(z)\exp\left[-C(\ell_{DNB} - z)\right] dz$$

$$C = 0.44\,\frac{(1 - X_{DNB})^{7.9}}{(G/_{10^6})^{1.72}} \qquad \text{(A-2)}$$

3) W-3 Uniform Flux DNB Correlation for Single Channel with Unheated Walls.

$$\frac{q''_{DNB\ with\ unheated\ wall}}{q''_{DNB,\ using\ D_h\ to\ replace\ De\ in\ eq.\ (A-1)}} = (1.36 + 0.12\, e^{9X}) * (1.2 - 1.6\, e^{-1.92\, Dh})(1.33 - 0.237 e^{5.66\, X}) \qquad (A-3)$$

$D_e$ = equivalent hydraulic diam.

$D_h$ = equivalent diameter based on only the heated parimeter (in).

The probability that the DNB heat flux has been exceeded for several values of the DNB ratio, is shown below ( 49 ) and on Fig. 7-5 . ( 56 )

Probability Distribution (DNB limits)

| DNB RATIO | Probability that DNB heat flux has beem exceeded. |
|---|---|
| 2.5 | 0.0000085 |
| 2.0 | 0.00018 |
| 1.75 | 0.001 |
| 1.50 | 0.01 |
| 1.30 | 0.05 |

REFERENCES.

1) H.D. Raleigh, " Economics of Plutonium Recycle in Thermal Reactors " Reactor and Fuel-processing Technology, Vol. 12, N°4, Fall 1969.

2) J. Haley, " EEI-Westinghouse Plutonium Recycle Demonstration Program Progress Report for the Period ending April 1970, May 1970 WCAP 4167-1

3) J. Debrue, P. Deramaix, F. de Waegh, " Plutonium Recycle Studies for the SENA PWR Reactor " Nuclear Applications and Technology Vol 9, October 1970.

4) R.G. Schweiger, " Managing Nuclear Fuel ", special report in " Power ", December 1969.

5) E.G. Andensam et al, " Computor Methods for Utility Reactor Physics Analysis " Reactor and Fuel Processing Technology, Vol 12, N°2, Spring 1969.

6) J. Chernick " Status of Reactor Physics Calculations " Reactor Technology, Vol. 13, n°4, Winter 1970-71.

7) C.G. Poncelet " LASER - A Depletion Program for Lattice Calculations Based on MUFT and THERMOS " WCAP-6073, Westinghouse Atomic Power Divisions (April 1966).

8) A.K. Addae et al, " The Reactor Physics of the Massachusetts Institute of Technology Reactor Redesign ", Aug. 1970, MITNE-118.

9) D.A. Goellner, J.J. Beaudreau, "Summary Description of the Fuel Depletion Code Cell " MIT -2073-8, MITNE-89, June 1968.

10) T.B. Fowler et al, " Exterminator-2 : A Fortran IV Code for Solving Multi-group Diffusion Equations in Two Dimensions " ORNL-4078 (1967).

11) M.A. Boling, W.A. Rhoades " NAA Program Description ANISN/DTF II Conversion to IBM System/360 " Atomics International, AI-66-MEMO-171.

12) K.D. Lathrop, "TWOTRAN, A Fortran Program for Two Dimensional Transport " Gulf General Atomic, GA-8747, July 1968.

13)-W.R. Cadwell, "PDQ-5- A Fortran Program for the Solution of the Two Dimensional Neutron Diffusion Problem-Part 1 : Steady-State Version " WAPD-TM-363,Febr.1963

-R.J. Breen et al, " HARMONY : System for Nuclear Reactor Depletion Computation" WAPD - TM -478, Jan. 1965.

14) Personal communication H. Spierling, Nucl.Eng. Dept. MIT.

15) D.F. Martin, " The Effect of Refueling Date Changes on Fuel Cycle Costs " Nucl. Eng. Dept. MIT, M.S. thesis 1971.

16) D.L. Delp et al " FLARE, A Three-Dimensional Boiling Water Reactor Simulator" GEAP-4598, AEC Research and Development Report, July 16, 1964.

17) P.N. Ontko, " Flare G, A Three-Dimensional Reactor Simulator " M.S. Thesis, Nucl.Eng.Dept. MIT, Febr. 1971.

18) D.S. Rowe, "Cross Flow Mixing between Parallel Flow Channels during Boiling-Part I, COBRA - Computor program for coolant boiling in rod arrays ", BNWL-371, pt.I, March 1967.

19) C.L. Wheeler, G.C. Main, D.C. Kolesar " COBRA II-A, A Program for thermal-Hydraulic Analysis in Very Large Bundles of Fuel Pins " BNWL-1422.

20) R.D. Brunell, " Heating and Heating 2, Program Description of a Generalized Heat Transfer Code for Solution of Transient and / for Steady-State Problems One, Two or Three Dimensional Cartesian or Cylindrical Coordinate Systems ". Atomics International, AI-64 Memo-177.

21) P.Loizzo et al, "Experimental and Calculated Results for $UO_2$ and $UO_2$-$PuO_2$ fueled $H_2O$-Moderated Loadings" Battelle Memorial Pacific Northwest Laboratories, BNWL-1379, August 1970.

22)-H.C. Honeck, "THERMOS, A Thermalization Transport Theory Code for Reactor Lattice Calculations " BNL-5826 (1961).-
-B. Toppel and I. Baksys " The Argonne Revised Thermos Code " ANL-7023 (March, 1965).

23) H.C. Honeck " The Calculation of the Thermal Utilization and Disadvantage Factors in Uranium Water Lattices ". Nuclear Science and Engin. 18, 49 (1964)

24) H. Bohl Jr. et al, "MUFT-4, Fast Neutron Spectrum Code for the IBM 704" WAPD-TM-72, July 1957.

25) T.R. England " CINDER, A one Point Depletion and Fission Product Program". WAPD-TM-334 (1962).

26) Gellings H., A. Sauer, " Programbeschreibung zu Dancoff Jr. " Allgemeine Elektrikcitäts Gesellschaft Report KEA-114 (1963).

27) R.F. Barry " LEOPARD, - A Spectrum Dependent Non-Spatial Depletion Code for the IBM-7094 " WCAP-3269-26, Sept. 1963 and revisions to WCAP-3269-26 Aug. 1968.

28) H. Amster, R.Suarez, "The Calculation of Thermal Constants averaged over a Wigner-Wilkins Flux Spectrum " WAPD-TM-39, Jan.1957.

29) E.P. Wigner, J.E. Wilkins Jr. " Effect of the Temperature of the Moderator on the velocitydistribution of neutrons with numerical calculations for H as moderator " AECD-2275, 1948.

30) D.L. Farrar " A Comparison of Simple Calculational Methods of Boiling Water Analysis " Aug. 1971. Nucl. Eng. Dept. MIT.

31) PDQ-5, Argonne Code Center Reference Material Abstract 336.
ANL, Building 203 Room C230, 9700 South Cass Avenue, Argonne, Ill. 60439.

32) A. Weinberg, E. Wigner " The Physical Theory of Neutron Chain Reactors ".
The University of Chicago Press, 1958.

33) G.C. Pomraning " On the Energy Averaging of the Diffusion Coefficient "
Nucl.-Sci. & Eng. (1965) p.250.

34) G.P. Calume, " A Few-Group Theory for Watergap Peaking " Nuclear Science and Engineering 8, 1960 p.400.

35) R.J. Breen, " A One Group Model for Thermal Activation Calculations ",
Nuclear Science and Engineering, 9, 1961 p.91.

36) W.J. Levedahl, " A Simplified Technique for Calculation Spectrum Dependent Water-Gap Peaking " General Electric Co. Report KAPL-M-WJL-5, December 1959.

37) J. Debrue et al, " A Basic Experimental Reactor Physics Programme on $UO_2$-$PuO_2$-$H_2O$ Lattices "
S.C.K./C.E.N. - Belgonucleaire Assoc. Mol, May 14, 1971.
Paper prepared for Presentation at the 17th annual ANS Meeting (Boston June 13, 1971)

38) F.D. Judge, L.S. Bohl, " Effective Hot Channel Factors for Flat Power Reactors"
Trans. ANS 7 (1964) p 497.

39) J. Celnik et al., " Representation of Fission Products in Thermal Power Reactors Containing $UO_2$ and Plutonium Recycle Fuel " Transaction A.N.S. 10, 516 (November 1967).

40) C.S. Rim " Neutronic and Thermal Analysis of Nuclear Fuels ", Ph.D.thesis Nuclear Engineering dept. MIT, August 1969.

41) C.G. Poncelet " Burnup Physics of Heterogeneous Reactor Lattices " WCAP-6069, Westinghouse Electric (June 1965)

42) L.E. Srawbridge, " Calculation of Lattice Parameters for Uniform Water Moderated Lattices WCAP-3742, Westinghouse Electric (1963).

43) R. Sher et al. " Least Square Analysis of the 2200 m/sec Parameters of U233,U235 and Pu 239, "BNL-918, Brookhaven National Lab. (March 1965)

44) C.H. Westcott et al, "Survey of Nuclear Data for Reactor Calculations " Paper A/Conf. 28/P/717. Proc. Third U.N. Intern.Conf. Peaceful Uses Atomic Energy, Geneva (1964)

45) B. Sturm " Refined calculation and comparison with measurements of the thermal neutron hyperfine structure in $D_2O$ moderated 4 and 7 UC cluster ". Energia Nucleare, Vol 13, n°8, Aug. 1966.

46) J.P. Schneeberger et al, "Distributions Fines dans des Grappes pour Réacteurs Uranium Métallique - eau lourde, refroidis par Gaz " "Heavy Water Lattices " Technical Series, 20, IAEA, Vienne 1963.

47) P.F. Palmedo " A semi-empirical description of the detailed thermal flux distribution in $UO_2$ clusters " Nucl. Sci. & Eng. 21 (1965) p.578.

48) W. Zernik, H.B. Currin et al "THINC - A Thermal Hydraulic Interaction Code for a Semi-Open or closed Channel Core " WCAP-3704 Westinghouse Atomic Power Divison (1962).

49) Allan , " Thermal-Hydraulic Design and Evaluation " YAEC-102, 8 6 71 Draft.

50) L.S. Tong, H. Chelemer et al " Hot Channel Factors for Flow Distribution and Mixing in Core Thermal Design ", WCAP-2211 (1963).

51) L.S. Tong and H.Chelemer, " Engineering Hot Channel Factors for an Open Channel PWR Core with Square-Latticed Fuel Rods ", WCAP-5182 (1961)

52) D.S. Rowe and C.W. Angle, "Cross Flow Mixing Between Parallel Flow Channels "- Par II - Measurement of Flow and Enthalpy in Two Parallel Channels " BNWL-371 pt 2 (December 1967).

53) R. Nijsing, " Temperature and Heat Flux Distribution in Nuclear Fuel Element Rods " Nuclear Engineering & Design 4 (1966) 1-20.

54) W.H. Jens and P.A. Lottes, " Analysis of Heat Transfer, Burnout, Pressure Drop and Density Data for High Pressure Water " USAEC Report ANL-4627, Argonne National Laboratory (1951).

55) J.R.S. Thom et al " Boiling in Sub-cooled Water During Flow up Heated Tubes or Annuli " Proc. Inst. Mech. Eng. 180, 226 (1965-66).

56) L.S. Tong, J. Weisman " Thermal Analysis of Pressurized Water Reactors " Published by the American Nuclear Society, 1970.

57) B. Rich, "Fuel-Clad Gap Conductance" United Nuclear Corporation, NEDO-1578 (August 1968)

58) R.B. Duncan, " Rabbit Irradiation of $UO_2$ " CVNA-142 (1962).

59) L.S. Tong, " An Evaluation of the Departure from Nucleate Boiling in Bundles of Reactor Fuel Rods " Nuclear Science & Engineering, 33, 7-15 (1968)

60) P.G. Mertens, Special Problem Report, January 1971, Prof. D.D. Lanning.